THE UNIVERSITY OF QUEENSLAND

AUSTRALIA

Cellular and molecular mechanisms of pancreatitis in atrophy and regeneration

Lynne Estelle Reid

BSc, MSc (Qual)

A thesis submitted for the degree of Doctor of Philosophy at

The University of Queensland in 2018

Faculty of Medicine

ABSTRACT

Pancreatitis is a debilitating disease with complex etiology, prognosis and pathology, limited treatment options and a burden on health resources. The main lesions of acute pancreatitis are injury to acinar cells and inflammation of the pancreas. Mild interstitial pancreatitis (or oedematous pancreatitis) is characterized by acute inflammation with oedema in the stroma and acinar tissue. Necrosis of acinar tissue, stroma or peri-pancreatic fat is absent and complete recovery, or regeneration of the gland is usual. Whilst there is universal agreement on many of the cellular changes that accompany acute pancreatitis, there is no clear distinction between the factors that determine whether regeneration can occur. The mechanism of regeneration and the cellular processes that influence regeneration form the primary basis of this study.

Experimental models of pancreatitis have been produced in rats, mice, dogs, cats and swine by various methods. The time course and final tissue regeneration, if it occurs, vary considerably among different models, with many having the limitation that pancreatic injury is extended, so that degenerative processes are superimposed on regenerative activity. Three *in vivo* models of pancreatitis in rats were chosen for this project, to study pancreatitis and pancreatic regeneration that occurs in the recovery phase. These models evolve slowly, allowing detailed morphological study. In general, they have similar early events but vary considerably in regenerative outcome. (1) The infusion of caerulein is a well-established model for inducing experimental pancreatitis in rats and pancreatitis is followed by a great reparative capacity. Caerulein is a decapeptide with biological activity on gastrointestinal smooth muscle contraction and pancreatic and gastric secretion. (2) In 1-cyano-2-hydroxy-3-butene (CHB)-induced pancreatitis, acinar cell regeneration is limited to small islands of acini which fail to endure. CHB is known to induce cell death in pancreatic acini. (3) The model of partial pancreatic duct ligation leads to atrophy of the gland with little or no regeneration ensuing. Although some characteristics are known about these models of pancreatitis, there is a general lack of information on the association between pancreatic atrophy and inflammation and investigating this association was one of my overall aims. In addition, as well as investigating the three different models of pancreatitis in rats, I aimed to compare the same initiating event in other animals. Because of the selective nature of CHB pancreatotoxicity, and the ease of producing the model in rats, I sought to investigate this method in a mouse model. In addition, I sought to establish and characterise a canine CHB model.

The pancreatic atrophy induced in the chosen models typically involved apoptosis of acinar cells and its removal by macrophages. In some situations, if acinar redifferentiation did not occur, development of fibrosis and scarring was a key to pancreatic repair. This atrophy took place in a coherent fashion with normal architectural relationships being maintained. Loss of the potentially dangerous enzyme-secreting cells by apoptosis led to regression of the underlying duct structure such that regeneration might occur should the circumstances change. This thesis has had a prolonged history because of part-time enrolment, through departure from the University of Queensland of my original Principal Advisor Dr Neal Walker, transfer of my Associate Advisor Dr Lyndell Kelly to Dunedin, New Zealand and necessary changes in my Advisory Team, an attempt to complete some of the research in New Zealand and the unfortunate death of the scientist I was working with, as well as my own personal and family issues. I am hoping to complete the project with my current re-enrolment.

The hypothesis tested was that different models of pancreatitis can be used to describe the processes of atrophy and regeneration in the pancreas. The specific aims of this study were:

1. To investigate rat models of pancreatitis using caerulein, CHB and duct ligation;
2. To validate a pancreatitis model with CHB in the mouse;
3. To establish a canine model of pancreatitis with CHB;
4. To compare and contrast the models with respect to:
   Stellate cells and the production of fibrosis
   The role of mast cells and macrophages
   The role of survivin in pancreatic regeneration

Summary of outcomes of this study

- Study of the three rat models of pancreatitis facilitated a comparison of markers and mechanisms within the lesion.
- All of the pathological processes studied, including fibrosis, stellate cells, mast cells and macrophages had specific roles in the different models that correlated with the initiation of pancreatitis, the deposition and degradation of fibrosis, and the ability of the pancreas to regenerate.
- Resorption of fibrosis may depend on the type of collagen deposited.
- Survivin appears to be maintaining conditions for the survival of cell populations.
- The models of CHB in mouse and dog were not suitable for the study of pancreatitis as the liver showed more severe damage at low doses than the pancreas

DECLARATION BY AUTHOR

This thesis is composed of my original work, and contains no material previously published or written by another person except where due reference has been made in the text. I have clearly stated the contribution by others to jointly-authored works that I have included in my thesis.

I have clearly stated the contribution of others to my thesis as a whole, including statistical assistance, survey design, data analysis, significant technical procedures, professional editorial advice, financial support and any other original research work used or reported in my thesis. The content of my thesis is the result of work I have carried out since the commencement of my higher degree by research candidature and does not include a substantial part of work that has been submitted to qualify for the award of any other degree or diploma in any university or other tertiary institution. I have clearly stated which parts of my thesis, if any, have been submitted to qualify for another award.

I acknowledge that an electronic copy of my thesis must be lodged with the University Library and, subject to the policy and procedures of The University of Queensland, the thesis be made available for research and study in accordance with the Copyright Act 1968 unless a period of embargo has been approved by the Dean of the Graduate School.

I acknowledge that copyright of all material contained in my thesis resides with the copyright holder(s) of that material. Where appropriate I have obtained copyright permission from the copyright holder to reproduce material in this thesis and have sought permission from co-authors for any jointly authored works included in the thesis.

ACKNOWLEDGEMENTS

I acknowledge and thank those who have given me support throughout this long journey. Prof Neal Walker, now Envoi Pathology, Brisbane, introduced me to pancreatitis as supervisor for my Masters Qualifying thesis and was first supervisor for the PhD thesis. Prof Grant Ramm (QIMR-Berghofer Research Institute) supervised a comprehensive but ultimately unsuccessful and aborted search for the elusive pancreatic stem cell. Dr Leila Cuttle (then, UQ School of Medicine) taught me how to use the ImagePro Plus® image analysis software. Dr Richard Malik (Centre for Veterinary Education, University of Sydney) and Dr Melanie Latter (veterinary pathologist, formerly UQ School of Veterinary Science) provided veterinary proficiency. Dr Anne Marie McNicol (now retired, Reader in Pathology, Glasgow University) perused some of the earlier manuscript. Work colleagues from the past, Clay Winterford, Estelle Schoch and from the more recent past, the brilliant staff too numerous to mention, of the Lakhani Breast Cancer Research Group, are sincerely thanked. Debates and discussions about research and protocols, sharing of knowledge and general moral support, were invaluable. Dr Lyndell Kelly (School of Medicine, University of Otago, New Zealand) has been a friend and colleague extraordinaire and a PhD supervisor: The Three Musketeers, Lyndell, Lynne and Pancreas have planned projects, finished some, made the acquaintance of lots of laboratory animals and enjoyed mutual scientific discovery. I could not have done this without you. A/Prof Glenda Gobe (School of Biomedical Sciences, UQ Faculty of Medicine), I am forever grateful for your expertise, patience and good humour in helping me achieve the finished product.

PUBLICATIONS

Peer-reviewed publications during candidature

Reid L and Walker N. Acinar cell apoptosis and the origin of tubular complexes in caerulein-induced pancreatitis. *Int. J. Exp. Pathol.* 1999, 80, 205-215.

Kelly LE, **Reid L**, Walker NI. Massive acinar cell apoptosis with secondary necrosis, origin of ducts in atrophic lobules and failure to regenerate in cyanohydroxybutene pancreatopathy in rats. *Int. J. Exp. Pathol.,* 1999, 80, 217-226.

Peer-reviewed published abstracts during candidature

Kelly LE, Goodall AR, **Reid L**, Walker NI. The effect of the pancreatotoxin cyanohydroxybutene on pancreatic ductal and acinar carcinoma cell lines. In Proceedings of the 5th International Symposium on predictive Oncology and Therapy, *Cancer Detection and Prevention,* 2000, 24, S-184.

Publications relevant to this thesis pre-candidature

Middleton G, **Reid LE**, Harmon BV. Apoptosis in the human thymus in sudden and delayed death. *Pathology*. 1994, 26(2), 81-89.

Publications during part-time candidature 1996-2012 not related to thesis

Peters AA, Simpson PT, Bassett JJ, Lee JM, Da Silva L, **Reid LE**, Song S, Parat MO, Lakhani SR, Kenny PA, Roberts-Thomson SJ, Monteith GR. Calcium channel TRPV6 as a potential therapeutic target in estrogen receptor-negative breast cancer. *Mol Cancer Ther.* 2012,11(10), 2158-68

Smart CM, Askarian Amiri ME, Wronski A, Dinger ME, Crawford J, Ovchinnikov DA, Vargas AC, **Reid LE**, Simpson PT, Song S, Wiesner C, French JD, Dave RK, Silva L, Purdon A, Andrew M, Mattick JS, Lakhani SR, Brown MA, Kellie S. Expression and function of the protein tyrosine phosphatase receptor J (PTPRJ) in normal mammary epithelial cells and breast tumors. *PLoS ONE,* 2012, **7** (7) e40742

Vargas AC, McCart Reed AE, Waddell N, Lane A, **Reid LE**, Smart CE, Cocciardi S, da Silva L, Song S, Chenevix-Trench G, Simpson PT, Lakhani SR. Gene expression profiling of tumour epithelial and stromal compartments during breast cancer progression. *Breast Cancer Res Treat.* 2012 135(1):153-65.

Waddell N, Arnold J, Cocciardi S, da Silva L, Marsh A, Riley J, Johnstone CN, Orloff M, Assie G, Eng C, **Reid LE,** Keith K, Yan M, Fox S, Devilee P, Godwin AK, Hogervorst FBL Fergus Couch F, kConFab Investigators, Grimmond S Flanagan JM, Khanna KK, Simpson, PT, Lakhani SR, Chenevix-Trench G. Subtypes of familial breast tumours revealed by expression and copy number profiling.*Breast Cancer Res Treat* 2010, 123, 661–677

Alexopoulou AN, Leao M, Caballero OL, Da Silva L, **Reid LE**, Lakhani SR, Simpson AJ, Marshall JF, Neville AM, Jat PS. Dissecting the transcriptional networks underlying breast cancer: NR4A1 reduces the migration of normal and breast cancer cell lines. *Breast Cancer Research* 2010, **12**:R51

Da Silva L, Buck L, Simpson PT, **Reid LE,** McCallum N Barry J. Madigan BJ, Lakhani SR. Molecular and morphological analysis of adenoid cystic carcinoma of the breast with synchronous tubular adenosis. *Virchows Arch* 2009, 454,107–114

Shin SJ, Simpson PT, Da Silva L, Jayanthan J, **Reid LE**, Lakhani SR, Rosen PP. Molecular Evidence for Progression of Microglandular Adenosis (MGA) to Invasive Carcinoma. *Am J Surg Pathol* 2009, 33, 496–504

Da Silva L, Parry P, **Reid LE**, Keith P, Waddell N, Kossai M, Clarke C, Lakhani SR, Simpson PT, Aberrant Expression of E-cadherin in Lobular Carcinomas of the Breast. *Am J Surg Pathol* 2008, 32, 773–783.

Simpson PT, Reis-Filho JS, Lambros MBK, Jones C, Steele D, Mackay A, Iravani M, Fenwick K, DexteR T, Jones A, **Reid L**, Da Silva L, Shin SJ, Hardisson D, Ashworth A, Schmitt FC, Palacios J, Lakhani SR. Molecular profiling pleomorphic lobular carcinoma of the breast: evidence for a common molecular genetic pathway with classic lobular carcinomas. *J Pathol* 2008, **215**, 231–244

Michael-Robinson JM, **Reid LE**, Purdie DM, Biemer-Hüttmann AE, Walsh MD, Pandeya N, Simms LA, Young JP, Leggett BA, Jass JR, Radford-Smith GL. Proliferation, apoptosis, and

survival in high-level microsatellite instability sporadic colorectal cancer. *Clin Cancer Res.* 2001, **7**(8), 2347-56.

CONTRIBUTION TO PUBLICATIONS INCLUDED IN THIS THESIS

Reid L and Walker N. Acinar cell apoptosis and the origin of tubular complexes in caerulein-induced pancreatitis. *Int. J. Exp. Pathol.* 1999, 80, 205-215. PMID: 10583630

Contributor	Statement of contribution
Lynne Reid (Candidate)	Designed experiments, wrote the paper (60 %)
Neal Walker	Designed experiments, edited the paper (40 %)

Kelly LE, **Reid L**, Walker NI. Massive acinar cell apoptosis with secondary necrosis, origin of ducts in atrophic lobules and failure to regenerate in cyanohydroxybutene pancreatopathy in rats. *Int. J. Exp. Pathol.,* 1999, 80, 217-226. PMID: 10583631

Contributor	Statement of contribution
Lyndell Kelly	Designed experiments, wrote the paper (40 %)
Lynne Reid (Candidate)	Designed experiments, wrote the paper (40 %)
Neal Walker	Designed experiments, edited the paper (20 %)

STATEMENT OF PARTS OF THE THESIS SUBMITTED TO QUALIFY FOR THE AWARD OF ANOTHER DEGREE

None

RESEARCH INVOLVING HUMAN OR ANIMAL SUBJECTS

All research was reviewed and approved by an independent review committee prior to commencement. Animal experiments were performed under National Health and Medical Research Committee guidelines and approved by the University of Queensland Animal Ethics Committee prior to project commencement. Animals were closely monitored for clinical signs of pain and distress. Ethics approval numbers were PATH/402/96 (caerulein), PATH/527/97/98 (rats with duct ligation); PATH/527/00 (rats with duct ligation with clips removed); PATH/QIMR/586/03 (CHB and duct ligation), PATH/457/04LF and PATH/725/05/LF (dogs); and PATH/102/04/PTPL (mice).

FINANCIAL SUPPORT

Some financial support was available from School of Medicine, University of Queensland for consumables and animals for this project.

KEYWORDS

Pancreatitis, fibrosis, cell death, apoptosis, regeneration, histology, electron microscopy

AUSTRALIAN AND NEW ZEALAND STANDARD RESEARCH CLASSIFICATIONS (ANZSRC)

ANZSRC code: 110307 Gastroenterology and Hepatology 50%
ANZSRC code: 110316 Pathology (excl oral pathology) 25%
ANZSRC code: 060103 Cell Development, Proliferation and Death 25%

FIELDS OF RESEARCH (FoR) CLASSIFICATION

FoR code: 1116 Medical Physiology 50%
FoR code: 0601 Biochemistry and Cell Biology 50%

TABLE OF CONTENTS

LIST OF FIGURES

CHAPTER 1

CHAPTER 2

CHAPTER 3

CHAPTER 4

CHAPTER 5

CHAPTER 6

CHAPTER 7

CHAPTER 8

LIST OF TABLES

CHAPTER 1

CHAPTER 2

CHAPTER 7

ABBREVIATIONS

All abbreviations are listed in alphabetic order

ANOVA	analysis of variance
αSMA	Alpha smooth muscle actin
ADM	Acinar-to-ductal metaplasia
AP	Activator protein
ATP	Adenosine triphosphate
Bcl2	B-cell lymphoma 2
BIR	Baclovirus inhibitor of apoptosis protein
BM	Basement membrane
BMP	Bone morphogenetic protein
CASR	Calcium sensing receptor
CCK	Cholecystokinin
CCL	Carbon tetrachloride
CCN	Cysteine-rich angiogenic protein
CFTR	Cystic fibrosis
CHB	1-cyano-2-hydroxy-3-butene
CK	Cytokeratin
CO_2	Carbon dioxide
COPD	Chronic obstructive pulmonary disease
COX	Cyclooxygenase
CPC	Chromosomal passenger complex
CTGF/CCN2	Connective tissue growth factor
CTRC	Chymotrypsinogen C
Cre-LoxP	Cre-recombinase protein/locus of x over P1
DAB	Diaminobenzidine tetrahydrochloride solution
DIABLO	Direct IAP binding protein with low p1
ECM	Extracellular matrix
EDTA	Ethylenediaminetetraacetic acid
EM	Electron microscopy

ERK	Extracellular-signal-regulated kinase
FFPE	Formalin-fixed paraffin-embedded
FGF	Fibroblast growth factor
GFAP	Glial fibrillary protein
GFP	Green fluorescent protein
HSC	Hepatic stellate cells
H&E	Haematoxylin and eosin
HRP	Horseradish peroxidase
IAP	Inhibitor of apoptosis protein
ICAM1	Intercellular adhesion molecule1
IGF	Insulin growth factor
IHC	Immunohistochemistry
IL	Interleukin
JAK-STAT	Janus kinase/signal transducers and activators of transcription
JNK	c-Jun N-terminal kinase
MAPK	Mitogen-activated protein kinase
MF	Myofibroblasts
MLKL	Mixed lineage kinase domain
MMPs	Matrix metalloproteinases
NF-κB	Nuclear factor kappa-light-chain-enhancer of activated B cells
NR5a2	Nuclear receptor 5a2
OCT	Optimal cutting temperature
P13K	Phosphatidylinositol 3-kinase
PAF	Platelet activating factor
PAS	Periodic acid Schiff
PBS	Phosphate buffered saline
PCNA	Proliferating cell nuclear antigen
PDGF	Platelet-derived growth factor
PDL2	Programmed cell death 1 ligand
PDX1	Pancreatic and duodenal homeobopx1
PERK	Protein kinase R-like endoplasmic reticulum kinase knockout

PTFA	Pancreas specific transcription factor
PDGF	Platelet-derived growth factor
PPAR-γ	Peroxisome proliferator-activated receptor gamma
PRSS11	Periostin, serine protease 11
PSC	Pancreatic stellate cell
Relma	Resistin-like molecule alpha
RER	Rough endoplasmic reticulum
RIP	Receptor-interacting protein kinases
RNA	Ribonucleic acid
ROS	Reactive oxygen species
R-Smad	Regulatory mothers against decapentaplegic homologues
SEM	standard error of the mean
SCF	Stem cell factor
SMAC	Second mitochondria-derived activator of caspases
SMAD	*Caenorhabditis elegans* protein SMA. *Drosophila* protein mothers against decapentaplegic homologues (MAD)
SPARC	Secreted protein acidic and rich in cysteine
SPINK	Serine protease inhibitor kazal type 1
STAT	Signal transducer and activator of transcription
TBS	Tris buffered saline
TGF	Transforming growth factor
TIMPs	Tissue inhibitors of matrix metalloproteinases
TNF	Tumor necrosis factor
TRAIL	Tumor necrosis factor related apoptosis inducing ligand
VCAM1	Vascular cell adhesion protein 1
VEGF	Vascular endothelial growth factor
WBN/KOB	Wistar Bonn/Kobori rats
Wnt	Wingless-type MMTV integration site
ZG	Zymogen granules

CHAPTER ONE
LITERATURE REVIEW

1.1 INTRODUCTION

Pancreatitis is a term that describes inflammation of the pancreas. More broadly, the term designates a group of diseases in which the basic lesions involve injury and death of acinar cells and inflammation of the pancreas. A spectrum of clinical pictures occurs with variety in the severity, duration and outcome of the disease. Due to the complexity of the disease, treatment is considered in terms of etiology and prognosis and remains largely supportive, with management to relieve symptoms and prevent further disease progression. Pancreatitis causes a significant burden on medical resources, and patients with chronic pancreatitis have reduced quality of life with substantially reduced employment and income.[1]

The worldwide incidence of acute pancreatitis ranges from 4.9 to 73.4 per 100,000 people per year with the risk of recurrence in the vicinity of 20%.[2] The incidence of chronic pancreatitis ranges from 4 to 14 per 100,000 per year. Approximately 35% of patients with at least one recurrence of acute pancreatitis risk progression to chronic pancreatitis, with the mortality rate of chronic pancreatitis at approximately 28-35%.[3]

Historically, pancreatitis has been divided into acute and chronic types. Acute pancreatitis is associated with elevated pancreatic enzymes in blood and urine due to inflammation and systemic responses of varying severity.[4] Mild interstitial or oedematous pancreatitis with acute inflammation and oedema generally resolves to normal morphology and function, however, the often fatal, severe, form of acute pancreatitis is haemorrhagic with necrosis and abscess, leading to the complete destruction of the gland, systemic complications and organ failure.[5] Chronic pancreatitis is an inflammatory disease, with the end result irreversible fibrotic destruction of the gland with impairment of exocrine and endocrine function.[1] The current view is that recurrent attacks of acute and chronic pancreatitis may represent a disease continuum due to repeated tissue destruction and subsequent remodelling.[6] Several classification systems have attempted to include etiology as an important criterion for the characterization of pancreatitis, particularly chronic pancreatitis.[7] These classification proposals attempted to include all relevant features of the disease: clinical presentation, outcome, pathology, and etiology. Currently, chronic pancreatitis is usually diagnosed when the

disease is already fully established with uncertain pathogenesis, unpredictable clinical course and unclear treatment, hence life expectancy is reduced.[8]

There is no reliable molecule, genetic biomarker or imaging system currently available for predicting the severity of acute pancreatitis.[9] These diagnostic aids would improve the ability to treat the early manifestation of the disease to prevent morbidity and mortality, as the early systemic inflammatory response has already occurred by the time patients present for treatment.[9] The models presented in this thesis allow pre-clinical analysis of etiology, outcome and pathology. In some experimental models of acute pancreatitis, acinar cells die by apoptosis. Without severe inflammation, the pancreas is able to regenerate and recover. In other models, no recovery takes place and the gland becomes fibrotic with loss of exocrine function. Although experimental studies do not completely mimic the human clinical situation, it is possible that a similar scenario is occurring in the human condition. It appears that the mode of cell death, apoptosis or necrosis, is important to the outcome, as is the production and resolution of fibrosis with accompanying interaction of inflammatory mediators. As evidence-based treatment options are limited, further exploration of the biomarkers and mechanisms involved in regeneration of exocrine pancreatic tissue is required to answer the question of how to prevent recurrence and progression of this disease. To do this, various animal models may be utilised.

Current treatment regimens have improved considerably over recent years with advances in intensive care medicine and pain relief, however, treatment is mainly symptom alleviation. In mild, acute pancreatitis, treatment is based on hydration and nutrition with laparoscopic cholecystectomy for biliary pancreatitis. Aggressive intravenous fluid, enteral feeding and intensive care monitoring are required for severe acute pancreatitis.[9, 10] For chronic pancreatitis, treatment is for maldigestion, and nutritional deficiencies resulting from exocrine insufficiency. Diabetes therapy is required for endocrine deficiencies. Complications such as obstruction of the pancreatic duct, gastric outlet and vessels, common in chronic pancreatitis, are treated with endoscopy and surgery.[1, 3] There is no current treatment for the fibrosis that causes the pathophysiology of chronic pancreatitis.

Chronic pancreatitis is considered a risk factor for pancreatic cancer.[6] The cancer is usually at an advanced stage at diagnosis, and it is rare to have complete resection of the tumour, and conventional cancer therapies such as radiation and chemotherapy have limited results with significant side effects.[11] 1-Cyano-2-hydroxy-3-butene (CHB) may represent a potential treatment for pancreatitis and acinar cell carcinoma of the pancreas as it may eliminate all or virtually all acinar cells and malignant cells derived from them. It is unknown whether the effect of CHB on the pancreas occurs in representative members of other species and whether this can be achieved safely.

This project aimed to improve descriptions of mechanisms and processes of acute and chronic pancreatitis. It used several pre-clinical animal models to complete this aim.

1.2 ANATOMY AND HISTOLOGY OF THE NORMAL PANCREAS

The human pancreas is an elongate, firm, gastrointestinal gland lying in the upper abdomen behind the stomach. It divides into the head near the duodenum, body, and tail approaching the hilum of the spleen (Figure 1.1). The pancreas is covered by a loose, thin connective tissue capsule which extends inwards as septa dividing the parenchyma into distinct lobules. The gland performs both exocrine and endocrine functions. The human exocrine portion forms the greatest volume (84%), ductular cells and blood vessels about 4 % of the gland, while endocrine cells comprise only 2%, and the remainder occupied by extracellular matrix. The exocrine pancreas is a branched, acinar gland responsible for secreting digestive enzymes into the intestine: the endocrine tissue, organized into islets of Langerhans, secretes hormones involved in stabilization of blood glucose homeostasis. In the human pancreas, the splenic artery provides the blood supply to the neck, body and tail, the superior and inferior pancreaticoduodenal arteries supply the head.[12] Most of the arteries are accompanied by veins that run into the splenic vein and by the pancreaticoduodenal veins into the portal and mesenteric veins.[13] Lymphatics from the pancreas follow the course of the arteries. The pancreas is richly innervated both by parasympathetic (cholinergic) fibres from the vagus nerve and by sympathetic fibres arising from the celiac, superior mesenteric and hepatic plexis.[14]

Pancreatic juice secretion is stimulated by parasympathetic activity and inhibited by sympathetic activity.[15] Rodent autonomic nerve distribution is homologous with human distribution, however innervation of exocrine tissue is poor in comparison to the rich innervation in humans.[15] Generally, the blood supply, lymphatics and nerves accompany the duct system to its terminus in the acini. The pancreas drains via a large pancreatic duct that penetrates the wall of the duodenum in association with the common bile duct. In the rat, the pancreas and biliary tract share a common conduit into the duodenum that results in the passage of bile into the proximal portion of the pancreatic duct prior to drainage into the duodenal lumen.[16]

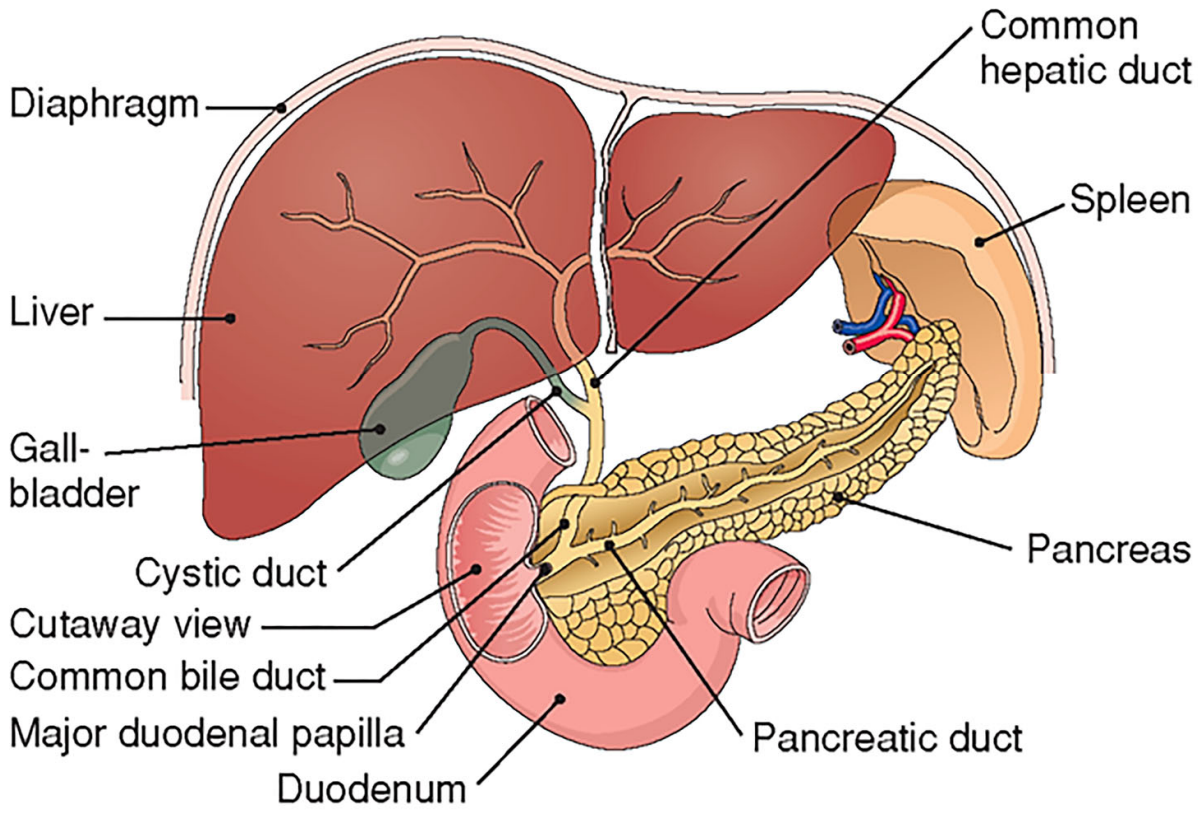

Figure 1.1 The pancreas as an accessory organ to the intestine

The human pancreas is an elongate, firm, gastrointestinal gland lying in the upper abdomen behind the stomach. It divides into the head near the duodenum, body, and tail approaching the hilum of the spleen.

Accessory organs of the digestive system. Physiology Plus 2017 [278]
http://physiologyplus.com/accessory-organs-of-the-digestive-system-and-their-functions/

There is interspecies variability in the proportion and distribution of endocrine tissue.[15, 17] The pancreas in rodents is soft and diffuse within the mesentery loosely attached to the stomach, duodenum and spleen and often described as gastric, duodenal, and splenic lobes.[15, 17] Adipose, connective and lymphatic tissues are dispersed in the rodent lobes.[15] The dog pancreas is solid, caudal to the liver and divided into three lobes, right, body and left, which form a reasonable V-shape.[17] Dog and rodent pancreatic blood supply is generally homologous to the human system.[15]

1.2.1 Light and electron microscopy

The exocrine pancreas is a complex anastomosing tubular network. The main functional unit is the acinus, comprised of approximately 50 cells bordering a common luminal space that with a few centroacinar cells forms the beginning of the duct system. In haematoxylin and eosin (H&E) sections, the closely packed acini appear as rounded units bounded by nuclei. Individual cells cannot be discerned. The endocrine Islets of Langerhans and ducts are randomly distributed (**Figure 1.2**). Cells appear pyramidal shaped with numerous darkly eosinophilic spherical zymogen granules situated in the apical cytoplasm. The basal cytoplasm is basophilic due to the high content of RNA in rough endoplasmic reticulum (RER) and the rounded nucleus eccentric towards the base. Nuclei contain one to two nucleoli (**EM in Figure 1.3**). The Golgi apparatus at the junction of the apical and basal poles appears as a paler zone. A basal lamina surrounds each acinus and the acinar unit is buttressed by a thin extracellular connective tissue matrix that contains numerous blood capillaries, nerves and connective tissue. The acinar cell height, granule content and the relative volume of the cell occupied by RER and zymogen granules vary with the stage of protein synthesis and secretion and this affects staining features. RER increases during synthesis, then, as zymogen granules increase, they occupy a greater proportion of the cell and RER is decreased.[18-20.]

Centroacinar cells constitute the beginning of the duct system continuous with the intercalated ducts that interpose between the acini and the intralobular ducts. The irregularly shaped centroacinar cells invaginate partly into the acinus, remaining in contact with the lumen that is not always obvious in light microscopy.[21, 22] Centroacinar cells are distinguished from acinar cells by a more irregularly shaped nucleus, less RER, no secretory granules and therefore paler cytoplasm. The intercalated and intralobular ducts have low cuboidal epithelium supported by a thin coat of connective tissue. The lumens of the ducts may contain homogeneous eosinophilic pancreatic proteinaceous secretion. Intralobular ducts comprise the largest percentage of all duct cells in the rat.[21] In the septa outside pancreatic lobules, the larger interlobular ducts are lined by cuboidal to columnar epithelium with

occasional goblet cells and are surrounded by a thick layer of connective tissue. Periacinar and periductular interstitial cells are predominately fibroblasts and macrophages.[23]

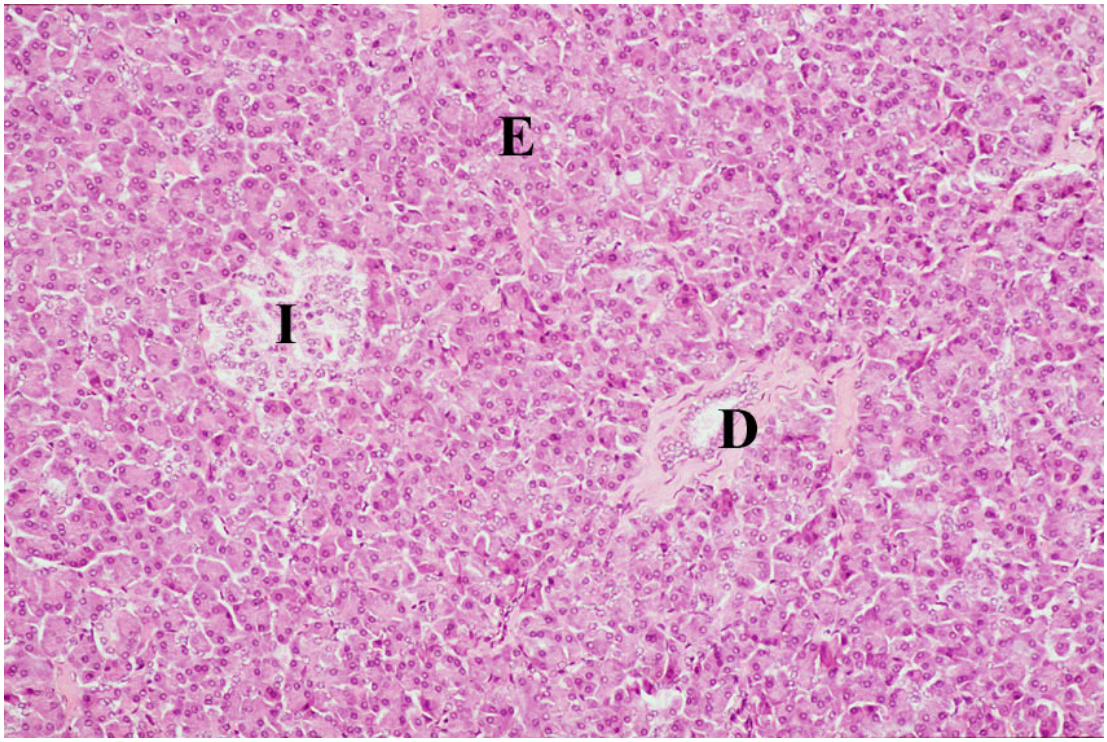

Figure 1.2 Histology of pancreas

The pancreas is made up of the exocrine segment (E) consisting of acini and randomly spaced ducts (D). The endocrine portion of the pancreas consists of the Islets of Langerhans (I). (Original magnification x400; haematoxylin and eosin stain).

The endocrine Islets of Langerhans, with a range of size of 50-250 μm, are mostly spherical in shape and dispersed throughout the lobules. They comprise approximately 1-2% of the pancreas in most mammalian species.[24] In rodent islets, the location of glucagon secreting α-cells is on the periphery of the islet with the insulin secreting β-cells mainly in the middle, whereas in human islets α-cells appear mixed with β-cells within the islets. The smaller α-cells can be seen with a trained eye in rodent islets with H&E staining but are particularly prominent with immunohistochemical (IHC) staining.[24] The distribution of organelles seen by electron microscopy (EM) in the acinar cell is highly polarised. Using EM to describe the ultrastructure of the pancreas, the nucleus has dispersed chromatin and the nucleoli are prominent (Figure 1.3). The basal pole of the cell is packed with abundant lamellar arrays of RER with ribosomes studded to the cytosolic surface of the membrane or occasionally free between the cisternae. The RER occupies approximately 20% of the cytoplasm and its membranes account for approximately 60% of the surface area of the cell's membranes.[18] The cytoplasm contains numerous mitochondria. Supranuclearly is a prominent Golgi apparatus with parallel arrays of stacked cisternae, many small vesicles, condensing vacuoles filled with low-density flocculent material, microtubules and microfilaments.[18, 25] Apical zymogen granules have a single limiting membrane; when well preserved their matrix has a high-density homogeneous electron opaque content, in pathological conditions or in immature granules the matrix may vary to pale staining with a dense irregular core. They vary in size from about 0.5-1.4 μm.[24]

Acinar lumina are approximately 1-3 μm in diameter and contain varying amounts of electron dense material.[25] The luminal end of the acinar cell has a few microvilli coated with a thin layer of fine filamentous material. The acinar basal plasma membrane is about 60 Å thick inside an amorphous basement membrane (BM) of 150-400 Å with associated collagen fibres.[25] The plasma membranes of adjacent cells fuse into well-developed zonulae occlendentes that seal the apical zone from access to digestive enzymes following exocytosis of zymogen granules. The relatively straight lateral cell membranes are separated by a narrow space joined by occasional desmosomes and adhering zonules.[18, 26] The acinar cell may also contain some dense, membrane-limited lysosomal bodies and multi-vesicular bodies. Connective tissue with capillaries and autonomic nerve fibres occupy the small spaces between the acini.[27]

Centroacinar, intercalated and intralobular duct cells similarly have little ER, a modest Golgi apparatus, ribosomes are free in the cytoplasm and mitochondria are few and smaller than those of the acinar cell.[28] A less extensive Golgi apparatus is found usually at the apical aspect of the nucleus.[25] The cytoplasm of duct cells contains considerable amounts of delicate fibrils but appears empty in contrast to acinar cells. The nucleus is large, mostly oval with marginal indentations. At least some

cells in each category of pancreatic duct possess cilia that project into the luminal space from a basal body in the supranuclear region.[21] The non-motile cilia have nine peripheral doublets but no central microtubules.[21, 29] Blebs are found on the surface of intralobular cells[25] but only occasionally on intercalated or centroacinar cells.[25] Intralobular duct cells have elaborate interdigitations at the lateral and basal plasma membranes.[28] Close packed and long microvilli border the surface of cells lining interlobular and main ducts. These cells contain mucin granules, have a more developed RER and some goblet cells.[21] The surface of duct cells secrete a coat of sialoglycoprotein that acts as a barrier to bicarbonate ions or pancreatic enzymes.[30]

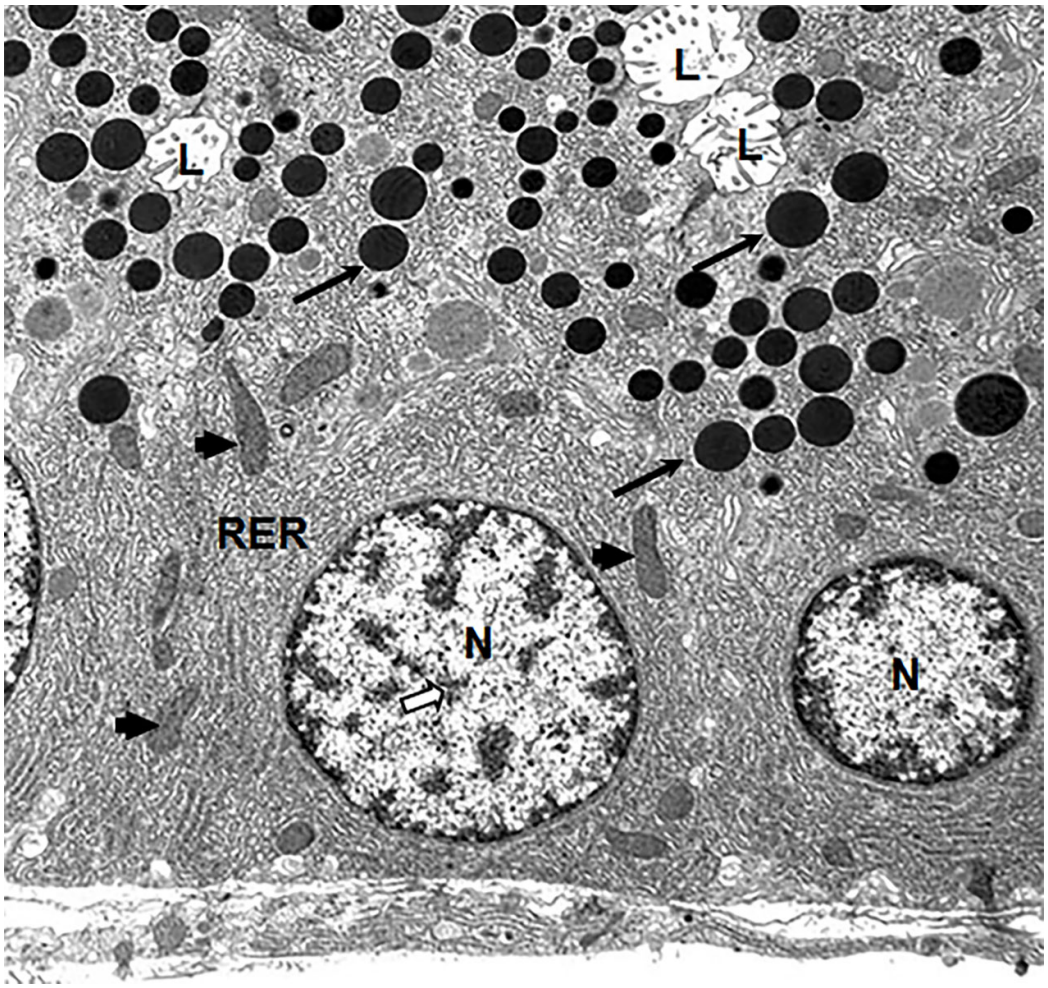

Figure 1.3 Electron microscopy of acinar cell of normal pancreas

The nucleus has dispersed chromatin (N=nucleus, open arrow=chromatin). The normally prominent nucleoli are not visible in this image. . There are abundant lamellar arrays of rough endoplasmic reticulum (RER) basally. The cytoplasm contains numerous mitochondria (short black arrows). Apical zymogen granules have a high-density homogeneous electron-opaque content (long black arrows). L= lumen.

The EM of fibroblasts and stellate cells has been well described. Fibroblasts have a spindle shape, an often elongated thin nucleus, long cytoplasmic extensions and lack of lipid droplets. In comparison, pancreatic stellate cells have a large triangular nucleus, more cytoplasm, prominent RER active in protein synthesis, abundant ribosomes, few mitochondria, and long cytoplasmic projections. Dilated cisternae of the RER may contain flocculent material. The cell surface has caveolae and closely aligned collagen fibres.

In the islets of Langerhans, the alpha cell secretory granules are round to ovoid with an eccentric core of high electron density separated from a limiting membrane by a halo of medium dense granular material. The more numerous beta cell secretory granules have an electron dense core surrounded by empty space. Dog and human granules have a dense core with bar like appearance. Delta cells have a similar distribution to alpha cells. Their secretory granules are larger, less dense than alpha granules and more uniform than beta granules.[31]

1.3 PANCREATITIS

Acute pancreatitis, chronic pancreatitis and pancreatic cancer account for the burden of exocrine pancreatic disease with high morbidity and mortality in severe cases.[1, 32, 33] More broadly, the term pancreatitis designates the group of diseases in which the basic lesions are injury of acinar cells and inflammation of the pancreas with a spectrum of pathologies displaying variety in the severity, duration and outcome.[34] Due to the complexity of the disease, treatment is considered in terms of etiology and prognosis and remains largely supportive with management to relieve symptoms and prevent further disease progression. Pancreatitis causes a significant burden on medical resources, and patients with chronic pancreatitis have reduced quality of life with substantially reduced employment and income.[1]

The worldwide incidence of acute pancreatitis ranges from 4.9 to 73.4 per 100,000 people per year with the risk of recurrence approximately 20%.[2] The prevalence of chronic pancreatitis ranges from 4 to 14 per 100,000 per year with mortality at approximately 28-35%.[3] Alcohol and gallstones make up the majority (80%) of all causes of pancreatitis and the overall risk of recurrence, 50% in alcoholic and 32-61% in gallstone pancreatitis.[35, 36] A retrospective study of patients with a first episode of acute pancreatitis of various causes showed recurrence in 17% of patients with 8% progressing to chronic disease within 5 years.[37] The risk was higher with smokers who abused alcohol. Generally, the causes of pancreatitis include obstructive (biliary and duct), toxic -metabolic (alcohol, tobacco, hypercalcaemia), vascular, trauma, autoimmune disorders, infectious, idiopathic, genetic

predispositions (cystic fibrosis). Hereditary and tropical pancreatitis are rare manifestations.[38, 39] Some examples of causes of pancreatitis are presented in **Table 1.1**. Patients with these rare types of pancreatitis pose an approximately 50 fold greater risk than the general population of developing pancreatic cancer however the risk for all chronic pancreatitis patients is approximately 5%.[38]

Table 1.1. Causes of Pancreatitis

Alcoholism
Gallstones
Abdominal surgery/haemorrhage
Certain drugs/medications
Cigarette smoking
Cystic fibrosis
Family history of pancreatitis
High calcium levels in the blood (hypercalcemia), which may be caused by an overactive parathyroid gland (hyperparathyroidism)
High triglyceride levels in the blood (hypertriglyceridemia)
Infection
Injury to the abdomen/haemorrhage
Pancreatic cancer

Adapted from Kleefe, J., *et al* (2017). Talukda P., Vege S., (2015)

Current treatment regimens have improved considerably over recent years with advances in intensive care medicine and pain relief, however, treatment is mainly symptom alleviation. In mild, acute pancreatitis, treatment is based on hydration and nutrition with laparoscopic cholecystectomy for biliary pancreatitis. Aggressive intravenous fluid, enteral feeding and intensive care monitoring are required for severe acute pancreatitis.[9, 10] For chronic pancreatitis, treatment is for maldigestion, and nutritional deficiencies resulting from exocrine insufficiency. Diabetes therapy is required for endocrine deficiencies. Complications such as obstruction of the duct, gastric outlet and vessels, common in chronic pancreatitis, are treated with endoscopy and surgery.[1, 3] There is no current treatment for the fibrosis that causes the pathophysiology of chronic pancreatitis.

Diagnosis of pancreatitis is made primarily on the basis of abdominal pain, serum amylase/lipase levels and abdominal imaging.[32, 40] Scoring systems to predict severity have high false positive rates

and individual assessment of patients is critical for recognition of the inflammatory response and local complications.[40] Diagnosing chronic pancreatitis is challenging as it can be easily confused with recurrent attacks of acute pancreatitis or features of other disorders, biopsy and direct visualisation are difficult and symptoms can be subtle and vague.[1, 38] There is no reliable molecule, genetic biomarker or imaging system currently available for predicting the severity of acute pancreatitis.[9] These diagnostic aids would improve the ability to treat the early manifestation of the disease to prevent morbidity and mortality as the early systemic inflammatory response has already occurred by the time patients present for treatment.[9]

Chronic pancreatitis is usually diagnosed when the disease is already fully established as the pancreas has a considerable functional reserve such that the symptoms of pancreatic insufficiency are not clinically recognised until most tissue destruction has occurred. Uncertain pathogenesis, unpredictable clinical course and unclear treatment result, so life expectancy is reduced.[8] There is no current treatment for the fibrosis that causes the pathophysiology of chronic pancreatitis as well as the lack of specific laboratory parameters for non-specific clinical symptoms.[3]

The classification of acute and chronic pancreatitis is multifaceted and has changed often due to the diverse aetiologies, symptoms, morphological patterns, the stage (early/late) and complications. Determinant-based classification (PANCREA) 2012[41] and Atlanta classification[42] for acute pancreatitis; and the M-ANNHEIM classification [43] and S3 Guideline for chronic pancreatitis are recent classification systems that introduce unifying concepts to pancreatitis.[3]

1.3.1 Acute pancreatitis

Acute pancreatitis is associated with elevated pancreatic enzymes in blood and urine due to inflammation and systemic responses of varying severity.[4] Mild interstitial or oedematous pancreatitis with acute inflammation and oedema generally resolves to normal morphology and function , however, the often fatal, severe form of acute pancreatitis is haemorrhagic with necrosis and abscess, leading to the complete destruction of the gland, systemic complications and organ failure.[5]

1.3.2 Chronic pancreatitis

Chronic pancreatitis is a fibro-inflammatory disease, the end result being irreversible destruction of the gland with impairment of exocrine and endocrine function.[1] The current view is that recurrent attacks of acute pancreatitis and chronic pancreatitis may represent a disease continuum due to

repeated tissue destruction and subsequent remodelling.[6] Chronic pancreatitis is irreversible once established but progression and symptoms can be modified by clinical intervention.[1] Chronic pancreatitis is considered a risk factor for pancreatic cancer.[6] The cancer is usually at an advanced stage at diagnosis, and it is rare to have complete resection of the tumour, and conventional cancer therapies such as radiation and chemotherapy have limited results with significant side effects.[11]

1.3.3 Cell death and its role in pancreatitis

Cell death is critical for tissue sculpting in development, in immunity and destruction of damaged cells. Best researched are necrosis, or accidental cell death, and apoptosis, or programmed cell death or cell suicide. Recently it has been suggested that there is cross talk between these forms of cell death, with necroptosis and pyroptosis utilising mechanisms distinct from necrosis and apoptosis to activate cell death.

Apoptosis, named by Kerr et al (1972), is an evolutionarily conserved innate process of regulated cell death executed to dispose of cell contents in a conservative manner. It is intentional cell suicide based on genetic mechanisms and activated in normal development and morphogenesis as well as in cellular injury and stress.[44] Apoptosis is regulated by extrinsic stimuli such as cell surface death receptors, tumour necrosis factor (TNF)α, Fas and TNF related apoptosis inducing ligand (TRAIL) leading to the activation of caspase-8, or by intrinsic stimuli via the mitochondrial signalling pathway through cytochrome c and Smac/Diablo that activate caspase-9.[45] Activated caspase-8 and -9 cleave and activate further caspases to result in apoptosis. The morphology of apoptosis is distinct. The nuclear chromatin becomes condensed and often marginated against the nuclear envelope, simultaneously with convolution of the nuclear outline. These sharply-defined chromatin masses often appear as crescent shaped. The cytoplasm condenses, microvilli disappear and protruberances, or blebs, appear on the cell surface. Cell attachments fail and cells separate from their neighbours. Cytoplasmic condensing causes crowding of organelles, ER rearranges into circumscribed whorls or circular profiles. Cell fragmentation occurs as the nucleus breaks into discrete fragments and the blebs on the cell surface separate with membrane sealing to form membrane bound apoptotic bodies of varying size and composition. Apoptotic bodies usually are rapidly phagocytosed by macrophages and adjacent epithelial cells or occasionally extruded into intercellular spaces or the pancreatic lumen. Most estimates are that apoptotic cells are recognized, ingested and degraded within approximately 1-2 hrs.[46]

Necrosis is regarded as an un-programmed cell death lacking signalling cascades, initiated by noxious or physical insult or lack of blood supply. Morphologically, the cytoplasm swells (oncosis) and nuclear chromatin clumps. Mitochondria swell with the appearance of densities in their matrix. The irregularly clumped nuclei become dispersed (karyorrhexis) leaving ghost like nuclei (karyolysis). Nuclear, organelle and plasma membranes rupture with dissolution of lysosomes and ribosomes. Cell boundaries become indistinct with blebbing and the cell contents leak into the intercellular space leading to an inflammatory response. Tissue architecture is lost and tissue appears eosinophilic. Cellular debris is ingested by macrophages.

Necroptosis resembles necrosis morphologically however it is a programmed form of necrosis driven by defined molecular pathways. It is induced by death receptors including TNF, Fas (under conditions of caspase inhibition), and involves activation of the receptor-interacting protein kinases/mixed lineage kinase domain (RIP1/ RIP3/ MLKL) pathway and other signalling pathways.[47] ROS, rapid depletion of ATP and mitochondrial dysfunction are also key events. Mice lacking RIP3/MLKL are protected from pancreatitis in an induced model.[48] Pyroptosis is a form of programmed cell death that depends on the action of caspase-1 therefore differs from apoptosis biochemically. Morphologically, pyroptosis is associated with cell swelling, plasma membrane lysis, nuclear fragmentation and lack of mitochondrial permeabilisation. It is suggested that pyroptosis functions to control infection or for release of inflammatory cytokines.[49]

1.3.4 Regeneration

Progenitor cell activity is active prenatally in the pancreas, however after birth, pancreatic cells do not regenerate continuously and lineage crossover is rare. It is possible to alter the growth of the pancreas by various types of experimental intervention, for example, with cholecystokinin (CCK) and after pancreatic resection.[50, 51] Mild pancreatitis in human and animal models appears to resolve through regeneration of acinar cells. Chronic pancreatitis endures with persistent inflammation, fibrosis and tubular complexes. Multiple mechanisms participate in regeneration including inflammation, metaplasia and differentiation. As well as acinar cells, cellular constituents contributing to repair are duct cells, inflammatory cells, and stellate cells. Fibrosis and the cellular interactions within the fibrotic milieu appears important in the regeneration process but is not well characterised.

In experimental regeneration conditions, acinar cells depleted by cell death are replaced by tubular complexes composed of cells positive for ductal markers that then appear to regenerate into acinar

cells. Whether this acinar cell regeneration is due to population expansion or acinar-to-ductal transdifferentiation and duct-to-acinar dedifferentiation has been debated passionately in the literature.[52] Recent knockout and genetic studies in mice, in particular the Cre-LoxP lineage tracing technique that links transcription factors to cell fate decisions have begun to unravel the molecular basis of regeneration.[53] Lineage tracing studies have determined to date that there are no stem cells in the exocrine pancreas although this issue is still under investigation.

Tamoxifen induced lineage tracing experiments show that when acinar cells are deleted and conditions support regeneration they are replaced by expansion of surviving acinar cells and not by progenitor cells. These acinar cells appear to retain lineage commitment as they do not differentiate into duct or endocrine cells.[54, 55] In these experiments residual acinar cells remain after injury. When acinar cells are erased completely, in a diphtheria toxin induced model, duct to acinar transdifferentiation appears to be the method of acinar renewal.[56] Furthermore, experimental models of regeneration from pancreatitis that have focused on the endocrine compartment have revealed a plasticity within acinar cells.[52] As well, recent evidence from experiments with genetically engineered mice suggests that acinar cells become duct-like through acinar-to-ductal metaplasia and are the source of pancreatic cancer. Acinar cells express the differentiation factors PTF1A, Mist1 and Nr5a2. Loss of PTF1A from acinar cells causes acinar-to-ductal metaplasia.[57] Under the influence of oncogenic KRAS, acinar-to-ductal metaplasia leads to the formation of precancerous lesions and thence to cancer. Mist1 and Nr5a2 normally expressed in acinar cells protect from transformation but equally, ductal fate controllers Sox9 and Pdx1 drive acinar cells toward a ductal state that may increase cancer cell growth.[58, 59] Exocrine regeneration is dependent on cell-to-cell interactions through disrupted gap junctions and ductal defects.[53]

Fibrosis is a common feature of failure to regenerate in pancreatitis. The persistence or withdrawal of pancreatic stellate cells affects regeneration, their role is uncertain and Cre lines for adult PSCs have not yet been developed. Macrophages and other immune cells such as dendritic cells, also persist in fibrotic pancreatitis. Their contribution to limiting or driving inflammation associated with injury resolution requires further investigation. Inflammatory signalling pathways associated in regeneration from pancreatitis are principally the nuclear factor-κB (NF-κB) and Janus activated kinase (JAK)-Signal transducer and activator of transcription (STAT) pathways implicated in inflammation, PSC recruitment and dedifferentiation, however findings to date are conflicting. As well, signals from factors expressed in embryonic development such as the Notch and Wnt signalling pathways, Pdx1 transcription factor, Hedgehog, Hippo and Wnt/β-catenin pathways may have regenerative roles

promoting acinar redifferentiation and proliferation. Communication between the fibrotic process, inflammation and developmental mechanisms may determine the outcome of regeneration.

1.4 PANCREATIC FIBROSIS AND INFLAMMATION

Progressive fibrosis is a characteristic feature of chronic pancreatitis of various etiologies. The cellular and molecular mechanisms leading to pancreatic fibrosis remain poorly understood.

1.4.1 Extracellular matrix

The extracellular matrix (ECM), the organic matter found between cells, is a framework that acts as a structural scaffold for the cellular components and determines cell function through cell-matrix biochemical and biomechanical interactions. It is indispensable in embryonic development and tissue remodelling, the ECM molecules playing a role in adhesion, migration, proliferation, differentiation and homeostasis.[60] ECM is composed of multifunctional proteins grouped primarily into structural proteins (collagen, elastin), proteoglycans and glycosaminoglycans (hyaluronan, perlecan), glycoproteins (fibronectins, laminins), and matricellular proteins (thrombospondins, tenascin).[61] Collagen and elastin classify as fibre-forming molecules, proteoglycans and glycoproteins are interfibrillary whereas other molecules regulate cell-matrix interactions The ECM molecules are strictly organised such that genetic abnormalities in ECM proteins can produce an array of disorders. Disturbances in ECM occur in a variety of human diseases such as coronary heart disease, hypertension, asthma, chronic obstructive pulmonary disease (COPD), hepatic fibrosis, chronic pancreatitis, Crohn's disease and some cancers.[62]

1.4.2 Basement membrane

The BM is a dense sheet-like structure that underlies and separates epithelial cells from interstitial tissue or endothelial cells, surrounds muscle, fat and Schwann cells and acts as a permeability filter in kidney glomeruli.[63, 64] BM is a complex, highly cross-linked meshwork of proteins secreted in soluble state and then organised into insoluble cell frameworks.[65] The essential BM components include collagen type IV in one or more variants, along with the proteoglycans laminin, heparin sulfate, perlecan and entactin/nidogen;[63, 64, 66] and also non-essential components such as secreted protein acidic and rich in cysteine (SPARC) and the integrin ligand nephronectin.[65] Collagens XV and XVIII are found tethered to the BM and stromal interfaces as are growth factors of the TGFβ family, proteinases and their inhibitors, and regulatory molecules.[65] Together these mediate local and

distant signals with complex signalling cascades, and support and protect the physical interactions of cells and tissues.

Morphologically, three layers of BM can be distinguished by EM; the electron dense lamina densa is 20-300nm thick; the lamina lucida, at 10-50nm thick, is clear or not electron dense; the lamina rara interna is 10nm thick and is the basal portion. The lamina reticularis of 200-500nm borders the lamina rara interna. BM formation is a laminin/collagen self-assembly, multi-step process involving binding and adhesion at the cell surface and polymerisation.[64, 65] Through laminins, the BM anchors to integrin and dystroglycan receptors[65] and sulfatides, nidogen and perlecan feature in assembly with considerable heterogeneity, resulting in different structural and biological properties at different locations.[63, 67, 68]

1.4.3 Collagen

Collagen consists of a large family of approximately 28 different collagens encoded by 42 different collagen genes.[60] Most bind and interact with other ECM proteins to form supramolecular aggregates that are classified into fibrillary, fibril-associated, network-forming, membrane-anchoring, interconnecting and developmental collagens.[60] They localise differently in the BM and/or the interstitial matrix. [69] The composition of collagens changes with age and tissue type and mature fibres can consist of multiple fibril types.[70] The collagen protein is elastic with a resilience of 90% thus collagen fibrils show reversible deformity and their mechanical properties are dependent on a variety of cross-linking pathways.[60] Collagen type IV is produced mainly by endothelial and epithelial cells whereas types-I, -III and -V collagen are synthesised intracellularly in fibroblasts.[69]

The common collagen triple helix forms by three polypeptide α-chains incorporating a repeating sequence of glycine X-Y, after which the molecule is called procollagen.[71] The existence of several alpha chains and molecular isoforms increases the structural and functional diversity of the collagen family.[60] The molecule is stabilised by covalent bonding along the chain before the formation of fibrils, end-to-end linear growth and lateral growth. In fibroblasts, collagen formation begins with translation of the protein in the RER. Packaging occurs in the Golgi apparatus. Two models of fibrogenesis are proposed; transport through the cytoplasm from Golgi to membrane by means of specialised, elongated compartments containing 28nm fibrils followed by exocytosis into the extracellular space via caveolae or membrane protrusions, or extracellular fibril assembly through an enzymatic fusion process.[60, 72]

EM can be used to illustrate the morphology of collagen. Collagen fibrils form from groups of filaments that contain proto-filaments of 0.5-0.3nm. In electron micrographs, the fibrils that form an aggregate of filaments 20nm-2µm in diameter often appear hollow or negatively stained due to artefact. Mature collagen fibrils show a full-banded and distinctive cross-striated pattern because they pack in a staggered arrangement. Very slender or young fibrils show only vague periodic structure. Each period consists of a light-dark band and 10-13 fine dark cross striations within each period. In ultra-thin EM sections, the length of period is approximately 52-62nm. Collagen fibres, often called heterotypic because they consist of a collection of several collagen fibril types, are usually 1-10µm in diameter and are wavy fibres of variable length. Collagen I consists of five molecules of twisted microfibrils interdigitated with neighbouring fibrils.[60] Reticular fibres are very fine branching collagen fibrils of collagen III. They are Periodic Acid-Schiff reagent (PAS) positive and argyrophilic, having an affinity for silver as used in a common histochemical stain.

1.4.4 Laminins

Laminins are a family of large molecular weight glycoproteins found in the BM. They function as structural components essential for BM formation and integrity and embryonic morphogenesis and mediate cell adhesion, proliferation, differentiation, cell shape and migration.[64, 73] Laminins interact with cell surface receptors like heparins, integrins and dystoglycans to initiate intracellular signalling that regulates cellular organisation.[64, 74]

Laminins are heterotrimers assembled from three genetically-distinct, disulphide-linked polypeptide chain subunits, and each laminin is named according to its chain constituents.[74, 75] The chains fold into many combinations stabilized by disulphide bonding into either cross-shaped, Y-shaped or rod-shaped trimers. This shaping determines how the laminin trimers interact with each other and other BM proteins for example, in cross-shaped laminins, the short arms can bind to other laminin molecules forming sheets that initiate BM assembly; the long arm binds to cells in an anchoring manner.[76] Laminins self and co-polymerise in the matrix; structure and assembly are reviewed elsewhere.[63] In different tissue locations and in different cell types they show heterogeneity due to diversity of assembly of their chain domains and the variety of interactions mediated by different binding sites.[63, 77] This leads to the formation of ECM with a diversity of laminin arrangement and biological properties.[77]

1.4.5 Fibrosis

Fibrosis is the excessive accumulation of fibrillary, collagen-rich ECM occurring either in persistent tissue damage or in tissue repair. Following damage to tissue or organs through trauma or disease, fibrosis may aid the restoration of cell and ECM components beneficially. However, the prolonged presence of fibrosis detrimentally leads to dysfunction and chronic disease. In skin wound healing, during inflammation, a platelet plug forms followed by a fibrin matrix scaffold. Growth factors activate neutrophils, mast cells, macrophages and fibroblasts to infiltrate and populate the scaffold. These cells defend against microorganisms, clear debris, produce fibrosis and signalling factors.[78] New tissue formation follows keratinocyte migration over the injured site to restore a barrier of epithelium and angiogenesis occurs to replace the fibrin matrix with granulation tissue. The endothelial, mast and macrophage cells undergo apoptosis or exit the wound, leaving a mostly acellular protein and collagen matrix. Activated fibroblasts (myofibroblasts) form the fibrotic scar of mainly collagen III and use mechanistic contraction to remodel the injury. Over time, matrix metalloproteinases secreted by fibroblasts regulate collagen turnover from collagen III to collagen I, until skin integrity and homeostasis is maintained.[79]

Studies of fibrosis are well documented in liver and have provided the basis for fibrosis research in pancreas. Although there are similarities to fibrosis in the pancreas, the liver has a population of resident macrophages (Kupffer cells), hepatic stellate cells have more and larger lipid droplets, the relationship with vasculature is different and a liver stem cell (oval cell) has been identified.[80] In liver, the deposition of fibrosis by collagens I, III, IV and V is accompanied by change in immune cell composition, altered angiogenesis and architectural changes. The collagen is produced by activated hepatic stellate cells (HSC) located in the peri-sinusoidal space and myofibroblasts located in larger vessels, portal tract stroma and sinusoidal endothelial cells.[81] In the liver, resident macrophages (Kupffer cells) and macrophages recruited from monocytes along with bile duct epithelial cells, the hepatic progenitor stem cells (oval cells)[80] and activated fibroblasts secrete cytokines and other mediators to recruit and activate HSC and myofibroblasts.[82] The environmental stiffness of ECM in advanced fibrosis activates HSC and MF and promotes the survival of HSC.[80, 83] Kupffer cells recruit monocyte macrophages that infiltrate and produce TGFβ1, TNFα and interleukins 1β, 6 and 13, which are pro-inflammatory or pro-fibrotic. Oval cells produce TGFβ1, TGFβ2, PDGF and sonic hedgehog for HSC proliferation and activation: HSC maintain oval cell growth through production of survival factors.[80] In acute liver disease, removal of excess ECM by matrix metalloproteinases (MMPs) leads to resolution of the disease state. However, in protracted or subsequent bouts of injury excess ECM deposition dominates permitting MMP downregulation and upregulation of tissue inhibitors of MMPs

(TIMPs). Fibrosis models optimised for liver fibrosis reversal include in rats treated with carbon tetrachloride (CCL4) or alcohol and bile duct ligation[84] and in mice CCL4 or thioacetamide induced fibrosis.[85] Factors associated with inefficient fibrolysis in the liver include advanced vascular remodelling with architectural distortion, extensive cross-linking of ECM components hindering proteolytic removal, and the disappearance of cells that digest and degrade scar tissue.[85]

1.4.6 Fibrosis in the pancreas

Injury to the pancreas, whether necrosis, apoptosis, inflammation or obstruction, leads to production and deposition of ECM depending on the site of injury and the tissue compartment or cell types involved.[86-88] Fibrosis may replace the normal exocrine and endocrine cell populations leading to both exocrine and endocrine deficiency. Pancreatic fibrosis ranges from interlobular (for example, alcoholic chronic pancreatitis), periductal (hereditary pancreatitis) or periductal and lobular (autoimmune pancreatitis).[89] It is the common pathological feature in chronic pancreatitis and a major risk factor for pancreatic cancer. There is a direct role of fibrosis in cancer invasiveness [90], apoptosis associated with cancer[91] and through molecular interaction between PSCs and cancer cells controlling pro-tumorigenic properties.[92-94] Treatment for pancreatic fibrosis remains problematic.

In the pancreas, injury to acinar cells activates the cascade of events that leads to fibrosis. Activated acinar cells and recruited inflammatory cells, macrophages, neutrophils and eosinophils, platelets,[95] induce the release of pro-inflammatory cytokines such as interleukins (IL)-1,-6,-8,-18 to -33 and TNFα that activate pancreatic stellate cells.[34] Matrix accumulates through activated pancreatic stellate cells (PSCs) secreting the ECM under the production of a wide range of cytokines and molecular signalling pathways, for example TGFβ/Smad, mitogen-activated protein kinase (MAPK), Rho kinase, JAK/STAT and phosphoinositol-3-kinase (P13K) pathways.[34] Macrophages produce pro-fibrotic cytokines such as TGFβ, platelet-derived growth factor (PDGF), fibroblast growth factor-2 (FGF2) and insulin growth factor-1 (IGF1). PSCs also regulate the degradation of ECM by secreting MMPs and TIMPs such that the balance between resolution of fibrosis and progression to fibrotic chronic disease depends on a complex process with multifunctional modes of action.

Dynamic autocrine and paracrine signalling pathways accompany the development of fibrosis in the pancreas. TGFβ regulates activation of PSCs in an autocrine manner through Smad and ERK pathways.[96, 97] Transforming growth factor (TGF)α increases proliferation and migration of PSCs via upregulation of MMP-1.[98] TGFβ also regulates other signalling pathways including the MAPK pathway whose members extracellular signal regulated kinase (ERK), c-Jun N terminal kinase (JNK),

p38 induce collagen synthesis.[99-102] The Rho kinase family is linked to the invasive nature of pancreatic ductal carcinoma[103], PDGF induces the proliferation of PSC by activating the JAK-2/STAT-3 pathway.[101]

Models used to study pancreatic fibrosis include repeated injections of caerulein[104], duct ligation[105], toxins injected into the pancreatic duct (trinitrobenzene sulfonic acid or IV dibutyltin chloride,[106, 107] over-expression of TGFβ,[108, 109] the WBN/Kob spontaneous chronic pancreatitis rat,[110] and alcohol-induced pancreatitis in rats[111] and in mice.[112]

1.4.7 Resolution of fibrosis

Fibrosis resolution depends on elimination of the pathological stimulus, clearance of PSCs and their stimulants such as macrophages, degradation and clearance of ECM components and regeneration of tissue epithelium. Identification and studies of the intracellular signalling pathways are important for the development of anti-fibrotic therapy. Reported pancreatic anti-fibrotic approaches in animal models include antioxidants;[113-116] silencing of TGFβ[117-119]; inhibition of TNFα;[113] anti-inflammatory drugs;[120] troglitazone, the peroxisome proliferation-activated receptor-γ (PPAR-γ) agonist;[121] angiotensin receptor blocker;[122] and a mouse model with inducible c-Jun.[123]

The withdrawal of the etiological source of chronic injury, the disappearance of PSCs, the recruitment of macrophages and the prevalence of MMPs over their inhibitors TIMPs are necessary for the reversal of fibrosis.[84] MMPs, a family of 28 members, also called matrixins, are zinc-dependent endopeptidases active in the degradation of most components of ECM.[124-126] They are commonly classified into collagenases, gelatinases, stromelysins, matrilysins, membrane-bound and other MMPs. Originally studied for their role in the turnover of ECM by degradation of ECM proteins in wound repair and embryogenesis, they are now known to be active in pathological conditions such as rheumatoid arthritis, chronic obstructive pulmonary disease, myocardial infarction, cancer metastasis and neurological disorders.[124, 126]

Through modulation of cellular and signalling pathways, MMPs have a role in cell proliferation, migration, differentiation, apoptosis, angiogenesis, cancer invasion and metastasis and immunity.[125] They are distributed in connective tissue as well as some vascular tissues and cells.[125] Most MMPs are secreted as inactive proenzymes by multiple cells including fibroblasts, macrophages, neutrophils and lymphocytes however some are membrane anchored to the cell surface of cells or the mitochondria or nucleus.[124] The core structure of MMPs consists of amino acids in a pro-peptide, a

catalytic metalloproteinase domain, a linker peptide and a hemopexin domain.[125] Generally, MMP-1, -8, -13,-14 cleave collagens I, II, III; MMP-2 cleaves collagen I.[126] TIMPs are a small family of four proteins that regulate the activity of all MMPs. In normal tissues, the ratio of MMPs to TIMPs is 1:1 however this balance is disrupted under pathological conditions.[124] Because the ratio of MMP/TIMP mostly determines the extent of protein degradation, MMPs are proposed as therapeutic targets for several pathological disorders.[124-126] Transmembrane receptors, integrins, are involved in resolution of fibrosis through the finding that liver, lung and kidney fibrosis are attenuated in mice with a constitutive MF-specific knockout of the αv integrin chain.[127]

1.4.8 Pancreatic stellate cells

Activated PSCs produce most of the components of the ECM, increasing synthesis and secretion of ECM components including collagen types I and III, fibronectin, laminins, proteoglycans and hyaluronan.[128-130] Historically, the activation of fibroblasts and fibroblast-like cells was observed in acute and chronic pancreatitis in the rat caerulein-induced pancreatitis.[105, 131, 132] Walker et al. (1992) identified myofibroblasts and fibroblasts in fibrotic areas of duct ligation rats. The importance of fibroblast-like cells in the peri-acinar region of the pancreas for collagen synthesis and fibrosis was identified by several authors[133-135] Cultured rat peri-acinar fibroblastoid cells were identified as myofibroblast-like cells producing the ECM proteins collagen, fibronectin and laminin.[136] A similar observation was made in transgenic mice models by others.[137,138] Alpha smooth muscle actin (αSMA) positive myofibroblast-like cells were recognised around the acini, ducts and vessels of the human pancreas.[139] Further studies with isolated and cultured fibroblast/myofibroblast cells from normal rat pancreas[140] and from human chronic pancreatitis, and from rats treated and untreated with caerulein[129] noted the similarity of the myofibroblast-like cells to hepatic stellate cells (HSC) and changed the terminology to PSCs.

Stellate cells, in general, have a perivascular location and store retinoids, a feature shared with HSC.[141, 142] In normal pancreas, quiescent PSCs (or inactive fibroblasts) are in low numbers (approximately 4% of the cells), have limited proliferation, rounded cell bodies with long cytoplasmic processes, possess vitamin A containing fat droplets[129, 140] and are negative for α-smooth muscle actin (αSMA).[140] They have a periacinar and interlobular distribution[129, 140] however may be detectable in islets.[143] When isolated and cultured *in vitro*[129, 140] and when activated *in vivo* during both human and experimental fibrosis,[144] PSCs transform to a myofibroblast-like phenotype. They lose their vitamin-A containing lipid droplets, enlarge and proliferate, stain positive for the cytoskeletal marker protein αSMA and synthesise large amounts of ECM proteins.

Quiescent PSCs are believed to reside in the normal pancreas, however histological stains for their identification and comparison with resident fibroblasts are limited. For both PSC and HSC, vitamin A droplets in the cytoplasm provide a target for staining, however the lipid marker Oil Red O is reliable only with frozen sections as processing with solvents for formalin-fixed paraffin-embedded (FFPE) sections dissolves the lipid. Markers previously reported to be effective in quiescent HSCs or PSCs in rats and cell culture, glial fibrillary protein (GFAP), nestin, desmin and vimentin, are either not specific and/or are not positive in human PSCs.[129, 140, 144-147] Many markers for quiescent PSCs in normal human pancreas have been evaluated recently.[148] They identified the limitations of previously proposed markers and suggested cytoglobin and adipophilin as possible but not perfect replacements.

Activated PSCs migrate and phagocytose.[149, 150] Activated PSCs are thought to transform from quiescent PSCs residing in the pancreas[129, 140] however, in mice with caerulein-induced pancreatitis approximately 5% of the total population of PSCs were derived from bone marrow.[151, 152] The bone marrow derived cells contributed to both quiescent and activated PSC populations.[153] Phillips et al. (2003) reported an increase in the numbers of PSC in pancreatic injury resulting not only from PSC proliferation but also via migration from surrounding areas to injured tissue. This migration of cultured PSC was stimulated by platelet-derived growth factor (PDGF)[149] and the migration is dependent in part on cell proliferation.[154] In an animal model of spontaneous chronic pancreatitis and diabetes mellitus using the male WBN/KOB rat, Shimizu et al. (2005) found phagocytic cells in the periacinar region with the same characteristic features of PSCs, suggesting that PSCs might act as resident phagocytic cells during pancreatic injury.

PSCs produce MMPs and TIMPs to degrade collagen.[155] PSCs therefore play an important role in the balance between synthesis and degradation of ECM. Proteins expressed in activated PSCs are different to those in the quiescent state according to proteomic studies of mouse, rat and human PSCs.[156, 157] Chronic pancreatitis with fibrosis is a complication of alcoholism and ethanol metabolites along with oxidative stress may perpetuate activated PSC. PSC were activated by exposure to ethanol in culture[158] via the metabolism of ethanol to acetaldehyde accompanied by oxidant stress.[159] The antioxidant retinol supplements prevented alcohol-induced PSC activation.[160] The authors propose that retinoic acid in quiescent stellate cells is responsible for keeping the cells in an undifferentiated state.[160, 161]

1.4.9 Fibrosis and the transforming growth factor beta family

TGFβ is a multifunctional cytokine residing in the ECM and synthesized by macrophages, lymphocytes, fibroblasts and PSCs, epithelial cells, and platelets. It has roles in cellular and development pathways and tumour promotion or suppression and is linked to the tight control of apoptosis.[162, 163] In mammals, TGFβ occurs as three isoforms, TGF-β1, TGF-β2, and TGF-β3, with TGF-β1 the most abundant. Stimulated TGFβ dimers mediate signalling via serine/threonine kinase Type-I and Type-II receptors.[164] TGFβ can activate the MAPK signalling pathways ERK, JNK and p38 and mediate Smad-dependent or independent effects. Loss of function of the components of the TGFβ pathway results in aberrant organ development and physiological performance. The TGFβ family has a role in embryogenesis and may be necessary for normal development of acini. In the exocrine pancreas, acini express TGFβ1 whilst duct cells are reactive for all three isoforms.[165] Inactivating TGFβ in transgenic mice resulted in increased proliferation, defective acinar differentiation and fibrosis with macrophage infiltration, suggesting the necessity for TGFβ in normal exocrine function.[166] TGFβ appears to support both fibrosis and hyperglycaemia in chronic pancreatitis. In fibrosis, TGFβ regulates PSC activation and proliferation through Smad 2, Smad3 and ERK-dependent autocrine pathways.[97] PSCs actively secrete TGFβ1 and express TGFβ receptors I and II. Exogenous TGFβ1 increases collagen protein synthesis significantly.[167]

1.4.10 Fate of pancreatic stellate cells

Prolonged activation of PSCs results in progressive fibrosis. PSCs activate by autocrine pathways, thus they may achieve a perpetually-activated state when triggers, for example ethanol, have ceased.[168] PDGF, TGFβ1 and activin A, cytokines (IL-1, IL-6 and TRAIL), and the pro-inflammatory molecules (cyclo-oxygenase-2/COX-2) can perpetuate the activated phenotype.[169] Mechanisms to terminate PSC activation are required for fibrotic resolution and tissue regeneration. Several studies have found that PSCs may revert to quiescence, or undergo cell death or senescence. *In vitro* and *in vivo* immunity studies in mouse and rat models showed the necrotic cell death of PSCs after engulfing necrotic acinar cells and apoptotic neutrophils.[150] The fate of rat PSCs in culture and in a chronic pancreatitis model was determined by senescence.[170] PSCs isolated from rat pancreas were susceptible to CD95L and TRAIL-induced apoptosis in culture and, in a model of explant cultures of rat pancreatic tissues, some PSCs disappeared by apoptosis whilst some reverted to non-activated fibroblast phenotype.[171] Apoptotic PSCs were demonstrated in an ethanol-fed endotoxin model of chronic pancreatitis.[172] Exposure to retinoic acid may counteract PSC activation, or promote the PSC

quiescent phenotype or stage.[102, 173] In cell culture of PSCs, studies demonstrated that activin A induced the expression of anti-apoptotic Bcl-xL.[174]

1.4.11 Pancreatic inflammation

Inflammatory cells (particularly macrophages), platelets, injured acinar cells and pancreatic cancer cells secrete cytokines and growth factors to activate PSCs in a paracrine manner. This stimulates PSCs to produce factors that act through autocrine signalling to regulate and sustain PSC activation.[175] The multiple signalling pathways involved in PSC activation and functions are summarised.[175, 176] They include the p38 MAPK pathway involved in activation and proliferation of PSCs; PPAR-γ in maintenance of quiescence; ERK mainly in proliferation with JNK and JAK-STAT3; Rho/Rho kinase pathway for regulation of the actin cytoskeleton and contraction; NF-κB , ERK, JNK, p38 kinase and activator protein-1 (AP-1) for cytokine production; and P13K/Akt for controlling migration.

Members of the Smad family regulate activation, α-smooth muscle actin (αSMA) and COX-2 expression and VEGF production. STAT1 and Smads are involved in growth inhibition. Mediators for the signalling pathways include growth factors such as platelet-derived growth factor (PDGF);[128, 130] TGFβ1[177] and activin A;[178] basic FGF (bFGF);[129, 130] connective tissue growth factor (CTGF/CCN2);[179, 180] and cytokines such as IL-1 and -6;[181] IL-8 and TRAIL;[169] and TNFα.[130, 181] The vasoconstrictor, endothelin-1 is expressed by PSCs however they also contract and migrate in response to endothelin-1 expression.[101, 182] Overexpression of the integrin ligand, periostin, produced by PSCs, may contribute to tumour desmoplasia in pancreatic ductal adenocarcinoma.[183] Oxidative stress, ethanol and pressure also act to stimulate and perpetuate the activation of PSCs.[158, 184, 185]

1.4.11.1 Macrophages in pancreatitis

Macrophages are mononuclear phagocytes involved in mammalian development, trophic support and homeostasis of tissues and are major coordinators of both the initiation and resolution of inflammation after tissue injury. For simplicity and mechanistic cell culture studies, macrophages are divided primarily into classically activated M1 macrophages by secretion of pro-inflammatory cytokines TNFα, IL1β and IL6, and alternatively activated M2 macrophages treated with IL-4 and IL-13.[186] However, as macrophages appear to be highly plastic, other subsets, phenotypes and changed physiology are described that respond to changes in environmental signals.[187] Studies in cancer and obesity indicate that macrophage populations do undergo a phenotypic switch associated with time and pathology.[188] The pancreas contains an unknown proportion of resident self-sustaining macrophages, however they are known to reside in the peritoneal cavity near the pancreas and in the

peri-pancreatic tissue and are recruited from blood and bone marrow under inflammatory conditions. Following injury, they expand exponentially. Peritoneal macrophages, alveolar macrophages and Kupffer cells become activated at different stages of acute pancreatitis.[189]

Macrophage-derived MMPs facilitate BM disruption and this expedites movement of inflammatory cells to the injury site.[190] Macrophages recognise cell surface markers expressed by acinar cells and act as phagocytes to clear dying cells rapidly and efficiently. Clearance of cellular debris alters the physiology of macrophages through endogenous signals from ingested material including alterations in surface protein expression and the production of cytokines and pro-inflammatory mediators.[188] This removal of intracellular contents appears to simulate the macrophages to express either an anti-inflammatory phenotype for the resolution of inflammation, or a suppressive phenotype that would continue inflammation.[191]

Macrophages produce several growth factors that promote wound healing through proliferation and angiogenesis including PDGF, IGF-1, and VEGF and also produce mediators such as TGFβ to activate PSCs. Thus, they stimulate PSCs to synthesise ECM products that result in the development of fibrosis. If the trigger for injury is removed, macrophages direct tissue repair through mechanisms that suppress inflammation, remove collagen and restore tissue architecture. Dysregulated cross talk between macrophages and other cells or the ECM, and transcription of pro-fibrotic genes by cytokines PDGF, IL-6, IL-13 results in survival and proliferation of PSCs.[79] This leads to pathological fibrosis and chronic pancreatitis. Studies of macrophages in cancers support a role of the ECM in guiding macrophage interactions where they support metastasis by mobilizing and co-migrating with tumour cells.[79]

1.4.11.2 Mast cells in pancreatitis

Mast cells are haematopoietic immune cells resident in all human tissues usually in close proximity to vasculature. Sensitive to pathological change, on activation they release a myriad of inflammatory mediators important in the context of allergic disorders and other inflammatory responses as well as in protection against toxins and infection.[192] The secretion and the regulation of the extent of mediator release is controlled by stem cell factor (SCF), the ligand of the receptor c-kit.[193] The precise role of mast cells in acute and chronic pancreatitis is not clear, however they are implicated in the development and progression of acute pancreatitis,[194] and identified as the cells responsible for perpetuating chronic inflammation in chronic pancreatitis.[195]

Mast cells have a high content of secretory granules filled with preformed compounds including histamines, cytokines and growth factors (TNFα, FGF2, TGFβ, IL-4), and lysosomal hydrolases and proteases (tryptase, chymase).[196] The many mediators and molecules that mast cells produce are pro-fibrotic. They demonstrate biological effects modulating fibrosis through directly influencing fibroblasts/PSCs or through recruitment and activation of other inflammatory cell types (overview of mediators and biological effects.[192] In particular, histamine, FGF-2, TNFα and proteases are implicated in fibroblast proliferation and migration, matrix protein and collagenase production and collagen synthesis in humans. Mast cells may be a source of TGFβ as TGFβ derived from cultured mast cells can enhance collagen 1 production.[197] Animal studies, particularly in knockout mice, have provided contradictory results on the effects of mast cells on fibrosis with detrimental, protective and no effects noted. Data from human and *in vitro* studies favour a pro-fibrotic function for mast cells.

1.4.12 Survivin and the processes of pancreatitis

Survivin is a member of the inhibitor of apoptosis protein (IAP) family. The eight IAP family proteins are identified by one to three copies of an ~70-amino acid zinc finger fold designated Baclovirus IAP repeat (BIR). Other domains include a carboxyl-terminus RING and a caspase-recruitment domain. At 16.5kDa and 142 amino acids, survivin is the smallest IAP containing a single N-terminal BIR and a carboxyl-terminus α-helix.[198] The human gene for survivin is found on chromosome 17q25.[199] Four alternative splice variants have been described, designated survivin 2B*,* survivin-ΔEx3, survivin 3B, and survivin-2α.[199] The splice variants appear to differ in subcellular localisation and function, however, anti-survivin antibodies recognise them all due to the existence of an identical amino-terminal peptide.[200] Survivin gene expression is activated by transcription factors for pathways of cell proliferation, cell survival or development, or inhibited by other molecules such as p53.[198]

Survivin is localised intracellularly in the cytoplasm (approximately 80%), nucleus and mitochondria, and as components of the mitotic apparatus.[201] It is present abundantly in embryonic tissues, and in fast dividing cells but is mostly absent in normal differentiated cells. It may be expressed in normal adult cells such as primitive haematopoietic cells, T-lymphocytes, polymorphonuclear neutrophils and vascular endothelial cells. It occurs prominently in nearly every human tumour where it is frequently associated with poor outcome and resistance to therapy. The IAP family is implicated in control of cell division or regulation of apoptosis however survivin is associated with both functions. Essentially, nuclear survivin is involved in cell proliferation, but cytoplasmic survivin participates in cell survival.

It is well established that survivin is essential for cell division with cell cycle dependent expression at G2/m and localisation of the mitotic apparatus. Many studies targeting deletion of survivin have shown mitotic defects.[198] As a member of the chromosomal passenger complex, survivin targets the centromere in chromosome-microtubule attachment and may regulate the spindle assembly checkpoint by repressing microtubule dynamics.[198] Survivin has an anti-apoptotic function at mitosis by inhibiting mitotic catastrophe (the activation of a dual necrotic/apoptotic pathway) through suppression of caspase-9 and segregation of Smac. During embryogenesis, the signalling pathways Wnt/β-catenin, Hedgehog, Hippo and Notch target survivin. Because human and mouse embryonic stem cells express survivin, it may be essential for the integrity of stem cells to have survivin protection from apoptosis.[198] It is well documented that survivin is a biomarker of poor prognosis in human metastatic tumours through inhibition of apoptosis, increased drug resistance and maintenance of stem cells, however it appears that survivin may participate in cell motility and invasion.[198]

Investigations with human cases of normal pancreas and chronic pancreatitis or pancreatic cancer have found conflicting results. Survivin expression was absent in normal pancreas and chronic pancreatitis but positive in tumour cells.[202] Survivin expression in ducts, acini and islets increased with the extent of fibrosis in human chronic pancreatitis cases.[203] In acute necrohaemorrhagic pancreatitis in rats, duct cells (cytoplasm and nucleus), acinar cells and infiltrating cells (nucleus only) were positive for survivin.[204]

1.5. EXPERIMENTAL MODELS OF PANCREATITIS

Exocrine pancreatic pathology is usually comprised of four conditions: acute and chronic pancreatitis, cancer and cystic fibrosis. Since it is difficult to study the pathophysiology of pancreatitis in humans, many animal models of pancreatitis have been established in an effort to elucidate the cellular and molecular mechanisms that initiate and precipitate the disease and the subsequent events that allow regeneration and recuperation of the pancreas. Experimental models attempt to mimic the clinical situation and whilst most do not in entirety, many result in the physiological and histological alterations that are relevant to clinical findings. Models using chemical administration, diet or surgical-induction have been developed in such diverse species as rats, mice, rabbits, dogs, cats, hamsters, pigs, opossum and ducklings.

Model-based bias is a difficulty for the extrapolation of findings in animal models to the human disease. In the rat, pancreatic ductal epithelium is less well developed, and ductal secretion may occur predominantly in interlobular ducts compared with intralobular/intercalated ducts in humans. The

physiological profile of rodent pancreatic acini is different to human with respect to CCK receptors and amines, and fluid secretion from acini differs markedly. Other species, for example dog and cat, exhibit a pattern closer to that in human.[205]

1.5.1 Caerulein

Caerulein is a decapeptide, structurally and functionally related to the intestinal hormone cholecystokinin (CCK), and was originally extracted from the skin of the Australian tree frog *Litoria caerulea*. Since Lampel and Kern [275] first showed it to have a striking stimulatory action on exocrine pancreatic secretion by producing reversible, oedematous pancreatitis in rats, it has become well-established as a model of experimental acute pancreatitis. In pharmacological doses, it also reproducibly induces acute pancreatitis in mice, dogs and Syrian hamsters.[206] This model, often referred to as secretagogue hyperstimulation pancreatitis, may be induced by intravenous, subcutaneous or intraperitoneal injection routes, the course and severity of pancreatitis varying with dose and route. At low doses, acinar cells are stimulated to activate the consecutive steps in the secretory process and pancreatic growth is accelerated; at maximal doses the secretory process is disturbed and acute pancreatitis ensues.[207] The model is found to be physiologically relevant to some aspects of human disease, although the effect of CCK is different in humans and rodents.[205] Whereas in rat and mouse it regulates exocrine enzyme secretion, human acini lack CCK receptors, and are regulated by neurogenic CCK stimulation.[208] Depending on dose and route of administration, caerulein induces a mild, self-limiting, reversible pancreatitis with oedema, increased serum levels of digestive enzymes, necrosis/apoptosis, inflammation and vascular permeability such that the early initial changes that occur in pancreatitis may be studied.[209] Repeated episodes of acute pancreatitis may induce chronic pancreatitis. Neuschwander-Tetri (2000A,B) developed a chronic pancreatitis model in mice using repeated doses of caerulein which results in a pattern of fibrosis similar to that found in human chronic pancreatitis. However, repeated doses of caerulein are not sufficient to cause the endocrine and exocrine insufficiency normally found in human chronic pancreatitis.[208] Wistar Bonn/Kobori (WBN/Kob) rats spontaneously develop chronic pancreatitis and may be supplemented with caerulein doses to produce a more severe effect.[110] The repetitive caerulein model may be combined with toxic agents such as lipopolysaccharides, dibutyltin dichloride and ethanol to enhance its effect.[208]

1.5.2 Ethanol

In humans, ethanol causes severe damage to liver but milder changes in the pancreas where ethanol may act merely as a sensitizer to chronic injury. Cofactors such as ethanol metabolites are probably responsible for producing the chronic pancreatitis that occurs in those who abuse alcohol. The majority of studies in rodents found that ethanol feeding and even continuous infusion of ethanol could not produce typical pancreatitis (comprehensively reviewed in Schneider et al 2002). However, supplementation with different feeding protocols for example, Lieber-DeCarli diet, Tsukamoto-French diet, deliver higher doses of ethanol. Similarly, models combining ethanol with other factors, including pancreatic duct obstruction, trinitrobenzene sulfonic acid, dibutyltin dichloride and caerulein have been investigated.[210] These models of ethanol administration do not produce classical acute or chronic pancreatitis however, they do facilitate the investigation of mechanisms that include enzymes, nutrition, metabolite changes and regeneration that are important in the course of alcoholic pancreatitis.

1.5.3 L-Arginine

A single intraperitoneal injection of high-dose amino acid L-arginine induces acute necrotizing pancreatitis.[211] This model has established pancreatitis in rats and mice with selective dose-dependent pancreatic acinar cell necrosis and is suitable for varying the degree of severity of disease and for investigating early and late phases, regeneration and multi-organ characteristics of acute pancreatitis.[212, 213] Results in chronic pancreatitis with administration of l-arginine for an extended time results in chronic pancreatitis with exocrine insufficiency.[214] This model is of unknown clinical relevance and is not used *in vitro*.

1.5.4 1-cyano-2-hydroxy-3-butene (CHB)

CHB is the stable breakdown product of a glucosinolate present in plants of the Cruciferae family, particularly the Brassica genus that includes vegetables such as cabbage, turnip and kale, condiments such as mustard, canola oil and certain forage and pasture plants. It is now well-established that in rats, at a reasonably high dose, CHB causes cell death in pancreatic acinar cells only[215, 216] but at higher doses lethality due to CHB is caused by extensive hepatocyte vacuolation and necrosis.[217] In the CHB study by Kelly and colleagues,[216] large animals were found to be more sensitive on a dose/weight basis than smaller animals, with females and males being equally sensitive. In rats, if the initial dose of CHB was high enough, death of virtually all acinar cells occurred with only very

occasional nests regenerating before 28 days. Subcutaneous administration gave a more consistent lesion, a more complete atrophic effect and liver toxicity could be lessened. An acute oedematous pancreatitis induced by synthetic CHB is non-invasive and requires but one subcutaneous injection of CHB. This model in rats has the benefit that the acinar cells are deleted completely by apoptosis so that regeneration and the fibrotic process can be assessed without the complication of residual acinar cells.[216] Bhatia et al. (1998) studied the early events of pancreatitis with a combination of CHB administration followed by caerulein-induced pancreatitis.

1.5.6 Ductal ligation

Gallstone or biliary disease is a common cause of pancreatitis. Historically, this instigated extensive research into the cause of pancreatitis from obstructed ducts. Invasive models of pancreatitis including the closed duodenal loop model, and duct injection models involving the retrograde injection into the pancreatic duct of bile, bile salts, with or without trypsin and pancreatic enzymes and bacteria result in severe pancreatitis with necrosis and haemorrhage. These were used to study pseudocyst and abscess formation, duodenal juice components and fat necrosis.[206] The perfusion of the bile acid sodium taurocholate induces biliary pancreatitis with severe haemorrhagic, necrotic pancreatitis with multi-organ failure.[206] The infusion of trinitrobenzene sulfonic acid into rat pancreatic ducts produces chronic pancreatitis with mono- and polymorphonuclear cell infiltrates, fibrosis and gland atrophy within 3 weeks.[106] Partial surgical ligation in rats as a model for ductal obstruction in the pancreas was modified by Pound and Walker.[218] The technique of tying off the body of the pancreas, but not the splenic vessels close to the hilus of the spleen, avoids interference with biliary drainage, preserves the blood vessels, minimizes constitutional disturbance and leaves some pancreatic parenchyma as an internal control with retained organ function so that animal experiments may be extended.[218] The resultant pancreatitis is considered to be precipitated by pancreatic ductal hypertension, due to pancreatic secretion into the obstructed ducts. In the exocrine portion of the pancreas, acinar cells progressively disappear by apoptosis and the lobules are reduced to groups of small ductular complexes lying in a fibrous stroma.[218]

1.5.7 Vascular causes

Vascular-induced pancreatitis includes methods to impair pancreatic vasculature, or disturbance of microcirculation.[206] This is achieved by inducing hypovolemic shock, permanent occlusion of pancreatic arteries, by venous ligation or retrograde injection of microspheres and

ischaemia/reperfusion models. Microcirculatory disorders are a major cause of death in the course of severe acute pancreatitis in humans.[194]

1.5.8 Genetic models

Following the sequencing of the genome of the mouse, transgenic mouse models and gene deletion studies facilitated understanding of the role of specific proteins in the complex processes where different proteins interact and co-react in pancreatitis. Genetically engineered mouse models recapitulating chronic pancreatitis,[219] and gene knockout models to examine the effects of cytokine and chemokine mediators plus their receptors have been targeted.[206] Mutations in genes identified from families with hereditary pancreatitis have led to investigations with trypsin/trypsinogen (serine protease inhibitor kazal type 1/SPINK1) and bicarbonate secretion (cystic fibrosis/CFTR) in the pancreas and to the development of mouse models with these genetic manipulations.[219] Mutations in genes PRSS2 (anionic trypsin), SPINK1, CFTR, CTRC (chymotrypsinogen C) and CASR (calcium sensing receptor) expressed in mouse models are associated with an increased risk of pancreatitis.[208] The connection that recurrent acute pancreatitis may precede chronic pancreatitis was identified by the PRSS1 mutations in chronic pancreatitis.

WBN/Kob male rats endogenously develop morphological and biochemical changes typical of chronic pancreatitis and unique genes not found in other inbred rats.[208] Other chronic pancreatitis genetic models are COX2, Sonic hedgehog, and knockouts KRAS, and TGFβ. Protein kinase R-like endoplasmic reticulum kinase knockout (PERK-/-) mice and mice overexpressing IL-1β have been developed to look at chronic inflammation.[208]

Multiple mouse models for pancreatic cancer now exist. They include the subcutaneous xenograft model where cell lines or human cancer tissue are implanted subcutaneously in nude mice or immunodeficient mice and have been used to study chemotherapeutic agents. The technically challenging orthotopic model that uses pancreatic grafted tissue, either cell lines or cancer tissue in immunodeficient mice allows study in *in vivo* conditions. Genetically engineered mouse models of pancreatic cancer include mutant KRAS and the TGFβ family.

1.5.9 Summary of models

The models of pancreatitis, whether invasive or non-invasive, simple or complex, employing high or low dose chemicals, induce a variety of lesions from mild interstitial to severe necrotizing pancreatitis

with considerable variation between species and with unique advantages and disadvantages. Many of the models mentioned above go some way to reproducing human pancreatitis in terms of histopathology and pathophysiology. However, they still lack effectiveness for clinical relevance, etiology, symptoms, treatment and outcomes. Ductal models have some relevance to gallstone disease, and none reproduce alcoholic pancreatitis. Nonetheless, the models of chronic pancreatitis are improving.

1.6 HYPOTHESIS AND AIMS OF THIS THESIS

The hypothesis tested was that different models of pancreatitis can be used to describe the processes of atrophy and regeneration in the pancreas.

The specific aims of this study were:

1. To investigate rat models of pancreatitis using caerulein, CHB and duct ligation;
2. To validate a pancreatitis model with CHB in the mouse;
3. To establish a canine model of pancreatitis with CHB;
4. To compare and contrast the models with respect to:
   Stellate cells and the production of fibrosis
   The role of mast cells and macrophages
   The role of survivin in pancreatic regeneration

CHAPTER 2
MATERIALS AND METHODS

2.1 INTRODUCTION

This Chapter presents the general materials and methods for this thesis. More specific details are given in the original research Chapters (Chapters 3-6) for methods specific to those Chapters.

2.2 STATEMENT OF ETHICS

Animal experiments were performed under National Health and Medical Research Committee guidelines and approved by the University of Queensland Animal Ethics Committee prior to project commencement. Animals were closely monitored for clinical signs of pain and distress. Ethics approval numbers were PATH/527/97 (caerulein) and PATH/527/98 (rats with duct ligation); PATH/527/00 (rats with duct ligation with clips removed); PATH/QIMR/586/03 (CHB and duct ligation), PATH/457/04LF and PATH/725/05/LF (dogs); and PATH/102/04/PTPL (mice)

2.3 MATERIALS

All chemicals were of high purity and, unless otherwise indicated, were obtained from Sigma-Aldrich (St. Louis, MO, USA). Food for the rodent diet was from Specialty Feeds (Glen Forrest, Australia).

2.4 ANIMALS, SOURCES, HOUSING AND CONDITIONS

Randomly bred mature male Wistar or Sprague-Dawley rats, aged approximately 7-8 weeks and weighing 170-250gm were bred, supplied and housed by the Herston Medical Research Centre, Herston, Brisbane. Wistar rats were used for CHB experiments and Sprague-Dawley for caerulein and duct ligation experiments, based on the original models. CD1 Swiss outbred mice (20-35gm) were purchased from the Animal Resource Centre (ARC) Perth, transported by air and an air-conditioned van then housed at the Herston Medical Research Centre. Randomly-bred dogs were obtained from Logan City Pound, transported by air-conditioned van and housed at the Herston Medical Research Centre. All of the above animals were acclimatised for one week before commencement of experiments.

Rats and mice were housed in standard stainless steel boxes. The animal house was maintained at 21ºC ± 1ºC and supplied automatically with artificial light in a 12 hrs day/12 hrs night cycle. Animals were fed a standard pellet diet and were allowed free access to water. Environmental enrichment was provided in the form of shredded paper and cardboard rolls. Dogs were housed in pens that allowed social interaction. They were fed a normal dry dog food and had free access to water. Dogs were exercised in a free run on a daily basis.

When tissues were to be fixed by immersion only, rats and mice were killed by CO_2 asphyxiation or lethal dose of pentabarbitone sodium. When rats were perfused with solutions via the aorta the animals died during deep pentabarbitone anaesthesia. Dogs were euthanased by intravenous injection of pentabarbitone. Animal remains were disposed according to University of Queensland (UQ) regulations.

Rats were divided randomly into three groups of four to six animals at each time point; normal animals not subjected to any experimental procedure; sham-operated animals subjected to the same procedures and handling as experimental animals but without caerulein, duct ligation or CHB, and experimental animals. Mice were divided into control sham and experimental animals. Dogs were experimental animals only; no control dogs were used in this experiment. Archival tissue from previous rat experiments by this and other researchers (with permission), as well as dog control tissue, liver and pancreas from the UQ Veterinary School, was accessed. A full necropsy was undertaken in one rat and mouse per experimental run and all dogs to assess the effect of the drugs in other organs. In rat, mouse and dog, pancreas and liver were the only organs affected.

2.5 CAERULEIN MODEL

Pancreatitis was induced in Sprague-Dawley rats using the method of Jurkowska *et al* (1992), by subcutaneous injection of caerulein (synthetic caerulein, C-9026, Sigma Chemical Co., St Louis, MO., USA), 24µg/kg, every 8 h for 2 days. The caerulein dose was dissolved in gelatine solution (G-2625, Sigma Chemical Co) in the ratio 75% gelatine to 25% distilled water to prolong its absorption. The caerulein dose was determined by earlier trials as the least dose producing a relatively uniform but maximal pancreatic lesion. Sham control animals were subjected to the same procedures and handling as experimental animals, but with saline substituted for caerulein. Groups of 4 rats were assessed 8, 12, 16 hrs and 1, 2, 3, 4, 5, 6, 7 and 10 days after the first injection. After assessment of

the histology, the time points 2, 4, 7 and 10 days were chosen as representative time points for developments in the lesion. Additional pairs of rats were used for EM analyses.

2.6 DUCT LIGATION MODEL

Figure 2.1 gives a diagrammatical representation of duct ligation. Randomly bred adult male Sprague-Dawley rats weighing 190-210gms were anaesthetised with pentabarbitone sodium (60mg/mL) given intraperitoneally at a dose of 40mg/kg for early experiments and later as this regime was no longer considered as best practice with Ketamine 60mg/ml+ Rompun 20mg/ml. Analgesia with bupenorphine 0.1-0.5mg/kg sc. was administered to the rats for recovery. Partial ligation was performed through a left paramedian incision. The lienal pancreas was freed from the colonic mesentery, two clips (Hemoclip Pilling Weck Inc, Research Triangle Park, NC, USA) were clasped about the pancreas at the superior pole of the spleen after separation of splenic vessels. The abdominal wall was closed as a single layer with chromic catgut sutures (Ethicon G121, Ethnor Pty. Ltd., Sydney) and the skin closed with metal clips (Medicon, Germany). The whole procedure took approximately 10 minutes. Rats were euthanased at 1, 2, 3, 4, 5, 10, 12, 18 days following ligation. Sham controls were treated accordingly, the pancreas handled but not ligated. In an attempt to produce regeneration in the duct ligation model a further group of 15 rats were subjected to ligation of the pancreatic duct (as above) with one clip only. Atrophy was allowed to develop for 1 week, then under anaesthesia and analgesia (as before), a paramedian incision was made and the clip removed with care to not damage the surrounding tissue. The wound was closed the animals were allowed to recover and the pancreata harvested after 7 days.

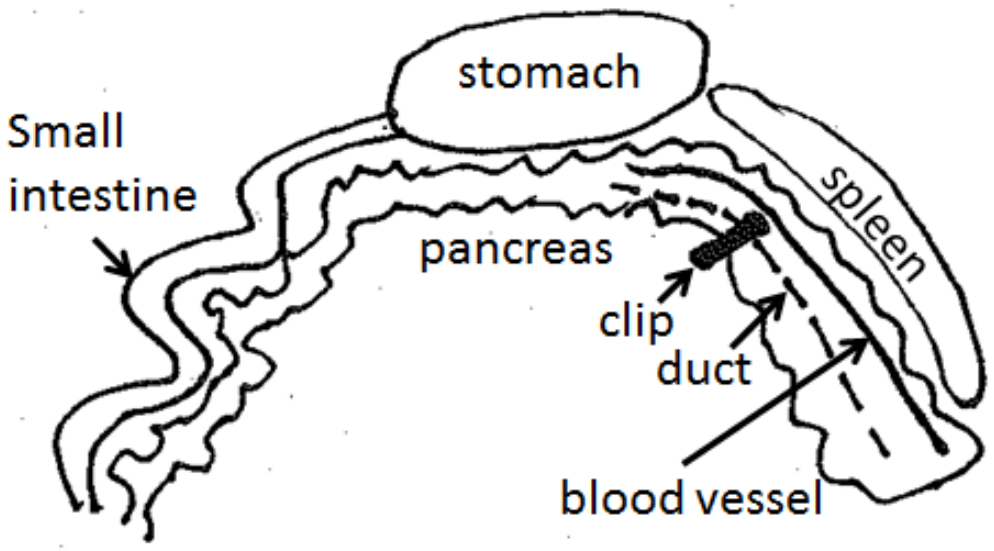

Figure 2.1 Diagrammatical representation of duct ligation

The technique of tying off the body of the pancreas, but not the splenic vessels close to the hilus of the spleen, avoids interference with biliary drainage, preserves the blood vessels, minimizes constitutional disturbance and leaves some pancreatic parenchyma as an internal control with retained organ function so that animal experiments may be extended. The lienal pancreas is freed from the colonic mesentery, and hemoclips are clasped about the pancreas at the superior pole of the spleen after separation of splenic vessels.

2.7 1-CYANO-2-HYDROXY-3-BUTENE (CHB) MODEL

Synthetic racemic CHB was obtained from Research Directions, Brisbane, Australia. Adult male Wistar rats weighing 200-250gms were used. At time zero, test animals were injected subcutaneously with 150mg/kg of CHB mixed in 0.5ml sterile saline and sham controls were given 0.5ml sterile normal saline. Groups of 4 experimental and 2 control rats were euthanased 1, 2, 4, 5, 7, 10, 12, 14, 16, 18, 28 days after the first dose. Pancreas was removed from all rats, liver was removed from selected rats.

Adult mice between 27.0-34.5gms were randomly divided and housed in pairs. One pair used for sham control purposes was injected subcutaneously with 0.25ml normal saline. Experimental pairs of mice were injected subcutaneous doses of CHB starting at 70mg/kg through 90, 110, 150, 170, 190, 210, 230, 250, 270, 290 and up to 310mg/kg. The dose increase was decided after review of histology of the previous dose pair. Euthanasia by carbon dioxide was performed 24 hrs later. Pancreas and liver were removed, a small piece of each placed in glutaraldehyde, some snap frozen in liquid nitrogen and the bulk placed in 4% buffered formalin. Three groups of eight mice were injected with a subcutaneous dose of 280mg/kg and one group euthanased at each time point of 12, 18 and 24 hrs, liver and pancreas removed and processed as above. Four smaller CD1 Swiss mice of 21 – 23 grams were given 280mg/kg subcutaneously and euthanased at 24 hrs, liver and pancreas removed and processed as above. This was performed to see whether some effect in mice was due to the adolescent status of the animals. Dogs (15-20kg) were given a pre-medication of 8mg of acepromazine and 8mg of methadone to induce drowsiness. CHB of the required dosage was placed in a 100ml bag of normal saline and infused intravenously over 15 minutes. Dosage for the first dog was commenced at 70mg/kg CHB and amended in subsequent dogs as required. Further intravenous Hartman's solution was administered at the rate of one litre every 12 hrs. Blood was taken at regular intervals. Dogs were kept sedated and comfortable with regular acepromazine and methadone and with monitoring of behaviour and blood parameters. Dogs were killed at selected times as detailed in the appropriate chapter, necropsy was performed by a veterinary pathologist, pancreas and liver tissue removed and processed as above.

2.8 MICROSCOPY

2.8.1 Light microscopy

Pancreas for histological study was fixed in 4% formalin in phosphate buffered saline at pH 7.2, dehydrated in graded alcohols, cleared in xylene and embedded in paraffin wax. Four micron sections were cut by microtome onto glass slides and stained with haematoxylin and eosin (H&E). Specific stains are noted in chapters and methods for these are in Appendix 1. Sections were visualised under a Nikon Eclipse E800 microscope with lenses of x10, x20, x40 and x100 (oil). The microscope was fitted with a Nikon digital camera DXM 1200F. A graticule was used for counting cells in tissue sections. The total area of the graticule at x400 magnification measured 250μm^2. Each square of the grid measured 25 μm^2.

2.8.2 Frozen sections

Small pieces of pancreas (1mm) were either placed into cryomatrix (OCT) and frozen on dry ice or small pieces were snap frozen in liquid nitrogen. Frozen sections (7μm) were cut onto glass slides on a Bright cryostat and fixed for 2.5 minutes in acetone.

2.8.3 Electron microscopy

Caerulein animals were deeply anaesthetised with intraperitoneal injections of pentabarbitone sodium. The abdomen was entered through a midline incision and a catheter (2mm outer diameter) was inserted into the abdominal aorta and secured using 6.0 silk (Ethicon, Ethnor Pty. Ltd., Sydney Australia) proximal to the coeliac artery. The ventricle was cut to allow free flow of the perfusing solutions. Fixation was carried out in sequence with 1) heparinised normal saline, 2) 1% paraformaldehyde and 1.2% glutaraldehyde in sodium cacodylate buffer and 3) 4% paraformaldehyde and 5% glutaraldehyde in sodium cacodylate buffer.[220] Tissue from duct ligation and CHB animals was immersion fixed in 3% glutaraldehyde in 4% paraformaldehyde. In all models the pancreas was removed immediately, trimmed of fat and lymph nodes. Small pieces (1mm) were left in fresh fixative for 2 hrs. The tissue was post-fixed in Osmium Tetroxide, stained *en bloc* in 5% aqueous uranyl acetate, dehydrated through a series of graded alcohols, cleared in propylene oxide, and embedded in an Epon/Araldite mixture. Semithin sections (1μm) were cut on an ultratome V microtome and stained with toluidine blue for viewing. Ultrathin sections from selected areas were stained with lead citrate and examined with a JEOL-1200 EX11 electron microscope.

2.9 IMMUNOHISTOCHEMISTRY

Heat antigen retrieval was performed in a decloaking chamber (Biocare Medical). Slides in 0.01M citric acid buffer pH6.0 or 0.001M Tris/EDTA buffer pH8.8 were subject to 5 minutes heat at 125ºC or 15 minutes heat at 105ºC respectively. After completion of the cool down cycle the container of slides was allowed to cool for a further 20 mins before transfer to Phosphate Buffered Saline. Enzyme pre-treatment consisted of prediluted Proteinase K (DAKO Corp., Carpinteria, California, USA.) or 0.1% trypsin in 0.05M Tris buffered saline (TBS) with 0.1% calcium chloride. Endogenous peroxidase was inhibited by treating sections with 1% hydrogen peroxide and 0.1% sodium azide in Phosphate buffered saline (PBS). Non-specific antibody binding was inhibited by incubation with 10% non-immune goat or donkey serum. Localization was demonstrated using peroxidase-labelled streptavidin biotin complex method (DAKO streptavidin AB Complex/Horseradish peroxidase (HRP) or DAKO Envision. Reactions were developed with 3,3'–diaminobenzidine tetrahydrochloride solution (DAB) (Zymed, San Francisco, California) or Vector VIP (SK-4600), Vector SG (SK-4700), Vector NovaRED (SK4800) peroxidase substrate kits (Vector laboratories, Inc. Burlingame, California, USA). Where double staining was performed with two mouse antibodies, Fab fragment was used after the first antibody. All sections were lightly counterstained with haematoxylin or nuclear fast red. Specificities of the antibodies used for identification was checked by inclusion of known positive control tissue (normal pancreas) in each run. Negative controls comprised test tissues without the addition of primary antibody. Antibodies used are detailed in Table 2.1.

Table 2.1 Antibodies for immunohistochemistry					
Primary Antibody	Manufacturer	Clone	Antigen retrieval	dilution	2° antibody
α-amylase rabbit anti-human	Sigma		Proteinase K	1:500	Jackson goat anti-rabbit
Bax rabbit anti-human	Santa Cruz	P-19	heat/citrate	1:100	Dako EnVision+
Bcl-xL rabbit anti-human	Santa Cruz	S-18	heat/EDTA	1:400	Dako EnVision+
caspase-3 rabbit anti-cleaved	Cell signalling	ASP-175	heat/EDTA	1:100	Dako EnVision+
CD68 mouse anti-human	Dako	PG-M1	heat/citrate	1:100	Dako EnVision+
CD117/c-kit rabbit poly	Dako		heat/EDTA	1:600	Mach 1 universal HRP kit
Cytokeratin mouse anti-human	Dako	AE1/AE3	Proteinase K	1:40	Jackson rat anti-mouse
glucagon porcine anti-human	Novocastra		Proteinase K	1:100	Dako EnVision+
Laminin 1+2 Rabbit poly	Abcam		chymotrypsin	1:300	mach
PCNA anti-mouse	Calbiochem	AB-1	HCl 0.2N	1:50	Dako EnVision+
αSMA mouse anti-human	Sigma	1A4	no AR	1:250	Dako EnVision+
Survivin, rabbit anti-human	Cell Signaling Technology	71G4	heat/EDTA	1:50	Dako EnVision+
Survivin rabbit anti-human	Novus Biologicals		heat/EDTA	1:150	Dako EnVision+

2.10 DIGITAL CAPTURE AND ANALYSIS FOR FIBROSIS AND STELLATE CELLS

Figures 2.2 and 2.3 demonstrate some methods for digital capture of images.

Semi-quantitative analysis of sections stained for Puchtler's picro-sirius red and αSMA expression was performed. Sections were captured with a spot RT slider cooled CCD camera as digital images. Ten fields of 50μm^2 from each slide were captured and variability associated with the light source was avoided by photographing all slides on the same day with the same settings. In particular, each field targeted a tubular complex or acinar cells, rather than interstitial areas, blood vessels, or large ducts.

ImagePro Plus® image analysis software was used to analyse image morphometry. This programme was adjusted to automatically calculate the area in square microns of defined stained proteins (as pixels) in each section. To define the pixels counted, coloured area ranges were selected that, through trial and error, selected a consistent intensity of the chosen colour, for example, in the fibrosis study the red of collagen staining; in the stellate cell study the brown of DAB, staining αSMA. The programme calculated ratios for each field and the average and standard error of the mean (SEM) were calculated for each time point in each animal model.

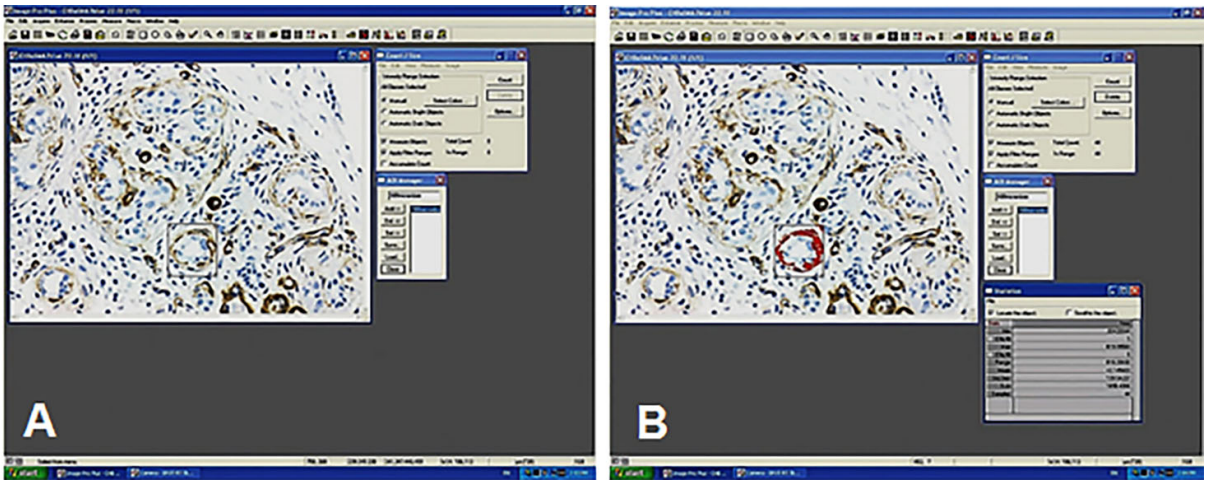

Figure 2.2 Captured screen of ImagePro Plus® image analysis software for αSMA IHC
Screen capture shows selected area on α-smooth muscle actin (αSMA) stained section (**A**) and corresponding calculated area of defined stained proteins for the brown pixels of αSMA staining (**B**), bright field image.

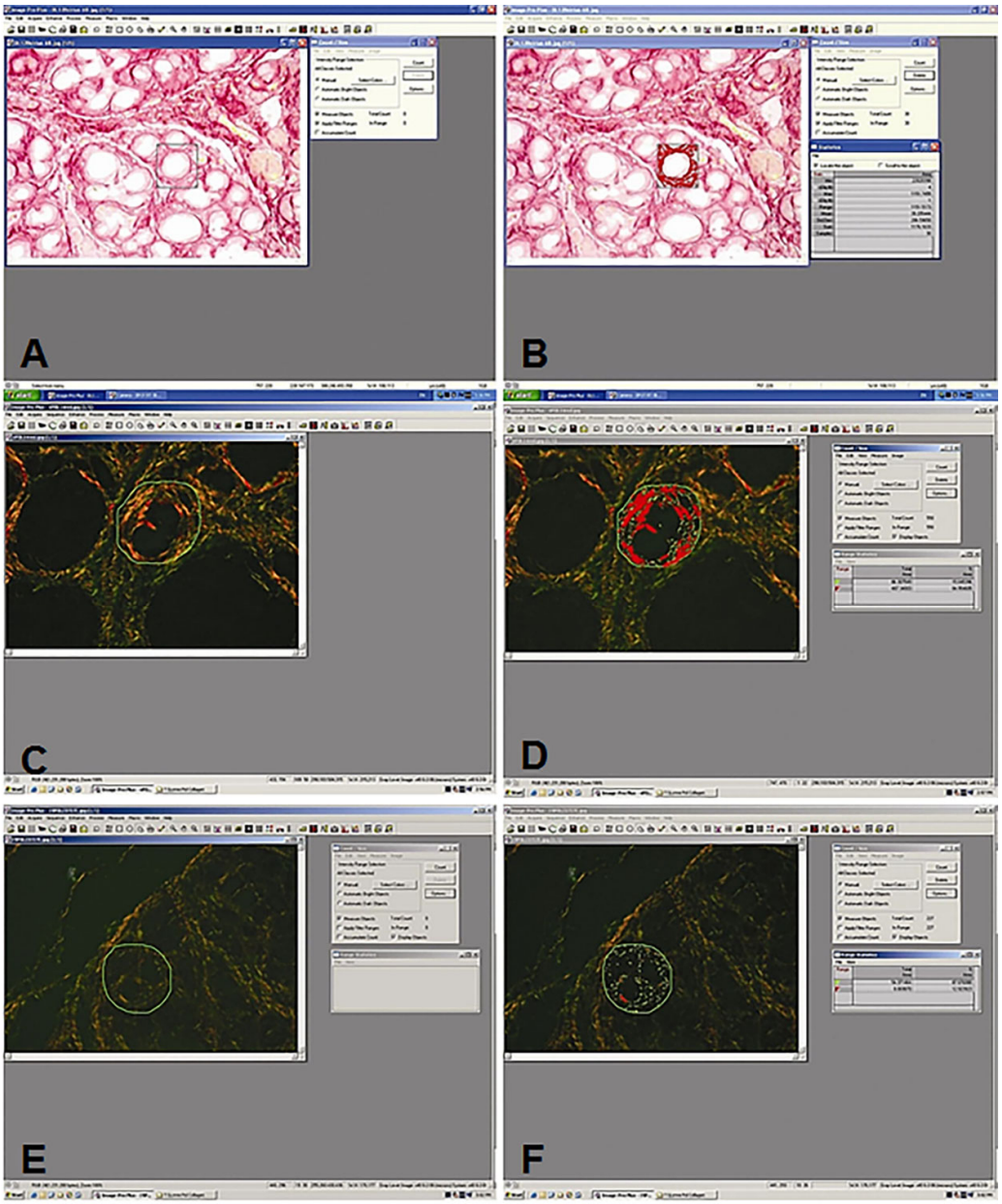

Figure 2.3 Captured screen of ImagePro Plus® image analysis software for fibrosis

Screen capture shows selected area on Sirius Red sections (**A**, **C, E**) and corresponding calculated area under different filters of defined stained proteins for Sirius Red pixels of (**B**) red (**D**) yellow/red and (**F**) green. A,B bright field images, (B) shows area of collagen deposition; **C**-**F** polarised light images discriminates and shows area of collagen III (D) and area of collagen I (F).

2.11 CELL DEATH AND PROLIFERATION

Apoptosis was identified using morphological criteria.[221] Immunoperoxidase stains for amylase were used to confirm residual intact acinar cells, which were otherwise difficult to identify. The following criteria were used to identify apoptosis in H&E sections; a single condensed cell or large single apoptotic body with typically marginated nuclear chromatin was given a single count; many apoptotic bodies clustered together were given a single count; any doubtful cells were disregarded. Necrosis was identified by cell swelling, mitochondrial swelling, lysosomal rupture, and plasma membrane rupture. The morphological characteristics used to distinguish mitosis were (i) formation of mitotic spindles occurring during metaphase and remaining visible in anaphase, or (ii) cells in the later stages of mitosis, telophase or undergoing cytokinesis. Cell senescence was approximated morphologically by the presence of large cells, at least 3-4 times the diameter of non-senescing cells.

2.12 STATISTICS

Values reported are mean ± standard error of the mean (SEM). Where indicated, data were analysed using one-way analysis of variance (ANOVA) and Tukey's post hoc analysis. Significance was established at $P < 0.05$.

CHAPTER 3
RAT MODELS OF PANCREATITIS

3.1 INTRODUCTION

We do not yet fully understand the complex interactions that comprise human pancreatitis. The current animal models are not comparable to the full spectrum and complexity of the human disease. In human pancreatitis, when acinar cells die by any cause they either regenerate or are followed by a progressive and gradual replacement of the glandular tissue with fibrosis. In order to study regeneration after pancreatitis I sought to use a model where the pancreatitis was severe enough to cause loss of acinar cells and production of a fibrotic infiltrate, though still mild enough that the pancreas could regenerate partially or fully. Three models that were standardized and fitted with this criteria were caerulein, CHB and duct ligation. They all have apoptosis as the mode of cell death to satisfy the interpretation of mild pancreatitis. They all develop fibrosis and considerable inflammatory infiltrate. The interesting factor is that they differ in regenerative ability which allows comparison of their outcomes. The caerulein model regenerates readily and fully; the CHB model regenerates partially but does not proceed; the duct ligation model does not regenerate at all. As no one model would be expected to be more suitable than another to answer specific questions these three rat models appeared to be a good compromise for a comparable study of the cellular interactions that occur in regeneration from pancreatitis. The three rat models, caerulein, CHB and duct ligation were chosen because of our expertise in all models, and the facilities available to produce all models. These were ethically acceptable, minimally invasive techniques with low morbidity and no procedural mortality.

3.1.1 Aim

The overall aim of this Chapter was to develop, reproducibly, a mild pancreatitis with fibrosis using three rat models, caerulein, CHB, duct ligation and to investigate patterns of cell death and regeneration.

3.2 MATERIALS AND METHODS

General materials and methods can be found in Chapter 2. Aspects of the three models have been described previously by this student, her PhD advisors and colleagues.[105, 216, 222] Some results for early time points were developed from review of available archival tissue from these studies.

A separate experiment was attempted with the duct ligation model to see if regeneration of acinar tissue could be achieved. This regeneration experiment, with rats subjected to duct ligation, clipped with one clip and the clip removed after one week, was abandoned. There was difficulty locating the clip after the first week due to adhesions and inflammation around the clip. Furthermore, the clip was difficult to remove without causing damage to the surrounding tissue. Whilst the distal pancreas of rats clipped with two clips was consistently atrophic, the pancreas of rats in trials with one clip showed variable results. Therefore, it was difficult to be certain whether the partial regeneration seen after the clip was removed and the pancreas allowed to recover for 7 days was due to actual regeneration or incomplete atrophy, or in cases where regeneration did not occur, whether this was due to the pancreatic duct being irretrievably damaged and failing to reopen.

3.3 RESULTS

3.3.1 Control

Pancreas from control rats appeared normal with widely spaced ducts and islets separated by closely packed acinar cells. Acinar cells have basophilic cytoplasm at their base due to a high content of RNA and the presence of nuclei. The apical cytoplasm is eosinophilic due to the high content of zymogen granules. The lobules are closely aligned, separated by narrow interlobular spaces **(Figure 3.1A).** High power clearly shows the centroacinar cell and intercalated duct cell at the beginning of the ductal system **(Figure 3.1B).** Immunohistochemistry for cytokeratin demonstrates the spacing of the ducts in normal pancreas **(Figure 3.1 C).**

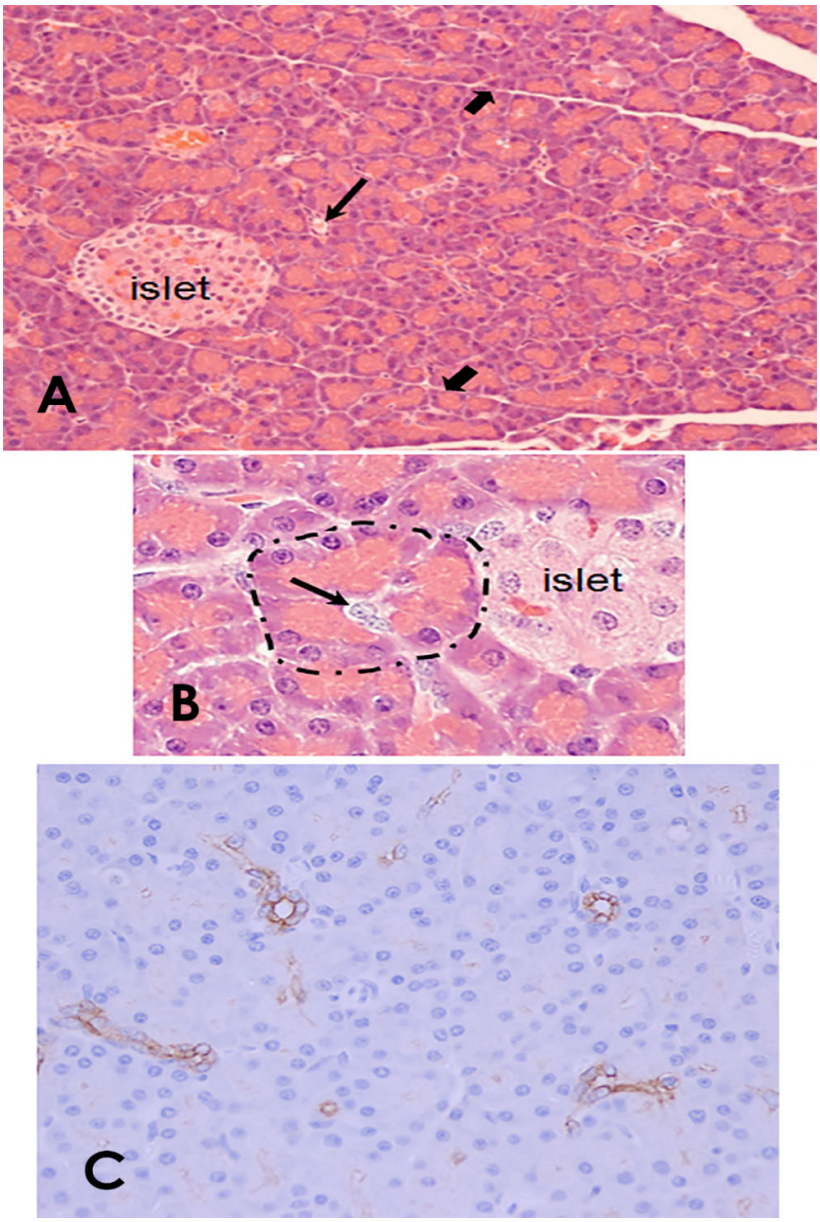

Figure 3.1 Control rat pancreas, light microscopy

A. Normal pancreas with islet and closely packed acini. Acinar cell cytoplasm is basophilic at base due to the staining of the nucleus and eosinophilic at apex due to the staining of zymogen granules. Intralobular duct (long arrow), The lobules are closely aligned, interlobular space (short arrows). H&E x200. **B**. High power of an acinus (dotted lines) shows a typical rounded acinus with several acinar cells surrounding a lumen. The beginning of the duct system at the lumen, shows a centroacinar cell nucleus (arrow) next to the nucleus of an intercalated duct cell. The islet is easily identified by paler cytoplasm and pale nuclei. H&E magnified to x1200. **C**. Normal spacing of ducts stained for cytokeratin immunohistochemistry (brown), haematoxylin counterstain.

EM demonstrated the polarised arrangement of organelles in the acinar cell. A whole acinus with round nuclei arranged around a central lumen and distinctly electron dense apical zymogen granules is shown (**Figure 3.2A**). Microvilli protrude from the luminal surface and zonulae occlendentes seal the cells at the lumen **(Figure 3.2B).** A basal view of the acinar cells show prominent RER and mitochondria, lysosomal bodies, interdigitations in the lateral space between cells, and BM closely aligned with the cell surface **(Figure 3.2C,D).** Duct cell nuclei are elongated and indented. Compared with acinar cells there are fewer mitochondria and RER **(Figure 3.3A)**. Blebs on the surface of the cells and lateral interdigitations are common on intralobular ducts **(Figure 3.3B)**. **Figure 3.3C** shows the start of the ductal system within the acinus. Centroacinar cells are smaller than acinar cells with fewer organelles and no zymogen granules (**Figure 3.3C**). Cilia are seen randomly projecting into the ductal lumen **(Figure 3.3D).**

3.3.2 Experimental results from three models

From 2 hrs in the models CHB and duct ligation (tissue distal to the ligature), and 6 hrs in the caerulein model, secretion leaked from lumens into intercellular and interstitial spaces. Oedema persisted for 48 hrs in CHB and duct ligation, less in caerulein. By 24 hrs all models had a cellular infiltration of mononuclear cells, fibroblasts and a moderate number of neutrophils. Acinar lumens began to extend. Apoptosis was the mode of acinar cell death in all models. Apoptotic nuclei were seen as pyknotic, condensed, rounded nuclei sometimes lying within cleared spaces or fragmented nuclei in eosinophilic or basophilic apoptotic bodies in H&E sections. Almost every acinus in the caerulein and duct ligation models had one or two apoptotic cells however in contrast in the CHB model, apoptosis was massive and synchronous with every cell affected **(Figures 3.4A-C).** In the EM images dilatation of RER and vacuoles were prominent early features of acinar cells with convolution of the cell membrane. There was disruption of junctional complexes between adjacent acinar cells. Zymogen granules discharged into increasingly dilated acinar lumens. Apoptotic cells were easily identified by their sharply demarcated condensation of chromatin against the nuclear envelope, with convolution of the nuclear outline, cell shrinkage and nuclear fragmentation to form apoptotic bodies **(Figures 3.4 D-F).** The apoptotic bodies contained pyknotic nuclear chromatin, intact or partially degraded zymogen granules, RER and mitochondria and later amorphous material and myelin figures.

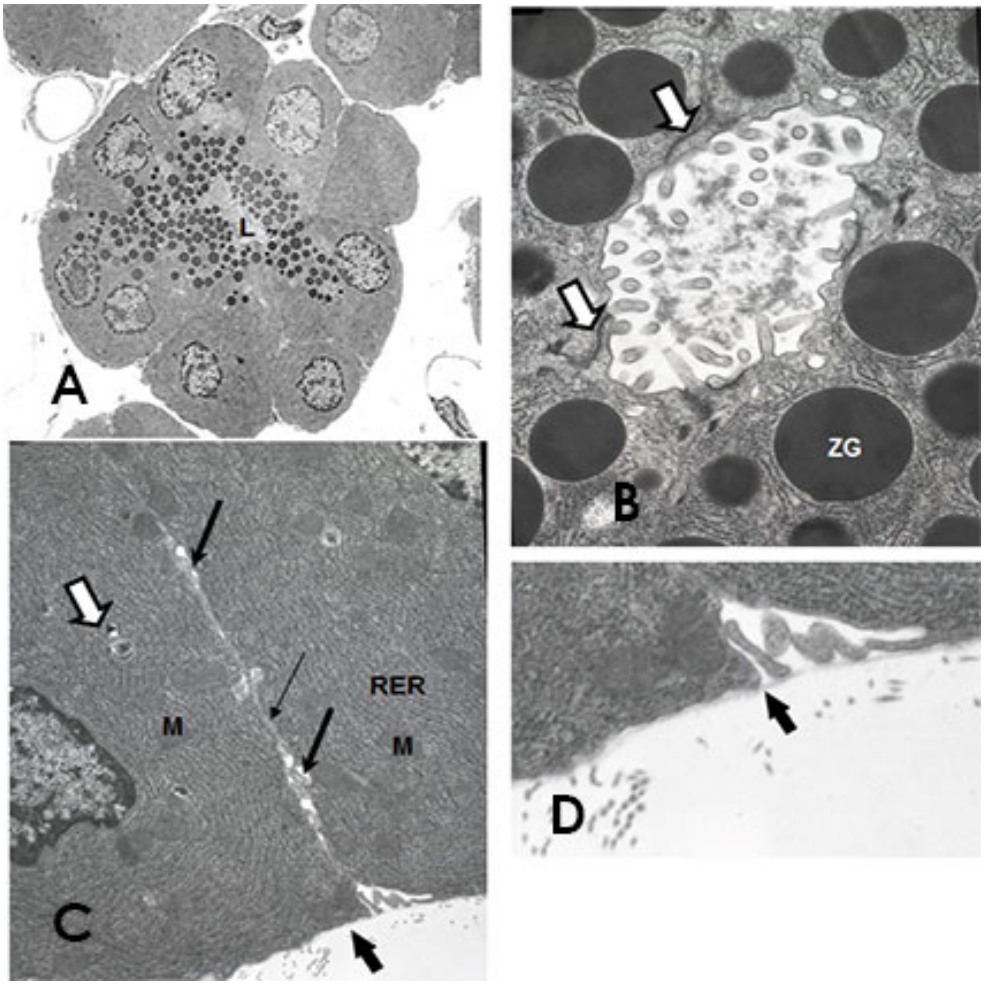

Figure 3.2 Electron microscopy of control rat pancreas with focus on acini

A. Control acinus. Note the pyramidal shaped acinar cells around a central lumen. The round nuclei are typically basal and apical electron dense zymogen granules congregate at the luminal pole. L=lumen. Electron microscopy (EM) x2000. **B**. High power of an acinar lumen with microvilli jutting into the luminal space. Zonulae occludentes form firm closures at the lumen to prevent unregulated release of zymogen granules (white arrows). Zymogen granules close to the lumen are ready for release ZG = zymogen granule EM x20000. **C**. Basal end of acinus. Interdigitations (long arrows) line the spaces between acinar cells, desmosome holds the acinar cells together (thin arrow), normal thin basement membrane (short arrow), lysosomal body (white arrow), rough endoplasmic reticulum=RER, mitochondria=M. EM x10000. **D**. High magnification of C showing the normal extent of basement membrane (arrow). Some collagen deposits are free in the intra-acinar space.

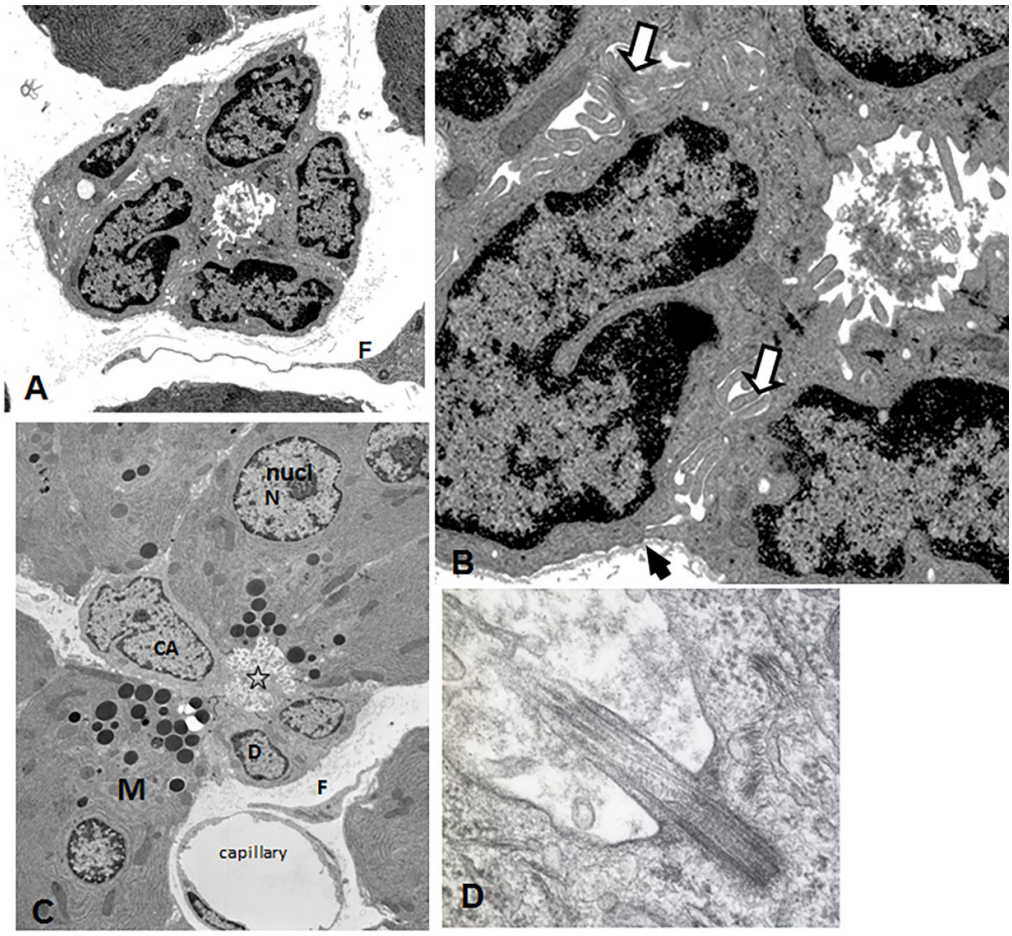

Figure 3.3 Electron microscopy of control rat pancreas with a focus on ducts

A. Intralobular Duct. Indented, elongated nuclei. F=fibroblast with a little collagen deposition. EM x5000. **B**. Magnification of A, with interdigitations on lateral membranes (white arrows), and basement membrane (black arrow). Electron microscopy (EM) x15000. **C**. Start of ductal system in acinus. CA=centroacinar cell, D= intercalated duct cell, N= nucleus, nucl= nucleolus, M=mitochondria, star =lumen. X4000. **D**. Cilia at lumen of interlobular duct. EM x 30000.

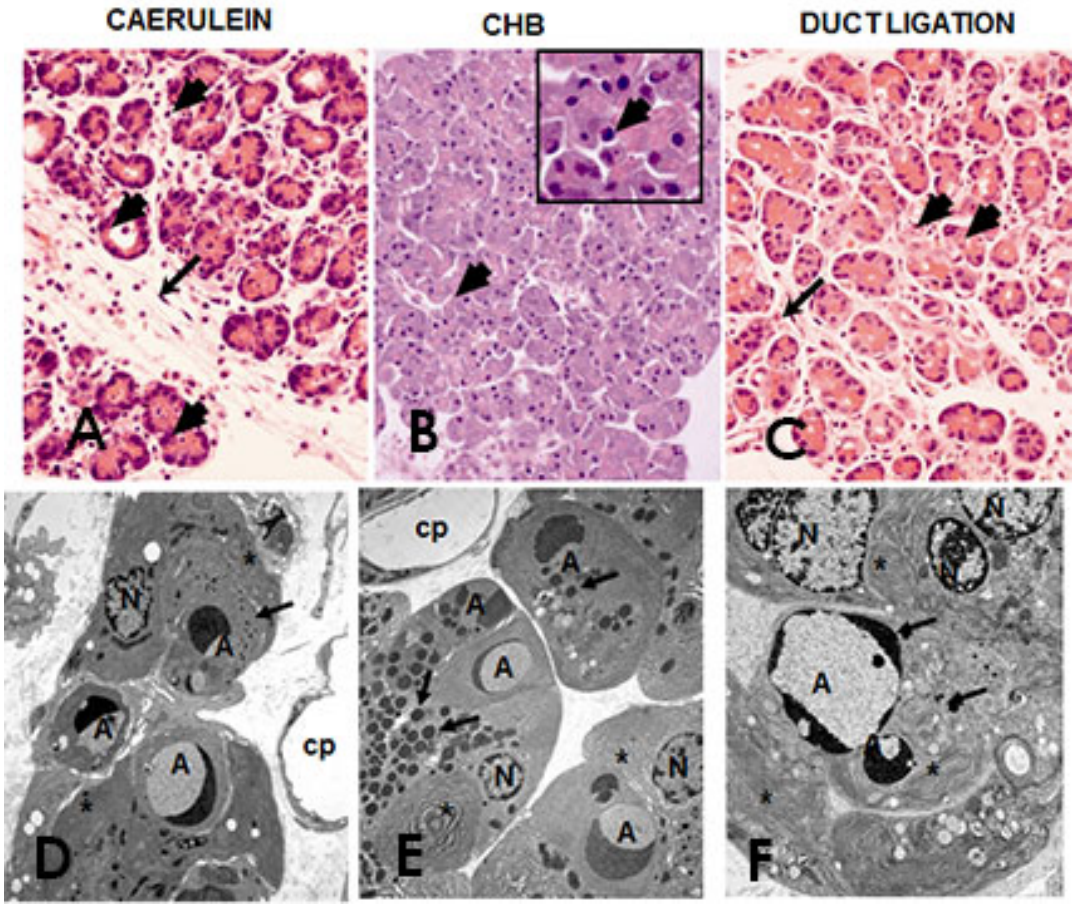

Figure 3.4 Apoptosis of pancreatic acinar cells in rat models

A. Caerulein at 24 hrs. Acinar cells undergo apoptosis as tubular complexes form. The inflammatory infiltrate is well advanced so that acini have lost adhesion to their neighbours. Haematoxylin and eosin (H&E) x400. **B**. CHB at 12 hrs. Apoptosis is present in most acinar cells in this model compared with only some to several in each acini of the other two models. The inflammatory infiltrate is not yet activated. H&E x400, insert x1000. **C**. Duct ligation at 24 hrs is similar to the caerulein model, H&E x400. **D**. Caerulein at 24 hrs, electron microscopy (EM) x 3000. **E**. CHB at 12 hrs EM x2500. **F**. Duct ligation at 24 hrs EM x4000. Figures **A-C**, short arrows show apoptotic nuclei, long arrows inflammatory infiltrate. Figures **D-F**, A=apoptotic nuclei, note crescent shaped chromatin. N=normal nucleus, arrows =zymogen granules; star=whorled rough endoplasmic reticulum; cp = capillary.

In the caerulein model, acinar cell apoptosis (**Figure 3.5A**) peaked at 3 days with a rapid reduction in acinar cell numbers, and by 4 days, few recognizable acinar cells remained. Similarly, by the 5th day in the duct ligation model all acini had disappeared. In contrast, in the CHB model, apoptosis was evident at 6 hrs and by 18 hrs almost all acinar cells had chromatin changes of apoptosis but also swollen vacuolated cytoplasm indicative of 'secondary necrosis' which subsequently progressed (**Figure 3.5B,C).** By 4 days no acinar cells remained.

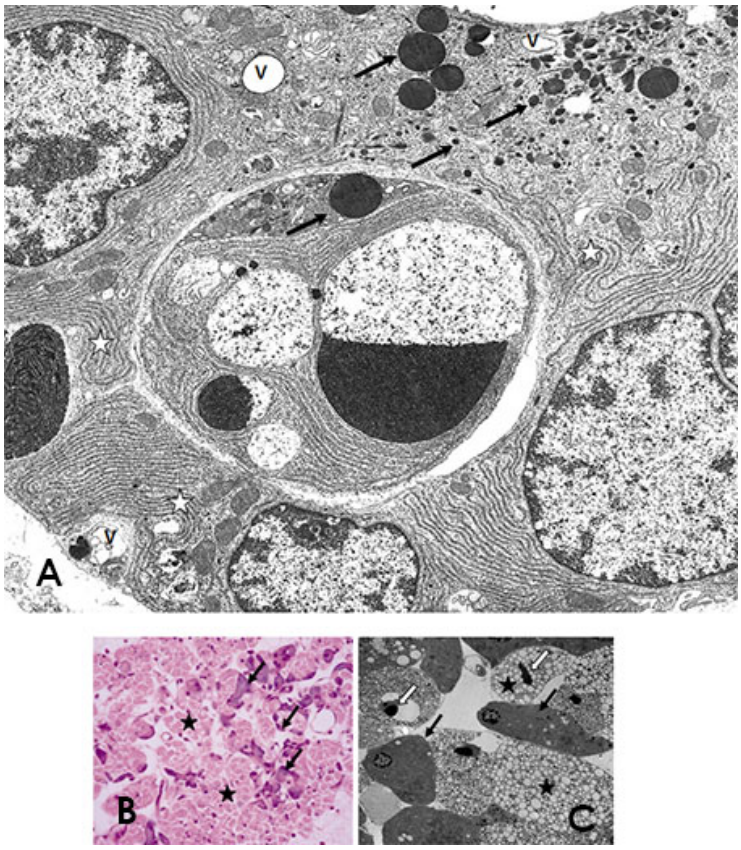

Figure 3.5 Typical apoptotic body and secondary necrosis in rat models

A. Electron microscopy (EM) of apoptotic body in duct ligation at 60 hrs. Note the condensed nuclear chromatin, multiple nuclear fragments within an apoptotic body becoming free from the surrounding cytoplasm, zymogen granules of varying size, many reduced in size, and whorling RER. Autophagic vacuoles are seen within the cytoplasm as are adjacent viable acinar nuclei. V=vacuole, arrows=zymogen granules of varying size, Star=whorled rough endoplasmic reticulum. **B**. 24 hrs after CHB massive apoptosis overwhelms the tissue until it appears degraded with both distended and condensed cytoplasm, however viable cells remain. Stars = degraded cytoplasm, arrows = viable cytoplasm. Haematoxylin and eosin x400. **C**. 18 hrs after CHB, stars = necrotic cytoplasm, black arrows = viable cells, white arrows = apoptotic bodies. EM x2000.

Apoptotic bodies were in the epithelium, in acinar lumens, free within the interstitium or phagocytosed within macrophages. In the CHB model, as apoptosis was a synchronous event, apoptotic bodies did not appear to be ingested by adjoining epithelial cells as in the other two models. The residual acinar tissue was mopped up predominantly by macrophages. Macrophage numbers were greatly increased in all models compared to controls **(Figure 3.6).** The macrophage results are expanded on in Chapter 4.

As a result of the depletion of acinar cells, lobules were rapidly converted into small groups of duct-like cells forming tubular complexes (**Figure 3.7)**. Tubular complexes were well established by 2 days in the caerulein model, by 4 days in the CHB and duct ligation models. The lobules and tubular complexes within them were separated by fibrosis and a persistent mononuclear inflammatory cell infiltrate **(Figure 3.7A-C).** Tubular complexes stained positive for cytokeratin confirming their ductal origin. Amylase immunohistochemistry indicated the few acinar cells or acinar debris remaining **(Figure 3.7D-F).** In the caerulein model particularly, as tubular complexes formed, residual acinar debris and duct cells coexisted **(Figure 3.7D).** The tubular complexes had distended lumens lined by flattened epithelial cells with the appearance of duct cells **(Figures 3.8A-F).** Mitoses were rarely seen in control sections but considerable numbers of cells lining tubular complexes showed mitotic activity by 2 days in all models (**Figure 3.8E).**

In the caerulein model, at 3-5 days clustered regenerative acinar cells in demilunes could be seen arising from tubular complexes and contained sparse small luminal zymogen granules (**Figure 3.9A-c).** Occasional cells were difficult to identify as ductal or acinar. Cytokeratin and amylase double staining showed clustered amylase positive cells around lightly stained brown tubular complexes (**Figure 3.9C**). Tubular complexes gave rise to islet cells with increased frequency (**Figure 3.9D).** By days 7-10 acinar cell mitoses were conspicuous, tubular complexes disappeared (**Figure 3.9F)**. By day 10 the lobular architecture had returned to a near normal appearance though mild fibrosis and a mild patchy inflammatory infiltrate persisted.

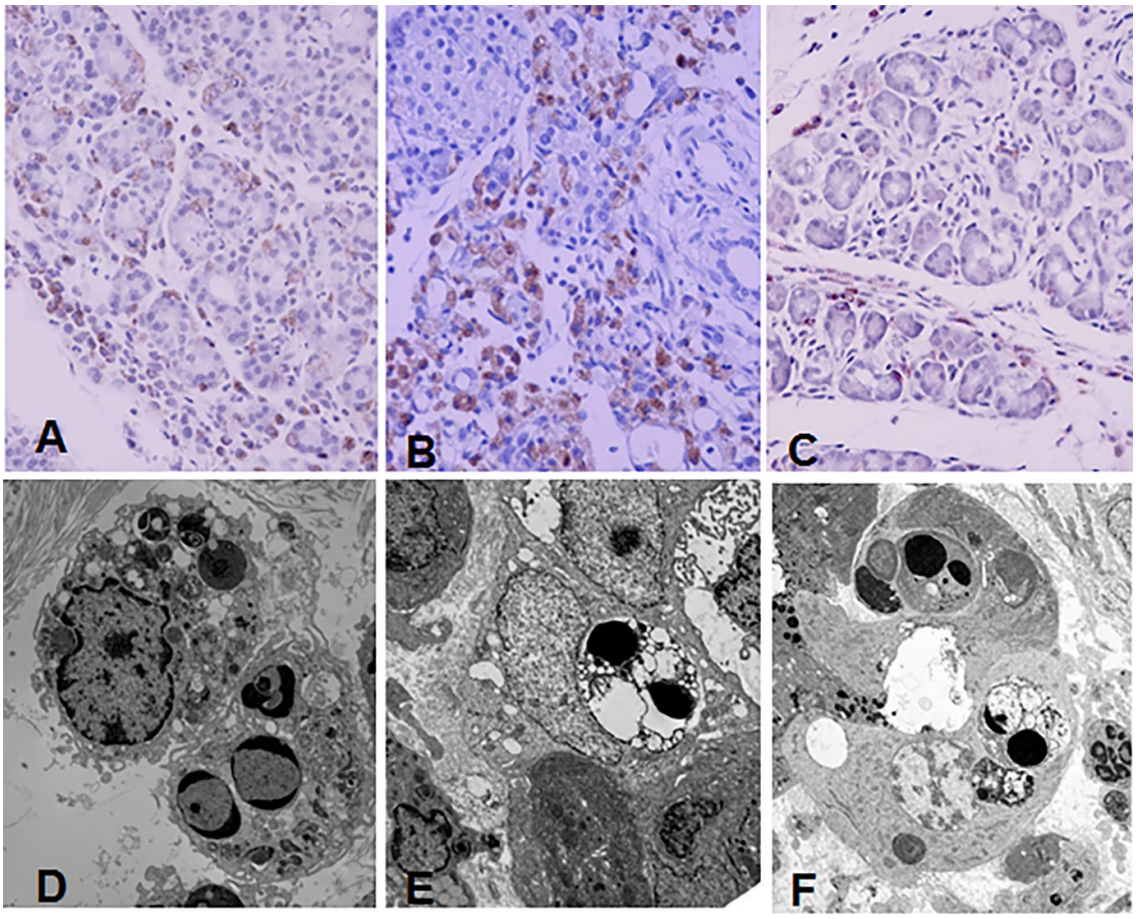

Figure 3.6 Macrophage or adjacent epithelial cell removal of apoptotic bodies in rat models

A. Caerulein 24 hrs, **B**. CHB 48 hrs, **C**. Duct ligation 48 hrs, all CD68 immunohistochemistry x 400, shows the extent of macrophage migration into the pancreas of each model. **D**. Caerulein day 4, apoptotic bodies being engulfed by a macrophage. Electron microscopy (EM) x 5000. **E**. CHB 48 hrs with secondary necrosis within a macrophage. EM x 4000. **F**. Duct ligation 60 hrs, apoptotic bodies were also engulfed by adjacent epithelial cells seen in this forming tubular complex with extended lumen and a viable acinar nucleus at the bottom of the complex. EM x2500

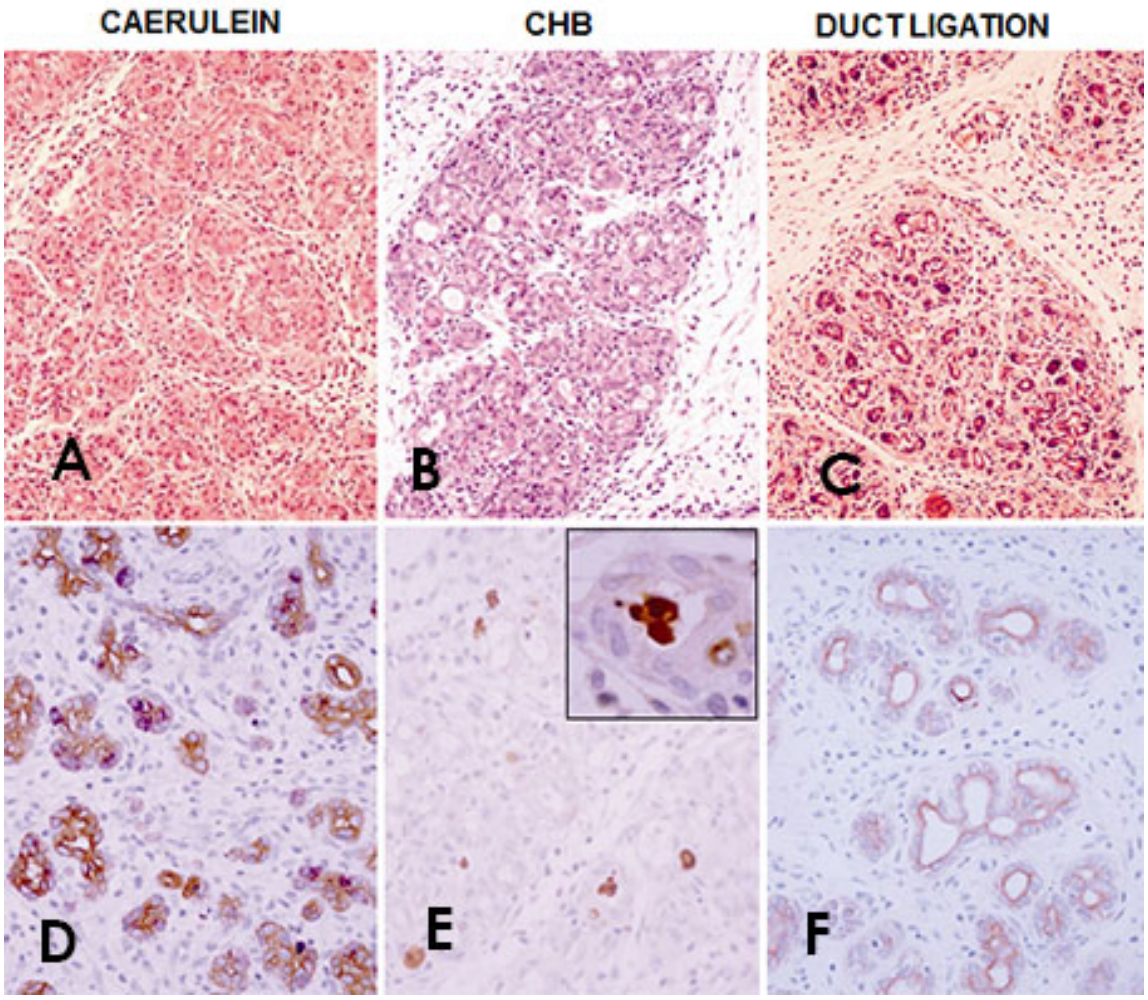

Figure 3.7 Acinar atrophy in rat models

A. Caerulein, day 2. **B**. CHB, day 3. **C**. Duct ligation, day 3.These micrographs show the parenchyma devoid of, or with few, acinar cells in all models. Tubular complexes fill the lobules which are surrounded by inflammatory infiltrate. All haematoxylin and eosin x 200. **D**. Caerulein, day 2, tubular complexes brown, acinar tissue purple indicate that most of the cells are ductal with only small residual acinar cells present, Immunohistochemistry for amylase (purple) and cytokeratin (brown) x400. **E**. CHB, day 3, residual acinar material is sparse amongst tubular complexes. Insert= residual acinar material lying in the lumen of a tubular complex. IHC for amylase (brown). x400, insert x1000. **F**. Duct ligation, day 4. Tubular complexes shown by IHC for cytokeratin (brown) are all that remain in the duct ligation model. x400. **D-F** counterstain is haematoxylin.

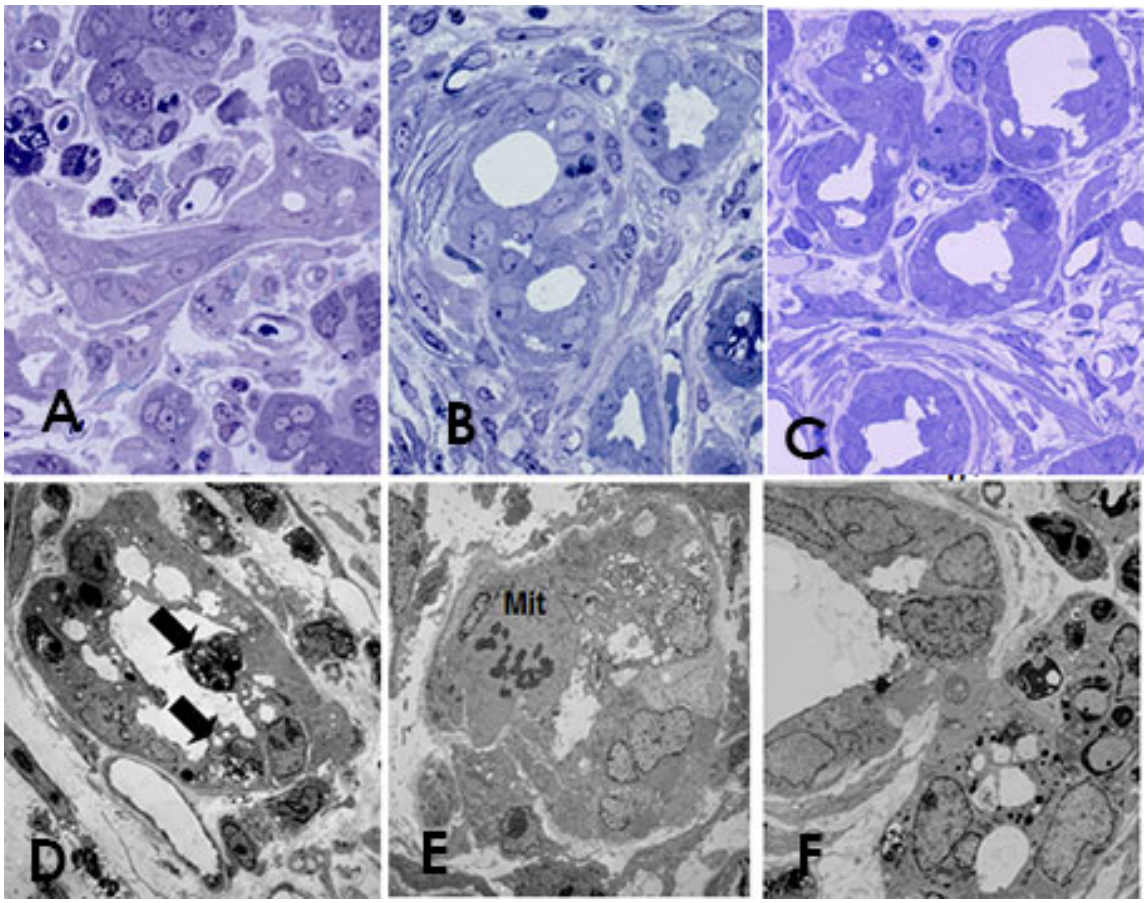

Figure 3.8 Tubular complexes in rat models

A. Caerulein, 36 hrs. **B**. CHB, day 5. **C**. Duct ligation, day 3. All toluidine blue stained semi-thin epoxy resin sections. Note the large lumens and flattened cells of the tubular complexes, surrounded by inflammatory infiltrate. In **A**, a tubular cell merges with a normal elongated duct and some dark condensed acinar material remains. All x1000. Electron microscopy (EM) is presented in **D-E**. **D**. Caerulein, day 2. **E**. CHB, day 3. **F**. Duct ligation, day 3. D shows tubular complexes forming with residual acinar debris and duct cells (arrows). **E**. shows mitosis in a ductal cell (Mit). **F** depicts a formed tubular complex next to one still forming with inclusions of residual material. **D**.= x2000, E and **F**. = x2500.

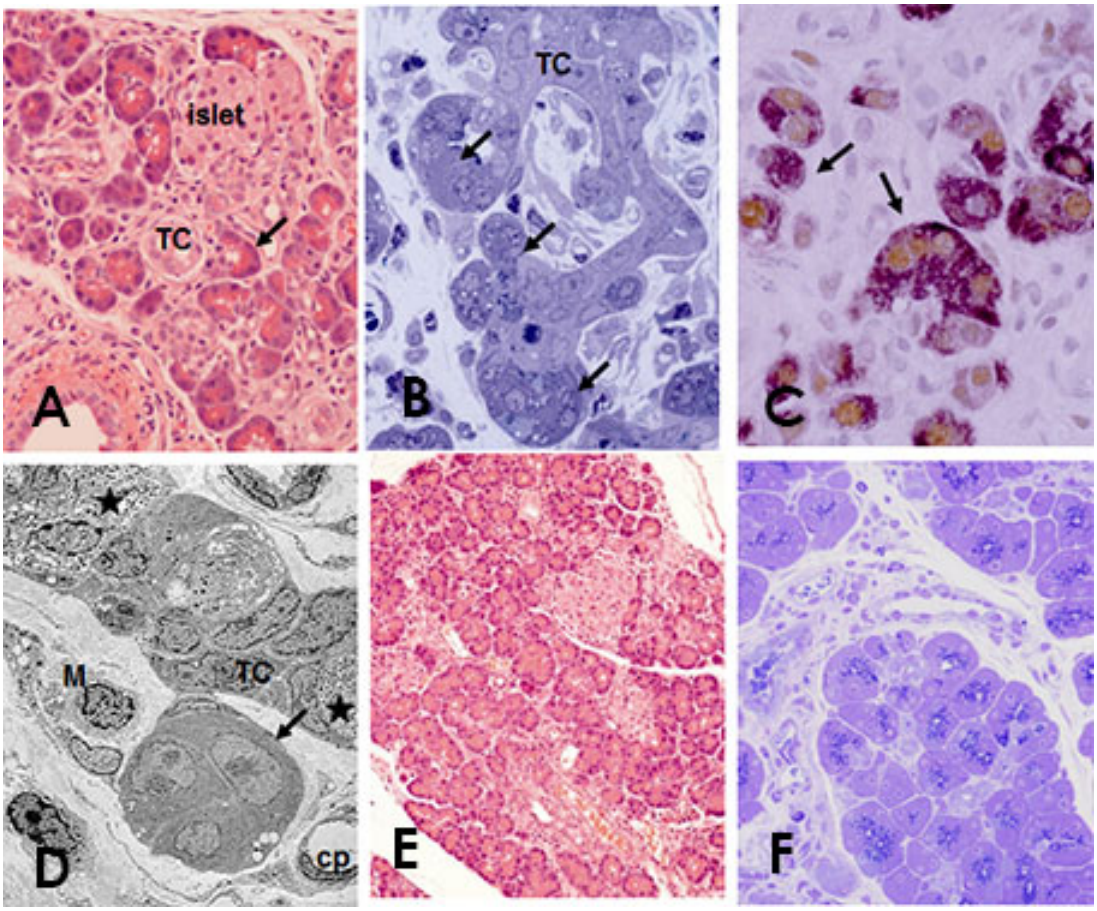

Figure 3.9 Regeneration in the caerulein model

A. Caerulein day 5, scattered regenerative acini are prominent because of eosinophilic cytoplasm and intense staining nuclei (arrow) in a lobule with residual tubular complexes and islet tissue. Haematoxylin and eosin (H&E), x400. **B**. Caerulein day 3, acinar cells regenerating in demi-lunes from tubular complexes was a particular feature of the caerulein model (arrows).Toluidine blue semi-thin epoxy resin, x1000. **C**. Caerulein day 4, acinar regeneration and proliferation. This particular staining combination highlights the zymogen granules with amylase content and the extent of cycling cells in regenerating acini, immunohistochemistry for amylase (pink) and proliferating cell nuclear antigen (PCNA) (brown), counterstain haematoxylin. x400. **D**. Caerulein day 4, an example of acinar cell regeneration (arrow), erupting from a tubular complex with its large elongated nuclei. Islet cell regeneration was a prominent feature in tubular complexes in this model. TC=tubular complex, cp=capillary, star=islet cell regeneration. Electron micrograph, x2500. **E**. Caerulein day 7, lobule almost fully regenerated with acini. H&E, x200. **F**. Caerulein day 10, regeneration varied between lobules and by day 10 considerable inflammatory infiltrate remained around some acinar lobules. x400.

In the CHB model, small numbers of apoptotic bodies continued to be seen within duct lumens and epithelium and by day 7 tubular complexes had larger lumens and flattened lining epithelial cells. Collagen was deposited both in and around lobules. Regenerative islands of acini appeared by 10 days but these were few and did not increase significantly in size or number **(Figure 3.10A-F)**. The regenerative acinar cells displayed both mitosis and apoptosis **(Figure 3.10B)**. Apoptosis was seen in the duct cells lining tubular complexes **(Figure 3.10E)** and the number of tubular complexes decreased with fewer remaining at 18 and 28 days. By 28 days the pancreas comprised largely fat, collagen, islets, blood vessels and nerves.

The duct ligation model followed a similar progression initially **(Figure 3.11A-F)**. By day 7 and up to day 18 lobules consisted of tubular complexes within a collagenous stroma. The tubular complexes were mostly smaller and more crowded than in the CHB and caerulein models. No regenerative acini were seen in this experiment except for a few sparse cells closely aligned with the ligature clips. Thickened basal lamina, and fibroblasts remained in the stroma with considerable adipose tissue around lobules.

3.3.2.1 Apoptosis counts

Figure 3.12 demonstrates mean ± SEM of counts of apoptosis for the three models over time points to 7 days. Compared with untreated controls (Time 0) where negligible apoptosis was found, all models had significantly increased apoptosis, but at varying periods of time after the cause of pancreatitis. The CHB model had massive apoptosis over 12 hrs, 1 and 2 days but this disappeared from 3 days where all acinar cells have disappeared through phagocytosis. While caerulein and duct ligation had a much lesser incidence of apoptosis compared with CHB, the incidence in caerulein was visible to 3-4 days, and the incidence with duct ligation to 5 days. **Figure 3.13** presents counts of cell proliferation using PCNA IHC. The graphs demonstrate the expected pattern of cycling cells. In the caerulein model, acinar cells were regenerating until experimental end at 10 days. The CHB model had duct cell regeneration up to 12 days when acinar cell regeneration started then declined by end of experiment. With the duct ligation model, duct cells were proliferating from 3 days to end of experiment at 18 days, with decreasing incidence from day 12.

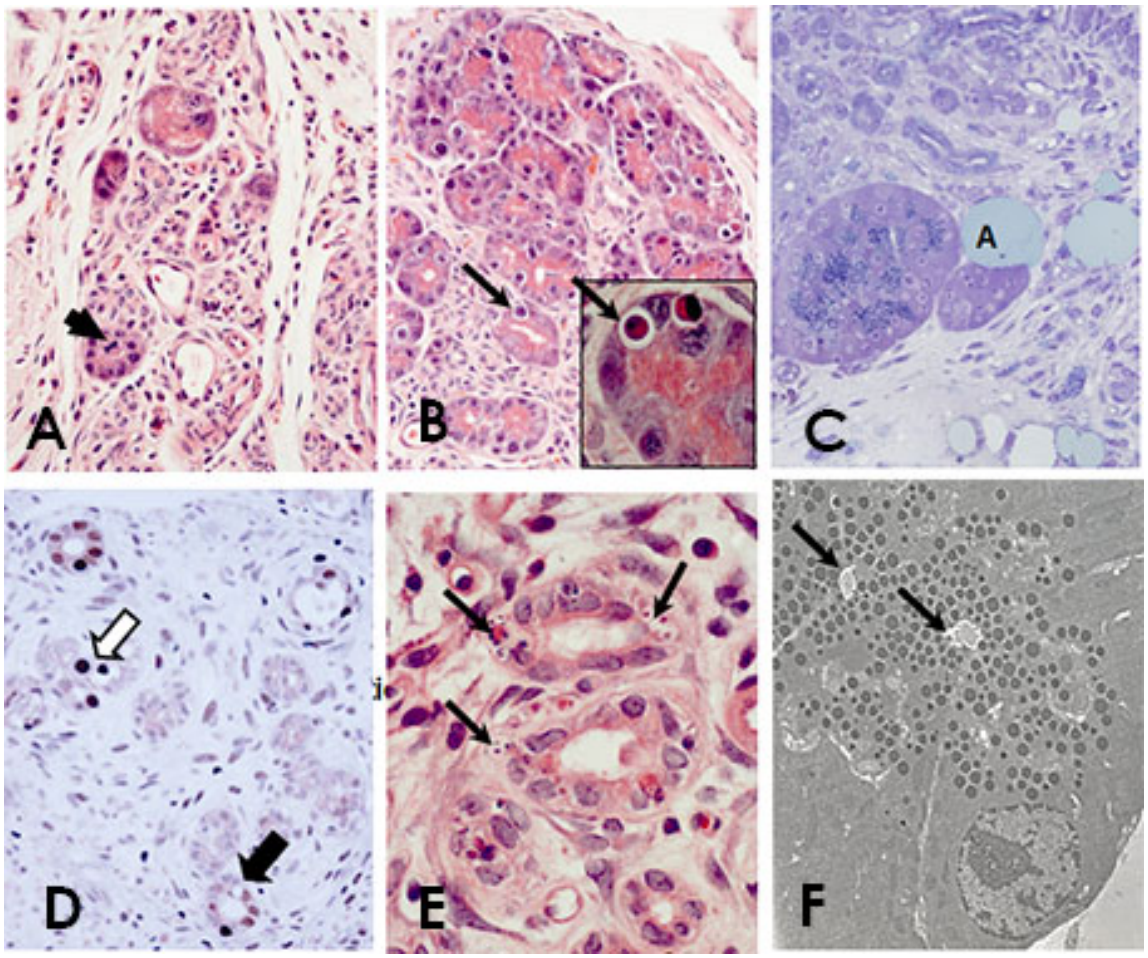

Figure 3.10 Regeneration in the CHB model

A. CHB day 10, small clusters of acinar cells with eosinophilic zymogen granules and intense purple nuclei stand out amongst residual tubular complex cells, arrow =mitosis. Haematoxylin and eosin (H&E) x 400. **B**. CHB day 12, Many of the regenerative acini at this time point are undergoing apoptosis at the same time as the acini are regenerating (arrows). The insert depicts a typical regenerating acinus with eosinophilic luminal cytoplasm and intensely stained nuclei as well as apoptotic nuclei, H&E x 400, insert x1000. **C**. CHB day 16, complete acinus on edge of lobule. Regenerating acini were often closely aligned with adipocyte formation. A=adipocyte. Toluidine blue semi-thin epoxy resin, x1000. **D**. CHB day 7, cycling cells were prominent both in tubular complexes (black arrow) and acinar cells (white arrow). Proliferating cell nuclear antigen (PCNA) immunohistochemistry x400. **E**. CHB day 7, apoptosis was often quite extensive in tubular complexes (black arrows). H&E x1000. **F**. CHB day 18, acinus with large autophagic vacuoles (arrows) indicates that these cells may be undergoing damage. Electron microscopy x2500.

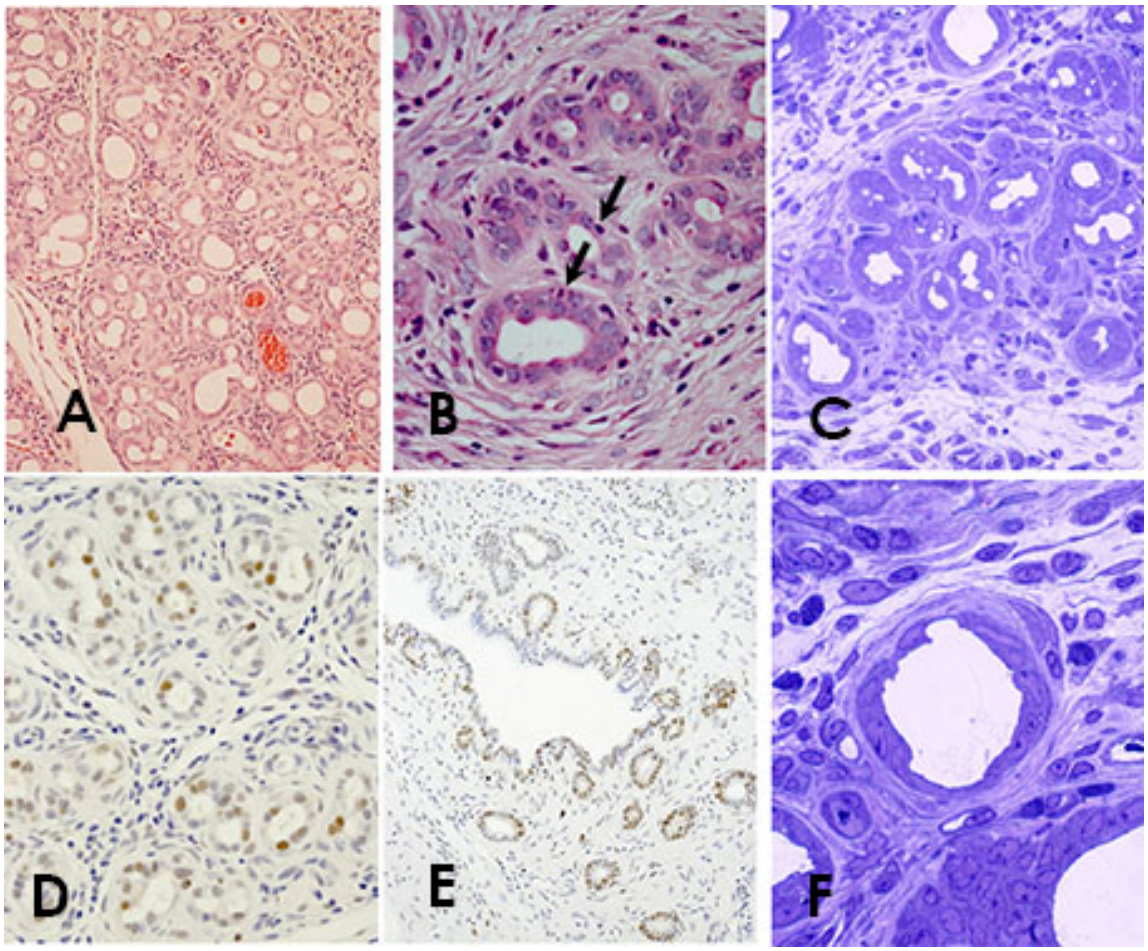

Figure 3.11 Regeneration in the duct ligation model

A. Duct ligation day 12, tubular complexes identified by their large lumens fill the tissue. No acinar cells can be seen. Haematoxylin and eosin (H&E) x200. **B**. Duct ligation day 10, apoptosis (arrows) in tubular complexes. The fibrous inflammatory infiltrate is prominent H&E x1000. **C**. Duct ligation, tubular complexes and fibrotic infiltrate remain, Toluidine blue x400. **D**. Duct ligation day 18, cycling cells are prominent in the tubular complexes. Proliferating cell nuclear antigen (PCNA) immunohistochemistry (IHC) x 200. **E**. Duct ligation day 16, large ducts also show increased cycling, interlobular duct. PCNA IHC x200. **F**. Duct ligation day 18, tubular complex with extended lumen and flattened, elongated lining cells. The inflammatory infiltrate is closely packed with collagen deposition stellate cells and macrophages. Stellate cells are also closely aligned with the tubular complex. Toluidine blue x1500

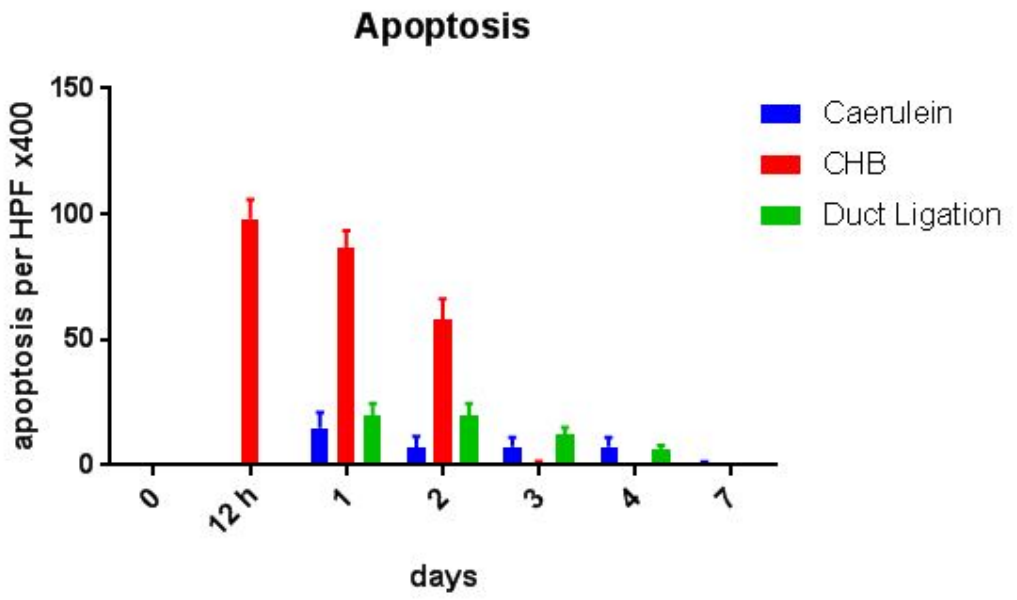

Figure 3.12 Mean ± SEM of counts of apoptosis for the three models

Apoptosis was counted in 10 random fields at x400 magnification of one 4µm thick section of whole pancreas per rat per time point. Data are the mean ± SEM of four rats (n=4) per time point from one experiment per model. Compared with untreated controls (Time 0) where negligible apoptosis was found, all models had significantly increased apoptosis, but at varying periods of time after the cause of pancreatitis. The CHB model had massive apoptosis over 12 hrs, 1 and 2 days but this disappeared from 3 days. While caerulein and duct ligation had a much lesser incidence of apoptosis compared with CHB, the incidence in caerulein was visible to 3-4 days, and the incidence with duct ligation to 5 days (barely visible on graph). One way ANOVA was used to compare apoptosis counts between the experimental groups. Tukey's multiple comparison test was used to compare individual groups. Apoptosis counts were significantly higher than controls in the caerulein, CHB and duct ligation models at days 1-2 ($P=0.0002$, $P<0.0001$, $P<0.0001$, respectively) and day 4 ($P<0.0001$, $P<0.0001$, $P<0.0001$, respectively).

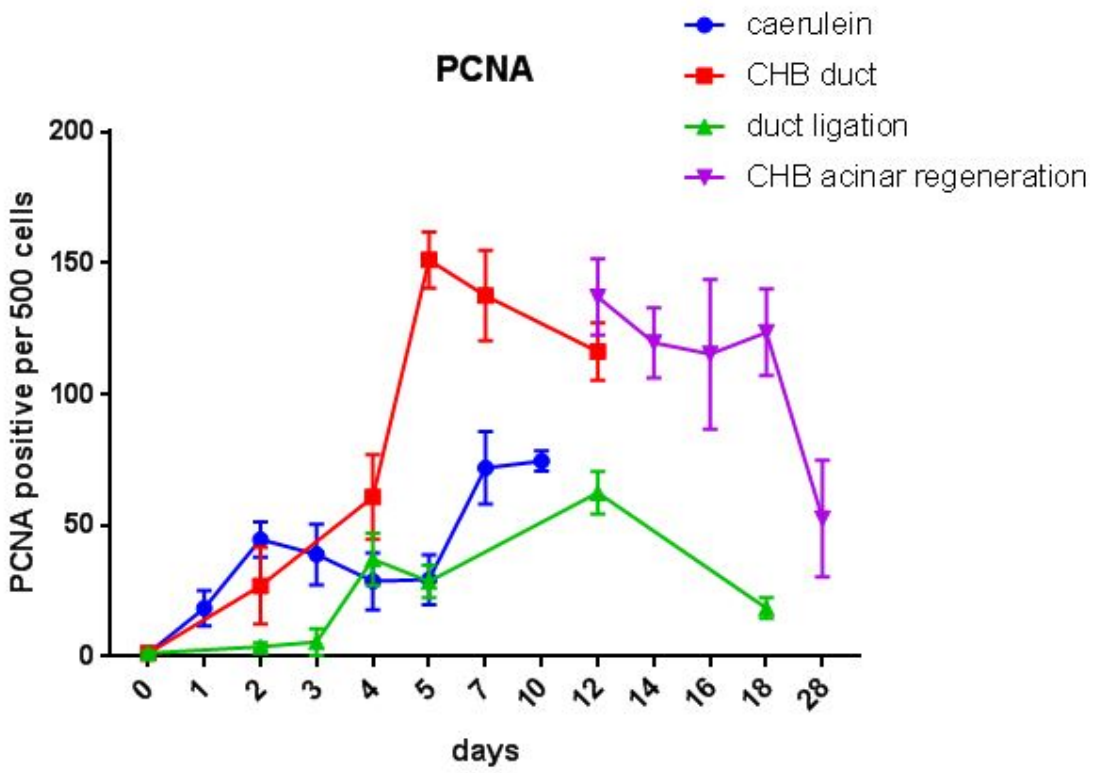

Figure 3.13 Mean ± SEM of cell proliferation measured by PCNA immunohistochemistry

Single nuclei stained for PCNA were counted in five to ten random fields at x200 magnification of one 4µm thick section of whole pancreas per rat (n=4) per time point. The number of fields counted varied with regard to reduced parenchyma at atrophic time points. Data are the mean ± standard error of the mean (SEM) of four rats (n=4) per time point for one experiment per model. Error bars represent the SEM. The graphs demonstrate cells that are undergoing cycling. In the caerulein model, acinar cells were regenerating until experimental end at 10 days. The CHB model had duct cell regeneration up to 12 days when acinar cell regeneration started then declined by end of experiment. With the duct ligation model, duct cells were proliferating from 3 days to end of experiment at 18 days, with decreasing incidence from day 12. One way ANOVA was used to compare PCNA expression in control groups versus experimental groups. Tukey's multiple comparison test was used to compare individual groups. PCNA expression in the caerulein, CHB and duct ligation models was significantly higher than controls at days 2, 4 and 7 (day 2, $P<0.0001$, $P<0.0001$, $P<0.0004$, respectively; day 4, $P<0.0001$, $P<0.0001$ $P<0.0001$, respectively; and day 7, $P<0.0001$ $P<0.0001$, $P<0.0001$, respectively).

3.4 DISCUSSION

This chapter shows the results of three models of pancreatitis produced experimentally in rats to understand the pathology and the cell biological and pathophysiological disease mechanisms and, eventually, as a step towards developing targeted therapies. The rat models were developed to reflect specific changes of human acute and chronic pancreatitis. Data relating to the molecular mechanisms of the disease are presented in later Chapters.

Although the timelines differed slightly, the models of caerulein, CHB and duct ligation successfully produced a mild pancreatitis with the mode of cell death as apoptosis. This was followed by fibrosis deposition with inflammatory cells prominent and differences in regeneration. Pancreatic atrophy in the caerulein model occurred randomly. In all rats the whole pancreas and every lobule was disturbed however there was considerable variation between the lobules from partial to complete atrophy that also varied between animals. In every rat pancreas there remained some viable acini. Loss of acinar cells by apoptosis, generation of tubular complexes, loss of tubular complexes and regeneration of acinar cells proceeded in concert. In the CHB model there was consistency between animals and the whole process seemed sequential. Acinar cells appeared to be completely absent from the lobules following apoptosis and re-emerged as small islands of regeneration later amongst tubular complexes. Compared with the caerulein model this was a slower process and regenerative acini in general often had a different appearance. In H&E sections the nuclei were larger and the cytoplasm was more intensely coloured as if the acinar cells were forming. Apoptosis occurred in the duct ligation model in a similar manner to caerulein, with one to several apoptotic cells visible in each acinus at any one time. However, in this case all of the acinar cells disappeared and no regenerating acini were seen. Tubular complexes were the only epithelia that remained in the fibrotic stroma. These models produce a mild pancreatitis with loss of acinar tissue. The inflammatory infiltrate proceeds to the deposition of fibrosis as may occur in humans. It is vitally important to elucidate the processes that lead to successful regeneration after fibrotic deposition in pancreatitis.

Most current knowledge of the pathogenesis of pancreatitis comes from animal studies as the human pancreas is relatively inaccessible especially in the early stages of the disease. Commonly used animal models focus on rodents and although widely used they have failed to produce noticeable clinical benefits. No model fully reproduces the human disease and each model has its advantages and disadvantages. Shortcomings aside, animal models are necessary for understanding the pathophysiology of this disease. It is unclear and possibly questionable if caerulein and CHB are clinically relevant stimulants in humans though the duct ligation model mimics gallstone obstruction

pancreatitis. The question addressed is of importance and in this case the generic models allow the study of specific elements common to the pancreatic disease. By comparing more than one model and the mechanisms by which they differ this analysis will progress our understanding of pancreatitis.

CHAPTER 4
FIBROSIS IN RAT PANCREATITIS

4.1 INTRODUCTION

Pancreatic fibrosis is a characteristic histopathological feature of many types of human pancreatitis including alcoholic, hereditary, autoimmune, idiopathic and tropical and obstructive chronic pancreatitis where it deposits in interlobular and periductal spaces.[7] It is typified by proliferation of connective tissue consisting mostly of densely packed ECM. Initially, pancreatic injury which involves the interstitial mesenchymal cells, the duct or the acinar cells leads to necrosis or apoptosis of parenchymal cells. These death processes, and immigrating inflammatory cells, release cytokines, growth factors and chemokines which in turn stimulate pro-fibrotic stellate cells of the pancreas (PSC) to activate, proliferate and migrate to the area of injury.[223] Activated PSC synthesise significant amounts of ECM, in particular collagens that are deposited in interstitial spaces.[135] In normal pancreas, quiescent PSC are in low numbers, possess vitamin A containing fat droplets and stain negative for αSMA. When activated, they lose the lipid droplets, enlarge and proliferate and stain positive for αSMA. They then increase secretion of ECM including collagens I and III and laminin, under the influence of molecular signalling pathways and cytokines released from recruited inflammatory cells.[130] In pancreatic pathology, the normal cell populations may be replaced by fibrosis, leading to both exocrine and endocrine deficiency. Accumulation of matrix leading to pancreatic fibrosis depends on an imbalance between ECM synthesis and degradation. PSC regulate this balance, however the role of other inflammatory cells such as macrophages and mast cells is not clear. As the three rat models of pancreatitis developed fibrosis and underwent different regenerative outcomes (Chapter 3), they have the potential to provide a good basis for comparison of the interactions between fibrosis and regeneration in pancreatitis.

4.1.1 Aim

The aim of this Chapter was to determine whether fibrosis in the three models of pancreatitis in rats followed a similar course with respect to inflammatory cell populations. The interaction of the PSC and other inflammatory cells (macrophages, mast cells) in the process of initiating, maintaining and degrading fibrosis was of particular interest.

4.2 MATERIALS AND METHODS

General materials and methods for this Chapter can be found in Chapter 2. Collagen stained histochemically by Puchtler's Sirius red (Appendix 1) was compared with an objective and quantitative scoring system of digital capture and image analysis of the histopathology. Comparison of collagen I and III was achieved by using a polarizing filter to visualise the birefringent collagen. Activated PSCs, mast cells and macrophages were identified by light and EM and IHC.

4.3 RESULTS – FIBROSIS AND STELLATE CELLS IN PANCREATITIS

4.3.1 Control pancreas for fibrosis studies

In the normal pancreas, the exocrine lobules are delineated by a thin line of connective tissue in the interlobular space and around ducts and blood vessels **(Figure 4.1A).** At a higher power the small amount of collagen was evident in the space between an intralobular duct and an acinus. The BM was closely attached to the cells **(Figure 4.1B).**

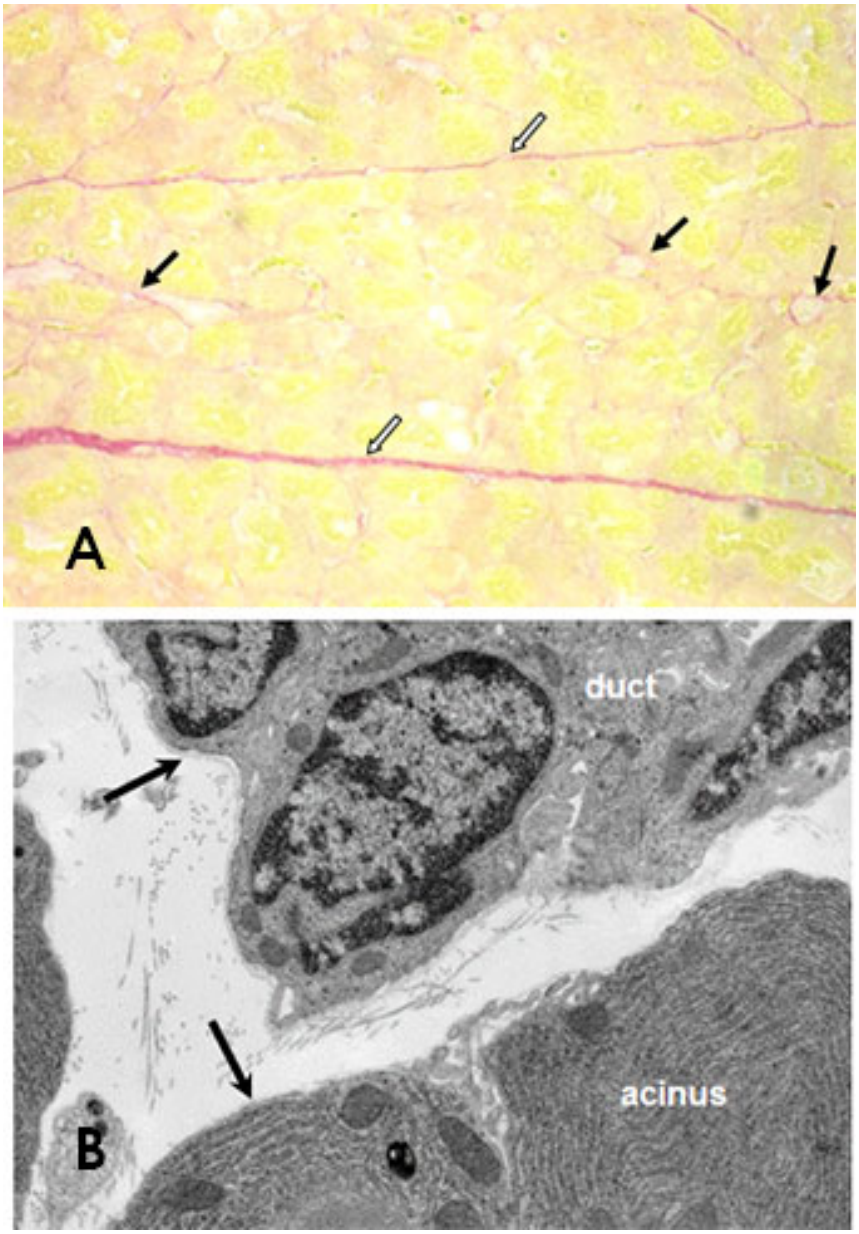

Figure 4.1 Fibrosis in the control rat pancreas

A. Collagen is indicated by the red staining of Puchtler's Sirius red. It shows fine threads of collagen in between acini and delineates the lobules which are closely aligned. Interlobular connective tissue (white arrows), blood vessels (black arrows). Red = collagen, yellow = parenchyma; Puchtler's Sirius red x400. **B**. Acinus and intralobular duct with small amounts of deposited collagen in the interstitial space. The basement membrane is a thin line along the extremities of the cells. Arrows = basement membrane. Electron microscopy x15000.

4.3.2 Fibrosis in the rat models

The different timelines demonstrated in the photomicrographs of **Figure 4.2** are used for specific features and as a comparison of fibrosis development in the different models. **Figures 4.2A-I** show the progression of fibrotic deposition through the course of the pancreatitis.

The increase in deposition of collagen occurred earlier in the caerulein model. Apoptotic acini were clearly delineated by fine strands of collagen as early as day 1 whereas in the CHB and duct ligation models at days 2-3 oedema was present and fibrosis was limited to wispy intralobular strands and intralobular ducts **(Figures 4.2A-C).**

By days 4-5, the caerulein model had reached the peak of fibrosis. Tubular complexes were surrounded by distinct wavy collagen, collagen was dense around intralobular ducts and ample in intralobular areas, wispy in interlobular areas **(Figure 4.2D).** By day 7 in the caerulein model, when acinar regeneration was widespread, collagen deposition was partially but not totally resolved. Collagen deposition was thin around newly formed acini but remained as wavy, thick strands in intralobular spaces and surrounding intralobular ducts **(Figure 4.2G)**.

By day 4 in the CHB model and day 7 in the duct ligation model, collagen deposition was approximately similar to that of the caerulein model (**Figures 4.2E,F).** In all models, the islets and nerves were surrounded by collagen but not infiltrated by collagen. Blood vessels were surrounded by dense collagen. From these times, collagen deposition in the CHB and duct ligation models increased in quantity and in density with thick, solid deposits around the tubular complexes and thick and wavy strands around intralobular ducts and in interlobular spaces **(Figures 4.2H,I).**

The collagen deposition remained around tubular complexes and interstitial areas in both CHB and duct ligation models until the end of the experiments. In the CHB model, where there was regeneration, fibrosis was sparse around the acinar bundles.

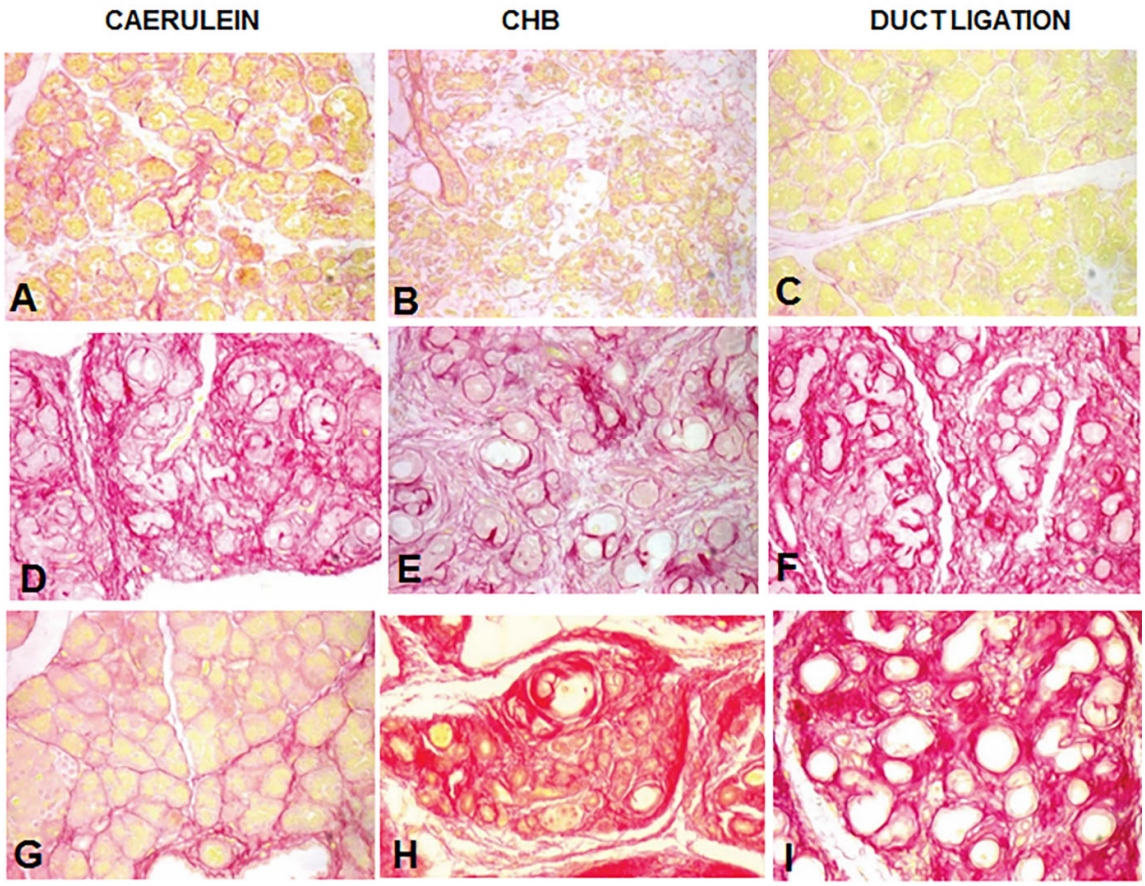

Figure 4.2 Collagen deposition in the rat models

Images show the deposition of fibrosis as collagen by Puchtler's Sirius red histochemistry. Collagen production is increased early compared with the controls in Figure 4.1. It progresses to being laid thickly around tubular complexes in each model, however regresses substantially in the caerulein model and remains thickly deposited in the others. Each experimental row depicts a comparable stage in the course of the pancreatitis for each model but not necessarily the same time point. All x200.

A, D, G. Caerulein, day 1, day 4, and day 7, respectively.

B, E, H. CHB model, day 2, day 4, and day 16, respectively.

C, F, I. Duct ligation, day 1, day 7, and day 18, respectively.

Polarised light was used to demonstrate how collagen deposition changed over time from green (collagen III) to yellow/red (collagen I), as the fibres became thicker and displayed more intensity. **Figure 4.3** shows the bright field image with the corresponding polarised light image. Vertical columns give examples for each of the models, with **Figures 4.3A-C** presenting the bright field images and **Figure 4.3D-F** presenting the corresponding fields under polarised light.

The type of collagen laid down varied in intensity and in type between the models **(Figure 4.4).** Early (days 1 and 4, **Figures 4.4A,D**) in the caerulein model and after regeneration (day 7, **Figure 4. 4G**), the collagen fibres were thin (green) around acinar cells. Blood vessels and ducts were easily seen as were occasional thicker strands **(Figure 4.4G).** At day 4 when tubular complexes were most prolific, collagen was a mixture of the collagen III type and the yellow colour of the denser strands of collagen I **(Figure 4.4D).**

CHB and duct ligation models showed similar patterns of collagen III early **(Figure 4.4B,C)** and a similar but more dense yellow/red colour as the lesion progressed **(Figure 4.4E,F)**. By the later stages, collagen visualised as predominantly collagen I (red). This occurred around tubular complexes, as interstitial collagen remained predominantly green as can be seen in **Figures 4.4H and I.**

Figure 4.5 compares the types of collagen deposited in a comparison between the three models. Collagen III was seen predominantly in the caerulein model, with CHB and duct ligation having mainly collagen I.

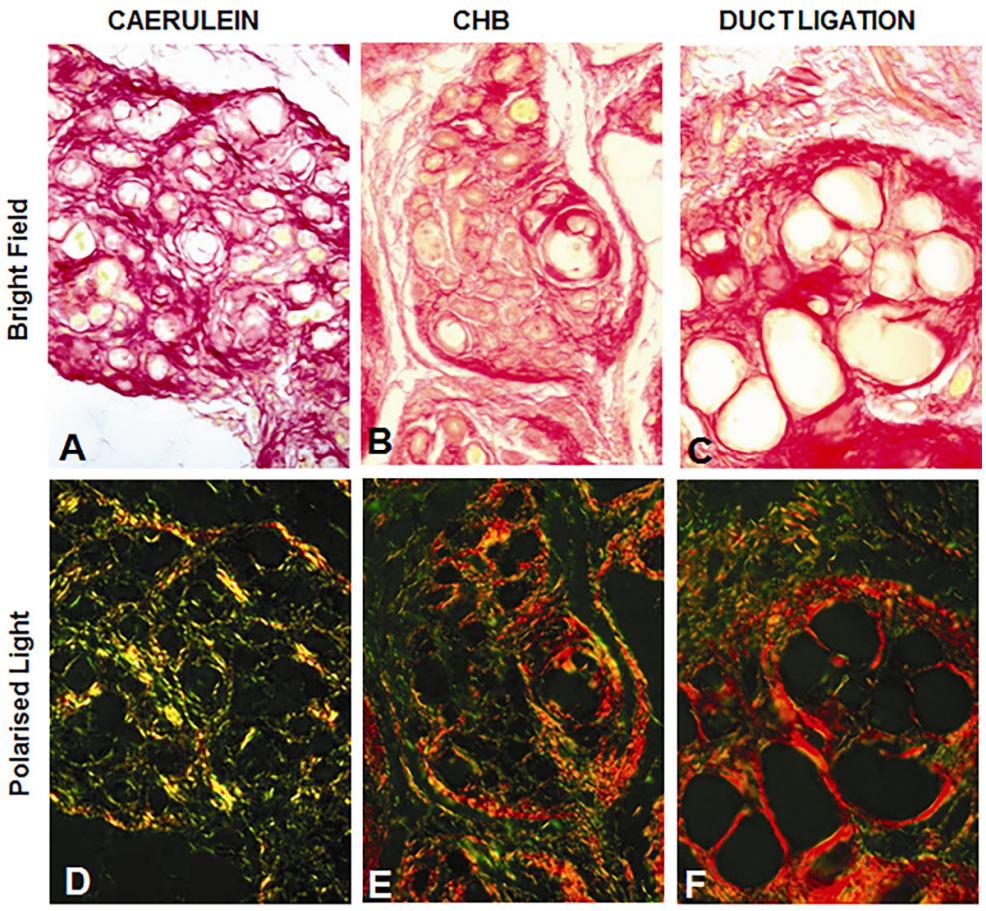

Figure 4.3. Comparison of bright field and polarised light images

Vertical columns are the same section example for each of the models. **A-C** present the bright field image, collagen=red, parenchyma=yellow. **D-F** demonstrate the corresponding field under polarised light. Collagen III=green, collagen I=yellow/red. Circular spaces portray the lumens of tubular complexes. Although the amount of deposited collagen looks similar in all models in the bright field images, the polarised light images show that the caerulein model has more green-coloured collagen III than the red of collagen I in the other two models. Puchtler's Sirius red is photographed under bright field and polarised light x400.

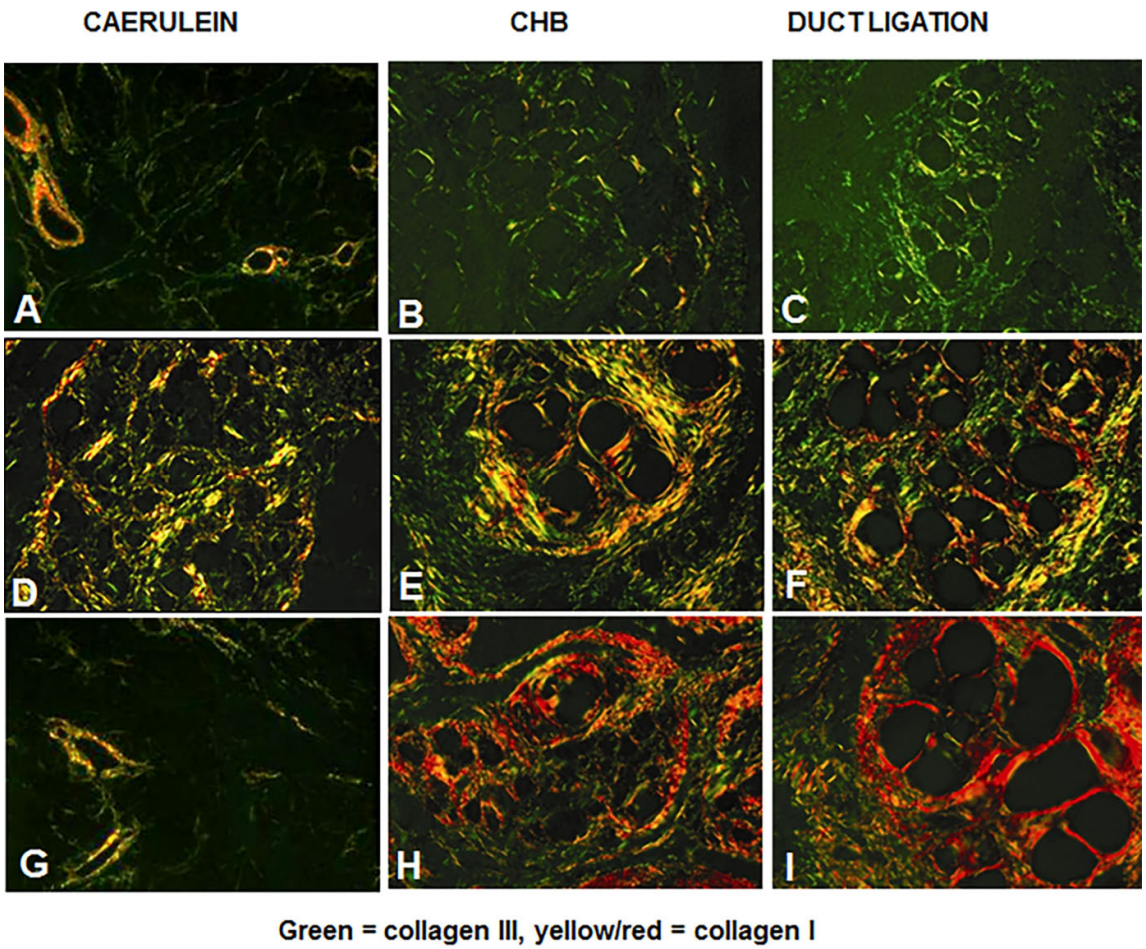

Figure 4.4 Polarised light images of collagen in the rat models

Vertical columns give examples for each of the models. Caerulein: **A** day 1, **D** day 4, and **G** day 7; CHB: **B** day 4, **E** day 14, and **H** day 16; Duct ligation: **C** day 4, **F** day 12, and **I**. day 18. Each experimental row depicts a comparable stage in the course of the pancreatitis for each model but not necessarily the same time point. Note how the progression of green collagen III deposition changes to collagen I deposition in the CHB and duct ligation models but does not progress to considerable amounts of collagen I in the caerulein model and regresses by day 7. Collagen III=green, collagen I=yellow/red. Puchtler's Sirius red is photographed under polarised light. All x400.

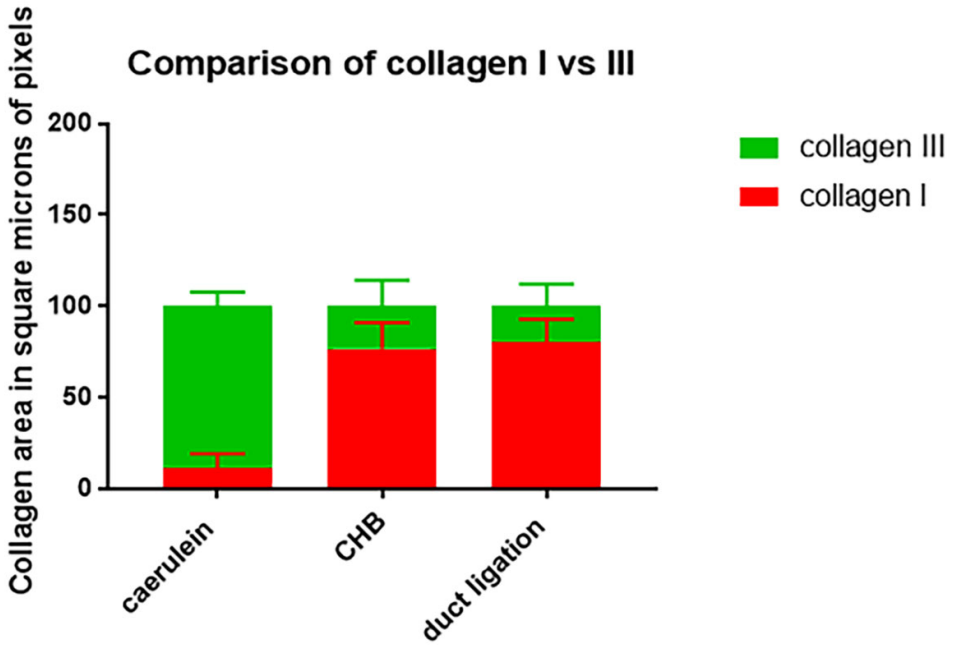

Figure 4.5 Comparison of the types of collagen deposited in the three models

Five fields of 50µm^2 of defined pixels were counted at x400 magnification for each 4µm thick section of whole pancreas for the time point of comparable collagen deposition between the models: caerulein and duct ligation day 4, CHB day 5. Data are the mean ± SEM of four sections (n=4) per time point for one experiment per model. Error bars represent the standard error of the mean. Collagen III was seen predominantly in the caerulein model, with CHB and duct ligation having mainly collagen I. One way ANOVA was used to compare the area of collagen III to collagen I between the experimental groups. Tukey's multiple comparison test was used to compare individual groups. Collagen III was significantly increased in the caerulein model compared to CHB and duct ligation ($P<0.0001$, $P<0.00010$, respectively). The CHB and duct ligation models were not significantly different from one another ($P=0.5430$). Collagen I was significantly increased in the CHB and duct ligation models compared to the caerulein model (($P<0.0001$, $P<0.00010$, respectively). The CHB and duct ligation models were not significantly different from one another ($P=0.5431$).

Using light microscopy and IHC and under EM, a comparison is made of structural similarities and differences for fibrosis in the three models. From day 1 in the caerulein model, collagen was deposited beside acinar cells undergoing apoptosis. This occurred earlier than in the other models **(Figure 4.6A)**. By day 4 when there were few acinar cells left, the collagen deposition increased around tubular complexes as the complexes became surrounded by PSC **(Figure 4.6B**). As apoptosis and acinar atrophy occurred BM became disrupted and folded. By day 4 remnant BM, immature and mature collagen fibrils were mixed in the interstitial space **(Figure 4.6C,D).** As regeneration occurred collagen levels around acini returned to near normal levels, however around ducts collagen was still obvious **(Figure 4.6E,F).**

During secondary necrosis negligible collagen was deposited in the CHB model **(Figure 4.7A)** however as tubular complexes formed more and more was laid down around them as typical long strands with striations **(Figure 4.7B).** By day 14, the interstitial space was distended with ECM. This was particularly obvious around tubular complexes **(Figure 4.7C).**

In the duct ligation model, the accumulation of ECM was aligned with the removal of acinar debris and the formation of tubular complexes (**Figures 4.8A-D**). From then, as tubular complexes persisted so did the level of fibrosis **(Figures 4.8C,D).** In the CHB and duct ligation models **(Figure 4.7 and 4.8)**, no collagen was laid down in the adipose tissue.

Figure 4.9 demonstrates patterns of fibrosis. Positive pixel counts of the red colour of Puchtler's Sirius red was measured as an approximate estimate of fibrosis. The different timelines for the three models relates to the progression of fibrosis in the three models. In caerulein, fibrosis peaked at 4 days then decreased. In CHB and duct ligation models, a similar pattern of fibrosis development was seen.

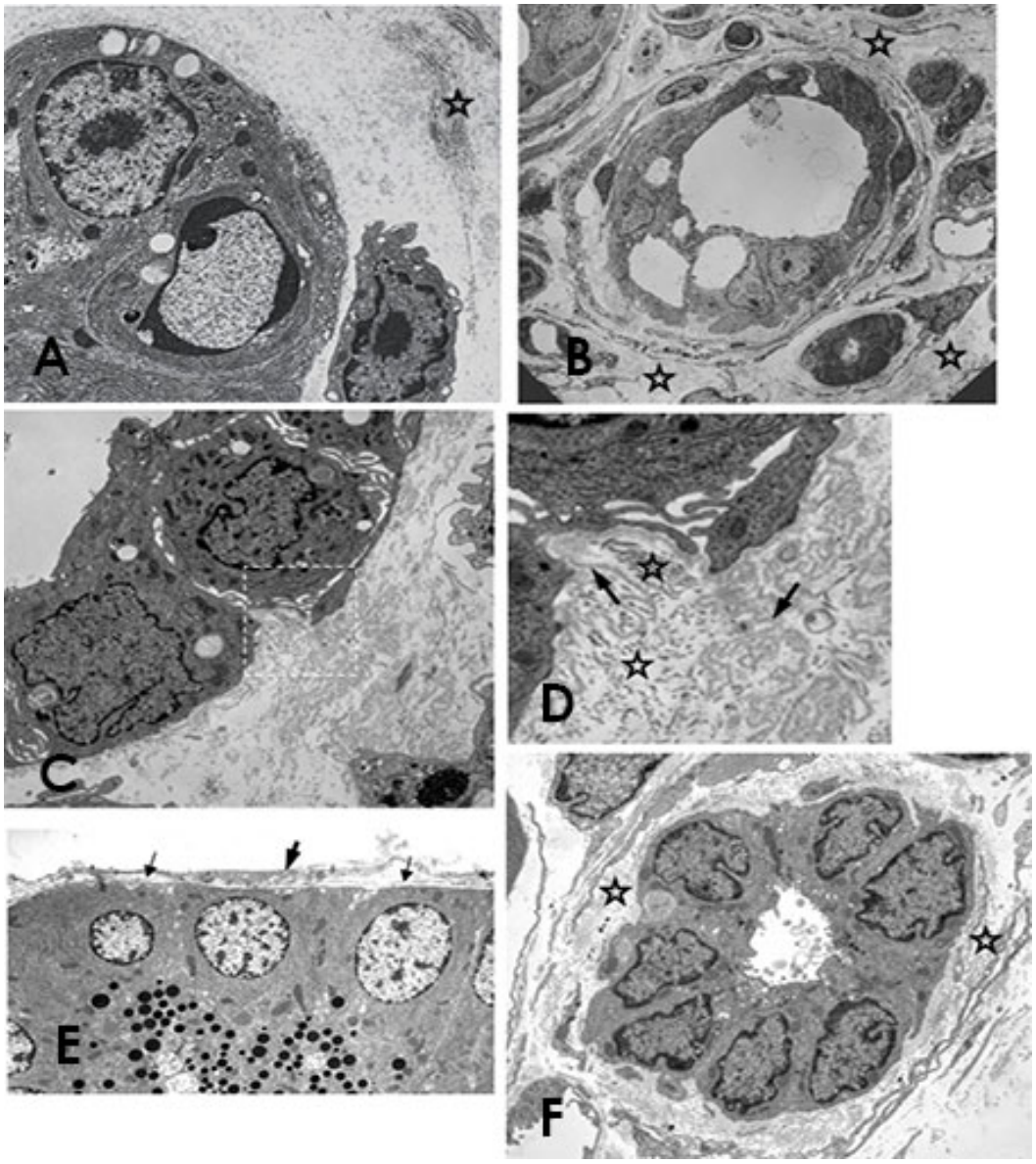

Figure 4.6 Fibrosis in the caerulein model

A. These electron micrographs show how in the collagen in the caerulein model is laid down early in thick swathes around tubular complexes but resorbs as regeneration occurs. Some areas of deposition remain after regeneration but this is mainly around ducts. Collagen deposit close to acinus, star=collagen, day 1, EM x4500. **B**. Tubular complex surrounded by collagen, day 4, EM x2500. C. Interstitial space next to a tubular complex is filled with collagen, day 4, EM x5000. **D**. Magnification of depicted area in **C**. Collagen appears as rods and in transverse (stars) with disrupted basement membrane (arrows), day 4, EM x10000. **E**. Regenerated acinar cells showing basement membrane (thin arrows) and the process of a stellate cell (thick arrow). Day 7, EM x4000. **F**. Intralobular duct showing collagen deposition (stars). Day 7 EM x4000.

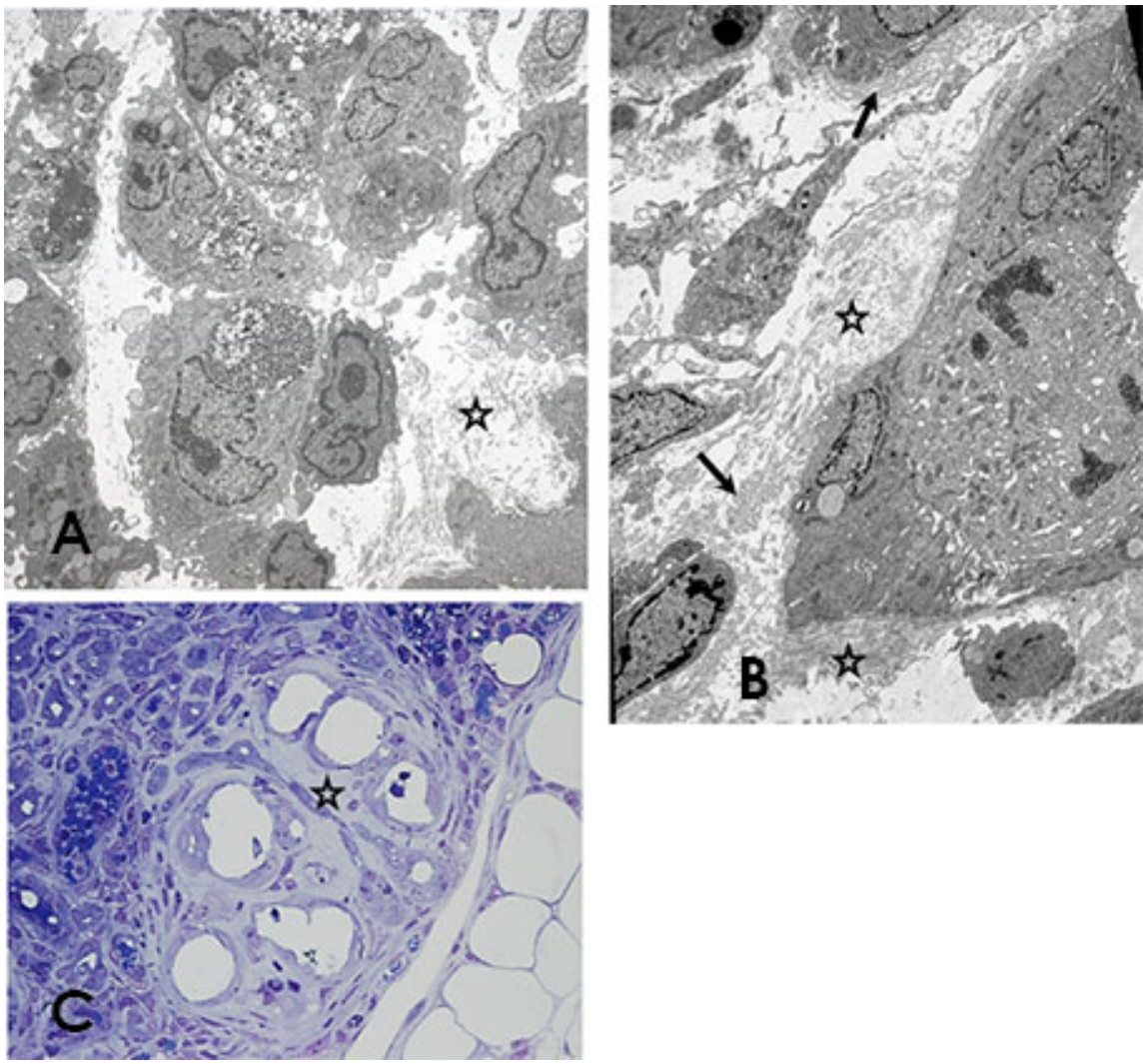

Figure 4.7 Fibrosis in the CHB model

In the CHB model, collagen is deposited thickly around and separating tubular complexes. This collagen does not regress and remains until the end of the experiment. **A** Collagen deposition, longitudinal and transverse. Day 3, EM x2500. **B**. Collagen deposits next to a duct cell in mitosis. Collagen=stars; basement membrane= arrows. Day 4, EM x2500. **C**. Collagen fills the interstitial spaces (star) surrounding tubular complexes. Day 14, toluidine blue x400.

Figure 4.7B is a cropped version of an electron micrograph from a publication by Kelly L, Reid L, Walker N. Massive acinar cell apoptosis with secondary necrosis, origin of ducts in atrophic lobules and failure to regenerate in cyanohydroxybutene pancreatopathy. Int. J. Exp. Path. (1999), 80, 217-226.[216.]

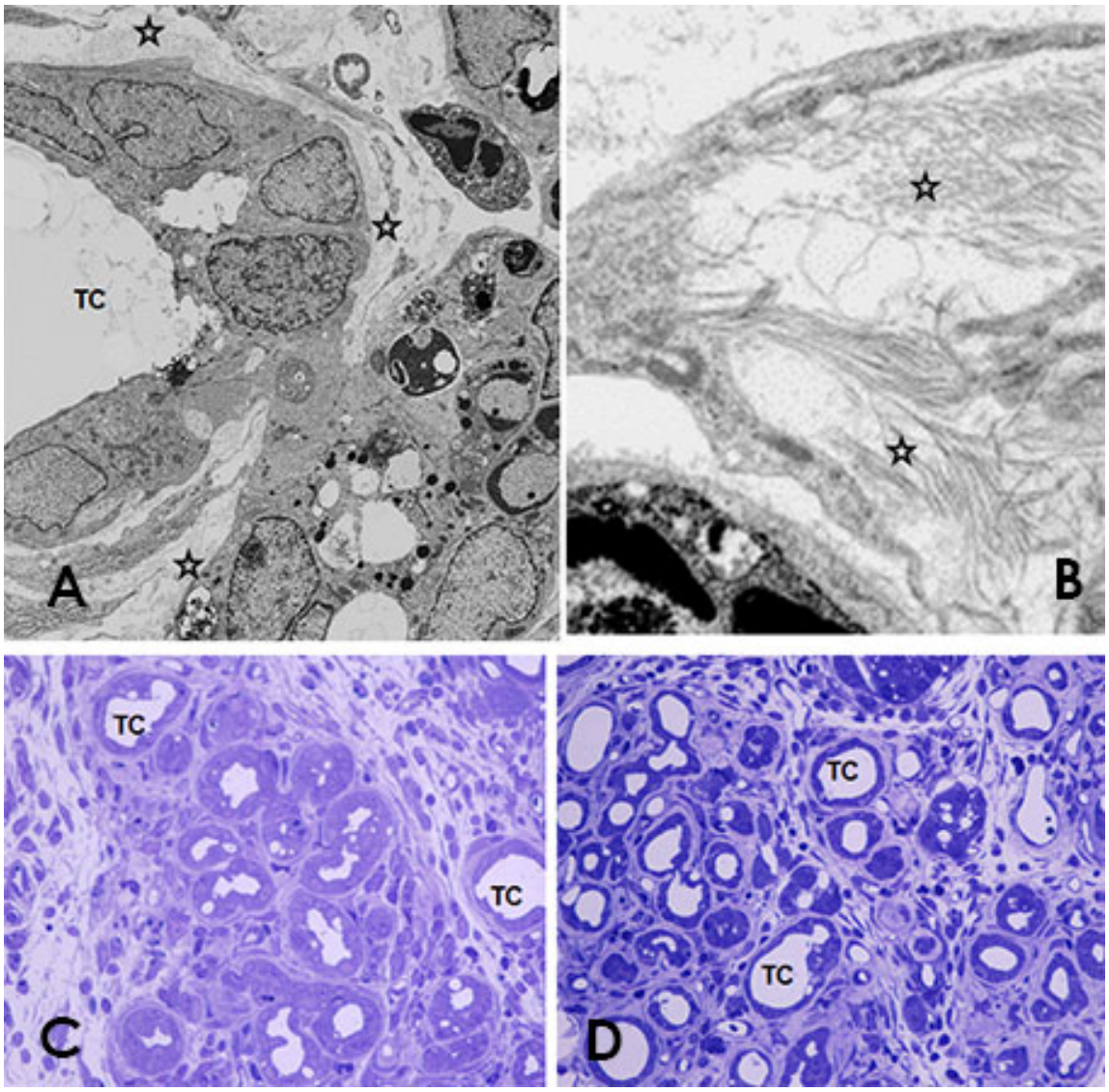

Figure 4.8 Fibrosis in the duct ligation model

Similar to the other models collagen is deposited thickly around tubular complexes in the duct ligation model. It surrounds and separates tubular complexes and fills the interlobular spaces along with supporting inflammatory cells. **A**. Collagen deposition in the interstitial space. Collagen=star, tubular complex=TC. Day 3 EM x2500. **B**. High power image of collagen seemingly emanating from a stellate cell. Collagen shown as longitudinal rods and in transverse (stars). Day 3, EM x8000. **C.** and **D**. Fibrosis between tubular complexes shown as opaque colouring compared to the white lumens of the tubular complexes (TC). **C** = day 10; **D** = day 18. Toluidine blue x400.

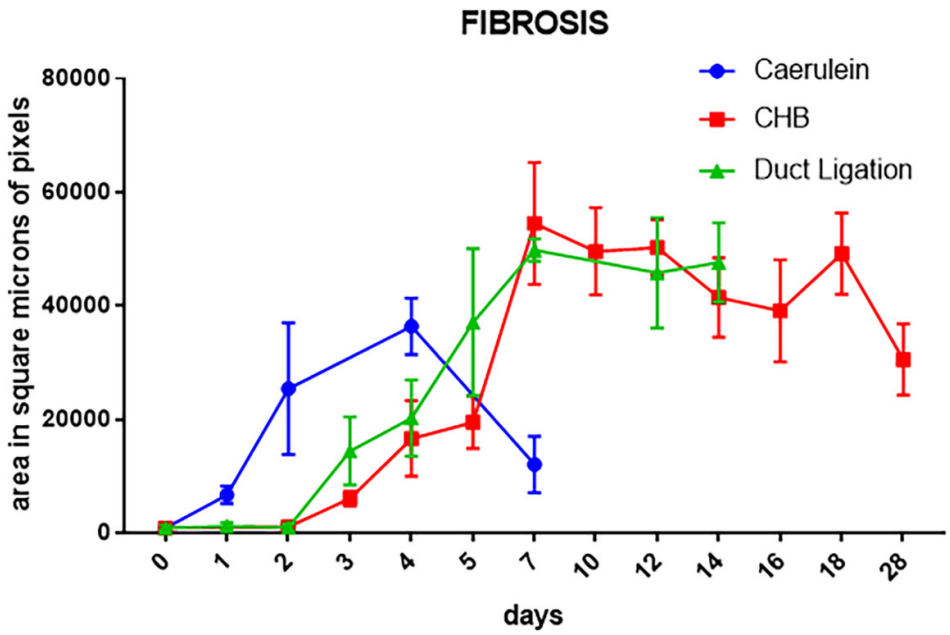

Figure 4.9 Mean ± SEM of estimate of fibrosis for the three models

Five to ten random fields of 50µm^2 of defined pixels were counted for one 4µm thick section of whole pancreas per rat per time point. The number of fields chosen varied with regard to reduced parenchyma at atrophic time points. Data are the mean ± SEM of four rats (n=4) per time point for one experiment per model. Error bars represent the standard error of the mean. The different timelines for the three models relate to the progression of fibrosis in the three models. In caerulein, fibrosis peaked at 4 days then decreased. In CHB and duct ligation models, a similar pattern of fibrosis development was seen. One way ANOVA was used to compare the area of Puchtler's Sirius red staining in control groups versus experimental groups. Tukey's multiple comparison test was used to compare individual groups. Sirius red expression in the caerulein model was significantly higher than in the control group at day 2 ($P<0.0001$) but not significant at day 4 ($P=0.9648$) and day 7 ($P=0.9996$). In the CHB model, it was not significantly changed at day 2 ($P=0.0783$) but was significantly higher than controls at days 4 and 10 ($P<0.0001$ $P<0.0001$, respectively). The duct ligation model was significantly higher for days 2, 4 and 10 ($P<0.0001$; $P<0.0001$ $P<0.0001$, respectively). At day 18 both CHB and duct ligation models were significantly higher than controls for Sirius red expression ($P<0.0001$).

Laminin IHC was used to investigate BM and ECM in the three models. There was progressive loss and disruption of the ECM in these models **(Figure 4.10).** Compared to the regular pattern of BM in the control image (**Figure 4.10A**), all three models showed considerable loss and disruption in early stages (**Figures 4.10B,C and D**). By day 4 in every model, the BM by laminin staining was disordered and thickened **(Figures 4.10E,-G),** as was seen in electron micrographs where BM appears folded and separated from the cell surface (**Figures 4.10D and 4.10B**). The laminin appears around tubular complexes randomly, with some surrounded thickly, some partially or thinly surrounded and some with a fuzzy appearance **(Figure 4.10F and at higher power in 4.10K).** Normal tissue such as blood vessels and pancreatic islets were not affected. In the caerulein model, by day 10 (**Figure 4.10H**) the BM has returned to a more normal appearance around acinar cells. In the other models (**Figures 4.10I,J**), with the persistence of tubular complexes, the BM remained denser.

4.3.3 Control pancreas stellate cells

Control pancreas stained for alpha-smooth muscle actin showed positive blood vessels but no activated stellate cells (**Figure 4.11A**). Electron micrographs show fibroblasts in high power and next to a normal acinus **(Figure 4.11B,C).**

4.3.4 Stellate cells in rat models

IHC of αSMA is demonstrated in **Figure 4.12** in the three models. Stellate cells activated by day 1 in the caerulein and duct ligation models, later in the CHB model probably due to the massive insult of apoptosis in this model compared to the others **(Figure 4.12A-C).** By day 4, stellate cells were prolific in all models **(Figure 4.12D-F).** When the caerulein model regenerated stellate cells disappeared **(Figure 4.12G).** This also occurred around regenerative acinar cells in the CHB model but not around tubular complexes **(Figure 4.12H)**. Tubular complexes in the duct ligation model remained surrounded by stellate cells **(Figure 4.12I)**.

A graph of the positive pixel counts for αSMA as an estimate of activated stellate cells is demonstrated in **Figure 4.13**. Staining of vessels by αSMA was not counted in these estimates. Similar to the figure for estimates of fibrosis (**Figure 4.5**), stellate cell area peaked earlier in the caerulein model than CHB or duct ligation, closely linking presence of stellate cells with development of fibrosis.

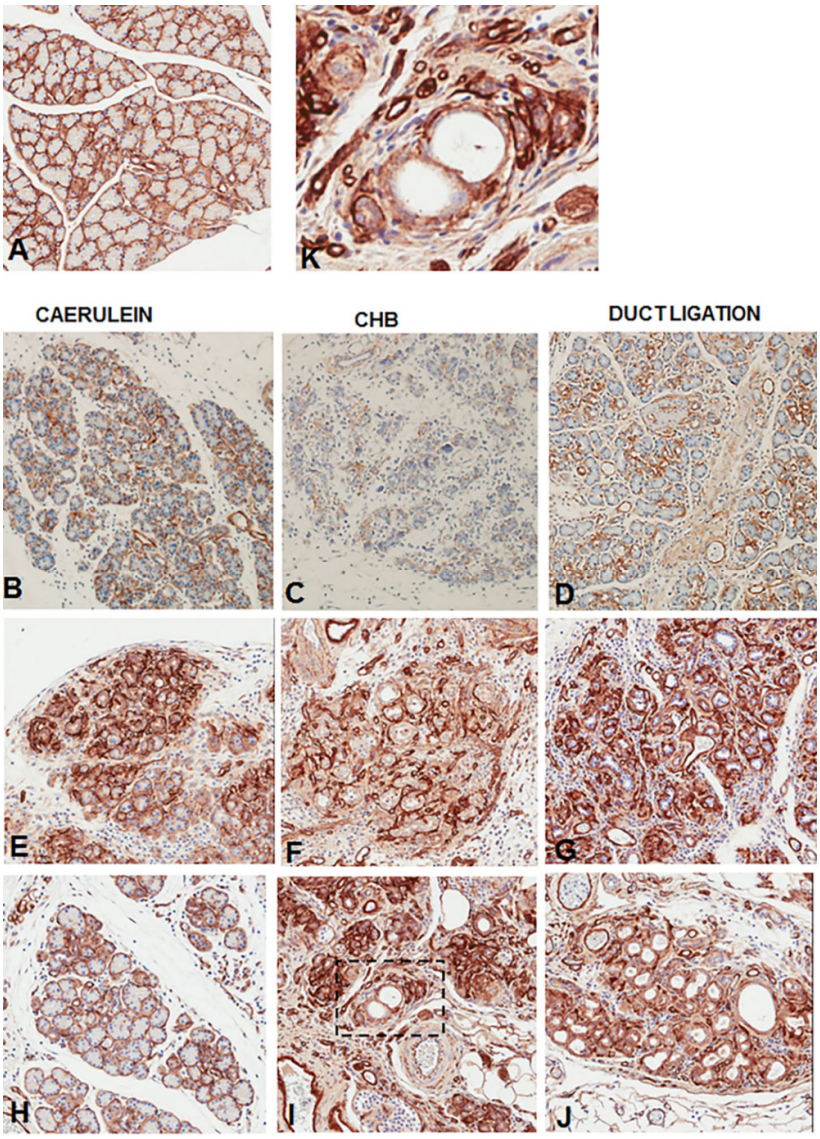

Figure 4.10 Laminin immunohistochemistry for basement membrane in the rat models

Images show basement membrane with positive brown staining for laminin using immunohistochemistry. Each experimental row depicts a comparable stage in the course of the pancreatitis for each model but not necessarily the same time point. Compared to the controls (Figure 4.10A), basement membrane of the treatments (brown staining) is much increased or disrupted. The disruption to the basement membrane is apparent in the caerulein model even at the stage of regeneration and very thickly evident in the other two models at the end of the experiment. All x200. **A.** Control section showing basement membrane surrounding normal acini. **B,E,**e,**H**. Caerulein **B.** day 1, **E.** day 4, **H.**) day 10. **C,F,I.** CHB **C.** day 2, **F**. day 4, **I**. day 18. **D,G,J**. Duct ligation **D**. day 2, **G**. day 4, **J**. day 18. **K**.) (Top right) High power image of selected area from 4.10I showing tubular complexes and normal ducts. Note: The caerulein experiment terminated on day 10 when tissue was almost completely regenerated. Duct ligation and CHB models were still proceeding at day 18 and were showing excess laminin positivity.

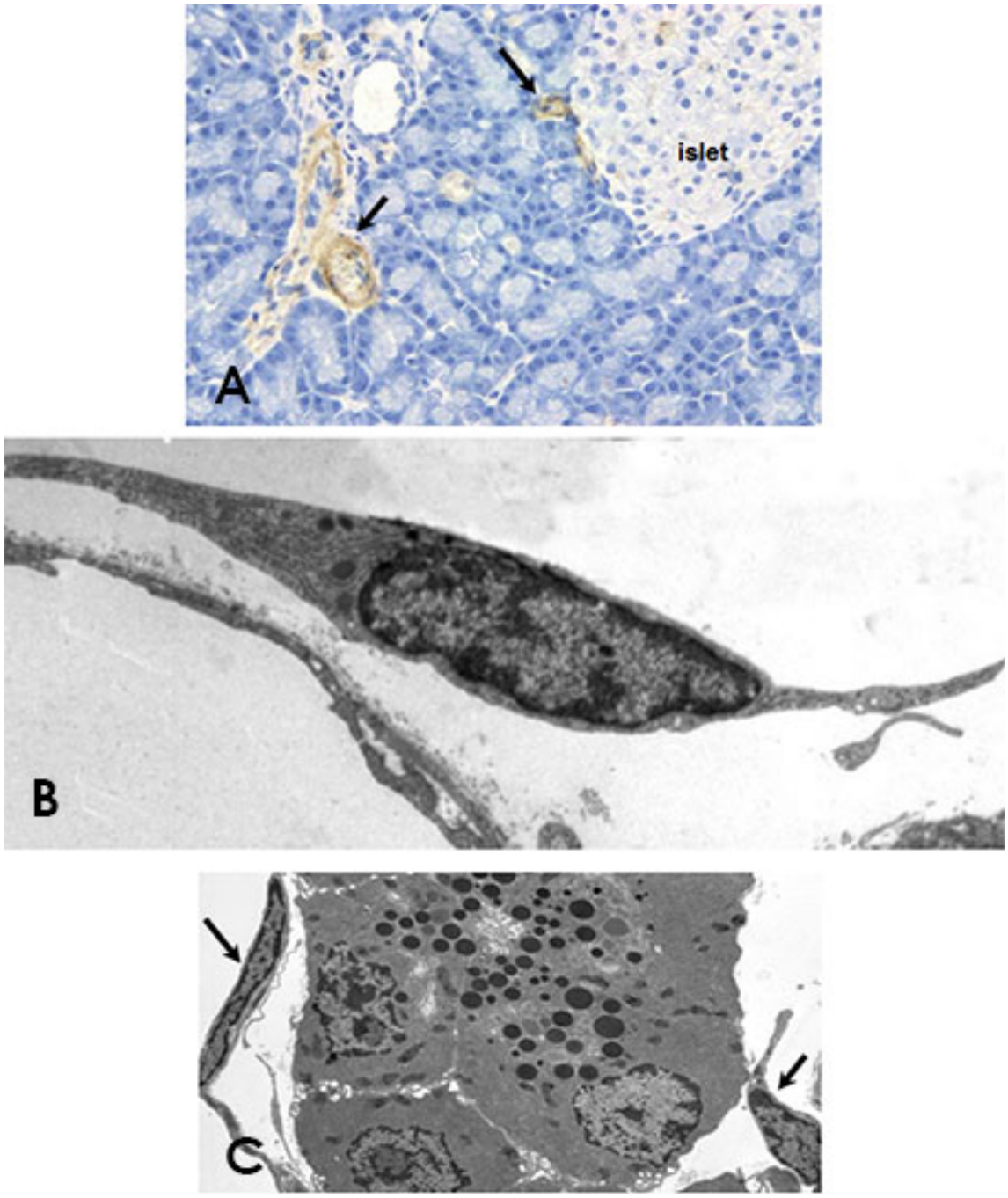

Figure 4.11 Stellate cells in control rat pancreas

Stellate cells do not stain positively for α-smooth muscle actin. The positivity in A is around blood vessels. Fibroblasts were difficult to find and identify in normal pancreas sections **A**. Control pancreas with α-smooth muscle actin immunohistochemistry for activated stellate cells. Arrows depict blood vessels. No stellate cells are seen. x400. **B**. Normal fibroblast from control pancreas. EM x1200. **C**. Normal acinus with fibroblasts (arrows). EM x3000.

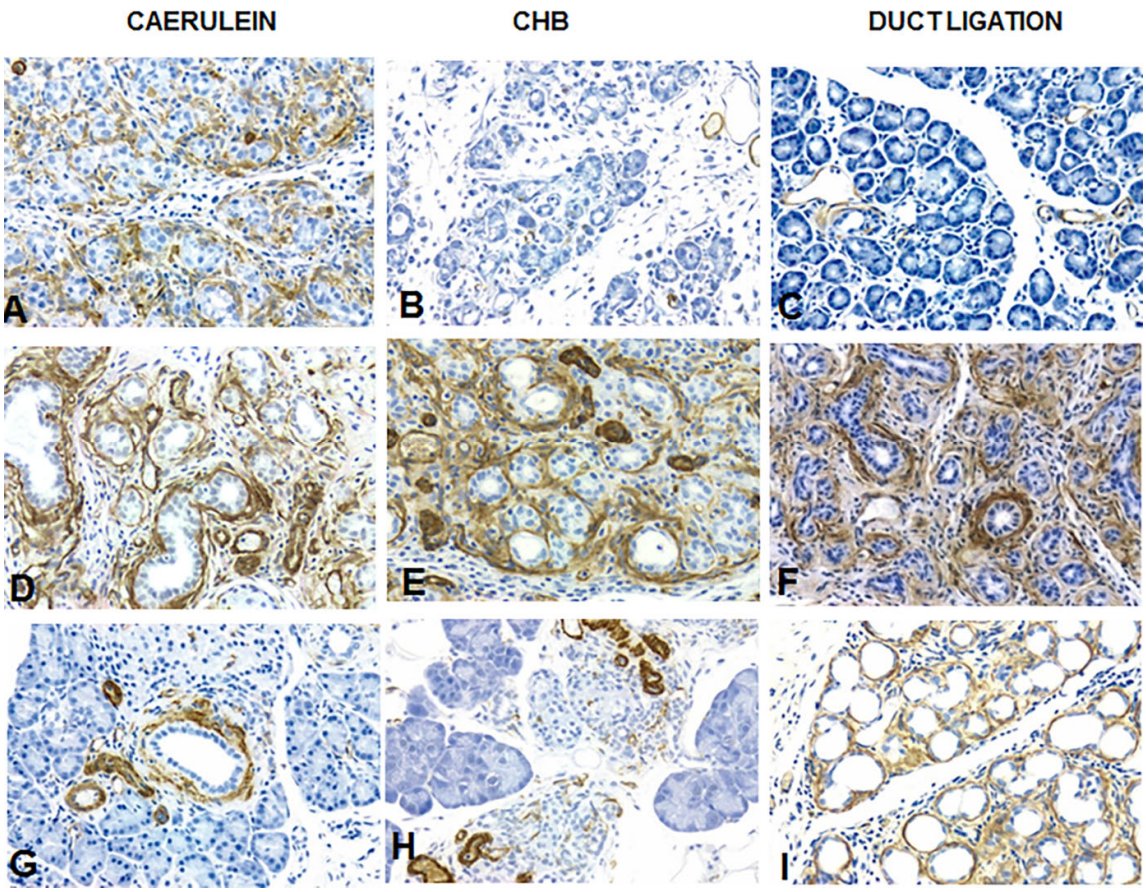

Figure 4.12 αSMA immunohistochemistry for stellate cells in the rat models

Images show positive brown staining for α-smooth muscle actin immunohistochemistry for stellate cells. Each experimental row depicts a comparable stage in the course of the pancreatitis for each model but not necessarily the same time point. Stellate cells activated earlier in the caerulein model than the other two models however they were soon very active particularly around tubular complexes where they remained in the CHB and duct ligation models. In areas of regeneration in the caerulein and CHB models stellate cells were scarce. All x400. **A,D,G**. Caerulein **A**. day 1, **D**. day 4, **G**. day 7. **B**,**E**,**H**. CHB **A**.day1, **E.** day 4, **H**. day 18. **C,F,I**. Duct ligation **C**. day 1, **F.** day 4, **I.** day 18.

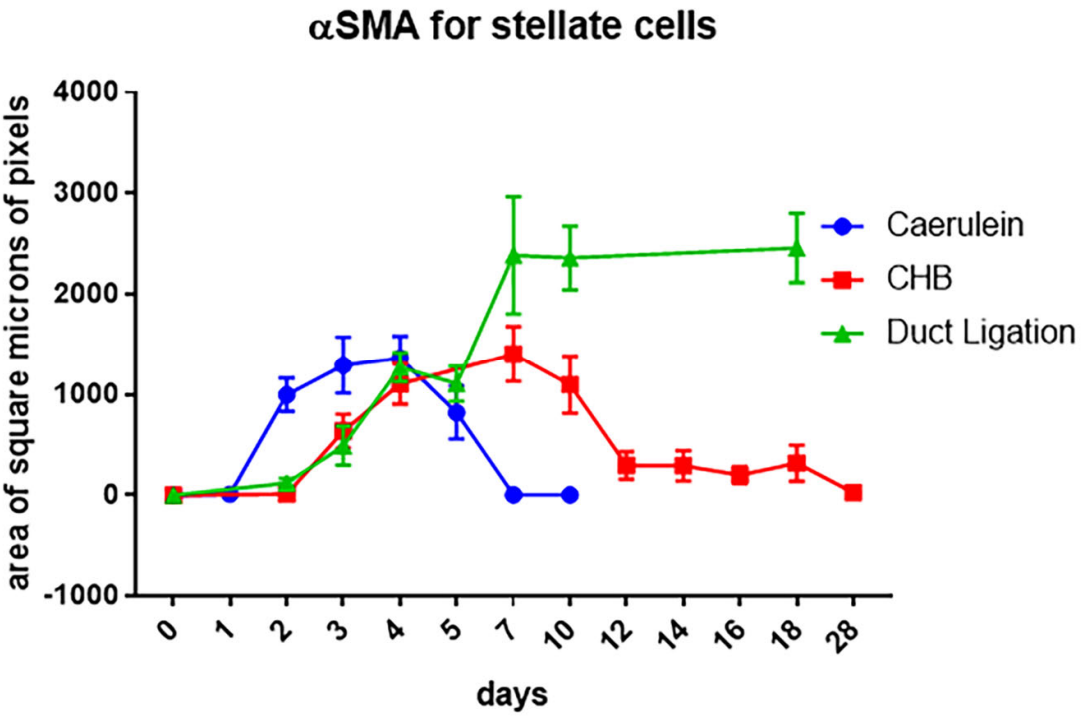

Figure 4.13 Estimate of activated stellate cell area using immunohistochemistry

Five to ten fields of 50μm^2 of defined pixels were counted at x400 magnification for one 4μm thick section of whole pancreas per rat (n=4), per time point. Fields were chosen randomly. The number of fields counted varied with regard to reduced parenchyma at atrophic time points. Data are the mean ± SEM of four rats (n=4) per time point from one experiment per model. Error bars represent the standard error of the mean. Positive pixel counts for αSMA are demonstrated as an estimate of activated stellate cells. Similar to the figure for estimates of fibrosis, stellate cell area peaked earlier in the caerulein model than CHB or duct ligation. Staining of vessels by αSMA was not counted in these estimates. One way ANOVA was used to compare the area of αSMA staining in control groups versus experimental groups. Tukey's multiple comparison test was used to compare individual groups. A-SMA expression in the caerulein model was significantly higher than in the control group at time points days 2 and 4 ($P<0.0001$, $P<0.0001$, respectively) but not at day 10 ($P=0.9999$). The duct ligation model was significantly higher compared to controls at days 2, 4, and 10 ($P<0.0001$, $P<0.0001$, $P<0.0001$, respectively). Staining in the CHB model was not significant compared to controls at day 2 ($P=0.9667$) but was significantly higher at days 4 and 10 ($P<0.0001$, $P<0.0001$, respectively). At day 18 both CHB and duct ligation were significantly higher than the control group ($P<0.0001$, $P<0.0001$, respectively) and also both significantly different compared to the caerulein model ($P<0.0001$, $P<0.0001$, respectively).

Electron micrographs and semi-thin sections in the caerulein model show the stellate cells producing collagen around acini and tubular complexes **(Figure 4.14).** Stellate cells have copious RER and when activating lose their lipid droplets (**Figure 4.14A**). The stellate cells were closely aligned to apoptotic acini with processes wrapped around cells and apoptotic bodies (**Figure 4.14B**). Collagen can be seen in close vicinity to the stellate cells such that immature and mature collagen fibres were mixed together **(Figure 4.14C).** By day 4 tubular complexes were tightly enclosed by stellate cells and their processes **(Figure 4.14D).** With almost complete regeneration stellate cells disappeared and stellate cells were inactive **(Figure 4.14C).**

Stellate cells were also activated in the CHB model as lipid droplets were extruded **(Figure 4.15A).** They were also closely aligned with tubular complexes **(Figures 4.15B,C)** becoming more tightly wound around them as the lesion progressed **(Figure 4.15D).** They were not around regenerative islands of acini or around adipose tissue but were in the interstitial space in the inflammatory infiltrate **(Figure 4.15E).**

The duct ligation model has a similar account with lipid droplets in the cell process **(Figure 4.16A)** and stellate cells and their processes in close proximity to apoptotic acini and tubular complexes **(Figure 4.16B,C,D).** In some cases the stellate cells were fewer however their processes remained encircling the tubular complexes **(Figure 4.16E). Figure 4.17** shows the extent of the stellate cells and their thin elongated processes producing collagen around an apoptotic body, acini and capillaries.

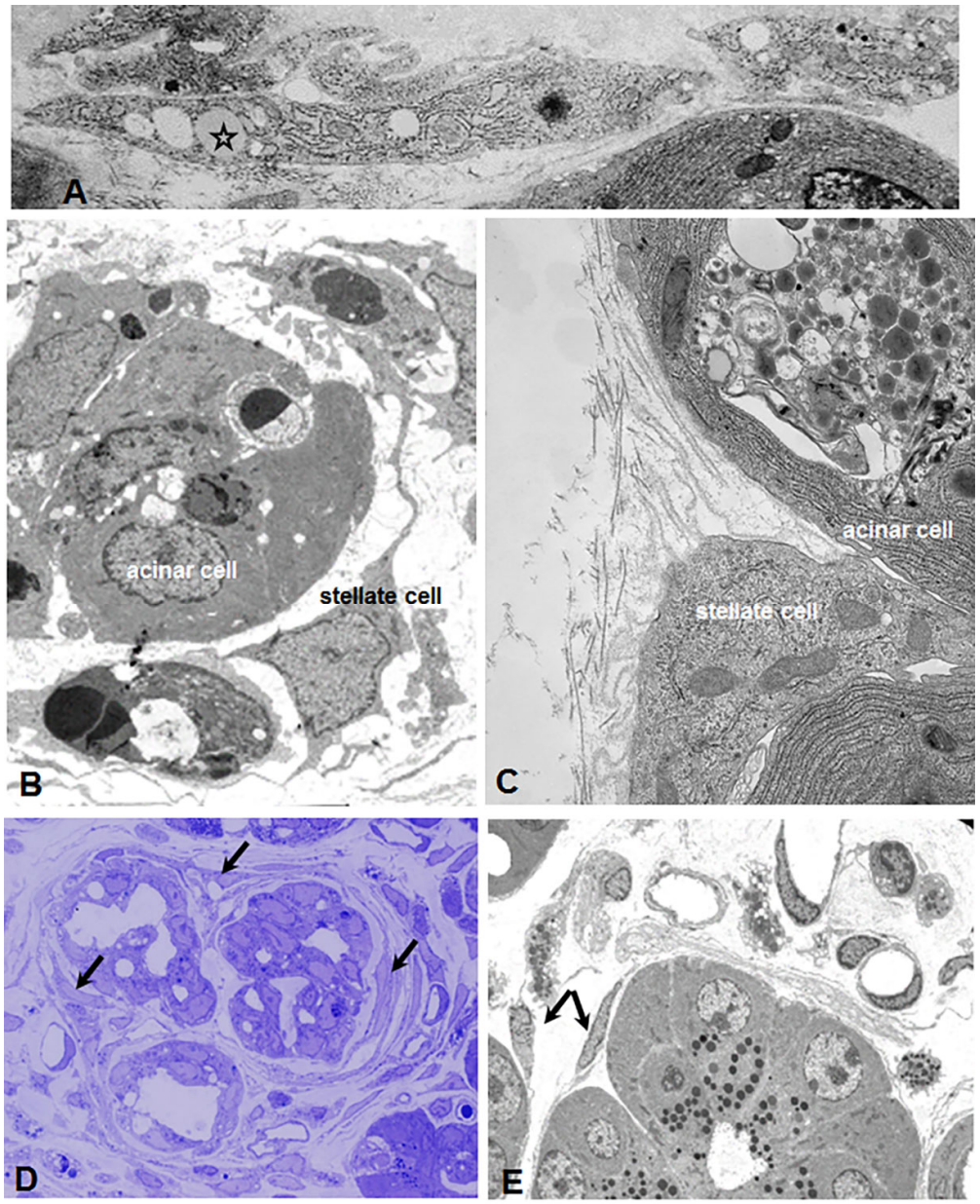

Figure 4.14 Stellate cells in the caerulein model

Stellate cells contain lipids and extrude these as they activate. Stellate cells were closely aligned with tubular complexes, their nuclei and processes appearing to wrap the tubular complexes into bundles. The stellate cell nuclei were either narrower and elongated around complexes, or expanded with rough endoplasmic reticulum (RER). The cytoplasm of stellate cells often appeared to be extruding collagen. **A**. Activating stellate cell with lipid droplet (star), copious RER. Day 1, EM x5000. **B**. Large stellate cells with long processes around apoptotic acinus. Day 2, EM x2500. **C**. Stellate cell extruding collagen. Day 2, EM x12000. **D**. Tubular complexes with stellate cells (arrows) wrapped closely around them. Day 4, Toluidine blue x1000. **E**. Acinus with cells approaching fibroblast phenotype (arrows) and remnants of interstitial collagen. Day 7, EM x1500.

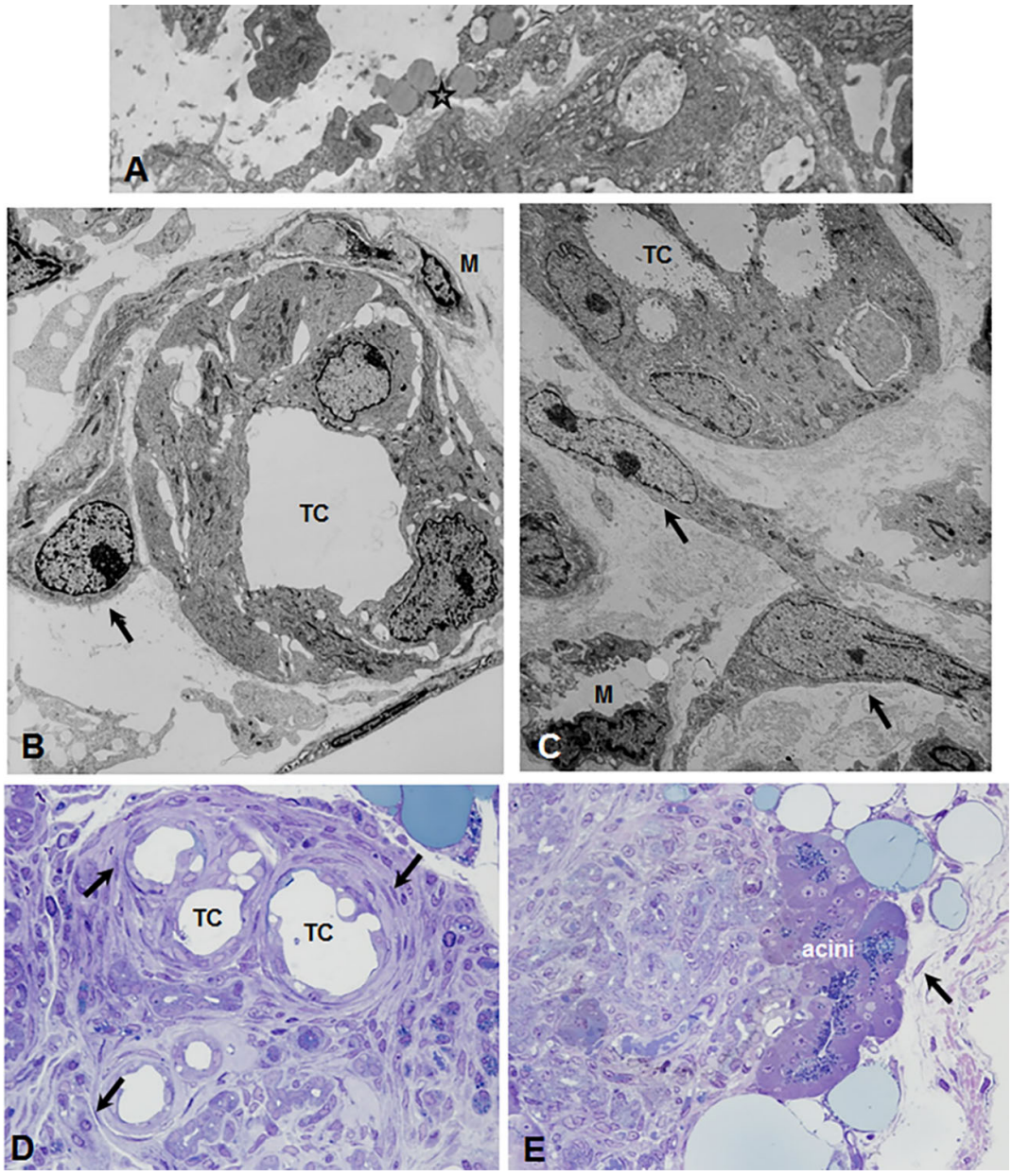

Figure 4.15 Stellate cells in the CHB model

Similar to the caerulein model, the stellate cells were closely associated with the tubular complexes and remained so. When regeneration did occur in the CHB model, no stellate cells wrapped around acini however they were still noted in the inflammatory infiltrate. Note also in this model the presence of lipid droplets in the toluidine blue-stained sections. **A**. Activating stellate cell process with lipid droplets (star) in the cytoplasm. Day 3, EM x5000. **B**. Tubular complex with stellate cell in close contact. Day 1, EM x5000. **C**. Stellate cells around tubular complex. Day 4, EM x2500. **D**. Stellate cells (arrows) closely wrapped around tubular complexes (TC). Toluidine blue day 14, x400. **E**. Regenerative acini with absence of close stellate cells. Stellate cells (arrow) are in the inflammatory infiltrate. Day 16, toluidine blue x1000.

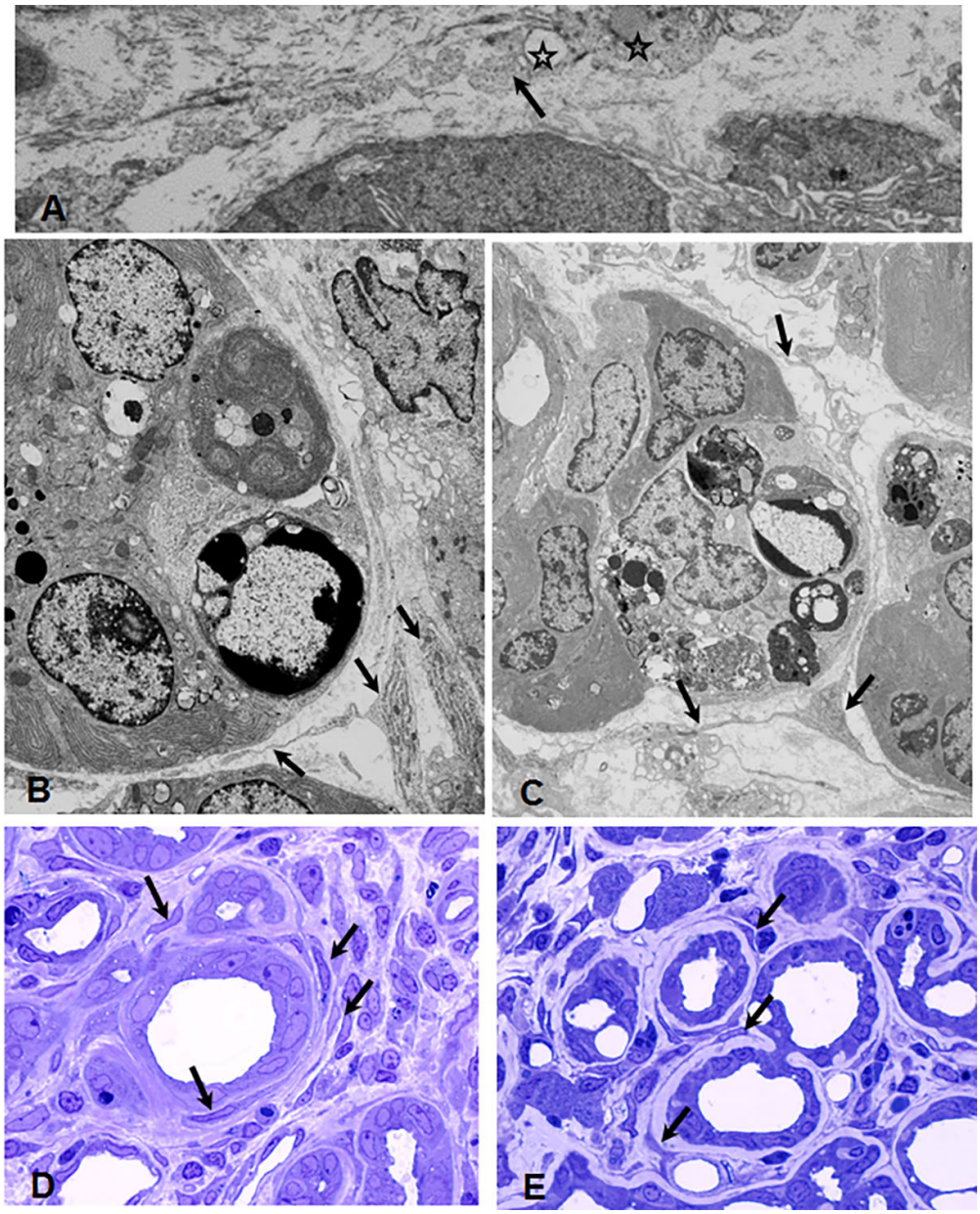

Figure 4.16 Stellate cells in the duct ligation model

The same pattern of stellate cell activation and localisation was seen in the duct ligation model with multiple cells wrapped around each tubular complex. **A**. Activating stellate cell process with lipid droplet (star) in the cytoplasm. Day 3, EM x5000. **B**, **C**. Stellate cells (arrows) closely aligned with tubular complex (TC). B=day 3, C=day 4, EM x2500. **D**, **E**. Tubular complexes with stellate cells (arrows) wrapped around them. D=day 10, E=day 18. Toluidine blue x1000.

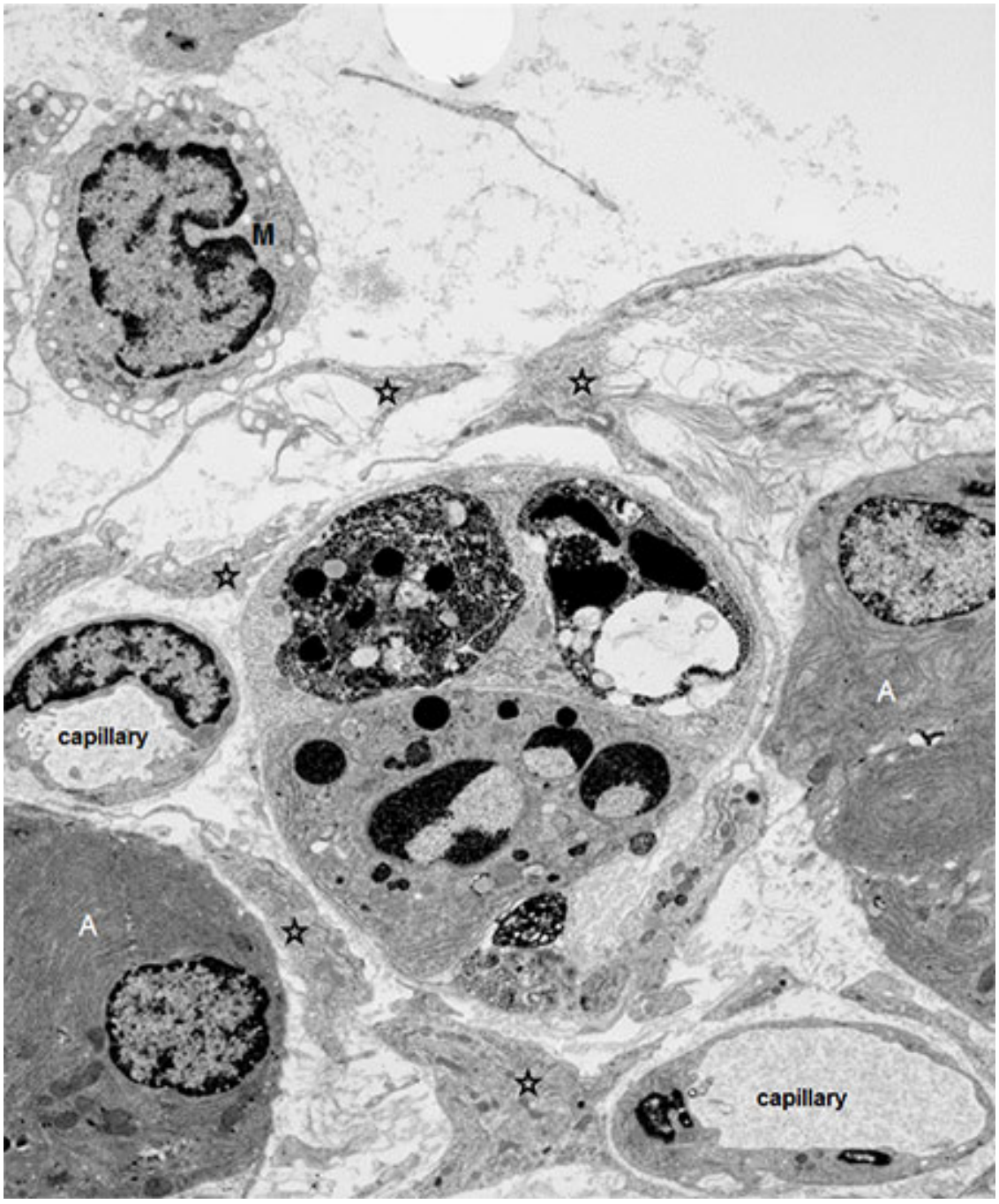

Figure 4.17 Stellate cells producing collagen

This micrograph shows activated stellate cells in the early stages of the duct ligation model. Multiple stellate cells surround a large apoptotic body, their long thin processes sliding around the residual body and the adjacent acini. There is much collagen deposition associated with the stellate cells. Duct ligation model, day 3. Stellate cells and processes (stars) around an apoptotic body. A=acinar cell, M=macrophage. Electron microscopy x6000.

4.4 DISCUSSION - FIBROSIS AND STELLATE CELLS IN PANCREATITIS

Traditionally, the pathological and physiological distinction between acute injury and chronic injury is blurred. Morphological characteristics which typify chronic pancreatitis are seen also in the model of acute pancreatitis. The three models of pancreatitis share a common pathogenesis in that atrophy of acinar cells via apoptosis leads to the formation of tubular complexes and the laying down of abnormal amounts of ECM. This study sought first to determine the differences in collagen deposition between the three models.

The experiments described here show pancreatic fibrogenesis in the caerulein model where degradation of fibrosis occurs and gland architecture is restored. The CHB model where regeneration is limited, and the duct ligation model where regeneration does not occur, proceed to chronic fibrosis. Fibrosis developed earlier in the caerulein model. This may be in part due to the CHB and duct ligation models undergoing considerably more oedema in the early stages and undergoing a later infiltration of macrophages into the gland. Once established, all models developed considerable fibrosis. That the peak of fibrosis did not last long in the caerulein model may be accounted for by the insult being removed earlier. It has been estimated that physiological activity of caerulein is absent from Sprague Dawley rats 8 hrs after one injection.[224] Resorption of fibrosis in this model proceeded swiftly once the insult ceased therefore the process for degradation of ECM is active in the caerulein model but not in the other models.

Pancreatic fibrosis is the result of the deposition of collagens I, III and IV, fibronectin and laminin.[225] One major difference between the models was in the type of collagen laid down. In the caerulein model the type of collagen laid down in intra- and inter-lobular areas was predominantly green under polarising light, typical of collagen type III and mostly of a wavy wispy nature. Around tubular complexes the collagen was a mixture of collagen type III and amounts of yellow, denser deposits that appeared to be collagen I. In contrast, in the CHB and duct ligation models under polarising light the collagen progressed from green to yellow then predominantly red, typical of collagen I. It was particularly thick around tubular complexes but also dense in swathes in the general tissue, with only a small amount of collagen III in some areas. Interestingly the overall amount of collagen laid down was approximately equal in all models at the peak of fibrosis respectively. It appears that in the caerulein model the process of degradation and resorption took place before collagen I fully replaced collagen III.

In the caerulein and duct ligation models, the BM became disordered and folded away from the cells as apoptosis and acinar atrophy progressed. In CHB, as synchronous apoptosis was followed by secondary necrosis BM was totally disrupted and scattered throughout the tissue. At the time point when tubular complexes were established in all models laminin staining showed the BM to be randomly dispersed around the complexes partially or fully encircling them and in thin or thick lines, Where regeneration occurred, the BM resumed an orderly thinner line around the acinar cells. Around tubular complexes, it remained thicker and disordered. BM is a highly cross-linked lattice of secreted proteins including collagen IV. The formation of BM depends on the binding and adhesion of laminin-collagen in a highly organised self- assembly process.[65] It requires laminin to anchor integrins, dystroglycan and other receptors in the process of assembly.[67] In all of the models laminin was disordered and dislocated to the same degree when tubular complexes formed after apoptosis. The laminin-collagen reassembly process occurs successfully around acinar cell regeneration as seen fully in the caerulein model and partially in the CHB model. The trigger for this is not yet known.

Fibrosis occurs as a result of the net deposition of excess collagen I and II and other matrix proteins that are synthesised by stellate cells. PSCs also synthesis MMPs that activate the resorption process in the extracellular space. The MMPs that play a key role in regulating matrix degradation are in turn, regulated by a family of specific inhibitors, TIMPs. A complex interplay exists between TIMPs and MMPs. In the caerulein/SHOP-induced chronic pancreatitis model in rats, fibrosis resolved by 18 days when MMP-1 and -2 expression was at a peak: MMP-9 did not significantly change.[226] MMP-2 and -9 also degrade BM proteins. Increased transcripts and protein for MMP-2 was reported during regeneration from caerulein-induced pancreatitis.[227] Other cells also play a part in collagen degradation, for example, in the liver Kupffer cells in matrix degradation.[228] Yokota et al. (2002) suggest that the MMP expression that is triggered by ECM injury enhances vascular basal membrane degradation and leads to an increase in polymorphonuclear leucocytes These leukocytes provide a further source of MMPs. Nakae and colleagues reported that the severity of disease in acute pancreatitis correlates with the ratio of TIMP-1/MMP-1.[229] The role that MMPs and TIMPs play in the regulation of ECM development progression and degradation was not explored in this current study and is a consideration for future studies.

Generally, fibroblasts with long thin nuclei and cytoplasm reside in the interstitial space closely aligned to parenchyma. These were identified in the control sections however they were not in great numbers. Non-activated stellate cells are reported to be identifiable by possessing vitamin A-containing lipid droplets.[142] These were not readily identified in controls in this study. Either the stellate cells were not resident in the controls, were too few to be easily observed and identified,

migrated into the injured pancreas, or activated from the resident fibroblasts. Others have observed that in the injured pancreas PSC populations resulted from bone marrow derived cells, migration from surrounding areas and PSC proliferation.[153] New special stains may aid in the identification of stellate cells in controls.[148] At the early stages of the experiments activating stellate cells were recognised by the presence of copious RER and lipid droplets in the cytoplasm and large regular shaped or elongated nuclei. The lipid droplets were seen up to three days in the CHB and duct ligation models, earlier in the caerulein model. After this no further lipid droplets were noted in stellate cell cytoplasm. The stellate cells were obvious by αSMA IHC, light and EM, migrating in the interlobular inflammatory infiltrate and in intralobular spaces and particularly closely arranged around tubular complexes. Mostly, the cells migrating in the inflammatory infiltrate had elongated nuclei and non-obvious cytoplasm more indicative of the shape of fibroblasts, however, in αSMA IHC sections they stained positively. In other areas their cytoplasmic processes were extremely long and thin and overlapped as they wrapped tightly around tubular complexes in a concentric fashion. By EM, they could be seen extruding preformed collagen into intercellular spaces. Stellate cells disappeared quickly as the caerulein model regenerated and were not apparent around regenerative acini in the CHB model. By the completion of the study in all models stellate cells remained around normal ducts and blood vessels. In the caerulein model they were there only; in the CHB model they remained also around residual tubular complexes; in the duct ligation model they were prevalent around tubular complexes. It was not obvious how the stellate cells departed other than they were seen migrating in the inflammatory infiltrate. Remaining cells in the caerulein model had an appearance approaching fibroblast morphology. No apoptosis or senescence was seen in stellate cells as were seen in other studies.[170, 171] This may have been missed as time points of two to three days apart in all models in the later stages are not close enough to account for all eventualities.

Future work could expand these parameters. It is apparent from this comparison of the models that stellate cells play roles in both the resorption of fibrosis and the ability of the pancreas to regenerate. Does the resorption of fibrosis first allow regeneration to occur? Do stellate cells drive regeneration? In the CHB model, fibrosis persists despite stellate cells waning. Does collagen I form a scar-like deposition in the CHB and duct ligation models that prevents the intercellular cross talk between other cells that promote regeneration?

4.5 MACROPHAGES IN INFLAMMATION AND FIBROSIS IN PANCREATITIS

4.5.1 An introduction to the role of macrophages in pancreatitis

The primary cause of morbidity and mortality in pancreatitis is the inflammatory response. Along with acinar cells, neutrophils, lymphocytes, monocytes and macrophages are a fundamental component of this immune response. Macrophages play a role in maintenance and resolution of tissue repair through communication with other immune cells. They are the major resident immune cell in the pancreas. They may be released into the blood stream from bone marrow to migrate into the tissue as monocytes and become activated and matured into macrophages. This section describes some of the potential roles that macrophages play in the inflammatory and fibrotic response of the injured pancreas.

4.5.2 Materials and methods

General materials and methods may be found in Chapter 2. Macrophages were identified by CD68 IHC, light and EM and semi-thin sections stained with toluidine blue.

4.5.3 Results for macrophages in inflammation and fibrosis in pancreatitis

Macrophages in control rat pancreas are demonstrated in **Figure 4.18**. Only few macrophages were identified in periacinar tissue (**Figure 4.18A**), however in select areas on the edge of lobules they were seen in greater numbers in connective tissue (**Figure 4.18C**). Ultrastructurally, macrophages have large nuclei that are often elongate with indentations and a thin rim of condensed chromatin, variable amounts of RER, mitochondria and Golgi apparatus. Inactive macrophages have poorly developed lysosomal vacuoles and the cell surface may or may not have cytoplasmic processes (**Figure 4.18B**). Remnants of apoptosis were predominantly ingested by macrophages in the early stages of the lesions and later when duct and regenerative acinar cell apoptosis occurred.

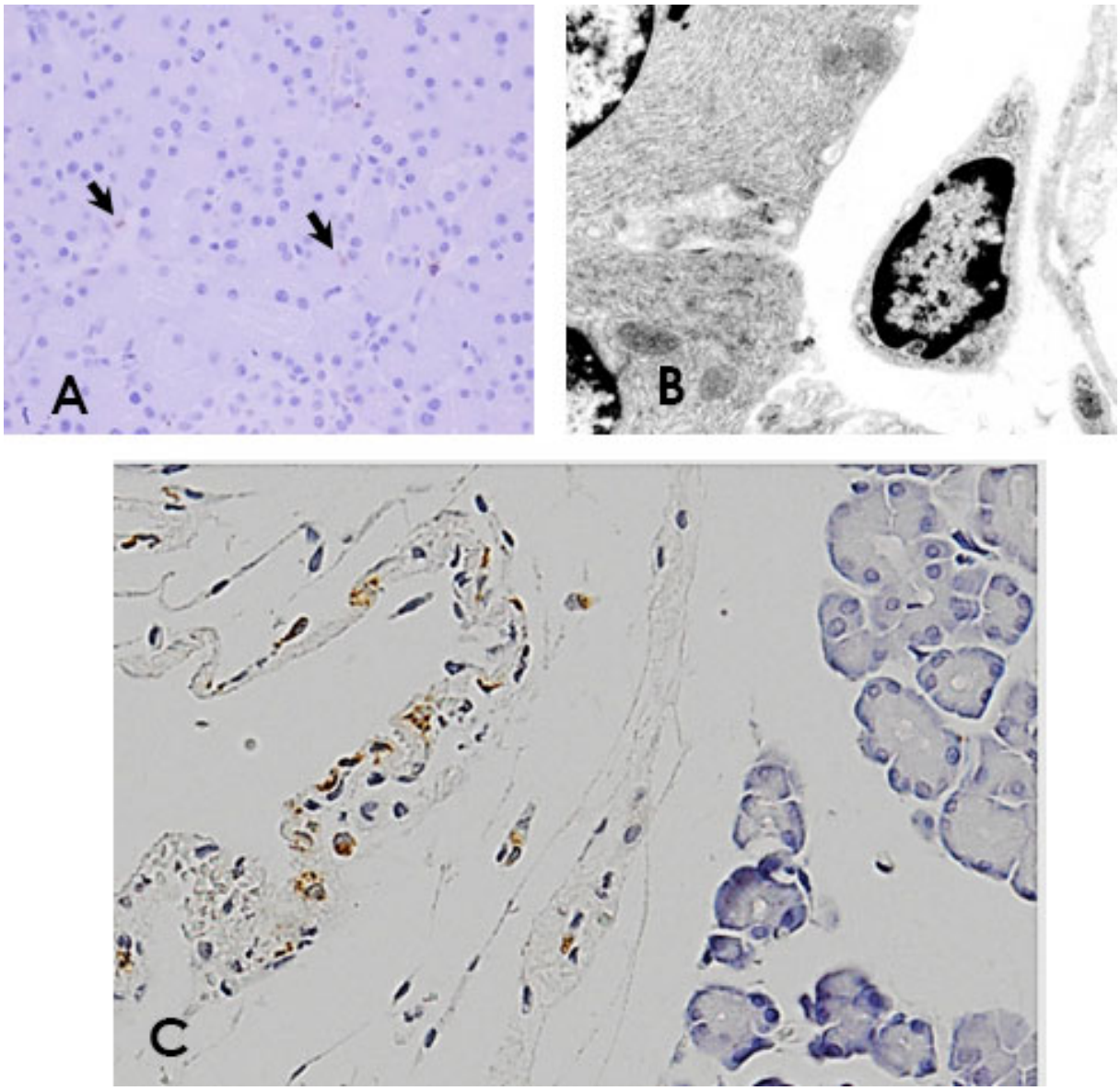

Figure 4.18 Macrophages in control pancreas

Macrophages were not obvious within the normal acinar population, however they were seen in numbers in connective tissue on the periphery of lobules. The macrophages were large cells with a large nuclear/cytoplasmic ratio, with or without chromatin clumped at the nuclear periphery and with obvious cytoplasmic rough endoplasmic reticulum. **A**. Rare macrophages were seen between acini in control pancreas. CD68, x200; **B**. A macrophage is seen next to an acinus. EM x5000; **C**. Macrophages are seen on the edge of a normal lobule, CD68 immunohistochemistry, x400.

Histology and EM are demonstrated in later figures. CD68 IHC showed that the macrophages appeared to migrate into the tissue through the inflammatory infiltrate and activate early in all of the models. They infiltrated into the spaces between apoptotic cells in great numbers as apoptotic cytoplasm was being scavenged (**Figure 4.19A-C**). In the caerulein model increased numbers of macrophages were seen early in the inflammatory infiltrate. The number peaked at 36 hrs in the infiltrate and in intralobular spaces however at 48 hrs they were mainly intralobular. By day 5-7 when there was less inflammatory infiltrate, fewer macrophages were seen (**Figure 4.19D**), however, by day 10 when regeneration was almost complete some lobules had few macrophages; other lobules had levels higher than normal with macrophages still in periacinar spaces and migrating in a residual inflammatory infiltrate (**Figure 4.19G; also see 4.21D**). In the CHB model the numbers of macrophages increased substantially up to 48 hrs (**Figure 4.19B**). Most macrophages were closely aligned with residual acinar cells rather than the inflammatory infiltrate. By day 5 macrophages were mainly in the inflammatory infiltrate but also singly around tubular complexes and close to stellate cells. From days 7-14 there remained considerable numbers of macrophages dispersed throughout the tissue, near tubular complexes, blood vessels and migrating (**Figure 4.19E**). Numbers decreased by days 18-28 but still remained above control levels (**Figure 4.19H**). In duct ligation the numbers of macrophages increased as apoptosis progressed up to day 4 when they were situated in the inflammatory infiltrate and around tubular complexes (**Figure 4.19C,F**). From days 7-18 numbers had declined but the macrophages were still active and occasionally formed giant cells **(Figure 4.19I**). As regeneration occurred in the caerulein model the number of macrophages decreased. In the CHB model the effect around regenerative nodules was varied with macrophages both absent and present in these areas (**Figure 4.19H, also see 4.22D**). In CHB and duct ligation models macrophages remained dispersed around tubular complexes, in the inflammatory infiltrate and randomly congregated in some areas (**Figures 4.19H,I**). A graph of the counts of macrophages (using IHC and CD68 antibody) is represented in **Figure 4.20**. In all experimental models, the number of macrophages increased from control levels.

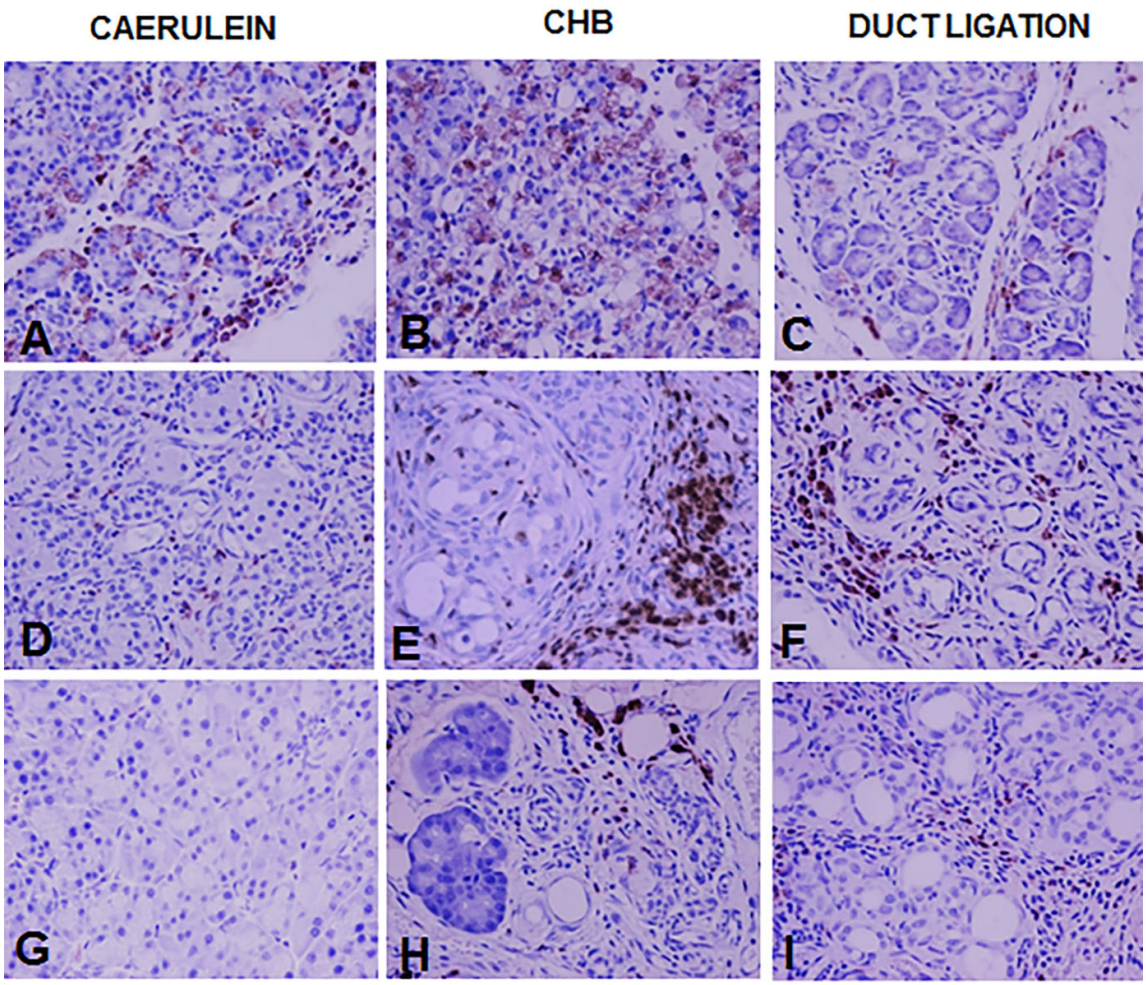

Figure 4.19 CD68 immunohistochemistry for macrophages in the rat models

IHC for macrophages showed clearly how activated they became early in pancreatitis in these models. They were mainly dispersed in all models but were seen both dispersed and congregated into large clumps in the CHB and duct ligation models. By regeneration in the caerulein model most macrophages had waned however large clumps persisted in the other two models. **A-C**. Increased numbers of macrophages in all models. **A**. caerulein, day1; (**B**. CHB, day2; **C**.duct ligation, day2. x 200. D-F. Macrophages around tubular complexes and in inflammatory infiltrate. **D**. caerulein, day4; (**E**.) CHB, day7; **F**.) duct ligation, day4. x 200. G-I. Macrophages returned to almost normal numbers around regenerated acini but prolific around tubular complexes. **G**.) caerulein, day10; **H**.) CHB, day16; **I**. duct ligation, day18. x200.

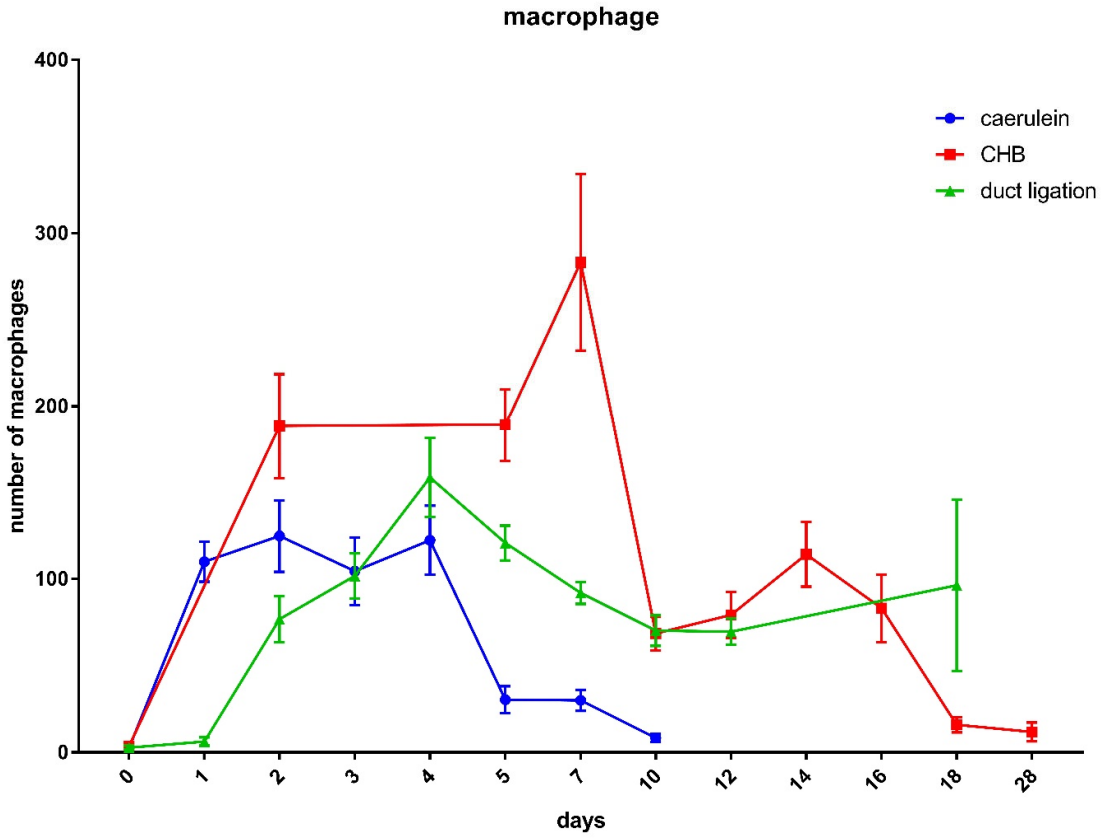

Figure 4.20 Mean ± SEM of counts of macrophages using CD68 antibody

Single macrophages were counted in five to ten random fields of x200 magnification for one whole pancreas section at 4µm per rat (n=4), per time point. The number of fields varied with regard to reduced parenchyma at atrophic time points. Data are the mean of four rats (n=4) per time point from one experiment per model. Error bars represent the standard error of the mean. In all experimental models, the number of macrophages increased from negligible numbers in controls. One way ANOVA was used to compare the number of macrophages in control groups versus experimental groups. Tukey's multiple comparison test was used to compare individual groups. The number of macrophages in the caerulein, CHB and duct ligation models were significantly higher (all $P<0.0001$) than in the control group at time points days 2 and 4, and at day 10 for the CHB and duct ligation models. At day 10 in the caerulein model, the number of macrophages was not significantly different compared to the control group ($P=0.2102$).

Figure 4.21A shows a typical activated macrophage in the interlobular space with a chromatin rimmed, irregularly-outlined nucleus. The cytoplasm contains membrane-bound spherical phagolysosomes of various sizes filled with cellular cytoplasm and organelles in different stages of degradation. Apoptotic nuclear fragments were present in the same manner. The lysosomal vesicles were also represented by clear vacuoles or spaces where digestion had occurred and lipids remained. These lipids mostly leached from the tissue during tissue processing leaving white spheres, however may remain in some electron micrographs as grey-coloured areas or in toluidine blue sections as bright blue-coloured areas. Stellate cells often aligned closely with macrophages. The macrophages used long, thin pseudopodia to snake around and extract apoptotic bodies from acinar cells (**Figure 4.21B**). In the caerulein model, the macrophages were very active in the periacinar space as acini underwent apoptosis and tubular complexes formed (**Figure 4.21C**). As regeneration progressed, macrophage numbers decreased quickly, however they were still found in periacinar areas and in residual inflammatory infiltrate in some lobules at day 10 (**Figure 4.21D**).

In the CHB model, the macrophage response was different as they were prolific early due the massive apoptotic response and secondary necrosis (**Figure 4.22A**). As the more disorderly removal of debris progressed, macrophages of all shapes and sizes filled with cellular debris packed the lobules (**Figure 4.22B**). By day 5, tubular complexes had formed although were undergoing continued apoptosis. Macrophages were often rounded up and lipid filled (**Figure 4.22C**). Where regeneration occurred, macrophages were often absent (also see **Figure 4.19H**) however in other areas they remained debris-filled around the parenchyma and in the inflammatory infiltrate, and associated with adipose tissue (**Figure 4.22D).**

Early in the duct ligation model, as acinar cells became vacuolated but not yet apoptotic macrophages migrated through the inflammatory infiltrate (**Figure 4.23C**). The macrophage response followed a typical procedure with respect to classic engulfment of apoptotic bodies in the same well-ordered manner as the caerulein model. Multiple macrophages filled with apoptotic bodies and lysosomal vesicles around apoptotic acinar cells and forming tubular complexes (**Figure 4.23A,B**). They persisted around tubular complexes and were seen migrating in the collagen rich inflammatory infiltrate (**Figure 4.23D**). Macrophages, mast cells and stellate cells shared the microenvironment in rat pancreatitis. They are illustrated in close proximity in the collagenous stroma in **Figure 4.24**.

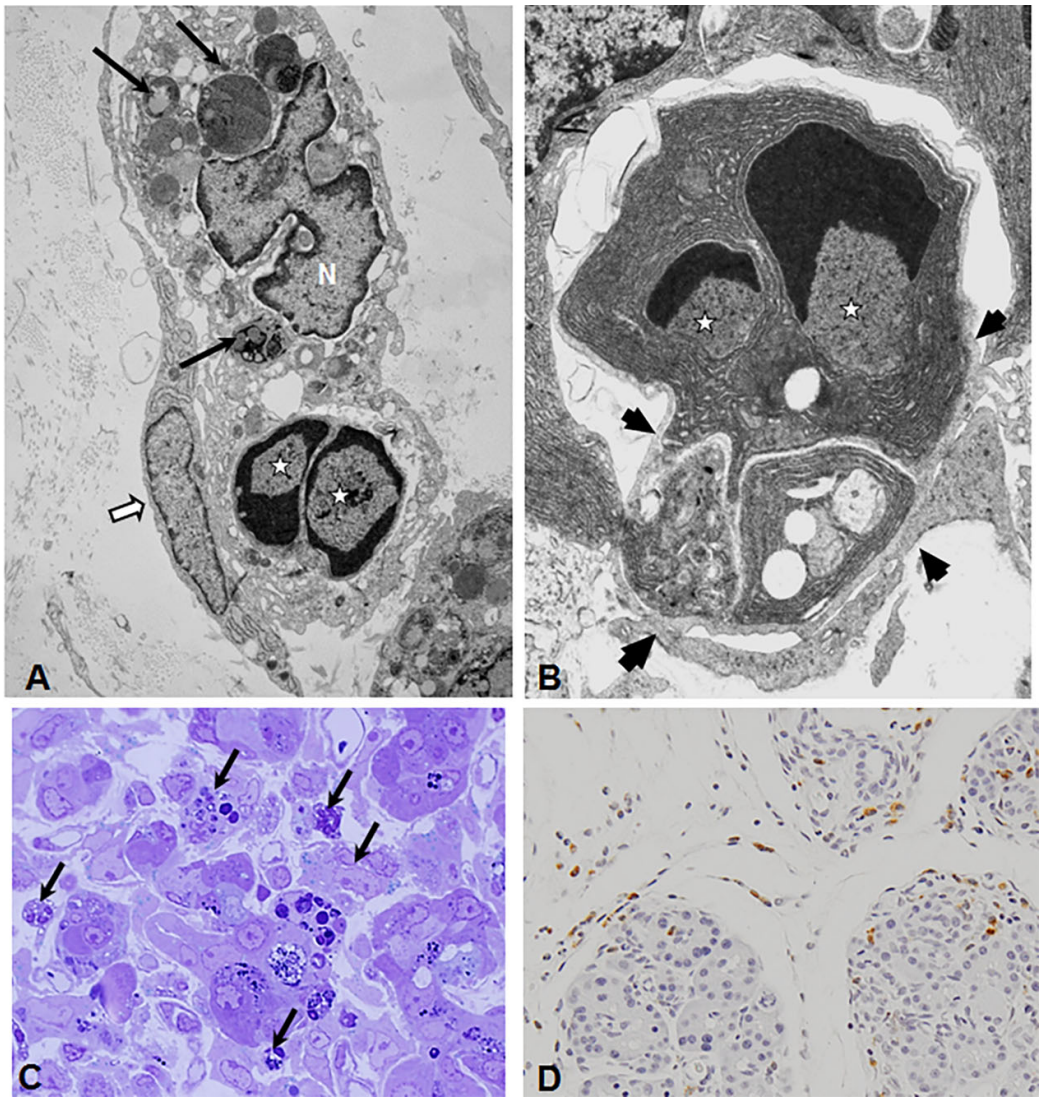

Figure 4.21 Macrophages in the caerulein model

Macrophages actively phagocytosed apoptotic bodies. They were close aligned with the acini, extending pseudopodia to remove detritus. They could be seen with inclusions in the inflammatory infiltrate well after most acinar cells has apoptosed. They were also still more visible than normal once regeneration had occurred. **A**. Macrophage in the interstitial space containing several phagolysosomes (black arrows) and apoptotic nuclear fragments (stars). N=macrophage nucleus, stellate cell (white arrow). Caerulein, day2. EM x5000. **B**. Macrophage (arrows) with thin pseudopodia removing an apoptotic body complex. Apoptotic nuclear bodies (stars). The macrophage nucleus is not visible. Caerulein, day2, EM x6000. **C**. Macrophages (arrows) within the interstitium around apoptotic acini and forming tubular complexes. Caerulein, day3, toluidine blue x1000. **D**. Macrophages (CD68+) remaining in intra- and interlobular spaces after regeneration. Caerulein, day10, CD68 x 400

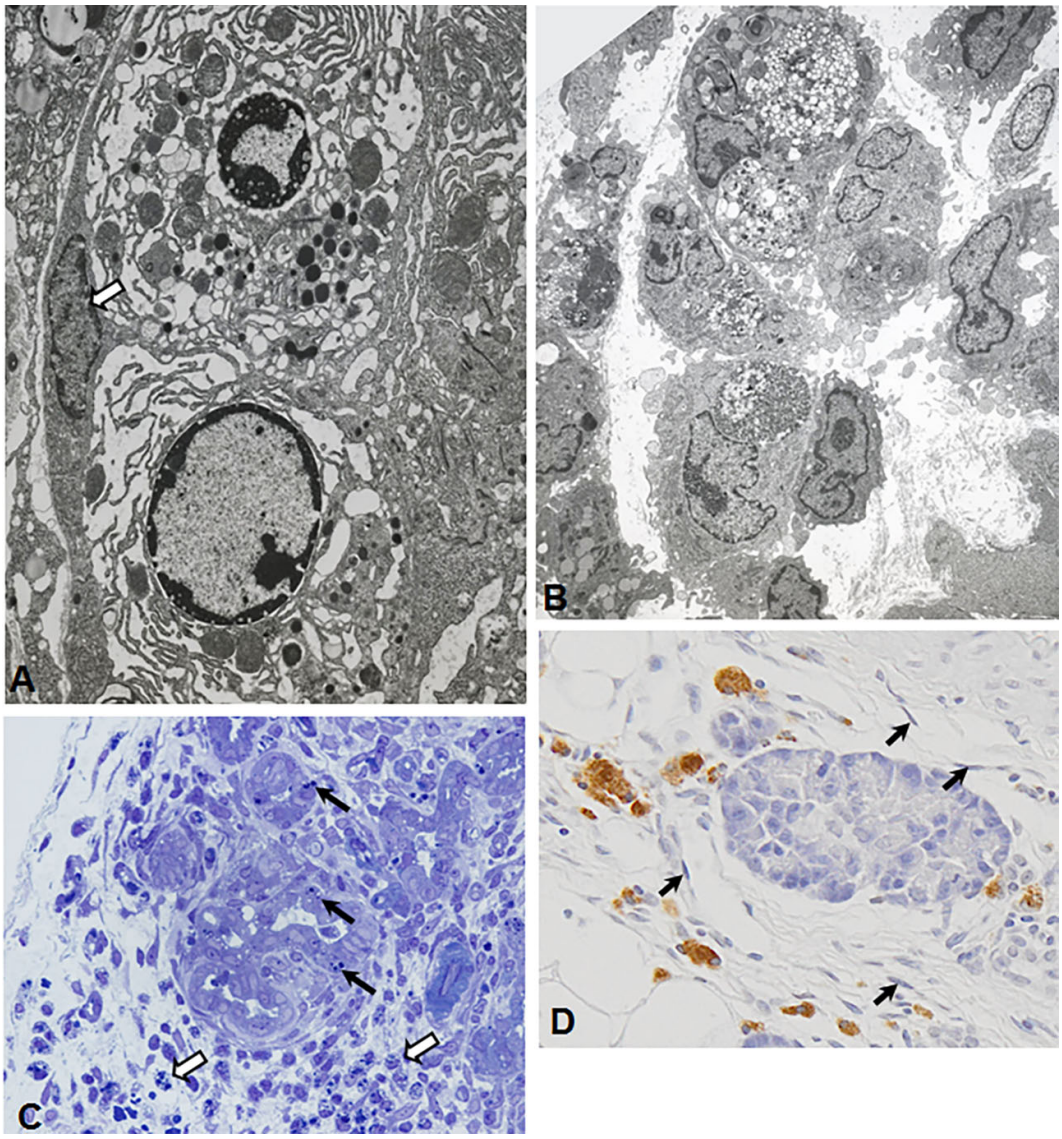

Figure 4.22 Macrophages in the CHB model

Macrophages were also active in the CHB model, engulfing the residue of secondary necrosis. They clumped together in numbers in this model and were seen in later stages with copious lipid inclusions in their cytoplasm which probably accounts for the large amounts of lipid in adipocytes in this model towards the end of the experiment. **A**. Macrophage in early activation (arrow) engulfing cells in secondary necrosis. CHB, day2, EM x4000. **B**. All cells in this image are macrophages engulfing residual acinar tissue. CHB, day3, EM x2500. **C**. Macrophages (white arrows) containing lipids in the inflammatory infiltrate around tubular complexes, apoptosis (black arrows). CHB, day 5, toluidine blue x1000. **D**. Large active macrophages in the inflammatory infiltrate around regenerating acini. Migrating stellate cells (arrows). CHB, day 10, CD68 x400

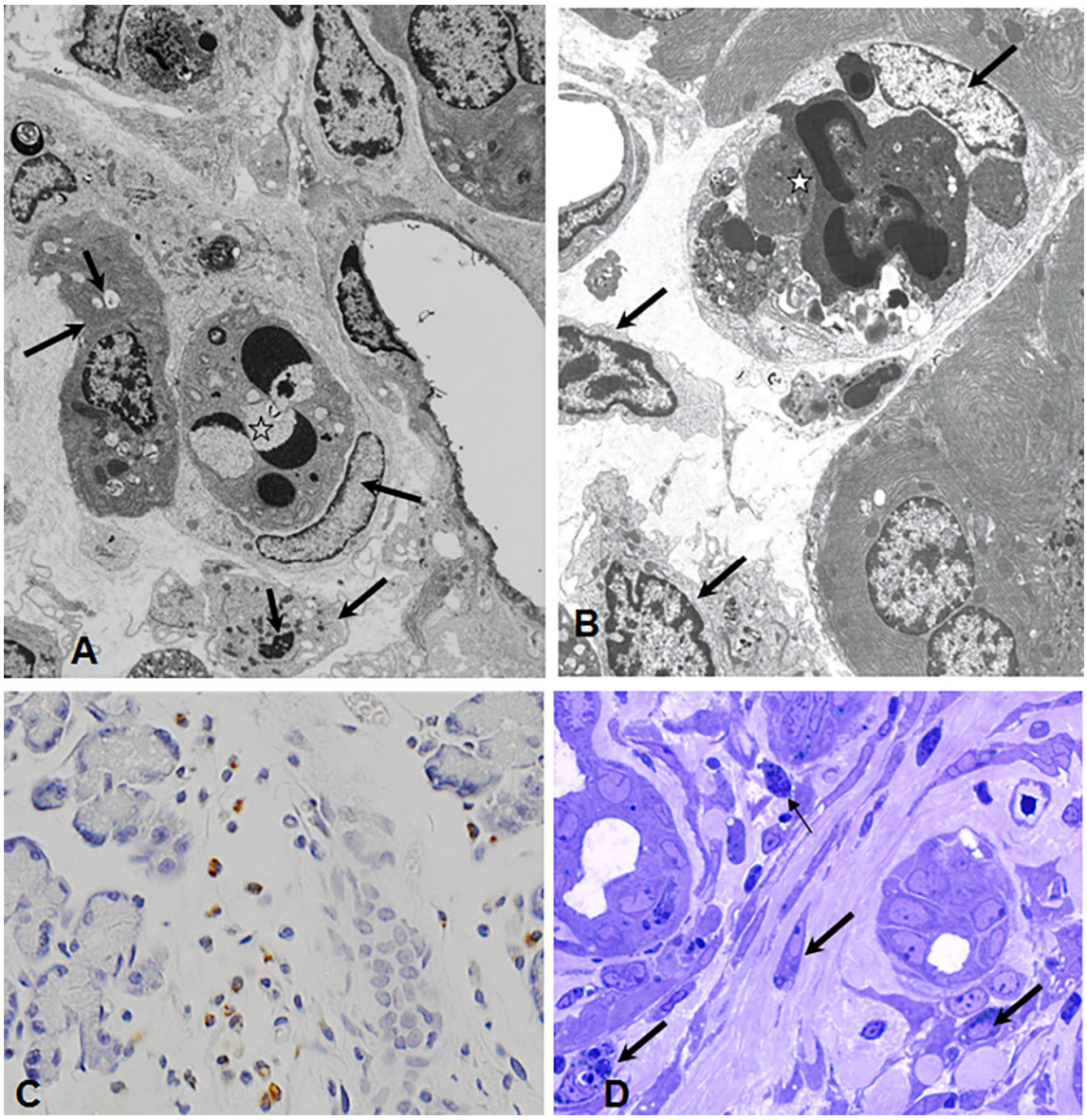

Figure 4.23 Macrophages in the duct ligation model

Macrophages in the duct ligation model followed a similar pattern to the other models of engulfing apoptotic bodies in large numbers. Macrophages were numerous in the inflammatory infiltrate at all stages of the lesion. **A**. Macrophages (long black arrows) are seen engulfing apoptotic nuclear fragments (star) and residual lysosomal bodies (short arrows). Duct ligation, day2, EM x3000. **B**. Macrophages (long arrows). Duct ligation, day3, EM x3000. **C**. Macrophages entering the pancreas through the inflammatory infiltrate. Duct ligation, day1, CD68, x400. **D**. Macrophages in the collagen rich inflammatory infiltrate and around tubular complexes (long black arrows), neutrophil (thin arrow). Day7, toluidine blue, x1000.

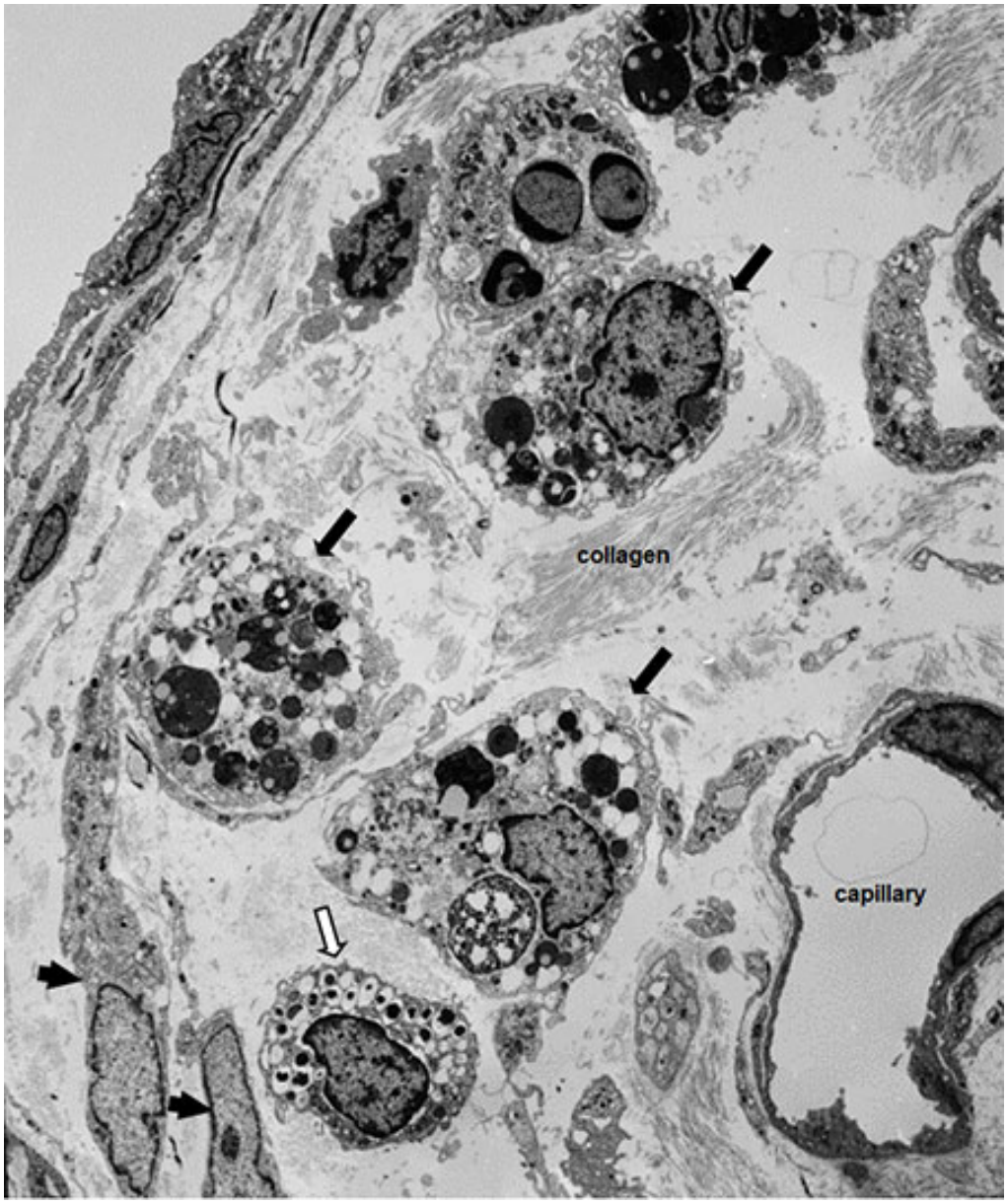

Figure 4.24 Inflammatory cells in pancreatitis

This electron micrograph shows a number of active macrophages within the inflammatory infiltrate with inclusions of detritus at various stages of degradation in lysosomes, and lipid droplets. Macrophages can be seen with residual bodies and lipid droplets (black arrows), mast cell (white arrow) and stellate cells (short arrows) in dense extracellular matrix at the edge of a lobule. Caerulein, day4, EM x2000.

The relationship between macrophages and adipose tissue is demonstrated in **Figure 4.25.** In the CHB and duct ligation models, macrophages filled with lipid droplets which coalesced to form large lipid filled cytoplasm **(Figure 4.25A**). Macrophages were noted often in adipose tissue presumably emptying lipid into forming adipocytes (**Figure 4.25B, C**).

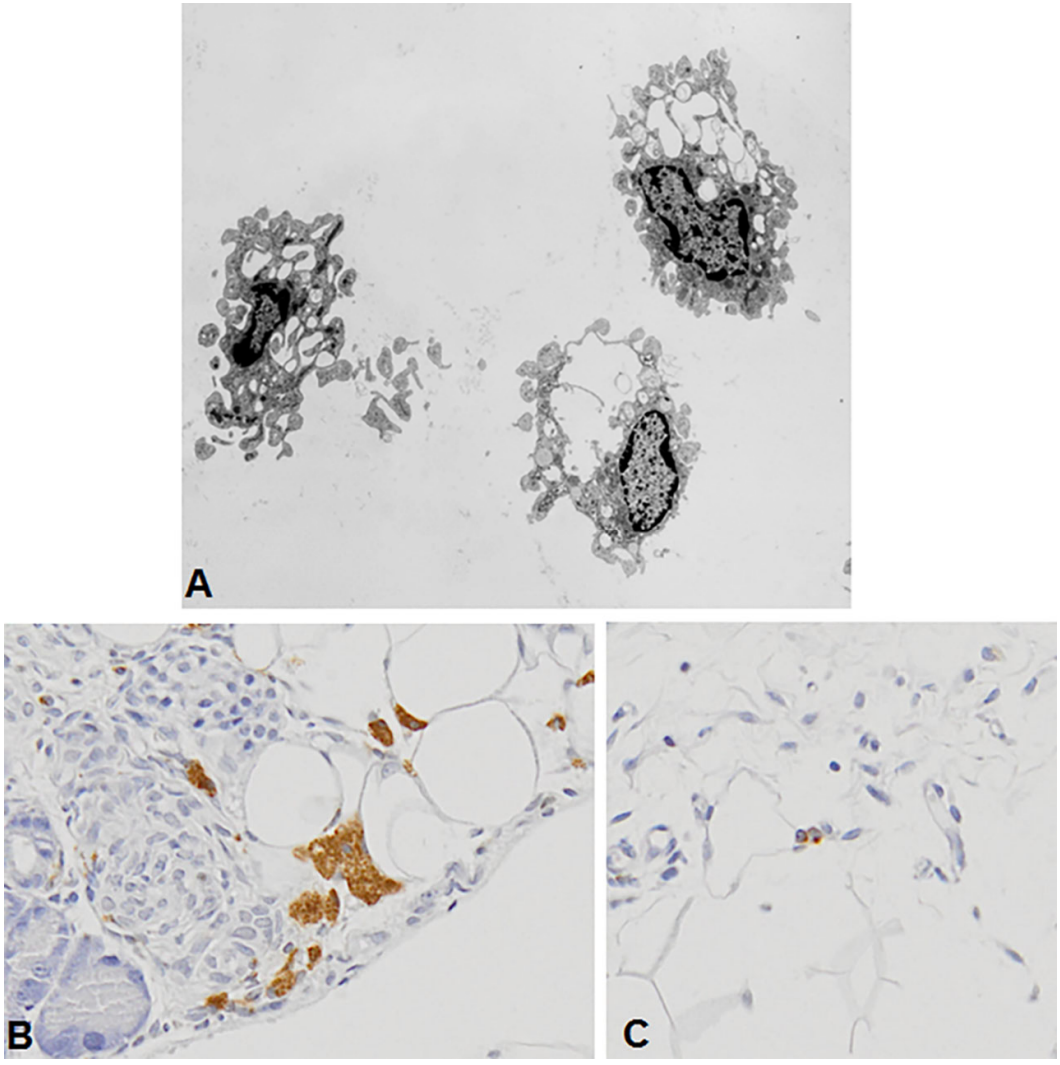

Figure 4.25 Relationship between macrophages and adipose tissue

Macrophages in the CHB model, particularly, had copious amounts of lipid droplets in the cytoplasm. They often clumped together as giant cells and were seen closely associated with adipose tissue. **A**. Macrophages can be seen with spaces that contained lipid (the actual lipid has been dissolved by tissue processing). CHB, day4, EM x2500. **B**. Adipose tissue is demonstrated with macrophages closely aligned. Note the size of the activated macrophages compared with Figure 4.18C. CHB, day18, x1000. **C**. Adipose tissue with macrophages (brown stain). Duct ligation, x1000.

4.5.4 Discussion of the role of macrophages in inflammation and fibrosis in pancreatitis

Macrophages are well known for their effectiveness as scavenger cells in wound repair and tissue injury. This was well demonstrated in the three rat models discussed here. Following apoptosis of acinar cells in all models macrophages, either recruited or resident, migrated within the inflammatory infiltrate to establish themselves within the parenchyma. There they effectively engulfed and removed injured cells until tissue architecture was reinstated as tubular complexes.

From there, macrophages possibly acted in the reparative process in the caerulein model as they disappeared in numbers as regeneration progressed. In the CHB and duct ligation models where regeneration did not remain or did not occur, macrophages may have aided the continuing inflammatory process. They remained in these models in numbers excessive of control levels.

Macrophages drive the initial inflammatory response by synthesizing inflammatory mediators such as chemokines and matrix metalloproteinases. Distinct roles for either resident or recruited macrophages as anti- or pro-inflammation have been proposed.[190] However, in models of liver injury phagocytosis functions in the conversion of inflammatory macrophages into cells displaying a restorative phenotype.[230] The removal of intracellular contents apparently stimulates macrophages to express an anti-inflammatory phenotype such that the depletion or diminution of macrophages may lead to the resolution of inflammation, resulting in repair and restoration. These macrophages suppress the immune system by expressing anti-inflammatory mediators such as IL-10 and TGFβ1 under the influence of interleukins.[190] Conversely, macrophages may adopt a suppressive phenotype that would continue inflammation and lead to the failure of the repair process. As well, fibrotic role of macrophages in chronic pancreatitis may be influenced by their release of cytokines such as IL-6.

As well as promoting proliferation and angiogenesis through PDGF, IGF-1 and VEGF, macrophages, through TGFβ, also recruit and promote the survival of the stellate cells that produce ECM. They also do this by producing MMPs such as MMP-2 and -9 that aid stellate cell migration via degradation of basement membrane.[186] Macrophages can secrete pro-fibrotic mediators such as TGFβ1, PDGF, FGF2, insulin-like growth factor–binding protein 5, CCL18, and Galectin-3, as well as various mediators that can influence fibrotic resolution such as IL-10, MMP-13, Relma-α, PD-L2, and Arginase-1.[186] For the caerulein model to regenerate through macrophage influence, presumably the macrophages must differentiate into anti-inflammatory macrophages that secrete the anti-fibrotic cytokines. These would stimulate the production of the matrix metalloproteinases that can directly

degrade interstitial collagen. Essential amino acids required for T cell and stellate proliferation and stimulation would need to be depleted. As macrophages are found in close association with stellate cells in these models the equilibrium between different macrophage populations or phenotypes, and stellate cells probably determines whether the outcome of pancreatitis is regeneration or pathogenic fibrosis.

4.6 MAST CELLS IN INFLAMMATION AND FIBROSIS IN PANCREATITIS

4.6.1 An introduction to the role of mast cells in pancreatitis

Mast cells are found in close proximity to vasculature in all tissues and are sensitive to pathological changes. On activation, they release a myriad of inflammatory mediators important in the context of allergic disorders and other inflammatory responses and are believed to play a role in fibrotic disease. The precise role of mast cells in acute and chronic pancreatitis is not clear however they are implicated in the development and progression of acute pancreatitis[194, 231] and have been identified as the cells responsible for perpetuating chronic inflammation in chronic pancreatitis. This study looks at the differences in mast cell distribution in experimental models of caerulein-induced, CHB-induced, and duct ligation-induced pancreatitis to see if they are involved in the inflammatory response or fibrosis or both. Mast cells have not been described in this CHB model.

4.6.2 Materials and methods

General materials and methods have been described in Chapter 2. For this section of the study, mast cells were stained histochemically with Alcian blue/nuclear fast red (Appendix 1). The presence of mast cells was confirmed with IHC for c-kit (CD117). The histochemical method was chosen as the preferred method for identifying mast cells in light microscopy. Semi-thin toluidine stained sections and EM were also used. Mast cells stained with Alcian blue/nuclear fast red were counted in ten fields x200 magnification for each slide. There was lobular variation in numbers of mast cells in all models which accounts for the large error bars.

4.6.3 Results for mast cells in inflammation and fibrosis in pancreatitis

Mast cells were sparse to non-existent in periacinar spaces but were found in small numbers around connective tissue, blood vessels and in lymph nodes in control sections (**Figure 4.26A-C**).

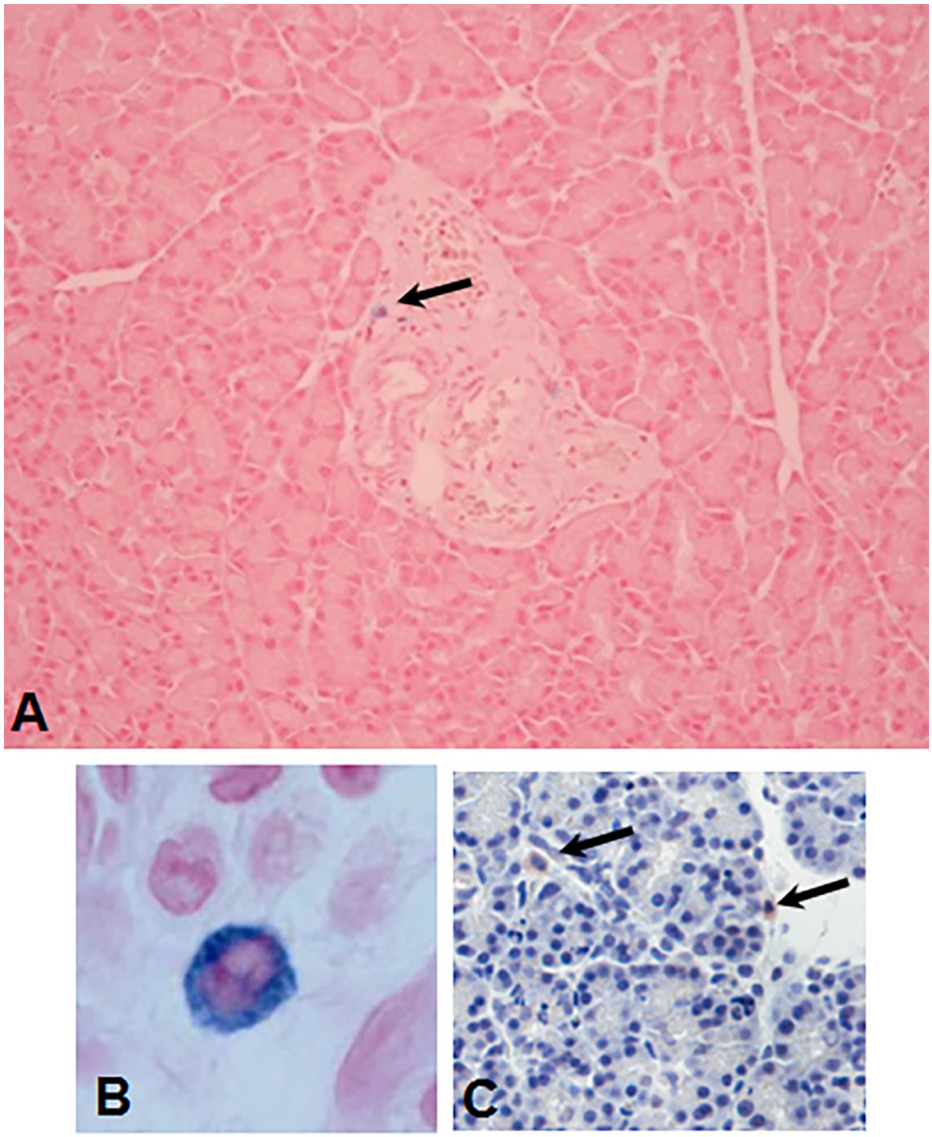

Figure 4.26 Control rat pancreas stained for mast cells

Mast cells were seen in control sections mainly close to blood vessels. They were not very numerous. With Alcian blue histochemistry, the mast cell granules stain brightly and distinctly. C-kit IHC may also be used however Alcian blue provides efficient identification, especially when degranulating when granules may be few. **A**. Control section shows a lone mast cell in connective tissue in the pancreas. Alcian blue/nuclear fast red, x200. **B**. High power image of a mast cell stained with Alcian blue/nuclear fast red. X1000. **C**. Mast cells stained with c-kit immunohistochemistry, counterstain haematoxylin.

In experimental sections, mast cells were distributed throughout the pancreas, congregated around blood vessels and nerves, in the interstitial and intralobular spaces and around tubular complexes and acini and close to adipose tissue (**Figure 4.27A-I**). Mast cell numbers increased by day 1 in the caerulein model, and to the same level by day 2 in the CHB model. In the duct ligation model, they increased slowly and by day 4 had reached the levels of the other models. Thereafter the caerulein model mast cell population rose markedly to an early peak at day 3-4 after which it decreased equally noticeably with regeneration. Mast cells in the CHB and duct ligation models increased slowly to a peak higher than caerulein by day 14 in the CHB model and day 28 in the duct ligation model. By the completion of the experiment in the caerulein model, the mast cell count remained considerably higher than the control levels in periacinar spaces. In the CHB model mast cell numbers decreased from the peak at day 14 however still remained high. In the duct ligation model there was no decrease in number. Mast cells were easily identified in light microscopy as their granules stain bright blue with Alcian blue. A graph of incidence of mast cells in the three models is depicted in **Figure 4.28**.

A typical mast cell is shown in **Figure 4.29**. The granules in the rat contain either finely granular electron dense material or scroll formations of loosely organised lamellae (**Figure 4.30A-C**). The appearance of the granules is affected by maturity of the granules and by degranulation. Immature mast cells demonstrate a smaller size and a higher nuclear cytoplasmic ratio with fewer granules.[232] Mast cells underwent massive degranulation in the early stages. Mast cells were in close proximity to macrophages and stellate cells especially in the earlier stages of the pancreatitis when apoptosis was occurring and tubular complexes formed. At later time points in the models, they were mainly in the interstitium.

In the semi-thin sections toluidine blue stains the granules metachromatically, seen in the sections of **Figure 4.31(D-F)**. In electron micrographs, the mast cells were identified by their numerous electron dense granules in the cytoplasm, an indented nucleus, and slender, cytoplasmic filiform projections on the cell surface.

Figure 4.32A,B demonstrate mast cells found in the regenerative phase. In this example, mast cells were found close to regenerated acini (**A**) or congregated in the interstitial space (**B**).

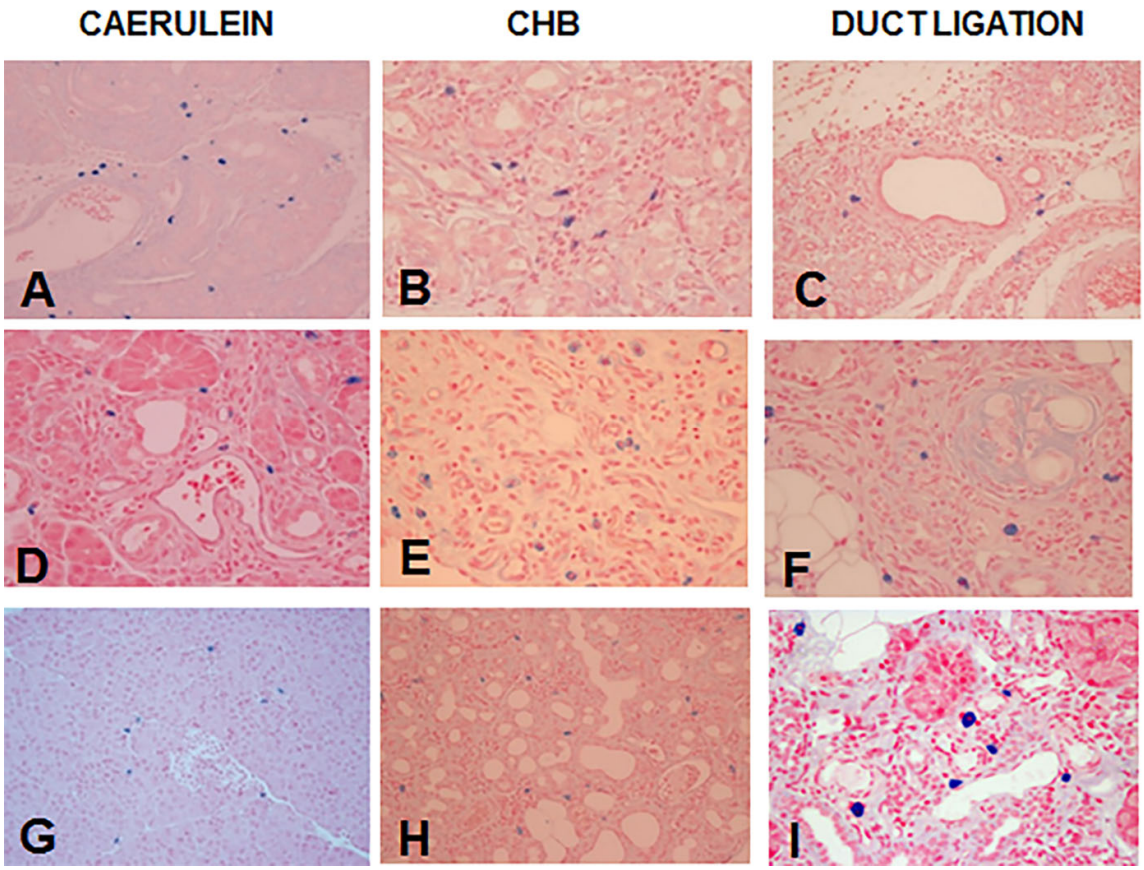

Figure 4.27 Distribution of mast cells in the rat models

In all of the models mast cells were seen within the parenchyma as well as around blood vessels during experimental conditions. In light microscopy the appeared randomly distributed and not particularly aligned with tubular complexes or acinar islands.

A,D,G. Caerulein, day2, day5, day10, x 200

B,E,H. CHB, day4, day12, day18, x200

C,F,I. Duct ligation, day4, day12, day28, x200

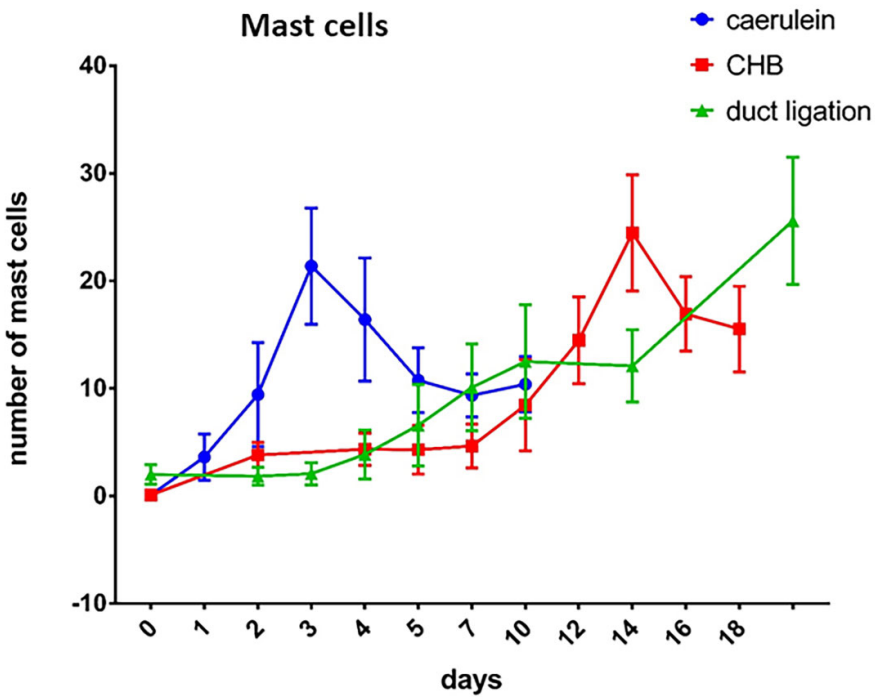

Figure 4.28 Mean ± SEM of mast cell numbers in the three models

Single mast cells were counted in five to ten fields of x200 magnification for one whole pancreas section at 4µm thickness per rat per time point. As mast cells tend to be more congregated around large blood vessels in the pancreas and the number of blood vessels were more closely aligned in reduced atrophic parenchyma over time and between models a less random but consistent system of field choice targeting parenchyma was used. Data are the mean of four rats (n=4) per time point from one experiment per model. Error bars represent the standard error of the mean. Mast cells peaked early in the caerulein model but took some days to peak in the CHB and duct ligation models. Mast cell numbers remained higher than normal (time 0) in all models. One way ANOVA was used to compare the number of mast cells in control groups versus experimental groups. Tukey's multiple comparison test was used to compare individual groups. The number of mast cells in the caerulein, CHB and duct ligation models were significantly higher than in the control group at time points days 2 and 4 ($P<0.0001$, $P<0.0001$, $P<0.0001$, respectively) and at day 10 ($P=0.0414$, $P<0.0001$, $P<0.0001$, respectively).

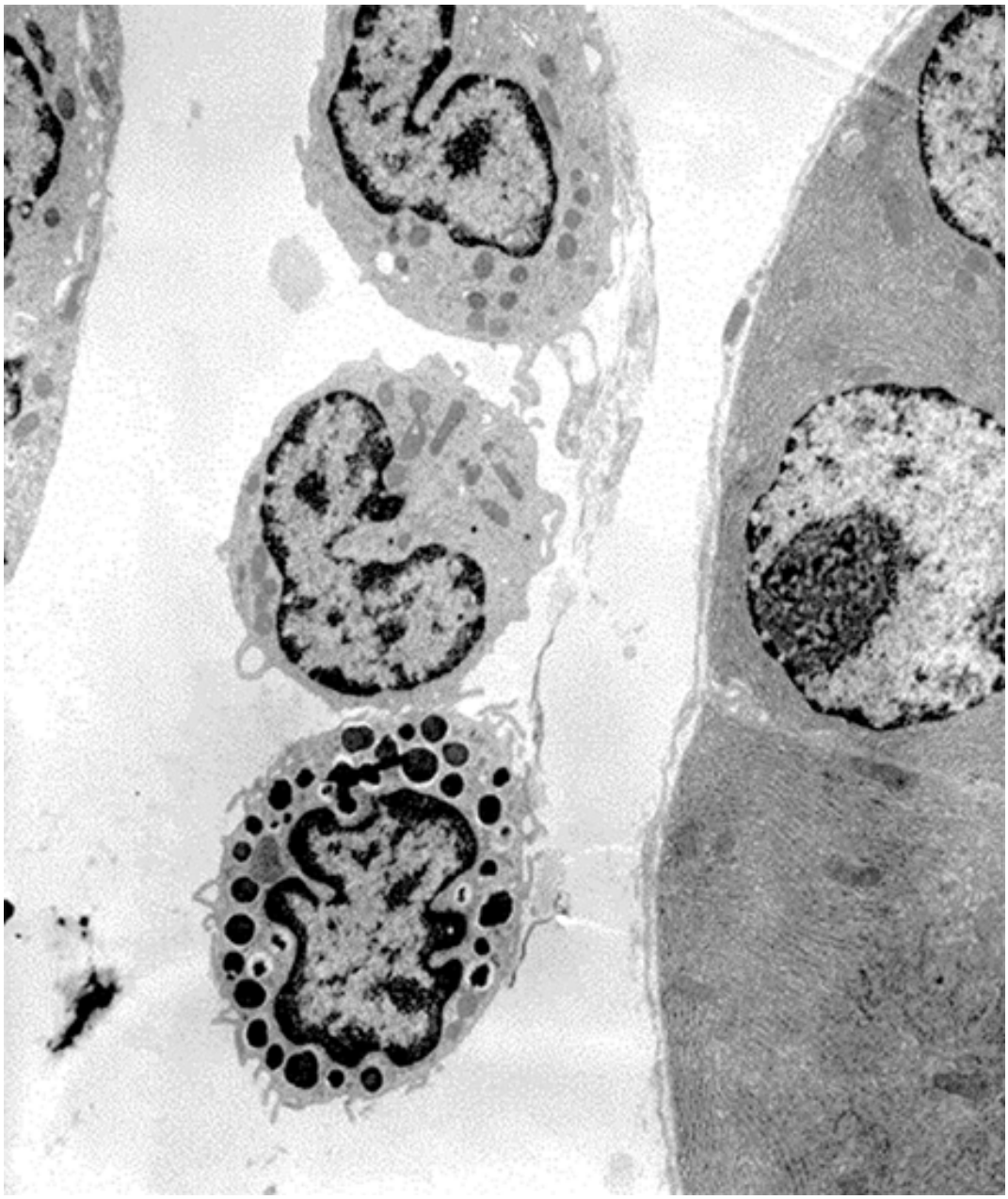

Figure 4.29 Typical mast cell with macrophages

This electron micrograph shows a typical mast cell with distinctive indented nucleus, high nuclear cytoplasmic ratio and cytoplasmic projections on the cell surface. The granules are electron dense and are of varying size as they degranulate and leave an empty space halo around the granule. Two typical macrophages are close by this mast cell in the interstitial space. By electron microscopy, mast cells, macrophages and stellate cells were seen closely associated in these experiments. A typical mast cell, with granulation is seen in the pancreatic interstitial space, close to two macrophages (top cells). Caerulein day2, x1000.

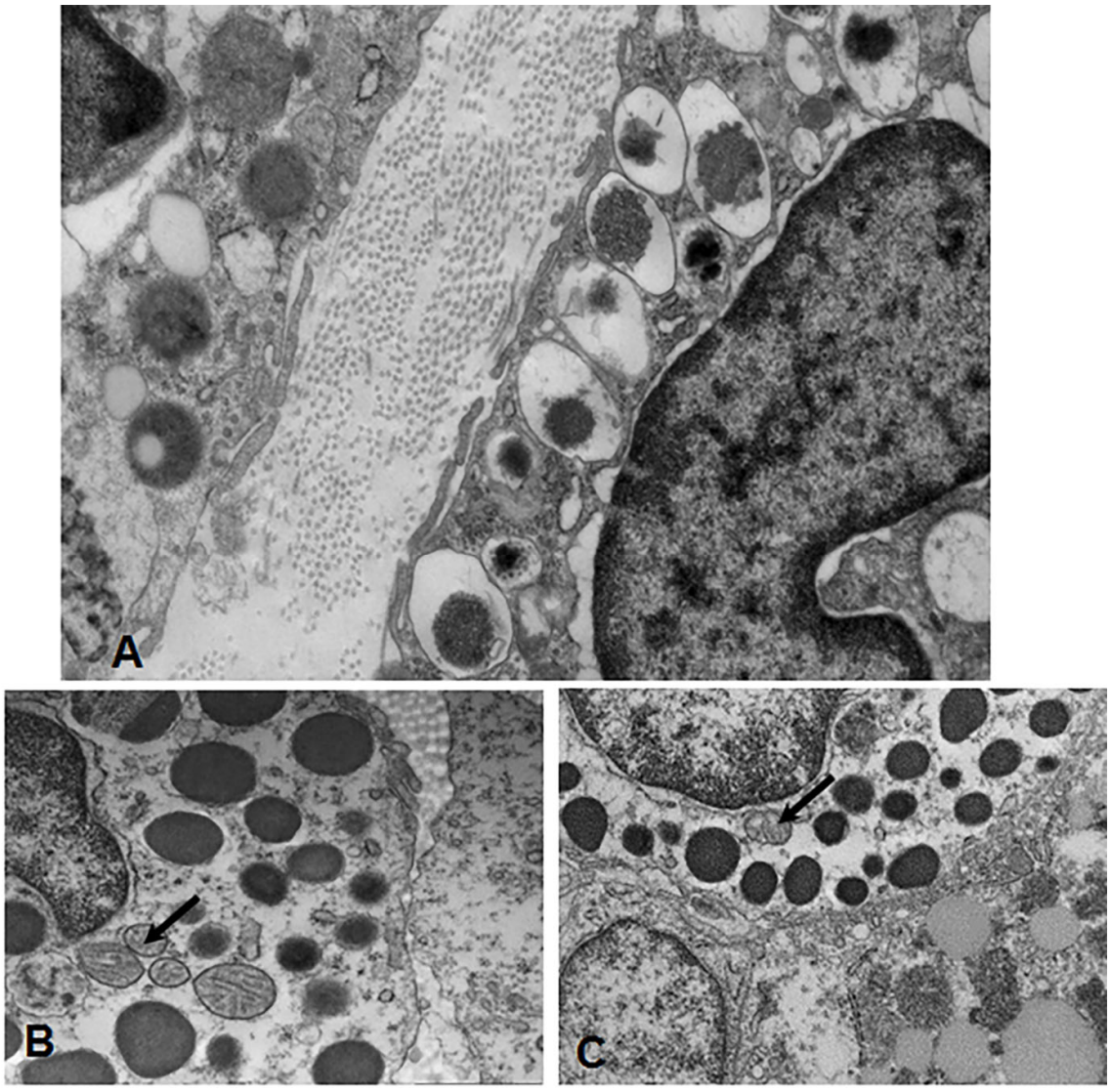

Figure 4.30 Mast cell granules

The mast cell granules in the rat contain either finely granular electron dense material or scroll formations of loosely organised lamellae. In4.30**B** and 4.30**C**, the arrow indicates a scroll formation.

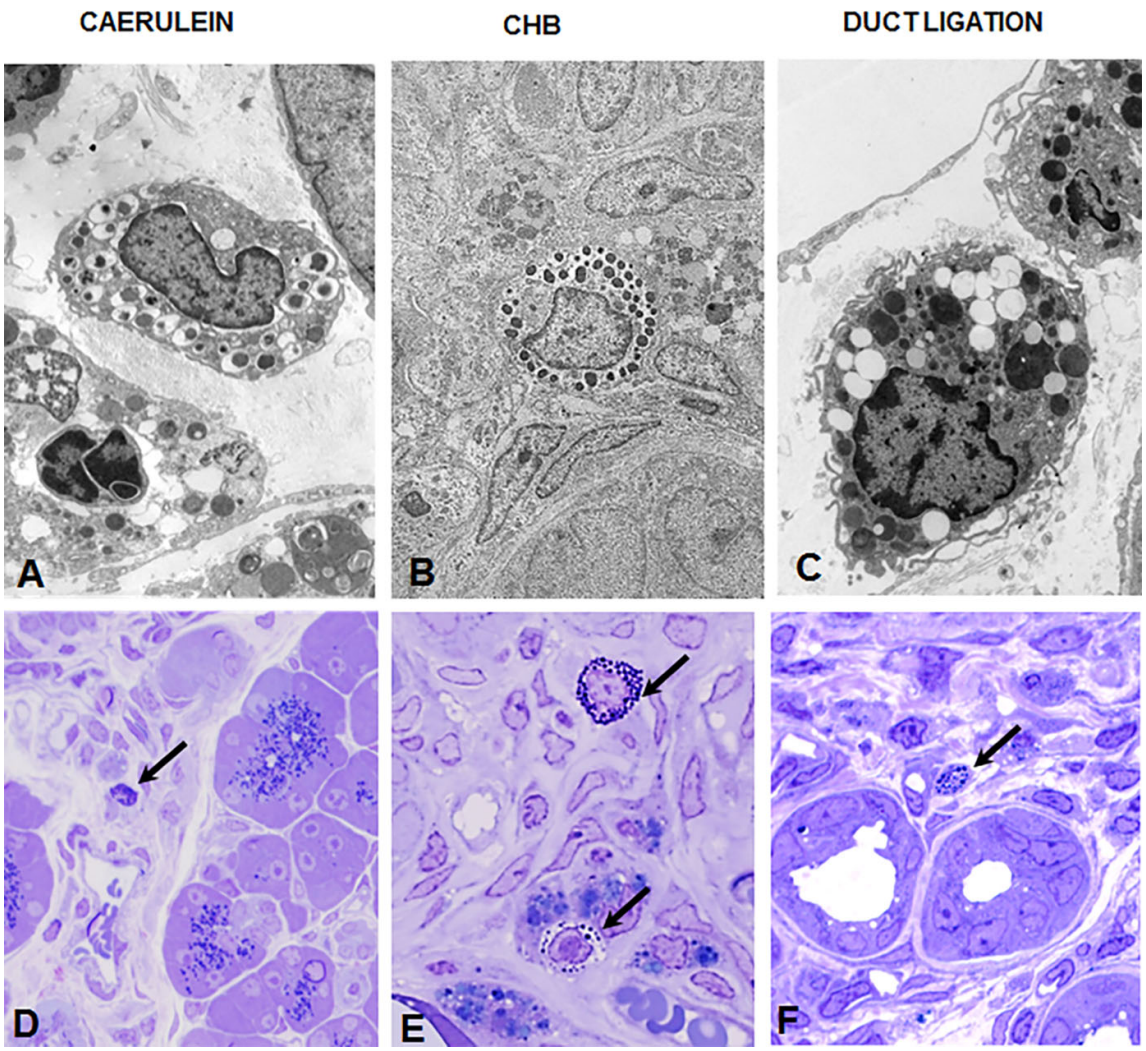

Figure 4.31 Mast cells in the rat models

In all of the models, mast cells could be seen actively degranulating, with some almost completely degranulated. They were sometimes seen randomly in the inflammatory infiltrate, often close to macrophages and, to a lesser degree, stellate cells. Apart from different numbers, there was little to distinguish between the three models for mast cells. **A**. Mast cell degranulating. Caerulein day 4, EM x10000. **B**. Mast cell in a compact stroma. CHB day14, EM x9000. **C**. Mast cell partially degranulated. Duct ligation, EM x10000. **D**. Mast cell in interstitial space (arrow). Regenerated acini. Caerulein, toluidine blue, day 10, x 1000. **E**. Mast cells one almost fully degranulated (arrows), CHB toluidine blue, day 14, x1000. **F**. Mast cell close to tubular complexes. Duct ligation (arrow), toluidine blue, day 10, x1000.

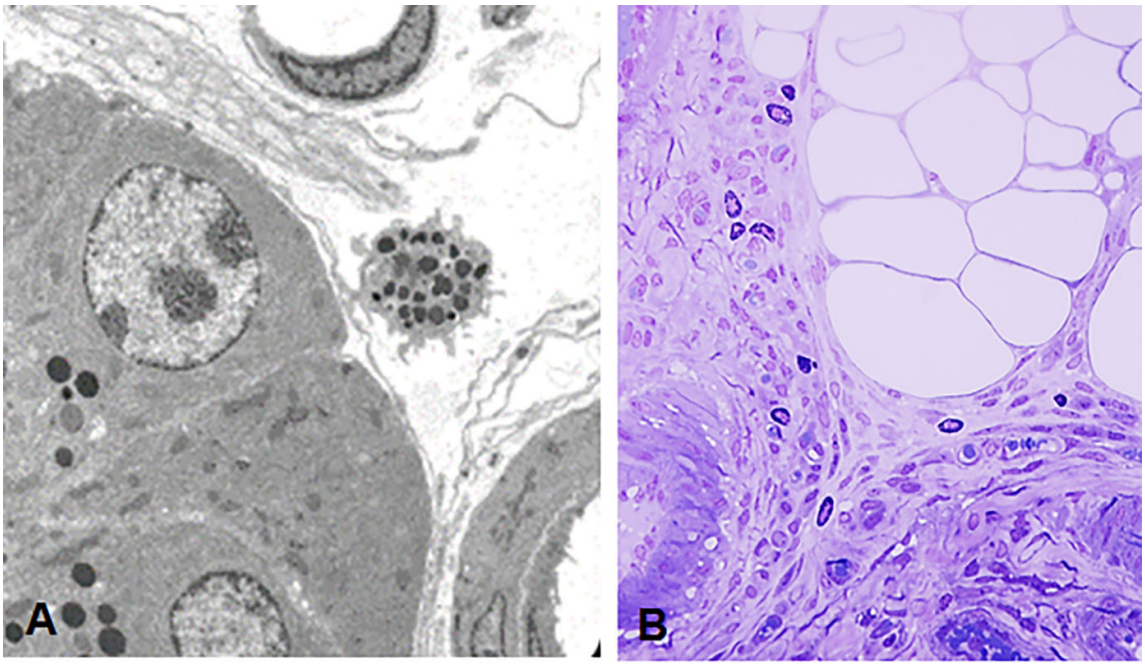

Figure 4.32 Mast cells found in the regenerative phase

In the CHB model in the later stages of the experiment, mast cells were seen to congregate in the inflammatory infiltrate **A**. Mast cell close to regenerated acini. Caerulein day10, EM x2500. **B**. Many mast cells congregated in the interstitial space. CHB, day 14, x1000.

4.6.4 Discussion on mast cells in inflammation and fibrosis in pancreatitis

Mast cells are widely distributed throughout normal connective tissues and are closely associated with the vasculature and nerves. In the models discussed here we show an increase in mast cell numbers early in pancreatitis and increased numbers of mast cells as fibrosis is developed. Increased numbers of mast cells were located near parenchymal cells, around nerves, in interstitial areas, in the mesentery and in adjacent lymph nodes. Mast cell degranulation was noted especially around tubular complexes and intralobular spaces.

Mechanisms proposed in the development of human acute pancreatitis are disturbance of acinar cell function, followed by the generation and release of inflammatory mediators combined with oxidative stress, that results in an exaggerated inflammatory reaction.[194] Thus, mast cell activation is proposed to be an important factor in the development of acute pancreatitis since many of the factors that stimulate mast cell activation such as platelet activating factor (PAF), ROS and oxidation products are implicated to trigger acute pancreatitis. Furthermore, inflammation could be further sustained by release of reactive oxygen species and PAF from mast cells. Of the three models only the caerulein model showed a dramatic increase in mast cell numbers early in the course of the lesion. Mast cell degranulation was found also at the 3-4 hour time-point in a mild model of caerulein-induced pancreatitis in rats. In the caerulein model, the presence of mast cell activation and the inflammatory response did not lead to a severe (or anaphylactic) outcome. Esposito and colleagues [195] reported that the mean number of mast cells in normal human pancreas was 7.6 ± 3.0 cells/mm^2 and in chronic pancreatitis 20.9 ± 9.3 mm^2. Mast cells were abundant both in fibrous tissue and in residual acinar parenchyma with diffuse infiltration around ducts, vessels and nerves. The mast cell counts from Esposito et al were similar to the results obtained in our experiment.

The role of mast cells in chronic pancreatitis is thought to follow a similar path to that of acute pancreatitis. According to Gruber[277] mast cells may initiate fibrosis indirectly. Endothelial cells are activated, adhesion molecules increase, release of chemotactic factors (in particular TGFβ) leads to leucocyte adhesion and migration. Fibroblast adhesion is upregulated with the increase in ICAM-1 and VCAM-1. The involvement of c-kit and other fibroblast factors leads to mast cell/stellate cell attachment, stellate cell activation and thus fibrosis. Concomitant with this, as mast cells degranulate, the release of TGFβ and TNFα stimulate stellate cell proliferation and the release of histamine, tryptase, heparin and MMPs.

In chronic pancreatitis and fibrotic disease, activated mast cells are identified as the cells responsible for perpetuating chronic inflammation.[233, 234] In these models, the highest count of mast cells coincided with the peak of fibrosis. Mast cells were also present in the CHB and duct ligation models as fibrosis persisted and remained active, though declined in numbers in CHB. In the caerulein model, mast cell count dropped noticeably as fibrosis resolved. In the models where fibrosis persisted, mast cell counts remained high. In these models, mast cells were located singly in the interstitium in the vicinity of stellate cells, macrophages and the cells of tubular complexes and surrounded by collagen deposition. They were found associated with both stellate cells and macrophages. The adherence of mast cells to stellate cells may be mediated by the interaction of membrane bound stem cell factors on fibroblasts with the c-kit receptor on mast cells.

The release of preformed mediators (histamine, tryptase, heparin, TNFα, TGFβ, bFGF, phospholipids and some cytokines) from mast cells is considered to be responsible for the activation of stellate cells which lay down ECM.[235] In the CHB model, the numbers of activated PSC decreased in the same timeframe as mast cell numbers decreased, despite the persistence of fibrosis and partial regeneration. In the caerulein model, fibrosis, mast cell and stellate cell decline were inversely related to regeneration of acinar cells. In the duct ligation model, there was no decline in mast cell and stellate cell numbers or fibrosis. This forms the basis of a relationship between stellate cells, mast cells and fibrosis.

4.7 OVERVIEW OF FIBROSIS IN PANCREATITIS

Fibrosis is a common feature of failure to regenerate in pancreatitis. The persistence or withdrawal of PSCs affects regeneration, but their role is uncertain. Macrophages and other immune cells such as mast cells, also persist in fibrotic pancreatitis. Their contribution to limiting or driving inflammation associated with injury resolution requires further investigation. Communication between the fibrotic processes, inflammation and some developmental mechanisms may determine the outcome of regeneration.

CHAPTER 5
SURVIVIN IN RAT PANCREATITIS

5.1 INTRODUCTION

Cell death and cell proliferation pathways are crucial to maintaining normal tissue homeostasis. During apoptotic cell death proteolytically-activated caspases cleave a range of substances that lead to nuclear and cell fragmentation. The inhibitor of apoptosis protein (IAP) family was identified in baculoviral genomes,[236] and in humans consists of eight regulators with the ability to block apoptosis through caspase inhibition by a wide range of triggers. The IAP family comprises two classes of molecules either indicated in control of cell division or regulation of apoptosis, however one member of this family, survivin, is implicated in both functions.[237]

The survivin protein has been extensively studied and is found to be unique in its differential expression in cancer compared with low to no expression in normal tissues and has been targeted as a potential cancer therapy due to its high expression in most human malignancies. It also has known functions in angiogenesis and cardiovascular diseases, and potentially has other roles. Most published reports concentrate on the involvement of survivin in cancer. The association of survivin in disease pathology is conceivably as important, however the expression and function of survivin in acute and chronic pancreatitis is not well defined.

5.2 AIM

The aim of this Chapter was to look at the expression and interactions of survivin with respect to apoptosis and cell proliferation in the rat models of pancreatitis.

5.3 MATERIALS AND METHODS

General materials and methods can be found in Chapter 2. IHC for survivin was performed using a monoclonal and a polyclonal antibody on serial sections from the experimental studies. The specification sheets from the antibody manufacturers suggest that both antibodies localize to the nucleus however examples provided for the antibodies showed some cytoplasmic staining in some tissues.

5.4 RESULTS

Serial sections of IHC for survivin are presented in **Figure 5.1** on alternate rows. The CST antibody localized well to nuclei although the cytoplasm often had a tinge of pale staining. Although there is the possibility that this was background staining, this appeared to be real staining as, though pale, it correlated with the cytoplasmic staining of the Nova antibody. The Nova antibody stained nuclei and cytoplasm, however it was particularly intense in the zymogen granules of acinar cells and the granules/cytoplasm of islet alpha cells during regeneration. Both antibodies showed some irregular staining or possible failed staining in random lobules, despite staining being performed in the same run or repeated. This was, however, a small percentage of the whole and the images presented here represent what is considered to be real.

The pancreas has a low turnover of cells in proliferation and in apoptosis. Nuclear survivin positivity in the control rat pancreas was more evident in the interlobular ducts than other ducts and acinar tissue and was similar in both antibodies. Nuclear positivity was seen occasionally in islets. Cytoplasm showed only very pale staining in the Nova antibody. (**Figure 5.1**). At day 1 in all models there was increased nuclear survivin expression in the acinar population, and in cells of the inflammatory infiltrate (**Figure 5.2A-E**). In Nova staining acinar cells and particularly the zymogen granules stained strongly in the cytoplasm, however the cytoplasm was negative in the duct ligation model (**Figure 5.2G,H,I**). As tubular complexes formed they were nuclear positive in both antibodies and also pale cytoplasmic positive in CST to strong positive in Nova. For both antibodies the duct ligation model was not as strongly stained **(Figure 5.2G-J**). As regeneration progressed in the caerulein and CHB models, acinar nuclei were strongly positive for survivin **(Figure 5.3A,B**). Nuclei in tubular complexes and islets were moderately positive (**Figure 5.3A-C**). With Nova IHC, the regenerative acinar cell cytoplasm was strongly positive, but islet cells were palely positive. The tubular complexes of the CHB model stained strongly in contrast to the duct ligation model where the cytoplasm was pale, however the nuclei stained strongly. Residual regenerated acini continued to express survivin strongly in the CHB model up to 28 days. Tubular complexes had random positive nuclei and some pale cytoplasm (**Figure 5.3G,H**).

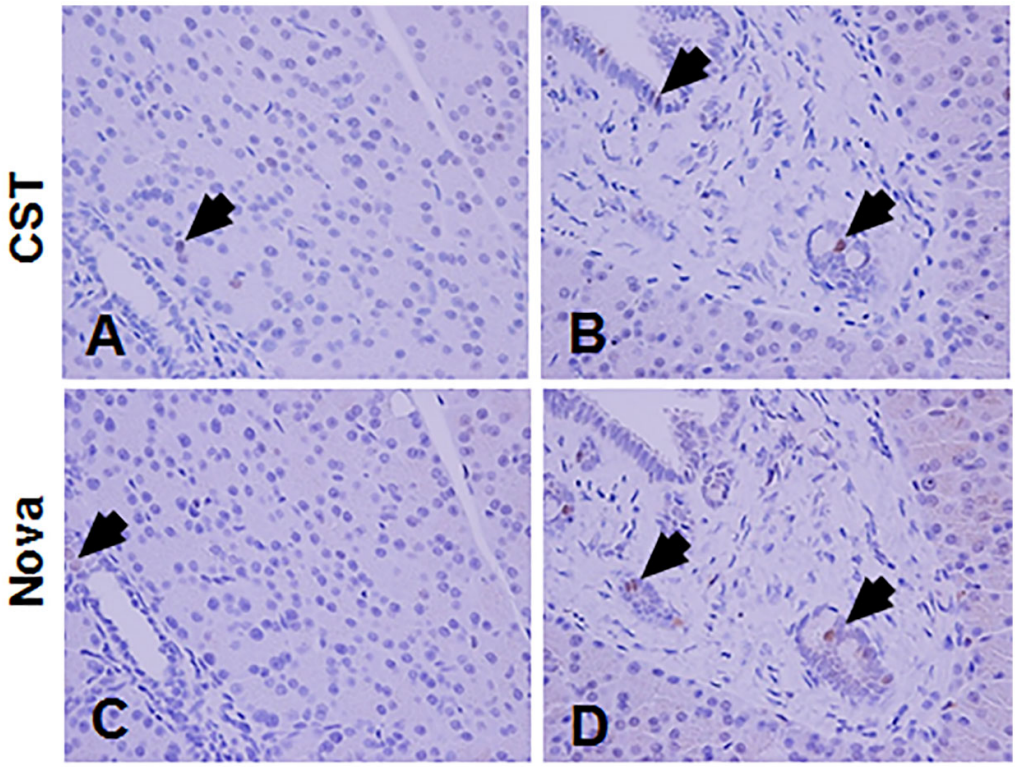

Figure 5.1 Control rat pancreas with survivin immunohistochemistry

Normal pancreas has a low turnover in proliferation and apoptosis Survivin nuclear positivity was seen in control sections primarily around or in ducts. **A**. CST antibody stains a probable acinar nucleus brown (arrow). In **B**, nuclei in the interlobular duct stain positive with both antibodies (arrows). In the corresponding section to **A** with Nova (**C**), there is pale staining in the ductal nucleus (arrow). In **D**, the cytoplasm and/or zymogen granules in acinar tissue at the bottom and right side of the Nova section (d) has a slight blush of colour.

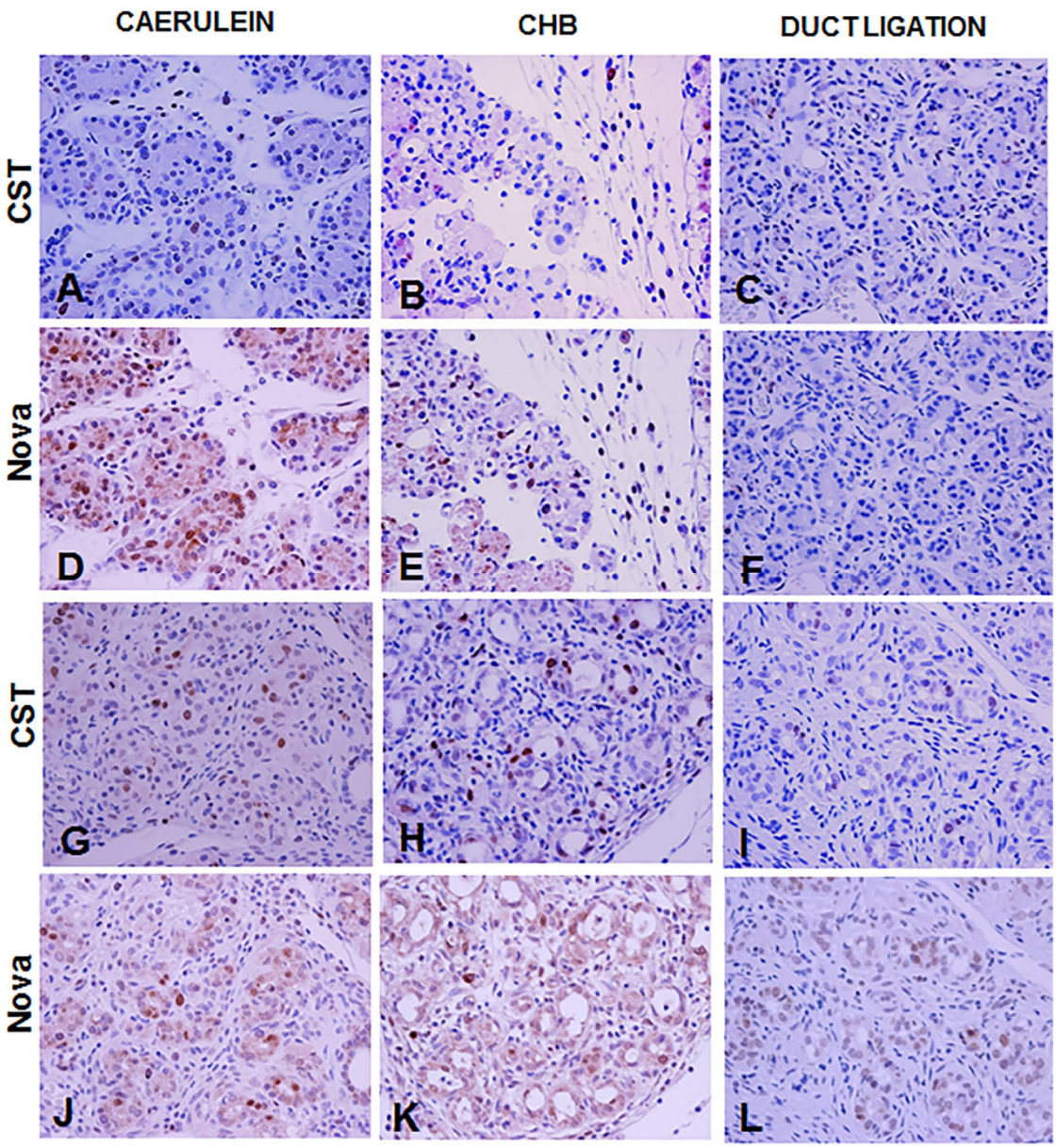

Figure 5.2 Distribution of survivin at early time points in the rat models

The CST antibody stained nuclei whilst the Nova antibody stained nuclei and cytoplasm.. When apoptosis was active acinar cell staining was prominent. Cells of the inflammatory infiltrate were nuclear positive and probably proliferating. Cytoplasmic staining in acini was weak in the duct ligation model. When tubular complexes formed they were also nuclear and cytoplasmic positive. Each experimental row depicts a comparable stage in the course of the pancreatitis for each model but not necessarily the same time point. Antibodies and models are indicated within the figure. **A,D**. caerulein, day1 x400; **B,E**. CHB, day1 x400; **C,F**. duct ligation, day1 x400; (**G,J**.)caerulein, day2 x400; **H,K**.) CHB, day4 x400; **I,L**. duct ligation, day4 x400

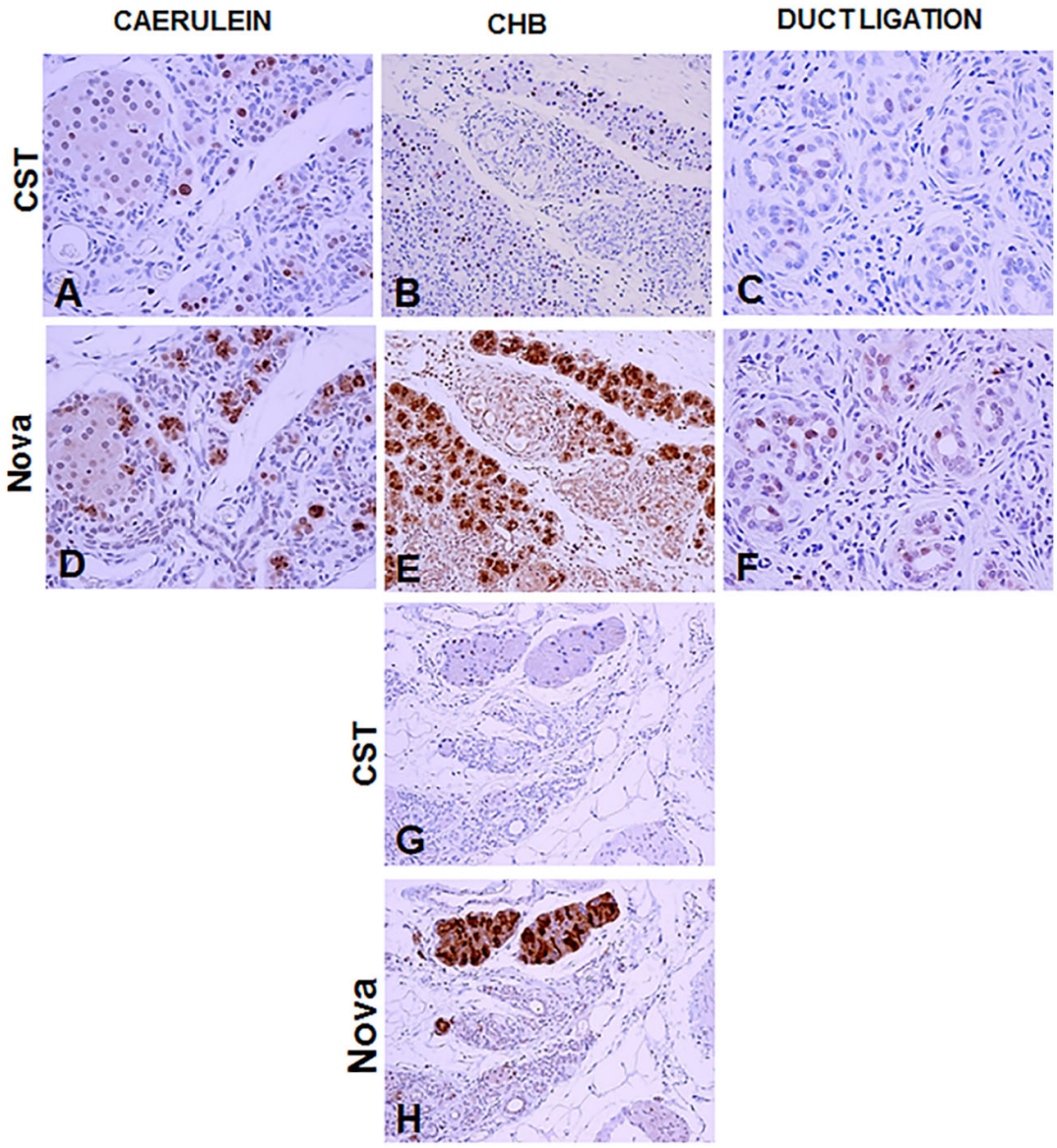

Figure 5.3 Distribution of survivin at later time points during regeneration

Models and antibodies are indicated within the figure. Each experimental row depicts a comparable stage in the course of the pancreatitis for each model but not necessarily the same time point. The Both antibodies indicate proliferative acinar cells by nuclear staining and zymogen granules are strongly positive in regenerating acini with the Nova antibody. **A,D** . Regenerating acinar nuclei show brown positivity with both antibodies, and cytoplasmic staining with Nova. Ducts and islets have pale cytoplasmic staining. Caerulein, day4 x400. **B,E**. Regenerating acini show positivity. Nova staining is prominent in acinar and tubular complex cytoplasm. CHB, day5 x200. **C,F**.Random tubular complex nuclei are positive. Nova stain is positive in the cytoplasm of tubular complexes. Duct ligation, day7 x400. **G,H**.) CHB, day28 x200 Nuclei are positive in regenerating acini and in tubular complex cells. Regenerated acini are still highly positive in cytoplasm, Nova. CHB, day28 x200

Other cell populations stained with the survivin antibodies. This was similar in all models although not all examples are demonstrated here. With Nova IHC but not CST IHC, the alpha/glucagon cells of the islets stained strongly **(Figure 5.4A,C**). This was also random as many but not every islet showed this staining effect (**Figure 5.4F**). **Figure 5.4C and F** compare the differences in staining of regenerative acini between the two antibodies. Interlobular ducts showed prolific nuclear positivity (**Figure 5.4G**,**J**) as did B cells and mast cells in the lymph nodes (**Figure 5.4H,K**). Nerve bundles and ganglion cells were cytoplasmic positive only in Nova but nerve bundles were negative and ganglion cells strongly nuclear positive in CST (**Figure 5.4I,L**). Cells of the inflammatory infiltrate were harder to judge. There were many seen strongly positive in the early time points however thereafter positive cells were few.

The proliferation marker PCNA on similar (but not serial) areas of the same models show that survivin nuclear positivity correlates with cell cycling in these models (**Figure 5.5**). **Figure 5.5A,D,G** compared islets stained for survivin, PCNA and alpha/glucagon cells. Survivin and PCNA staining are compared in interlobular ducts **(Figure 5.5B,E**), and in tubular complexes (**Figure 5.5C, F**). Regenerated acini in the PCNA stained image (**Figure 5.5D)** can be compared with the CST stained image of **Figure 5.3A**.

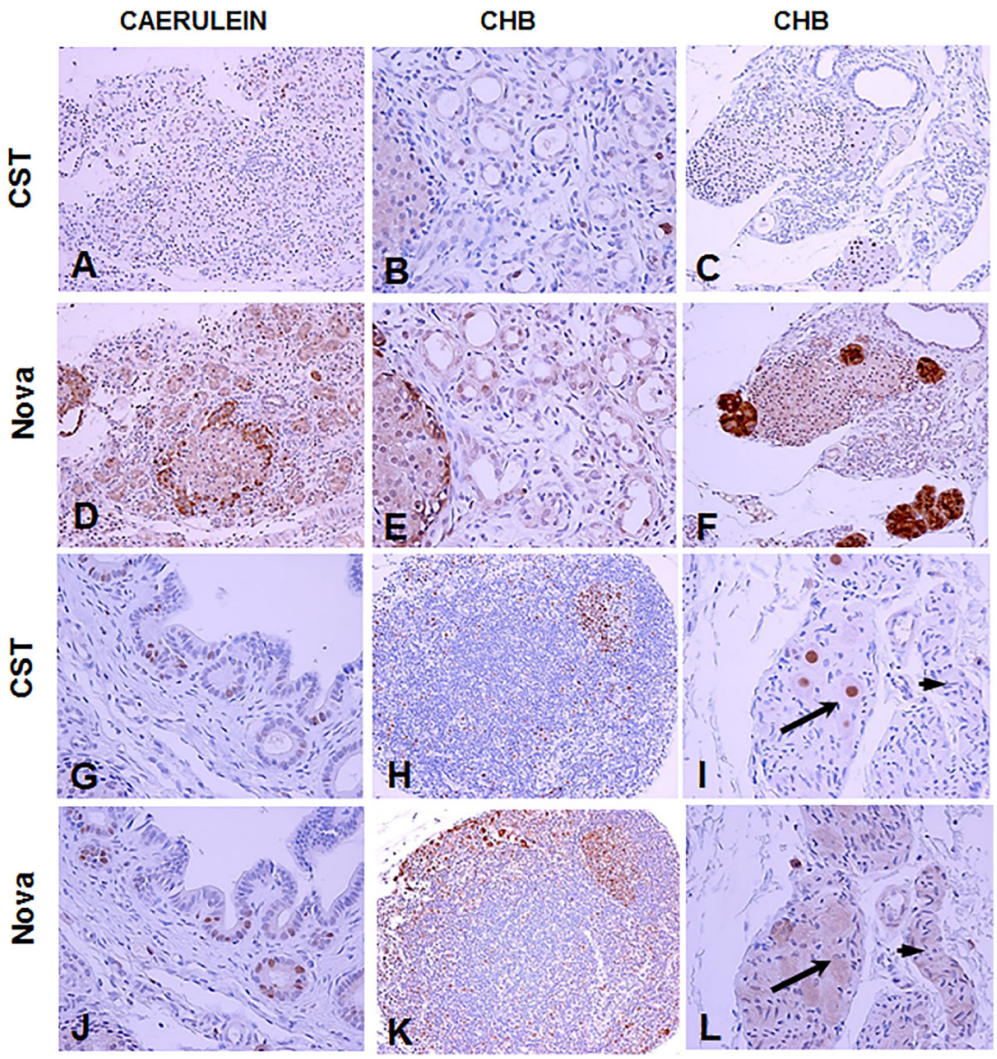

Figure 5.4 Survivin staining in other cell populations

Models and antibodies are indicated within the figure. Islets, large ducts, lymph nodes and nervous tissue also stained with the survivin antibodies. In serial sections (**A,D)**, markedly positive staining was noted on islet alpha cells with Nova but not CST. Caerulein, day 2, x200. This also applies to **B,E** which are CHB, day 4, x400. **C,F** show darkly positive staining of regenerating acinar cells, and variation in staining between antibodies for the islet. CHB day 18, x200. **G,J.** Nuclear staining of proliferative cells is similar between antibodies. Interlobular duct, caerulein, day10 x400. **H,K**. Lymph node with staining of B cell and mast cells. (**I,L**.) Ganglion cell nuclei stained with CST, cytoplasmic only with Nova. Nerve bundles were more prominently stained with the Nova antibody. This pattern of ganglion staining was consistent between the antibodies. Ganglion cell (long black arrow, nerve bundle (short arrow).

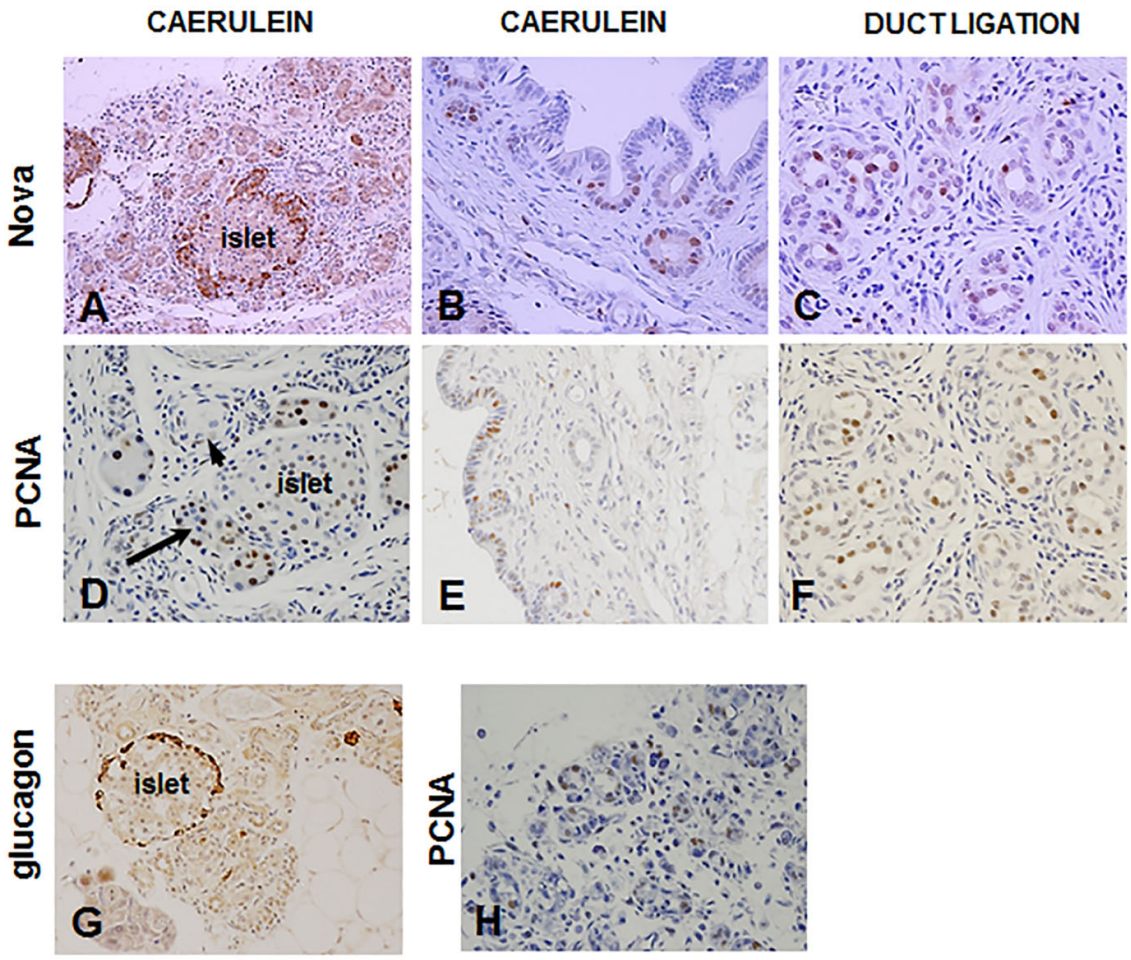

Figure 5.5 Comparison of survivin with proliferation marker PCNA

These images are not from serial sections. **A**. Islet alpha cells are strongly stained in the cytoplasm with survivin antibody, Caerulein, day 2 x200. For comparison, the distribution of alpha cells in an islet are indicated with IHC for glucagon in image **G**, CHB, day 18, x200. Interlobular duct nuclei stained positively with both survivin and PCNA. **B**, survivin, Caerulein, day 10 x400, **E**, PCNA Caerulein, day 10 x400. Tubular complex nuclei were positive both with survivin and PCNA, **C**, Duct ligation, day 7 x400, **F**, Duct ligation, day 7, x400. **D** shows cycling regenerating acinar cells (long arrow), islet cells, tubular complex (short arrow). Caerulein, day 2, x400; **H** shows cycling acinar cells. CHB, day 1, x400, both with PCNA IHC.

5.5 DISCUSSION

Survivin, the smallest member of the IAP family, is a multifunctional protein indicated in control of cell division and in regulation of apoptosis. It is usually found in all common cancers including pancreatic cancer, and selectively in normal cell development but it is not expressed in terminally differentiated tissues. It has a complex role in cell development as demonstrated by the impaired cell proliferation, apoptosis, cell cycle arrest and mitotic spindle formation that occurs when survivin is depleted or knocked down.[238] Survivin is expressed precisely in the G2/M phase of the cell cycle. It is involved in the cytokinesis process of mitosis by chromosome passenger protein behaviour and associates to centromeres from prophase to metaphase. Survivin has an anti-apoptotic role regulated by several mechanisms. Inhibition of apoptosis by survivin may occur during mitosis via the mitotic spindle checkpoint[239] or through mechanisms functionally-distinct from the mitotic role, including directly binding and inhibiting cell death proteases caspase-3 and caspase-7.[240]

Survivin is located in the nucleus contained in the mitotic apparatus and in the cytoplasm predominantly localized to mitochondria. Consistent with its function in cell survival and cell division is the proposal that nuclear survivin promotes cell division and cytoplasmic survivin controls cell viability. However, survivin is assumed to shuffle between nucleus and cytoplasm and has a number of splice variants with identical amino acid peptides that differ in subcellular locality and have different functional properties. The antibodies used in this study recognize all or most survivin splice variants and do not discriminate between the splice variants, thus the exact function of survivin in the cellular populations in these pancreata is subject to postulation.

The results show that acinar cells expressed survivin early in pancreatitis. Acinar nuclear survivin expression was noted also in acute necrohaemorrhagic pancreatitis in rats induced by sodium taurocholate.[204] This group recognised that survivin expression was not in every nucleus, proposed that the lack of survivin expression in other nuclei indicated that apoptosis may be activated in acinar cells and thus the nuclear expression of survivin is the anti-apoptotic effect. In the present study, survivin was expressed both in acinar nuclei and in the cytoplasm, depending on the antibody. Nuclear survivin expression was not in every cell and indicates that some acinar cells were cycling, confirmed by PCNA IHC. The early acinar cytoplasmic survivin expression was consistent in both the caerulein and CHB models but not in the duct ligation model. Whether the effect in the duct ligation model is real or a possible fixation artefact is unknown. It is clear, however, that the expression of survivin is increased in acinar cells early in this pancreatitis. Because the majority of these positive cells soon became apoptotic, the expression of survivin is not likely to have an anti-apoptotic effect. It may

indicate only that cell death pathways are activated and other factors determine which pathway of cell death or survival proceeds. Alternatively, the expression of survivin may indicate that acinar cells are differentiating.

It is important to understand the regulation of the death pathways in pancreatitis. Apoptosis, the primary mode of cell death in these models, is a tightly regulated process encompassing the caspase family of cysteine proteases. As a member of the IAP family, survivin inhibits the caspase system and several studies have reported the role of IAPs in regulating cell death in pancreatitis.[237] In caerulein pancreatitis in rats and mice, where apoptosis and necrosis were the modes of cell death respectively, the IAP called XIAP has been studied. In the rat model, XIAP was degraded and caspases activated leading to apoptosis in contrast to the mouse model where XIAP was not degraded and caspases were inhibited, resulting in necrosis.[241] PKD/PKD1 is the predominant isoform of the serine/threonine protein kinase family expressed in rat pancreatic acinar cells.[242] It is reported to mediate signal pathways in pancreatitis through NF-κB zymogen granule activation. In this study of experimental caerulein-induced pancreatitis, the Pandol group discovered that this protein kinase inhibits caspase activation and apoptosis but promotes necrosis by increasing the level of anti-apoptotic proteins such as survivin.[242]

In tubular complexes and normal ducts, survivin expression increased from normal values in both nuclei and cytoplasm, depending on the antibody. Comparison with PCNA expression, in tubular complexes and ducts at equivalent time points, indicates that this nuclear expression represents cycling cells. It is tempting to describe the consistent cytoplasmic tubular complex survivin expression as anti-apoptotic. Duct cells have an anti-apoptotic tendency as shown by expression of the Bcl2 family proteins compared with the pro-apoptotic tendency of acinar cells.[243] Regenerating acinar cells in the caerulein and CHB models strongly expressed survivin in the nucleus and in zymogen granules and cytoplasm. Again, the nuclear staining equated with cycling cells but the cytoplasmic staining is not easily explained other than survivin expression is involved in the regeneration of acinar cells and that the cells of the tubular complexes may not be terminally differentiated.

In the three rat models of pancreatitis, islet cells had nuclear expression of survivin in random cells consistent with cycling cells. General cytoplasmic staining may be explained as anti-apoptotic. The islet cells remain, presumably unaffected and non-apoptotic, under caerulein, CHB and duct ligation pancreatitis. Islet cells do undergo apoptosis in normal development and in diabetes pathology and are affected by disturbances in the cell cycle in development.[244, 245] With only a few exceptions, the

alpha cells that produce glucagon were strongly cytoplasmic positive, the beta and delta cells pale. These inconsistencies indicate increased survivin expression requires further investigation. IHC for survivin was demonstrated in human fetal alpha and beta cells but expression was noted only in alpha cells of newborns and adults.[244] High survivin expression in islets has been reported previously.[203] Hasel and colleagues report high survivin expression with immunohistochemistry in chronic pancreatitis in islets surrounded by fibrosis. As islets are stimulated for the TRAIL receptor lacking a death domain, and pancreatic stellate cells produce TRAIL, this suggests that an apoptosis-inhibitory program may be imposed on islet cells by stellate cell regulated TRAIL. Beta cell survivin expression has also been reported. Postnatal mice deficient in survivin in beta cells develop disordered insulin production and growth of beta cells due to lack of cell cycle progression.[245] Expression of the survivin protein, in this case, was due to EGF signalling through the Raf-1/ERK pathway. Survivin was strongly expressed in the nuclei of ganglion cells with the CST antibody but not with the Nova antibody. In Nova IHC, the ganglion cytoplasm was moderately stained as were nerve bundles that were negative in CST. The pancreas is richly innervated with mainly unmyelinated nerves with sympathetic and para sympathetic pathways and neural cell bodies known as intra-pancreatic ganglia aggregated randomly throughout the lobules.[14] The sensory nerves are damaged in pancreatitis by inflammation leaving them susceptible to factors released from inflammatory and acinar cells.[246] The damaged and sensitized nerve cells may be utilizing an adaptive and local defence response to injury by activating survivin.

This study in three models of rat pancreatitis has shown that survivin expression is increased in the major cell populations in pancreatitis. As cell death, cell proliferation and differentiation are implicated in pancreatitis and with survivin expression, the challenge will be to better define the role of survivin. The change in expression in different populations at different phases of the disease is not well defined and forms the basis for future investigation, particularly with respect to regeneration.

CHAPTER 6
THE EFFECT OF CYANOHYDROXYBUTENE IN MICE

6.1 INTRODUCTION

The common animal models of pancreatitis have been developed in a variety of species and are reviewed comprehensively in Chan and colleagues.[274] Models using chemical administration, diet, or surgically-induced have been developed in such diverse species as rats, mice, rabbits, dogs, cats, hamsters, pigs, opossum and ducklings. These models, whether invasive or non-invasive, simple or complex, employing high or low dose, induce a variety of lesions from mild interstitial to severe necrotising pancreatitis with considerable variation between species.

Following the sequencing of the genome of the mouse, transgenic mouse models and gene deletion studies facilitate understanding the role of specific proteins in the complex processes where different proteins interact and co-react in pancreatitis.[247] The model of CHB in rats eliminates all, or virtually all, acinar cells, produces fibrosis and regeneration occurs transiently. The possibility of using CHB as a model for pancreatitis in transgenic mice to study fibrosis and regeneration required exploration. It was, therefore, critical to assess whether the effect of CHB on the pancreas occurs, and whether this can be achieved safely.

Bhatia et al.[276] found that in mice a single intravenous dose of CHB (70mg/kg) induced apoptosis of pancreatic acinar cells. We are collaborating with a group at the Johns Hopkins Hospital in Baltimore, Maryland, USA (led by Dr Steven Leach) who has tried unsuccessfully to reproduce in mice the work by Bhatia et al. We reasoned that a successful regimen of subcutaneous dosage could develop a similar lesion in mice to that developed with subcutaneous dose in the rat, that is, with a more atrophic effect, and total loss of acinar cells. The effect of CHB is dose-related in rats[216, 248] and a sufficiently high dose in mice might be expected to initiate apoptosis within a relatively short time frame. Subcutaneous injections provide a method for minimal handling of animals in line with current ethical standards.

6.1.1. Aim

These experiments attempted to establish the CHB model of pancreatitis in mice. The aim was to induce pancreatitis in mice by the same method as that produced previously in rats.

6.2 MATERIALS AND METHODS

General materials and methods have been included in Chapter 2. Three separate experiments were performed to determine a dose and time frame that would produce pancreatitis in mice. Light and EM and IHC were used to investigate results. The weight of mice decreased between 0.5 and 2.5 g over the experimental period.

Experiment 1 Subcutaneous dose regime of CHB to produce apoptosis in mice

Adult mice between 27.0-34.5gms were randomly divided and housed in pairs. One pair used for sham control purposes was injected subcutaneously with 0.25ml normal saline. As this was an attempt to reproduce the work by Bhatia et al.,[276] and our collaborating group had already been unsuccessful by following that method exactly we proposed to use subcutaneous instead of intravenous injection which was successful in rats. As well, we treated the attempt as a pilot experiment starting with low doses with the intention of increasing the dose after histological review of the previous dose pair. Subcutaneous doses of CHB started at 70mg/kg through 90, 110, 150, 170, 190, 210, 230, 250, 270, 290 and up to 310mg/kg. Light microscopy, EM and IHC were used to investigate outcome.

Experiment 2. Optimal dose of CHB over time

As the results of experiment 1 were not optimal for apoptosis, we sought to expand the experiment with time frame to see if we had missed some effect. We chose a dose which produced cell death, either apoptosis and/or necrosis but did not cause excessive liver damage. Three groups of eight mice were injected with a subcutaneous dose of 280mg/kg and one group euthanased at each time point of 12, 18 and 24 hrs, liver and pancreas were removed and processed as above.

Experiment 3. Effect of mouse adolescent status with optimal dose of CHB

Four smaller CD1 Swiss mice of 21 – 23 grams were given 280mg/kg subcutaneously and euthanased at 24 hrs, then liver and pancreas taken as above. This was performed as some effect in rats may have been due to the adolescent status of the animals and we wanted to test if the same applied to the mice.

6.3 RESULTS

6.3.1 Experiment 1. Subcutaneous dose regime of CHB to produce apoptosis in mice

Effects of CHB on apoptosis and mitosis are represented in **Figure 6.1**. The effect on mice of a subcutaneous injection of CHB did produce apoptosis as hoped however not to the desired degree. Mitosis levels were slightly above normal**.** Damage to acinar cells occurred but the lesion did not proceed to classical pancreatitis. Liver necrosis caused fatal injury to the mice before pancreatitis could develop. In H&E sections the control mouse pancreas demonstrates typical closely packed acini with basophilic nuclei basally situated and eosinophilic zymogen granules at the cell apex. The acini are closely packed with minimal intercellular space (**Figure 6.2A**). The normal liver shows typical rows of hepatocytes separated by sinusoids. Two central veins are visible with a portal tract on the far right (**Figure 6.2B**). At a low dose of 70mg/kg CHB, there were mild changes of intra-and inter-lobular oedema in the pancreas shown by the increase in intra-acinus space. Both apoptotic cells and mitotic cells were evident in small numbers (**Figure 6.2C**). High power microscopy of the pancreas revealed vacuoles in acinar cells indicating the loss of zymogen granules via disordered autophagy, and change to RER was indicated by whorling. Nuclei had slightly clumped chromatin and there was loss of adhesion between individual acinar cells. (**Figure 6.2D**).

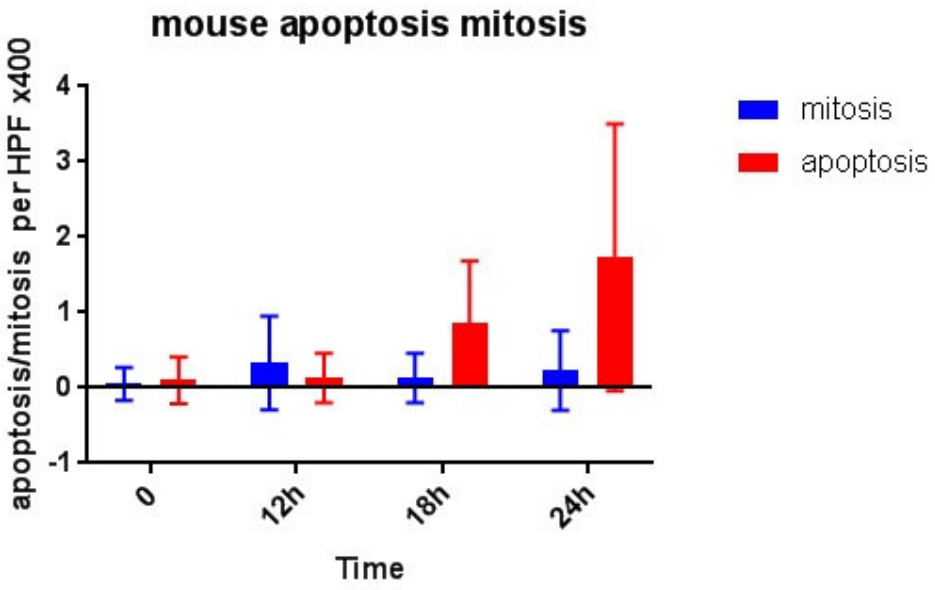

Figure 6.1. **Effects of CHB on apoptosis and mitosis over 24 hrs**

Apoptotic and mitotic nuclei were counted in ten fields of x400 magnification for one whole pancreas section at 4µm thickness per mouse per time point. Data are the mean ± SEM of eight mice (n=8) per time point from one experiment. Error bars represent the standard error of the mean. HPF=high power field. The effect on mice of a subcutaneous injection of CHB did produce apoptosis at 18 and 24 hrs, as hoped, however not to the desired degree. Mitosis was slightly above normal (time 0). One way ANOVA was used to compare apoptosis and mitosis in control groups versus experimental groups. Tukey's multiple comparison test was used to compare individual groups. Apoptosis counts were not significantly different from controls at time points 12 hrs and 18 hrs (P=0.9988, P=0.0924, respectively) but were significantly higher than controls at 24 hrs (P<0.0001). Mitosis was significantly higher than the control group at 12 hrs (P<0.0001) and 24 hrs (P=0.0315) but not significant at 18 hrs (P=0.4875).

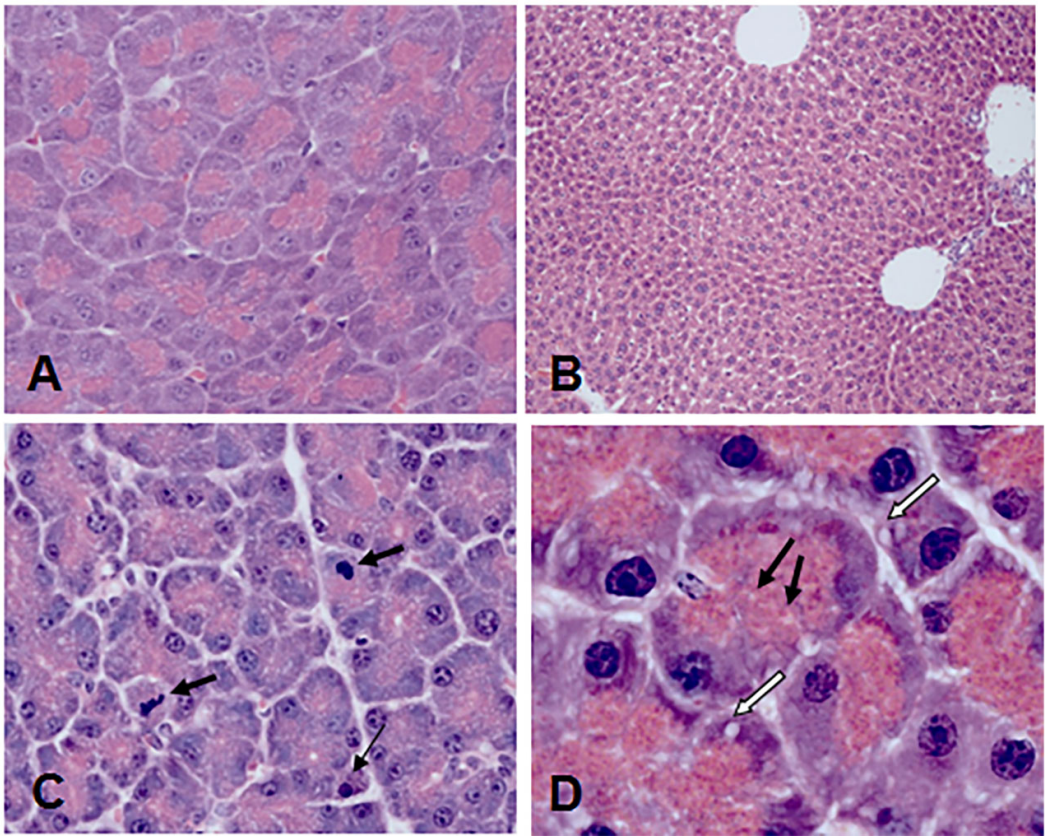

Figure 6.2 Mouse pancreas and liver for controls and experiment 1 (70mg/kg CHB)

Mouse control pancreas typically showed closely packed acini with minimal interacinar space, basophilic basal nuclei and apical eosinophilic zymogen-filled cytoplasm. The liver consisted of plates of hepatocytes separated by sinusoids. Central veins and portal tracts formed a typical triad with the bile ducts. Mild changes occurred at a dose of 70mg/kg CHB. There was intra- and interlobular oedema, seen by increased spacing between acini, some apoptosis and mitosis. At high power, vacuoles from disordered autophagy were visible, loss of zymogen granules was indicated by condensed cytoplasm and loss of adhesion between individual cells. Nuclear chromatin was condensed. **A**. Control pancreas with closely packed acini, luminal cytoplasm eosinophilic, basal cytoplasm basophilic. H&E, x400. **B**. Control liver, portal area and central vein of normal liver. H&E, x200. **C**. Pancreas treated with 70mg/kg CHB, intralobular oedema, mitosis (short arrow), apoptosis (thin arrow). H&E x400. **D**. Pancreas at 70mg/kg CHB, vacuoles (black arrows) distension of RER (white arrows), loss of cellular adhesion. H&E x1000

These mild pancreatic changes were consistent up to doses of 190mg/kg. At doses of 190-250mg/kg, the pancreatic lobules showed patchy changes consistent with increased disruption to acinar cells. This pathology was similar at doses of 270-310mg/kg, however the effect was more widespread. Basophilic and shrunken pancreatic cytoplasm reflected increased loss of zymogen granules (**Figure 6.3A**). High power view of a similar damaged area showed fewer nuclei, some with condensed chromatin, apoptotic figures, and large autophagic vacuoles in the cytoplasm (**Figure 6.3B**). Apoptosis was more prevalent at this stage but apoptotic counts were variable between animals and between lobules. Cell loss was obvious in some areas with acini consisting of only a few cells and many acini showed loss of adhesion between the remaining cells. In some lobules apoptosis and mitosis were juxtaposed.

There was no obvious liver pathology at doses less than 270mg/kg. Between 270mg and 310mg/kg mice had liver damage but four of fourteen mice had extensive liver pathology. This varied in the extent of necrosis, haemorrhage and apoptosis between lobules. Intact areas of liver were sharply demarcated from necrotic areas (**Figure 6.3C**). Cell death tended to be more obvious in portal areas of the lobule. Ghost cells coexisted beside apoptotic cells with pyknotic nuclei. Margination of inflammatory cells was present in veins and other cells, either apoptotic Kupffer cells or apoptotic bodies in Kupffer cells and/or lymphocytes were present in sinusoids (**Figure 6.3D**).

Pancreata from experiment 1, for example samples with doses of 270, 280, 290 and 310 mg/kg were chosen for further study with Bax and BclxL, immunohistochemistry. Nuclei showed positivity for both Bax and Bcl-x however the results were inconsistent with considerable variation between and within pancreatic lobules (**Figures 6.3E,F**).

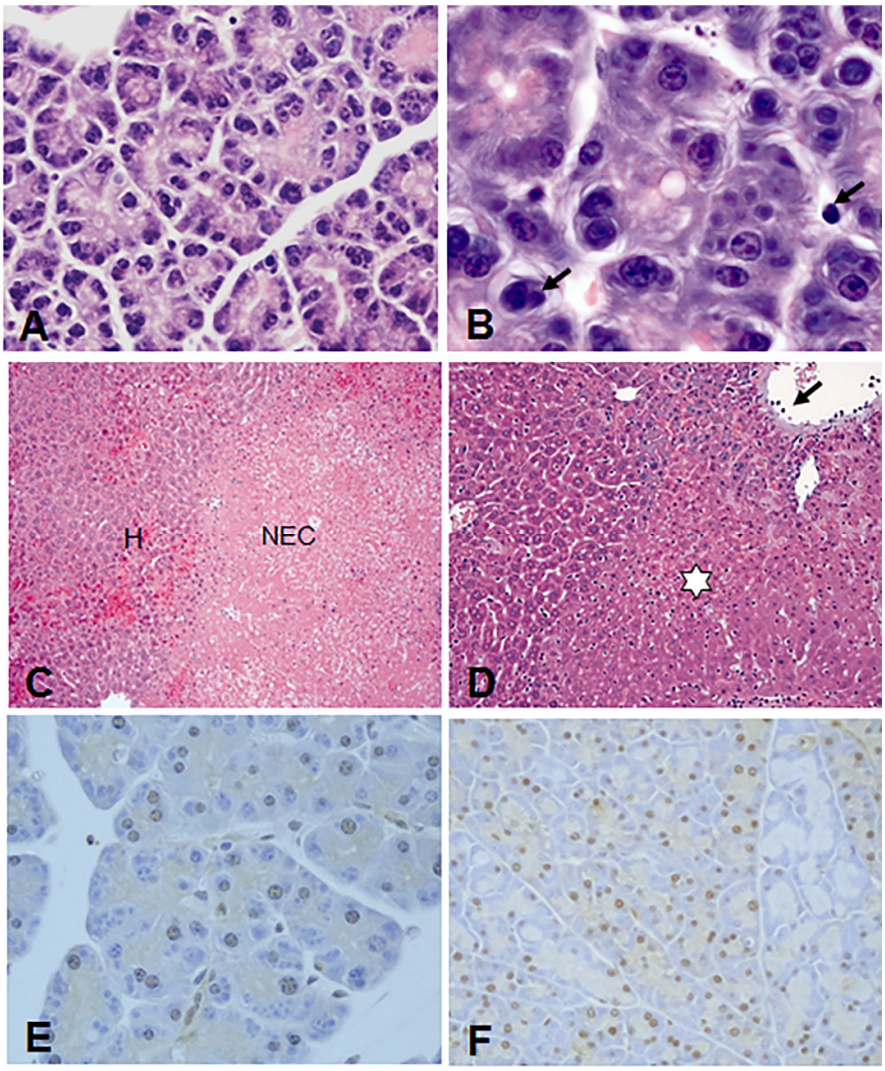

Figure 6.3 Mouse experiment 1. Pancreas and liver in mice treated with 270mg/kg CHB

Apoptosis was more prevalent at this dose with apoptosis and mitosis juxtaposed. Cell loss and lack of adhesion was more obvious. Liver damage included necrosis and haemorrhage, intact areas of liver were sharply demarcated from necrotic areas. Cell death was more prominent in portal area and inflammatory cells marginated in veins. Nuclear positivity for Bax and Bcl-xL was inconsistent with significant variation between lobules. **A**. Slightly damaged pancreas with basophilic cytoplasm reflects loss of zymogen granules. H&E, x400. **B**. Pancreas with whorling of RER, condensation of cytoplasm and nuclei, apoptosis (short arrows), loss of cell adhesion and architecture. H&E, x1000. **C**. Liver, necrosis (NEC) and haemorrhage (H). x200. **D**. Liver necrosis, haemorrhage and apoptosis; intact areas are sharply demarcated from damaged areas; margination of inflammatory cells (arrow), ghost cells devoid of nuclei (star). H&E x400. **E**. Bax positive nuclei brown counterstain haematoxylin. X400. **F**. Bcl-xL positive nuclei brown counterstain haematoxylin. X200.

EM of the mouse pancreas showed marked dilatation and whorling of endoplasmic reticulum in acinar cells. Nuclei appear normal. Inclusion bodies were present in lysosomes within the cytoplasm and extruded into enlarged intracellular spaces (**Figure 6.4A**). At a higher power electron dense zymogen granules are seen in the cytoplasm ready to be extruded as well as enclosed in extruded bodies with residual RER. Mitochondria appeared normal (**Figure 6.4B**). In **Figure 6.4C,** nuclei showed early margination of chromatin. Intercellular spaces were distended with widening gaps between neighbouring cells due to failure of desmosomes and gap junctions in lateral membranes. Flocculent material and residual RER is seen in these gaps. Zymogen granules were depleted, those remaining being small. Mitochondria were changed, dilated slightly with swollen cisternae. Few and small zymogen granules, many vacuoles and tightly wound RER are a typical picture of apoptosis, however in apoptosis the nuclei are apoptotic at a similar stage, and apoptotic bodies begin to form within the acinar cytoplasm. The mitochondrial swelling is more typical of necrosis (**Figure 6.4D**). A macrophage appears poised to mop up debris (**Figure 6.4D**).

A more advanced necrotic picture is depicted in **Figure 6.5A,B** with cell contents being extruded into the interstitial space through breakdown of the cell membrane. Vacuoles with debris have moved towards the cell surface, debris accumulating in the interstitial space. Mitochondria have increasingly swollen cisternae.

6.3.2 Experiment 2. Optimal dose of CHB over time

In mice with CHB doses over 280mg/kg, liver damage increased with dose concurrent with more pancreatic necrosis than apoptosis. The next experiment was designed to investigate the time effects on mice given a dose of CHB that achieved some apoptosis without too much liver necrosis. The pancreas from mice given 280mg/kg CHB in the time course from 12 to 24 hrs showed a similar progressive loss of zymogen granules in acinar cells. Whorling of RER, oedema and loss of adhesion between acinar cells and whole acini became widespread with time in most samples. The effect was mostly necrotic, however apoptosis and mitosis were again coexistent (**Figure 6.6A**). By 24 hrs apoptotic counts reached 1.29% compared to control 0.05%; mitosis reached 0.17% compared to control 0.03%. With increased time liver necrosis was more consistent, obvious and advanced, and haemorrhage was common in the 24 hour mice (**Figure 6.6B).**

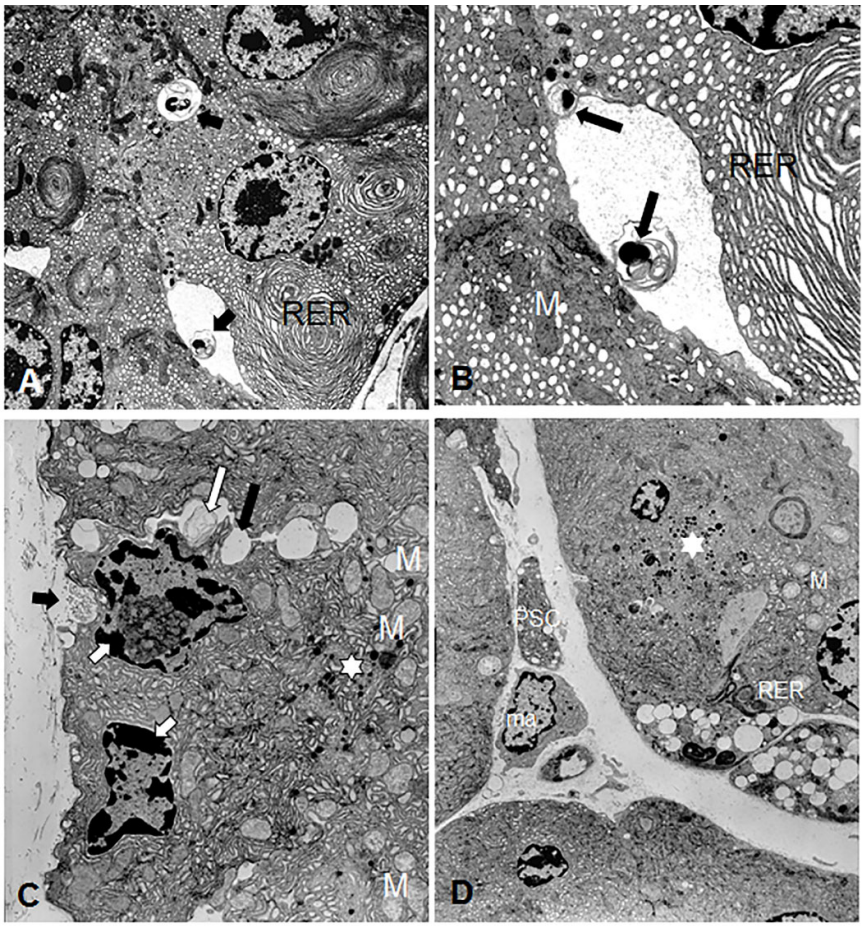

Figure 6.4 Non-lethal acinar cell damage in mouse pancreas

By electron microscopy damage to pancreatic acinar cells was obvious. There was marked dilatation and whorling of RER. Inclusion bodies were in active lysosomes, in the cytoplasm and in intracellular spaces. Inter- and intracellular spaces were distended with failure of desmosomes and gap junctions causing spaces between cells where flocculent and residual RER gathered. There was some early margination of nuclear chromatin. Zymogen granules were depleted and the mitochondria had slightly swollen cisternae. **A**. Intercellular separation at bottom and vacuoles with extruded residual material (short black arrows), RER is whorled. EM x3000. **B**. High power of A shows extent of whorling and distention of RER. Zymogen granules and RER are being extruded (black arrows). Mitochondria (M) appear normal. EM x9000.**C**. Nuclei show early margination of chromatin (short white arrows). Lateral membranes are separated by gaps (long black arrow) containing extruded RER (long white arrow). Basement membrane is disrupted (short black arrow). Few small ZGs are scattered in the cytoplasm (star). EM x5000. **D**. Acini with swollen mitochondria (M), large vacuoles (short black arrows), few ZG (star) and residual RER. Stellate cell (PSC), macrophage (ma). EM x2500.

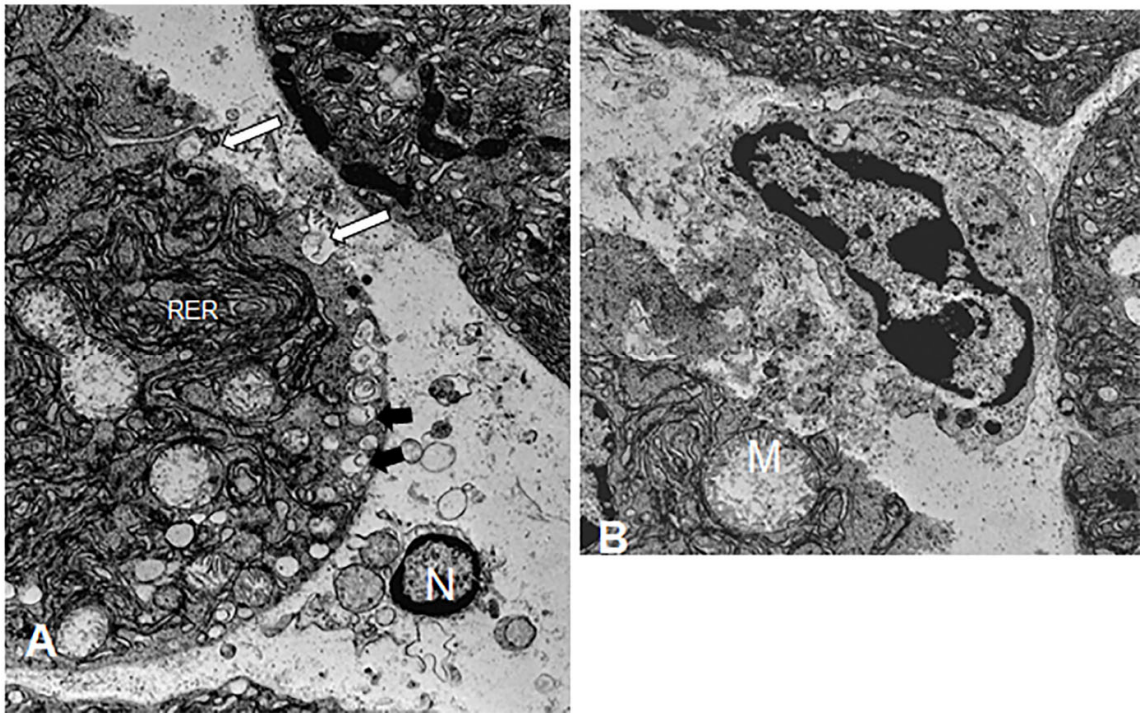

Figure 6.5 Acinar injury with necrosis in the mouse model

These images show a more advanced scenario of acinar cell damage than in Figure 6.4. This damage is more consistent with necrosis. **A**. Acini with whorled, condensed rough endoplasmic reticulum (RER) and swollen mitochondria. Breakdown of cell membrane with extruding debris (long white arrows), nuclear debris (N), extensive autophagic vacuoles (short arrows). EM x3000. **B**. Swollen mitochondria (M), debris and macrophage EM x7500

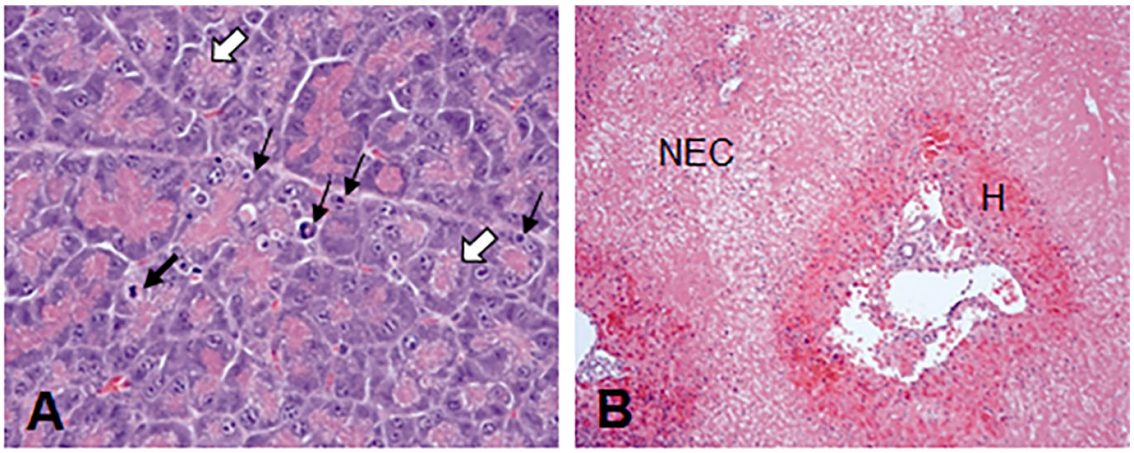

Figure 6.6 Experiment 2. Pancreas and liver in mice treated with 280mg/kg CHB for 24 hrs

The pancreas of mice treated with a high dose of CHB for 24 hrs showed the most apoptosis however this coexisted with mitosis. The typical picture was of loss of zymogen granules and cellular adhesion, vacuoles, condensation of cytoplasm. Liver necrosis was more obvious and advanced with haemorrhage common. **A**. Pancreas, cytoplasmic vacuoles (white arrow), mitosis (short arrow), apoptosis, (thin arrows), note less numbers of cells comprising acini. H&E, x400. **B**. liver H&E. necrosis (NEC) and haemorrhage (H). x200.

6.3.3 Experiment 3. Effect of mouse adolescent status with optimal dose of CHB

As there was no histological difference in the pancreatic or liver effects in younger mice given 280mg/kg and euthanased at 24 hrs compared to older and heavier mice, the pathology was no longer considered relevant and no images are presented.

6.4 DISCUSSION

The desired outcome of massive synchronous apoptosis by 12 hrs, and subsequent atrophy of exocrine pancreas as was found in the rat under similar experimental conditions was not achieved. At 24 hrs after a single subcutaneous injection of CHB to mice the apoptotic count reached seven per high power field (HPF) magnification x400 or 1.29% of acinar cell total compared with control levels of 0.03%. This is only a slight increase in apoptosis, far below that found in intravenous dose by Bhatia et al.[276] In their study, when CHB was given as a single intravenous dose of 70mg/kg to mice, apoptotic acinar cells reached 30-40 per high power field (magnification x250) 12 – 24 hrs after injection but apoptotic labeling diminished between 24-36 hrs post CHB administration and at 48 hrs, substantial viable acinar tissue remained.

Walgren and colleagues[273] evaluated the sensitivity of peptide markers for pancreatitis in rats treated with CHB and caerulein, and mice treated with CHB. Mice were administered a single subcutaneous dose of CHB (50 or 150mg/kg) however details of the method of CHB synthesis was not given. Minimal histological changes were noted in the mouse pancreas. Both diffuse and multifocal changes were seen, mainly mild vesiculation in the RER and ZG zones. No apoptosis or necrosis was reported. The Steven Leach group (Johns Hopkins, Boston) reported a similar unsuccessful dose response regime with intravenous CHB in mice (personal communication, Prof Sandra O'Toole, Garvan Institute of Medical Research). At low doses there was mild injury to the pancreas. At high doses, liver necrosis killed the mice with little change to the pancreas.

Given the half-life of apoptotic bodies of 1-2 hrs[249, 250] and the fact that small increments in apoptotic indices of the order of 1-2% can halve the total cell population of a tissue within 24 hrs,[251] the observed high apoptotic indices in the Bhatia[276] experiment should have been sufficient to delete all or most acinar cells by 48 hrs. The apoptotic staining methods used in that experiment (Fluorescent dye Hoechst H33258 and *in situ* staining by Apoptag method) may be demonstrating cleaved strands of DNA that have chosen the apoptotic pathway but go on to repair rather than continue to the final

stages of apoptosis. That substantial tissue remained at 48 hrs would indicate that apoptosis leading to acinar atrophy was also not achieved in the Bhatia model.

It would appear that the results in our experiment reflect that of a mild effect of CHB, and that liver damage occurs before atrophy of acinar cells. The histological picture seen in our experiments with mice closely resembles the mild effect described by Wallig and colleagues[248] on rats 150-225gm given a single dose of CHB (extracted from the seeds of Crambe Abyssinica) daily in 0.25-0.50ml corn oil. Note: corn oil is not miscible with CHB. In those experiments, the most consistent lesion over 1-4 days was dilatation of the cisternae of RER in pancreatic acinar cells. The degree of dilatation varied from cell to cell but was present to some degree on virtually all acinar cells. In most acini 1-4 cells were reduced in size and had rounded profile, severely dilated ER cisternae, decreased numbers of zymogen granules and varying degrees of cytosolic condensation. Nuclei and mitochondria were unaltered. Some apoptosis was seen (shrunken cells and cell fragments) in acini, macrophages, autophagic vacuoles and within the interstitium.

Clinically and experimentally, apoptotic and necrotic cell death are seen in pancreatitis. The mechanisms which determine whether acinar cells undergo the apoptotic or necrotic cell death pathway are still to be fully understood and involve an array of molecules. Mareninova et al [240] investigated the differences in cell death responses between rats and mice in a model of caerulein-induced pancreatitis, with up to seven hourly injections of 50µg/kg caerulein. The rat pancreatitis was mild and characterised predominantly by apoptosis; the mouse model more severe with predominantly necrosis. Detection of caspase activity determined that in the rat model the effector caspase-3 and the initiator caspases-8 and -9 were swiftly increased compared with no caspase activation in the mouse model. The intrinsic pathway of apoptosis involves mitochondrial damage that releases cytochrome-c to form a complex with Apaf-1 and procaspase-9 that in turn activates the effector caspases through caspase-9. This appeared to be the pathway initiated in both rats and mice however in the mice the caspases-8 and -9 were blocked in the acinar cells. In caerulein-induced pancreatitis, therefore, it appears that mice are more susceptible to necrosis than apoptosis and vice versa for rats. Furthermore this group found that caspases protected the rats from necrotic cell death.

Marked depletion of pancreatic glutathione (GSH) within 1-2 hrs of CHB administration[248, 252] suggests that CHB causes oxidative injury to acinar cells that initiates apoptosis.[253] In rats, there was a dose relationship between GSH elevation and pancreatotoxicity following intravenous and oral administration of CHB.[248] Plasma levels would be expected to peak much higher following intravenous administration compared to subcutaneous and oral dosing thus toxicity and GSH

elevation are most likely both related to plasma levels. The data on intravenous administration showed that both toxicity and GSH elevation are dose dependent. Wallig and Jeffery[252] showed a mild protective effect of low dose CHB against the toxicity of subsequent high-dose CHB. It may be that the induction of glutathione after CHB administration in the mouse confers a relative resistance to further similar insults. The Bhatia group[276] showed a protective effect of CHB against caerulein induced injury, especially when given 12 hrs after CHB but not after 18 or 24 hrs.

In this experiment there was considerable inter- and intra-lobular variability in the pancreatic lesion indicating that the dose effect was less than optimal. Some acinar cells had swollen mitochondria indicating early necrotic injury. Loss of zymogen granules was more marked than in the rat model - an indicator of either a necrotic or apoptotic pathway to cell death. Necrosis in this setting may be a high dose effect, but at lower dose (70mg/kg) we saw little evidence of apoptosis. We have speculated that in the rat, early apoptosis is a mechanism protective against necrosis.[216] This does not appear to exist in mice and this is confirmed by the study of caspases between rats and mice by Marienova et al.[241] The morphological features of apoptosis are well defined in the nucleus as crescentic margination of chromatin against the nuclear membrane. In this mouse experiment, besides classical apoptosis, electron micrographs show margination of nuclear chromatin different from the classical manner of apoptosis. This partial margination bears resemblance to that depicted as the morphological features of nuclei in autophagic cells.[254] Autophagy may be involved in the degradation of damaged organelles such as mitochondria and endoplasmic reticulum as a survival mechanism for cells as opposed to a death pathway. Vacuolisation in the cytoplasm is seen in both necrosis and autophagy. In this mouse lesion it can be seen that the processes of autophagy, apoptosis and necrosis are seen concurrently.

In the mouse pancreas there was no evidence of a substantial inflammatory infiltrate. Various triggers dictate the course of pancreatitis whether acute or acute-on-chronic. Generally, activation of complement and other serine proteases and fibrinolytic cascades occurs early.[194] Caerulein administration in rats excites a vigorous inflammatory response[255] however in rats given CHB inflammation is delayed, reaching moderate density only at 48 hrs,[215, 252] or from early in the subcutaneous lesion it is mainly mononuclear with the number of neutrophils remaining small throughout.[216] Although macrophages and stellate cells were noted in the mouse pancreas their numbers were not observed to increase. Weight loss in most mice would suggest that some acinar attrition had occurred, however mitosis was present just above normal levels from 12 hrs, indicating that the pancreas may have been attempting to maintain homeostasis. With viable acinar cells

remaining it is difficult to ascertain whether regeneration was from remaining acinar tissue, from duct cells or from other stem cells.

Mitochondrial membrane permeabilisation (MMP) is the event that defines the point of no return in most programmed cell death models. Bax and/or Bak are the pro apoptotic, pore-forming molecules of the Bcl-2 family that can trigger MMP and the release of death-inducing molecules from the mitochondrial intermembrane space. The anti-apoptotic Bcl-2 proteins, Bcl-2 and Bcl-xL oppose MMP.[256] Immunohistochemistry for Bax on the mouse sections showed an increase in expression with dose but not an increase with time compared to controls. Bcl-xL immunohistochemistry showed an increase in expression compared to controls that did not relate to either dose or time and varied between lobules. The inconsistent balance of Bax to Bcl-xL most likely reflects the inability of this model to undergo significant apoptosis. Rats may have a lower threshold for apoptosis of acinar cells than do mice where $Bclx_L$ and Bax are evenly switched on and may protect from low threshold apoptosis. As these results were inconsistent no statistical analysis was completed with Bax to Bcl-xL here however an expanded future comparison with mouse versus rat Bcl-2 family proteins may be worthwhile.

In these experiments, the dose of CHB was not increased past 310mg/kg as this high dose proved to be hepatotoxic to mice. This is in itself an important and interesting observation for the role of CHB in the liver. In mice given 250mg/kg CHB liver necrosis was more obvious with time. When given orally in water to rats, CHB is toxic to liver at a lower dose than to pancreas as expected with the portal circulation. In contrast when given subcutaneously the pancreatotoxic effects are the first to occur, followed by hepatotoxicity. In rats high dose CHB was hepatotoxic when administered orally, intravenously and subcutaneously.[216, 217, 248] Rats given high dose CHB died of massive liver necrosis with little or no change to their pancreata. A fine balance between the dose and route of administration determines the outcome between liver and pancreatic toxicity in rats. We were not able to find this balance in the mouse.

6.5 CONCLUSION

This study was a dose response study to find a dose which caused pancreatic acinar cell atrophy. We found that in mice, liver toxicity occurred at a lower dose than complete pancreatic toxicity, which limits the usefulness of it as an experimental model. Given the marked difference between our findings in rats and mice it may be that the pathway to cell death is completely different in these rodents, an interesting conundrum for the administration of pharmaceuticals in animal models.

CHAPTER 7

DOG MODEL OF PANCREATITIS

This chapter presents the investigations using a dog model of pancreatitis. The chapter is presented as a manuscript for submission "Cyanohydroxybutene (crambene) causes massive liver damage in dogs" by Lynne E Reid, BSc, Melanie Latter, BVSc, and Lyndell E Kelly, MBBS, PhD, FRANZCR. Methods are again in detailed format. Some abbreviations previously defined in this thesis are, of necessity for submission of a manuscript, redefined here. Please note that references for this Chapter are listed at the end of this Chapter.

Note that mature pound dogs were the only dogs available for this experiment although an unsuccessful attempt was made to secure greyhounds to limit variability among breeds. Use of pound dogs was not optimal as it was not possible to choose dogs individually and, therefore, it was challenging to get dogs of similar weight and age. No veterinary history was available for the dogs used. Clinical veterinary checks showed that they were in good health, however the variability in our results would indicate that some may have had unknown underlying conditions.

7.1 SUMMARY

Cyanohydroxybutene (1-cyano-2-hydroxy-3-butene, CHB) is a breakdown product of glucosinolates in cruciferous vegetables. In rats, a dose of 150mg/kg causes selective destruction of pancreatic acinar tissue principally by apoptosis. CHB was given to 14 dogs (12-21kg) in doses ranging from 70 down to 30 mg/kg intravenously over 15-30 minutes, followed by euthanasia and necropsy. These doses had little effect on the pancreas, but frequently produced fatal hepatic necrosis. Dogs were well and active or developed fatal liver failure, perhaps indicating that antioxidant capacity had been overwhelmed. Hepatic injury was reflected by depression and lethargy, and sometimes by abdominal discomfort. Laboratory testing showed marked elevations in hepatic cytosolic enzyme activities, bilirubin, creatine kinase activity and moderate to severe hypoglycaemia. Haematology showed marked thrombocytopaenia. A coagulopathy was suggested by bleeding into the peritoneal cavity of some dogs with advanced hepatic necrosis. Oral administration of antioxidants did not ameliorate liver injury. Clearly, CHB is of no value for treating chronic relapsing pancreatitis or acinar pancreatic

carcinoma in canine patients. There is a remarkable similarity in physical and laboratory necropsy findings between intoxications referable to the 5-carbon CHB and xylitol, a 5-carbon sugar used as an artificial sweetener.

7.2 INTRODUCTION

A model of pancreatitis induced using synthetic racemic 1-cyano-2-hydroxy-3-butene (CHB), sometimes called crambene, had been established in rats [1]. CHB is present in many foods such as canola and cruciferous vegetables and is a selective pancreatotoxin in the rat and mouse. It is thought to be beneficial in low doses because it induces glutathione, an antioxidant [2]. At high doses, it causes apoptosis of pancreatic acinar cells. At a critical dose, this causes almost complete loss of acinar tissue. CHB administration results in cell death in acinar tumours transplanted into rats making it a potential treatment for acinar cell carcinoma of the pancreas [3]. At present, it is unknown whether this effect occurs in other mammals.

Total and permanent loss of acinar cells constitutes a valid investigation for acute relapsing or chronic pancreatitis, common diseases both in human and canine patients, often secondary to inherited lipid disorders and ingestion of high-fat meals [4,5]. One purpose of this experiment was to see if a safe drug-induced exocrine pancreatectomy could be achieved with CHB in the dog. We have tried to assess the effects and potential toxicity of CHB in randomly-bred dogs. All experiments were approved by the University of Queensland Animal Ethics Committee (PATH/457/04/LF).

7.3 MATERIALS AND METHODS

CHB was synthesized by and purchased from Research Directions, Auchenflower, Queensland. The Animal Research Ethics Committee of the University of Queensland gave ethics approval. This pilot study was conducted in stages, with the intention of finding a dose of CHB that would selectively destroy acinar cells of the pancreas without excessively damaging the liver, islets of Langerhans or other tissues. Given that the most effective parenteral doses in mice and rats are 280 mg/kg and 150 mg/kg subcutaneously, respectively, and taking into account allometric scaling, we elected to start with 70 mg/kg. Based on studies in rats and mice, CHB is more toxic on a mg/kg basis in large animals [6].

Experimental subjects (N = 14) were dogs destined for euthanasia at a local pound. They were apparently fit and healthy as assessed by routine physical examination and were of mixed breeds. For ease of handling, dogs of 15-20 kg were chosen. Dogs were continuously monitored by one or two veterinarians for the duration of the experiment. If required, dogs were kept sedated, however, if well, the level of sedation was reduced, and dogs were taken on regular walks in runs to permit urination and defecation. At these times, strength and demeanour was assessed and the abdomen was gently palpated to assess if pain was evident.

Dogs were given 0.05 mg/kg of acepromazine and 0.3-0.4 mg/kg of methadone subcutaneously to provide sedation and analgesia. The required volume of CHB was placed in a 100 ml bag of normal saline (0.9% NaCl) and infused intravenously through an indwelling cephalic catheter over 15 minutes. Hartman's solution was subsequently administered intravenously (IV) at the rate of 1 litre every 12 hours using an infusion pump. Blood was taken at 4, 8 and 12 hours for dogs 1 and 2, and at 0, 12, 24 and immediately prior to euthanasia for dogs 3-6.

Dog 1 was given 70 mg/kg (x 18 kg = 1.26 g CHB). Dog 2 commenced 10 hours after Dog 1 but was given a reduced dose of 50 mg/kg (x 15kg = 750 mg CHB). Both dogs were kept sedated and comfortable using incremental doses of acepromazine and methadone, given to effect. The first dog was euthanased by an IV overdose of pentabarbitone sodium 12 hours after CHB administration, the second at 20 hours after CHB. The experiments were terminated at these time points when it was clear that dogs had severe liver damage, likely to be fatal, on the basis of numerous physical and laboratory findings.

Given the apparent hepatotoxic effect on dogs 1 and 2 (Table 1), the CHB dose was reduced in subsequent experiments, and the drug was administered more slowly. As serum biochemistry demonstrated hypoglycaemia, blood glucose was monitored in subsequent experiments using a point-of-care glucometer so that glucose infusions and boluses could be given to maintain euglycaemia. Two dogs received 30 mg CHB/kg (x 18 kg = 575mg; x 15.5 kg = 465 mg); two received 40 mg/kg (x 20 kg = 820 mg; x 12 kg = 450 mg). The IV infusion of CHB was given over 30 minutes, rather than 15 minutes. It was intended that one dog from each pair be euthanased at 24 hours, and the other dog at 48 hours. Dogs were kept sedated, analgesed and comfortable as above with continuous monitoring of behaviour, biochemical measurements and continuous support with intravenous fluids and glucose.

In order to assess whether a dose of CHB could be found that was consistently 'safe' and to assess the effect of CHB on tissue over a longer timeframe, dogs 7-10 were given 35 mg/kg with euthanasia planned for 96 hours. As the mechanism of action of CHB is thought to consist of membrane oxidation, a further experiment was conducted with dogs 11 – 14 following premedication with antioxidants vitamin C (200 mg) and vitamin E (200 mg) given orally (by mouth) 90 minutes prior to the 35 mg/kg dose of CHB. The intention was to use the first-pass effect following oral administration of these antioxidants to selectively protect the liver from CHB toxicity.

Complete necropsies were performed on each of the dogs by a veterinary pathologist. Tissues were fixed in buffered formalin and paraffin-embedded for haematoxylin and eosin (H&E) staining (4 μm sections).

7.3.1 Immunohistochemistry

PCNA IHC was used to examine proliferation of cells in pancreatic sections. The mouse anti-human monoclonal PCNA (Calbiochem Oncogene Research Products cat#NA03) was used at a concentration of 1:100. Sections were pre-treated with 0.2N HCl for 20 minutes and processed using a Dako EnVision+ Dual Link System-HRP (DAB+) kit (DakoCytomation) and lightly counterstained with Mayer's haematoxylin. Total acinar cells and PCNA-positive acinar cells were counted in 10 high powered fields (HPF) for each pancreatic sample. The PCNA index was calculated as a percentage of total acinar cells.

7.4 RESULTS

7.4.1 Biochemical parameters and gross pathology

Biochemical parameters after treatment with CHB are presented in Table 1. There was a marked variation in response to the dose of CHB. Doses up to approximately 35 mg/kg were mostly tolerated with eight dogs clinically normal. Doses in excess of 35 mg/kg were fatal to six dogs due to a severe hepatotoxic effect.

Dogs given 70 mg/kg and 50 mg/kg over 15 minutes (dogs 1 & 2) after 11-12 hours showed marked thrombocytopenia, moderate leukopenia, slightly elevated bilirubin concentration. Alanine aminotransferase (ALT), alanine aminotransferase (AST) and creatine kinase (CK) activities were markedly elevated, while amylase and lipase were normal. These dogs were euthanased early. At

necropsy the liver was enlarged, dark and friable, the pancreas edematous and pale. Petechial haemorrhage was evident throughout the gall bladder and stomach and a large volume of free blood was present in the abdominal cavity in one dog.

Dogs with dosage 40 mg/kg over 30 mins (dogs 4 & 6), 35 mg/kg over 30 minutes (dog 7), and 35 mg/kg over 30 mins after oral antioxidants (dog 12) were unwell from 7-24 hrs. Blood results showed reduced platelet and white cell counts (WCC), markedly elevated bilirubin, AST, ALT, and CK activities. Amylase and lipase dropped but remained within reference intervals. One dog died at 21 hours. The others were euthanased at 22, 24 and 33 hrs. At necropsy, the pancreata were edematous and swollen, the livers ranged between normal size with multiple areas of darkened parenchyma, to swollen and friable. There were multiple haemorrhages into the intestinal wall, urine was dark and there was a serous nasal discharge with dog 12.

Dogs with dosage of 30 mg/kg over 30 minutes (dogs 3 & 5) were well throughout the experiment and were euthanased at 24 and 48 hrs. Glucose dropped slightly at 12 and 24 hours. There was moderate elevation of AST, ALT and CK activities. Platelets remained within the reference interval, but neutrophils were elevated at 12 hours, settling by 24 hours. Both liver and pancreas appeared normal at necropsy examination. Dogs with dosage 35 mg/kg over 30 minutes (8-10) and 35 mg/kg after oral antioxidants (dogs 11, 13, 14) remained clinically well, eating and evacuating normally, bright and responsive until euthanased.

7.4.2 Histopathology

7.4.2.1 Pancreas

Compared to the normal pancreatic tissue reviewed from the archives, all dogs showed some evidence of histological change within the pancreas, from relatively normal pancreatic architecture with mild cellular damage (**Figure 7.1A**) to increased and variable amounts of injury. These changes varied within and between lobules of the same organ. Isolated single cells displayed either classic apoptosis [7] or necrosis, both being randomly distributed (**Figure 7.1A**). Large clusters of acinar cells displayed cell shrinkage and loss of adhesion with varying degrees of pyknosis from partial to fully condensed nuclei (**Figure 7.1B, 7.1F**). Many nuclei exhibited pallor; nuclei often appeared pale with chromatin clumping towards the nuclear membrane. Areas of 'dark' cells [7] were prominent. The cytoplasm of acinar cells was vacuolated both apically and basally and increased basophilia was noted. (**Figure 7.1D and 7.1E**). Periacinar oedema was usually evident (**Figure 7.1C and 7.1D**). The ductal system remained microscopically intact with the exception of periductal fibrosis in dog 1, most probably

from a pre-existing lesion. Some islet cells appeared apoptotic and occasional mitotic figures were seen in acini. Neutrophil numbers were increased marginally compared to control tissues in some sections. PCNA immunohistochemistry was positive above control levels in acinar cells, centroacinar cells, macrophages and stellate cells to various degrees in all tissue specimens tested (**Figure 7.1G and 7.1H; Table 7.1**).

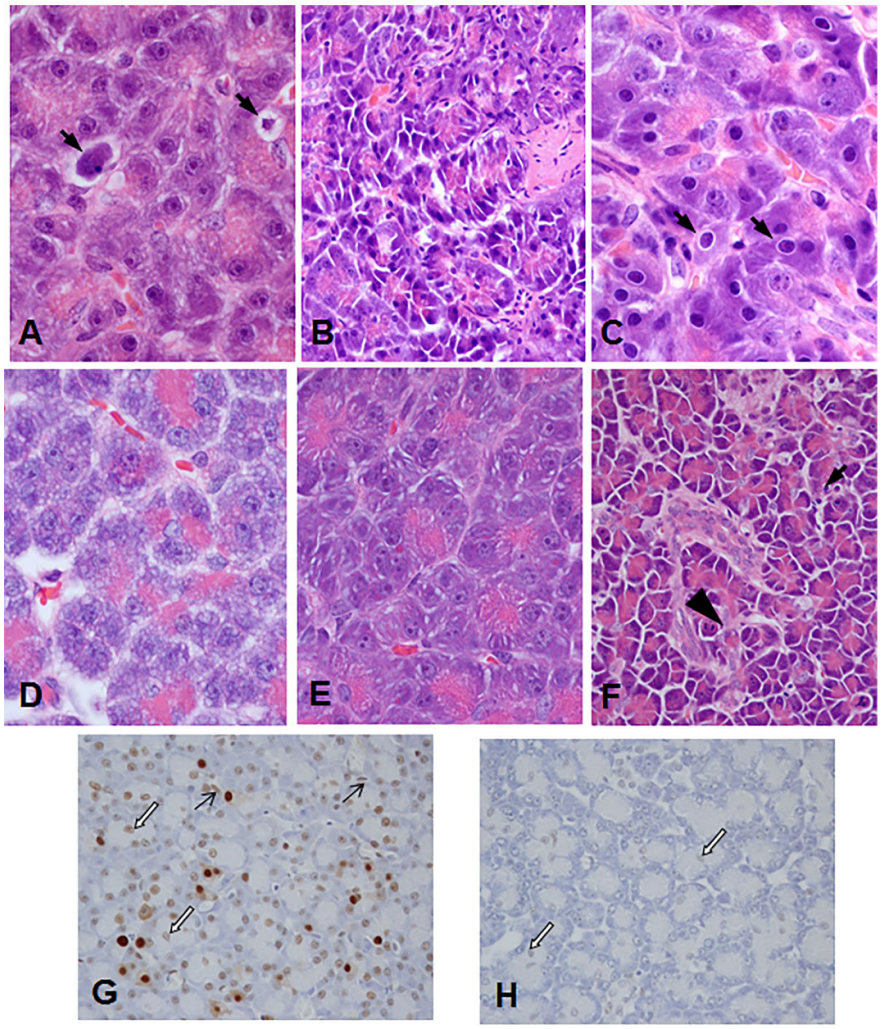

Figure 7.1 Range of pancreatic damage after treatment with CHB

A. dog 3 x 1000 **B**. dog 14 x400, **C**. dog 14 x1000, **D**. dog 7 x1000, **E**. dog 10 x 1000, **F**.) dog 11. All x 400, all H&E. Apoptotic cells and nuclei with halos (short arrows) are shown in **A,C,F**. Cells with condensed cytoplasm and disrupted cell attachment are shown in **B**. and **F**. D and e show cytoplasmic vacuoles in acinar cells, overall increased basophilia and periacinar oedema. Apoptosis and mitosis (arrow head) coexist **F**.. (**G**. dog 12 x 400 and **H**. dog 11 x 400 show range of PCNA immunohistochemistry with brown staining of centroacinar cell nuclei (white arrows) and stellate cells (thin arrows); counterstain haematoxylin.

7.4.2.2 Liver

Normal dog liver from archival blocks consisted of multiple lobules organised around a central vein, in which hepatocytes form single cell cords from portal area to central vein, separated by sinusoidal spaces [8]. The livers of dogs 3, 5, 8, 9, 10, 11 and 14 were histologically normal, some showing mild hydropic change (**Figure 7.2A**). Apoptosis was scattered, predominantly in Küpffer cells, and there was mild periacinar congestion.

The livers from the other dogs demonstrated moderate to severe changes ranging from periportal necrosis (dogs 6, 13) to massive necrosis and haemorrhage with complete disruption of lobular architecture (dogs 1, 2, 4, 7, 12). Hydropic change with sinudoidal congestion is depicted in Dog 3 (**Figure 7.2B**). Hepatic cells in dog 4 demonstrated necrosis, pyknosis, karyolysis and karyorrhexis, with haemorrhage (**Figure 7.2C**). In general, neutrophilic infiltration was prominent and margination was apparent in blood vessels, especially the central vein. The liver of dog 6 showed periportal necrosis with inflammation and haemorrhage whilst in dog 13 coagulative necrosis was midzonal to periportal with haemorrhage (**Figure 7.2D, E**). Periportal activation of stellate cells was noted in dog 13. Congestion in dog 7 was extreme, with haemorrhagic necrosis, loss of sinusoidal integrity and haemorrhage (**Figure 7.2 F**).

In dogs with massive liver injury, haemorrhage in other organs such as bladder and intestinal wall was noted consistent with thrombocytopaenia plus likely disseminated intravascular coagulation. Quantification of the apparent haemorrhagic diathesis was not performed apart from platelet counts (**Table 7.1**).

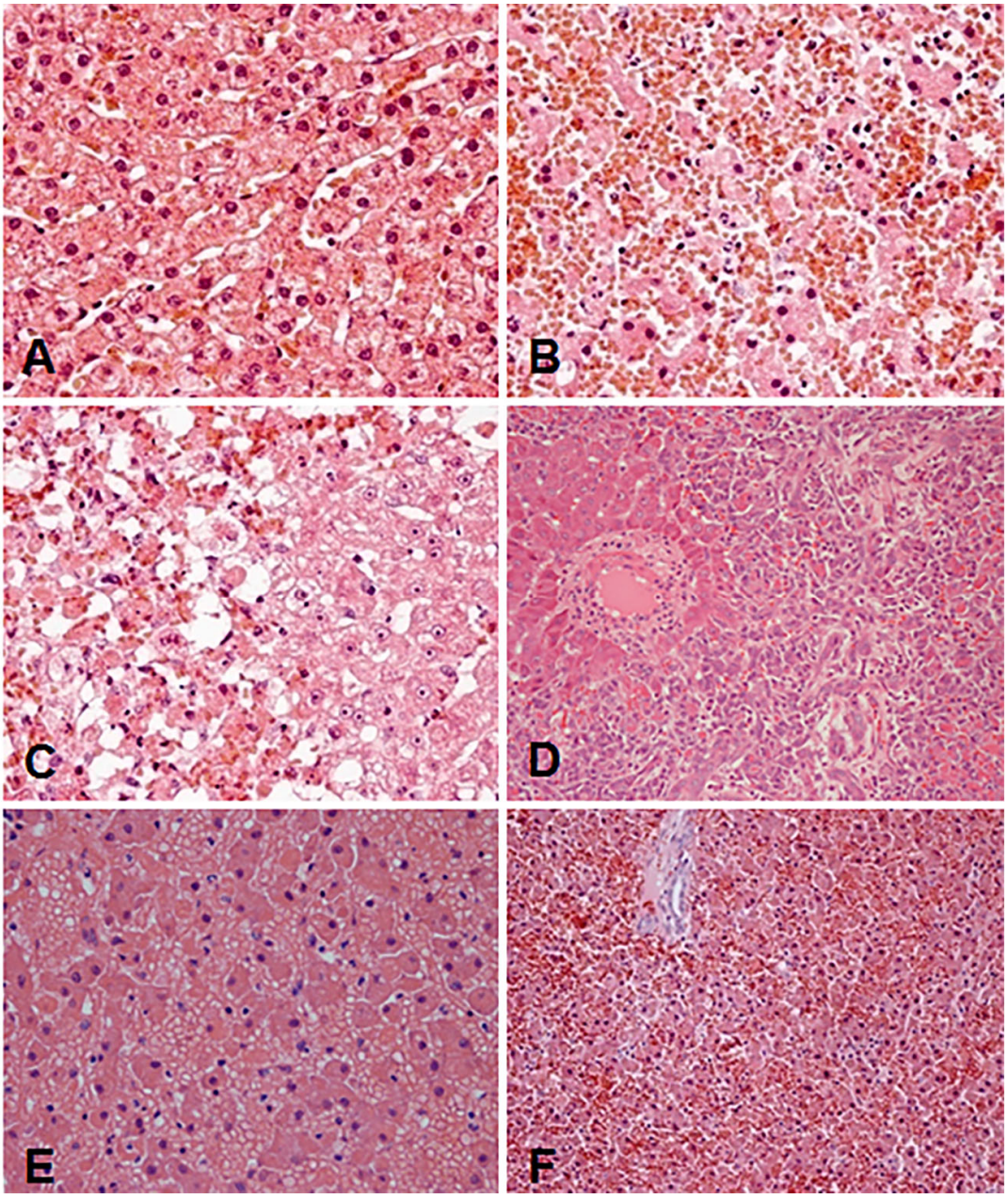

Figure 7.2. Range of liver damage after treatment with CHB.

All images are H&E stained sections at x 400. Normal liver is demonstrated **A**.. Dog 3 showed hydropic change with sinusoidal congestion **B**.. Dog 4 had massive necrosis with pyknosis, karyolysis, karyorrhexis and haemorrhage **C**.. Dog 6 had periportal necrosis with inflammation and haemorrhage **D**.. Dog 13 had periportal coagulative necrosis **E**. Dog 7 had extreme congestion, massive haemorrhagic necrosis with loss of sinusoidal integrity and haemorrhage **F**.

Table 7.1

DOG	1	2	3	4	5	6	7	8	9	10	11	12	13	14
Weight (kg)	18	15	18	20	15.5	12	17.6	15.4	16.2	17.8	20.6	14	29	19
Time blood taken	8hrs	12hrs	15hrs	14hrs	24hrs	24hrs	18hrs	15hrs	15hrs	15hrs	15hrs	15hrs	15hrs	15hrs
Dose CHB	70mg/kg	50mg/kg	30mg/kg	40mg/kg	30mg/kg	40mg/kg	35mg/kg	35mg/kg	35mg/kg	35mg/kg	35mg/kg	35mg/kg	35mg/kg	35mg/kg
Absolute dose	1260mg	750mg	575mg	800mg	465mg	480mg	616mg	539mg	567mg	605mg	700mg	490mg	850mg	665mg
Clinical state	Sick	sick	well	sick	well	sick	sick	well	well	well	well	sick	well	well
Platelets (200-900)	125	4	485	11	414	247	37	324	351	clumped	176	clumped	158	248
Neutrophil (4.1-9.4)	1.0	0.8	7.4	2.5	10	15.3	2.9	13.4	11.7	6.0	14.9	4.4	13.6	16.7
AST(1-80)	328	1348	118	4822	1738	13815	7,750	110	157	50	355	8494	730	458
ALT(0-80)	166	1668	42	5652	1763	16795	7180	44	49	59	174	11301	809	137
GGT(0-5)	<5	5	6	6	6	10	21	6	6	6	9	7	5	<5
CK (0-400)	5938	2888	1155	2071	1832	1830	1658	1064	2613	405	1377	1073	5074	4769
Bilirubin (0-10)	17	30	4	19	<2	23	27	3	<2	2	12	24	13	8
Amylase (0-2400)	260	310	300	370	370	350	200	550	400	610	310	140	740	460
Time of death Early (E) Scheduled (S)	13hrs E	20hrs E	48hrs S	22hrs E	25hrs S	24hrs S	22hrs E	48hrs S	96hrs S	96hrs S	72hrs S	33hrs E	72hrs S	72hrs S
PCNA %	2.5	1.2	36.6	1.5	34.6	30.3	8.1	48.1	31.9	10.2	66.9	1.4	59.6	78.9

Aspartate aminotransferase AST, alanine aminotransferase ALT, gammaglutamyl transferase GGT, creatine kinase CK

7.5 DISCUSSION

This experiment was an attempt to reproduce in dogs the CHB pancreatopathy which occurs in rats [1]. The rat pancreatic lesion is unusual in that there is marked early oedema with an acute inflammatory infiltrate, rapid synchronous onset of acinar cell apoptosis and total acinar atrophy with only a very limited regenerative response. In contrast, the dog pancreas exhibited cellular damage of acinar cells consistent with both reversible and irreversible injury. Apoptotic and necrotic acinar cells were present, with cytoplasmic vacuolisation, cell shrinkage and increased basophilia. In acinar injury, vacuolation of the apical cytoplasm of acinar cells is due to loss of zymogen granules whereas in basal areas it is due to distension and whorling of rough endoplasmic reticulum (RER) a common feature in apoptosis of acinar cells [1,9,10]. Increased basophilia in H&E-stained sections reflects loss of zymogen granules and subsequent cell shrinkage. Dark cells as described by Walker *et al.* [7], have markedly condensed cytoplasm and nuclear compaction, and are considered to be necrotic and dying. In this study, by 96 hours, whilst loss of acinar cells had occurred to some extent this was not nearly as complete an effect as in the rat.

By 18 hrs in CHB-induced pancreatitis in the rat, the apoptotic acinar cells are swollen with secondary necrosis followed by ingestion by macrophages. By 3-4 days no acinar cells remain and duct cells proliferate to convert the lobules into small groups of tubular complexes. In the dog, although substantial cell injury had occurred, this was not sufficient to cause considerable atrophy of acinar cells, nor the conversion into tubular complexes. Periacinar oedema, loss of zymogen granules, whorling of RER and loss of adhesion between acinar units was present in the necropsy specimens similar to that found in the rat. Centroacinar cells, stellate cells and macrophages were positive for PCNA indicating proliferation and activation of these cell populations, as occurs in the rat CHB model and other rat models of pancreatitis [1,9,11]. PCNA counts varied between animals but not between lobules in the same animal (Table 1). In rat pancreas, the percentage of PCNA positive cells reflects the pool of cycling cells, not only representing S-phase cells but also cells that have recently completed the cell cycle [12]. The high PCNA positive counts in dog acinar cells indicates that in some instances the pancreas was attempting to maintain a regenerative balance of cells. This was particularly, but not exclusively so, for those animals with less severe liver pathology.

All dogs had histological changes in the hepatic parenchyma ranging from mild hydropic change to moderate or massive liver necrosis with haemorrhage, neutrophilic vascular margination and parenchymal infiltration. Hepatocellular damage was more severe in dogs that received higher doses of CHB. The necrotic changes in liver were comparable to those observed in rats given high doses of CHB orally [13] and mice dosed with CHB (previous Chapter). In this experiment in dogs, liver toxicity appeared to occur at comparable doses to those which cause pancreatic toxicity, similar to the toxicity profile in mice, but dissimilar to the rat. In rats, the dose of CHB which elicited an apoptotic response in the pancreas is lower than that which causes liver damage. From studies of varying sized rats, as well as our comparative study of mice, CHB is much more toxic on a mg/kg basis in large animals, as is true for most toxins. It is difficult to extrapolate the variation in effect of toxins from one species to another.

As CHB is thought to damage cells by oxidizing membranes, we attempted to protect the liver with antioxidants given orally, and expected this to work preferentially on the hepatic parenchyma because of the first-pass effect. The most effective ameliorating agent in rat pancreas [6], reducing both edema and apoptotic cell counts was the antioxidant 2-octadecylascorbic acid, a synthetic vitamin C analogue with a small molecular weight and a high affinity for biomembranes [14,15]. Recent work showed the most likely initiating lesion in CHB toxicity to pancreatic acinar cells *in vitro* was loss of mitochondrial membrane potential with consequent release of cytochrome c [16]. Carbon tetrachloride is also a potent hepatotoxin. It oxidizes the hepatocyte membrane and thereby initiates a cascade of necrosis by being metabolized to oxygen free radicals which peroxidise fatty acids in the phospholipid membrane, activating both Kupffer cells and an inflammatory cascade [17]. This effect is ameliorated by vitamins C and E. This is in contrast with our experiments where no protective effect could be discerned. Indeed one of 4 dogs pre-treated with these antioxidants died early and the others also developed liver damage as evidenced by liver enzyme elevations (Table 7.1).

The pancreatic acinar cell changes indicated damage which might proceed to cell death, or resolve. Ninety-six hour studies were therefore undertaken to show the progression of the lesion. They showed that the lesions resolved rather than progressed, but reduced cell numbers in acini were noted subjectively indicating apoptotic cell drop out. However, liver damage

worsened, indicating a possible inflammatory cytokine cascade as occurs following ingestion of carbon tetrachloride [17].

Early and sometimes severe thrombocytopenia (dogs 2, 4 and 7) developed. We postulate this to be due to sequestration and a consumption of platelets on sinusoid walls as liver necrosis developed. The timing of venepuncture for dog 1 probably precluded observation of this effect. Thrombocytopenia has been reported after liver damage due to radiation in children and is worse with both increasing dose and volume irradiated [18]. The underlying histological lesion is thought to be congestion of the sublobular veins, with venous congestion of both spleen and liver, leading to a hypersplenism with platelet sequestration. In the therapeutic setting it is rare for this effect to have discernible clinical consequences.

Liver failure in this experiment was so fulminant that glucose metabolism was disordered. This could be due to either a loss of glycogen stores or a failure of gluconeogenesis, or both. It is quite possible also that CHB caused insulin release. This would likely be an early effect in all dogs and at lower doses. When euglycaemia was restored in dog 4, its mental state improved temporarily. Disordered glucose metabolism after CHB has been reported in rats also [19] with increased urine glucose at eight hours and lower than control serum levels from 24 hours, indicating a possible effect on the endocrine pancreas.

Xylitol ingestion in dogs is associated with hypoglycaemia following increased insulin release [20]. It is known that dogs who accidentally ingest xylitol develop acute hepatic failure with a moderate to severe increase in liver enzyme activities, hyperbilirubinemia, hypoglycaemia (due in part to increased insulin release), hyperphosphatemia, prolonged clotting times and thrombocytopenia [21]. Like CHB, xylitol is also a 5-carbon molecule. It may be that xylitol and CHB are metabolized to a similar compound which is the actual toxicant. Necropsy and laboratory findings on dogs with naturally-occurring xylitol intoxication are remarkably similar to those seen in our experimental subjects treated with CHB. Xylitol at a dose of 1.4-2.0 g/kg consistently causes increased insulin release. It is unknown whether CHB also causes this elevation of insulin, as acute liver failure *per se* can result in hypoglycemia. Direct measurement of insulin in subsequent studies will be able to resolve this issue. Xylitol is safe in humans but toxic to dogs. Interestingly, CHB also shows inter-species variability in toxic effects between rats and dogs.

Another model of experimental pancreatitis in dogs has been described, copying a well-established model in rats and mice [22]. D, l-ethionine produced exocrine necrosis in dogs leading to complete acinar atrophy [23]. These dogs were mature pound dogs of mixed breed of either sex weighing 15-22 kg similar to our study. Regeneration was not complete four weeks after the onset of the experiment, with areas of fibrosis and inflammatory infiltrate coinciding with regenerative acini. As in the current study, the largest dogs, given higher absolute doses of ethionine, were more severely affected.

In this study there was marked variation in response between animals of the same weight given the same dose – in some, the dose was fatal, others were clinically normal. The effects of CHB on the hepatic parenchyma appeared to have a marked threshold effect. Doses up to ~30 mg/kg appeared to be tolerated, whereas doses in excess of 40 mg/kg were almost always fatal, indicating that up to a certain level, the oxidant effect could be reversed, and although there was obvious evidence of hepatocellular injury, the changes could be somehow circumvented. If a threshold was exceeded, perhaps as a result of glutathione depletion, then an irreversible cascade of changes ensued, consisting of neutropenia (often with a left shift), thrombocytopenia and hyperbilirubinemia. These changes are remarkably similar to those seen in dogs with xylitol intoxication, and it is unclear to us whether this is because both toxicants have a common cellular mechanism of action such as damage to mitochondrial membranes, or whether they cause diffuse hepatic injury by different initial mechanisms, with an identical 'final common pathway' culminating in acute liver failure. More work is required to shed light on this issue, however it is of great interest that recent data has shown dogs with xylitol intoxication appear to benefit from acetylcysteine +S-adenosyl methionine (SAM-E), agents whose presumptive effect is due to repletion of glutathione levels within the liver [24]. In rat liver, CHB initially depletes glutathione levels to about 17% [2]. Bohus [19] found that the major CHB metabolite in urine of rats was a conjugate of N-acetyl-cysteine. Clearly further work should examine the benefit of acetylcysteine in CHB toxicity.

Our histological observations suggest that neutropenia is due to loss of mature neutrophils into the damaged liver, with overwhelming demand exceeding the capacity for the bone marrow to respond acutely. We suspect a similar mechanism causes thrombocytopenia with loss of platelets into the liver, and secondary hypersplenism due to hepatic vascular congestion and acute portal hypertension. Although disseminated intravascular coagulation is another possibility, we could find no evidence for this in histological specimens examined. Another

consistent biochemical finding was moderate to severely elevated CK activity in plasma, suggesting diffuse damage to muscle cell membranes in skeletal muscle and possibly the myocardium.

7.6 CONCLUSION

One purpose of this experiment was to see if a safe drug-induced exocrine pancreatectomy could be achieved with CHB in the dog. In rats, this is routinely achieved with a dose of 150 mg/kg subcutaneously. It is clear that there will not be a safe and reliable medical pancreatectomy with CHB in the dog. Even more importantly, extensive primate studies would be required before any attempt is made to trial it in humans. This study indicates there is a possibility of unpredictable fatal hepatotoxicity. From a veterinary standpoint, the similarity between toxicity due to CHB and xylitol is of interest, and further studies may shed light on a final common pathway involved in the pathogenesis of both intoxicants.

7.7 REFERENCES FOR THIS CHAPTER

1. Kelly LE, Reid, L, and Walker NI. Massive acinar cell apoptosis with secondary necrosis, origin of ducts in atrophic lobules and failure to regenerate in cyanohydroxybutene pancreatopathy in rats. *Int. J. Exp. Pathol.,* 1999, 80, 217-226.

2. Wallig MA and Jeffrey EH. Enhancement of pancreatic and hepatic glutathione levels in rats during cyanohydroxybutene intoxication. *Fundam. Appl. Toxicol.,* 1990, 14, 144-159.

3. Kelly LE, Goodall, AR, Reid L, and Walker NI. The effect of the pancreatotoxin cyanohydroxybutene on pancreatic ductal and acinar carcinoma cell lines. In Proceedings of the 5th International Symposium on Predictive Oncology and Therapy, *Cancer Detection and Prevention*, 2000, 24, S-184.

4.Kluger EK, Malik R, Ilkin W, Snow D, Sullivan DR, Govendir M. Serum triglyceride concentration in dogs with epilepsy treated with Phenobarbital or with Phenobarbital and bromide. *JAVMA,* 2008, 233(8), 1270-1277.

5. Xenoulis PG, Steiner J M. Lipid metabolism and hyperlipidemia in dogs. *Vet. J.,* 2010. 183(1), 12-21.

6. Kelly LE, Toxicology of cyanohydroxybutene and its effect on carcinoma of the pancreas. University of Queensland, Australia, PhD Thesis 2002.

7. Walker NI, Harmon, BV, Gobe GC, Kerr JFR. (1988). Patterns of Cell Death. *Meth. Achiev. Exp. Pathol.,* 1988, 13*, 18-54.*
8. Dellman H-D, Brown EM. eds. Textbook of Veterinary Histology. 2nd ed., Lea and Febiger, Philadelphia 1981.
9. Reid L. and Walker N. Acinar cell apoptosis and the origin of tubular complexes in caerulein-induced pancreatitis. *Int. J. Exp. Path.,* 1999, 80, 205-215.

10. Walker NI, Winterford CM, Kerr JF. Ultrastructure of the rat pancreas after experimental duct ligation. II. Duct and stromal cell proliferation, differentiation, and deletion. *Pancreas,* 1992*,* 7 (4), 420-430.

11. Walker NI. Ultrastructure of the rat pancreas after experimental duct ligation. (1) The role of apoptosis and intraepithelial macrophages in acinar cell deletion. *Am. J. Pathol.,* 1987, 126, 439-451.
12. Elsässer HP, Biederbick, A, Kern HF. Growth of rat pancreatic acinar cells quantitated with a monoclonal antibody against the proliferating cell nuclear antigen. *Cell.Tissue.Res.,* 1994, 276 (3), 603-9.
13. Nishie K. and Daxenbichler ME. Toxicology of glucosinolates, related compounds (nitriles, R-goitrin, isothiocyanates) and vitamin U found in cruciferae. *Fd. Cosmet. Toxicol.,* 1980, 18, 159-172.
14. Hirano T. (1996). New synthetic free radical scavenger, 2-octadecylascorbic acid (CV-3611), prevents pancreatic lipid peroxidation in rats with caerulein-induced pancreatitis. *Med. Sci.Res.,* 1996*,* 24, 3-5.
15. Nonaka A, Manabe T, Kyogoku T, Tamura K, Tobe T. Evidence for a role of free radicals by synthesized scavenger, 2-octadeclyascorbic acid, in caerulein-induced mouse acute pancreatitis. *Dig. Dis. Sci.,* 1992, 37, 274-279.
16. Cao Y, Adhikari A, Ang AD, Clement MV, Wallig M and Bhatia M. Crambene induces pancreatic acinar cell apoptosis via the activation of mitochondrial pathway. *Am. J. Physiol. Gastrointest. Liver. Physiol.,* 2006, 291, G95-G101.
17. Roomi MW, Kalinovsky T, Roomi N W, Ivanov V, Rath M, Niedzwiecki A. A nutrient mixture suppresses carbon tetrachloride-induced acute hepatic toxicity in ICR mice. *Hum. Exp. Toxicol.,* 2008, 27, 559-566.

18. Tefft M, Mitus A, Das L, Vawter GF, Filler R M. Irradiation of the liver in children: review of experience in the acute and chronic phases, and in the intact normal and partially resected. *Am. J. Roentgenol. Radium. Ther. Nucl. Med.,* 1970, 108(2), 365-385.
19. Bohus E, Racz A, Noszal B, Coen M, Beckonert O, Keun HC., Ebbels TMD, Cantor GH, Wijsman J., Holmes E, Lindon JC, and Nicholson JK. Metabionomic investigations into the global biochemical sequelae of exposure to the pancreatic toxin 1-cyano-2-hydroxy-3-butene in the rat. *Magn. Reson. Chem. 2009,* 47, S26-S35.
20. Kuzuya T, Kanazawa Y, Kosaka K. Stimulation of insulin secretion by xylitol in dogs. *Endocrinology,* 1969, 84(2), 200-207.
21. Dunayer EK, Gwaltney-Brant SM. Acute hepatic failure and coagulopathy associated with xylitol ingestion in eight dogs. *JAVMA,* 2006, 229 (7), 1113-1117.
22. Walker NI, Winterford CM, Williamson RM, Kerr J.F. Ethionine induced atrophy of rat pancreas involves apoptosis of acinar cells. *Pancreas,* 1993, 8(4), 433-449.
23. Govendir M, Canfield M, Church D. Effect of d,l-ethionine administration on the histomorphology of canine pancreatic acinar and β-cells. *Exp. Toxic. Pathol.,* 2002, 54, 77-83.
24. Webster CRL and Cooper J. Therapeutic use of cytoprotective agents in canine and feline hepatobiliary disease. *Vet. Clin. Small Anim.,* 2009*,* 39, 631-652.

CHAPTER 8
DISCUSSION

8.1 OVERVIEW

Pancreatitis is an inflammatory disorder of the exocrine pancreas in both acute and chronic forms. It causes considerable morbidity and mortality, as the disease varies widely in severity, and the approach to management and outcome is uncertain. Due to the relative inaccessibility of pancreatic tissue for examination, animal models are used to investigate the pathogenesis of the disease. Fibrosis is a serious complication of pancreatitis and leads to the destruction of the exocrine gland, pancreatic insufficiency and ultimately death. Understanding the processes of fibrosis and its role in the imbalances that drive the pancreas to regenerate or not is the basis for this study.

8.2 MODELS

Experimental animal models of pancreatitis vary in their relevance to clinical disease, their ease of use, reproducibility and the basic features of injury and reparation. For this reason it was decided as wise to compare more than one model to examine the progressive and overlapping pathology of the disease. The caerulein and duct ligation models are well-established models in rats with simplicity, strong reproducibility and predictable results. Fibrosis can be established in mice with both models however depends on the right mouse strain in the case of caerulein.[257] The CHB model is not reported widely, is simply achieved with one subcutaneous dose and is reproducible with the caveat that results do vary between rat colonies. This latter effect is not restricted to the CHB model and creates substantial inconvenience for researchers from personal experience. Unfortunately, CHB does not translate into a mouse model, however the beauty of the CHB model in rat pancreatitis is that regeneration does occur briefly, but does not persist. This provides a perfect medium between the caerulein and duct ligation models and a good model to investigate how the pancreas can retain the capacity to regenerate but cannot sustain the regenerated population. One would suppose that this has some relevance to the human chronic disease. A summary and comparison of results of the parameters studied in the three models is presented in **Figure 8.1.**

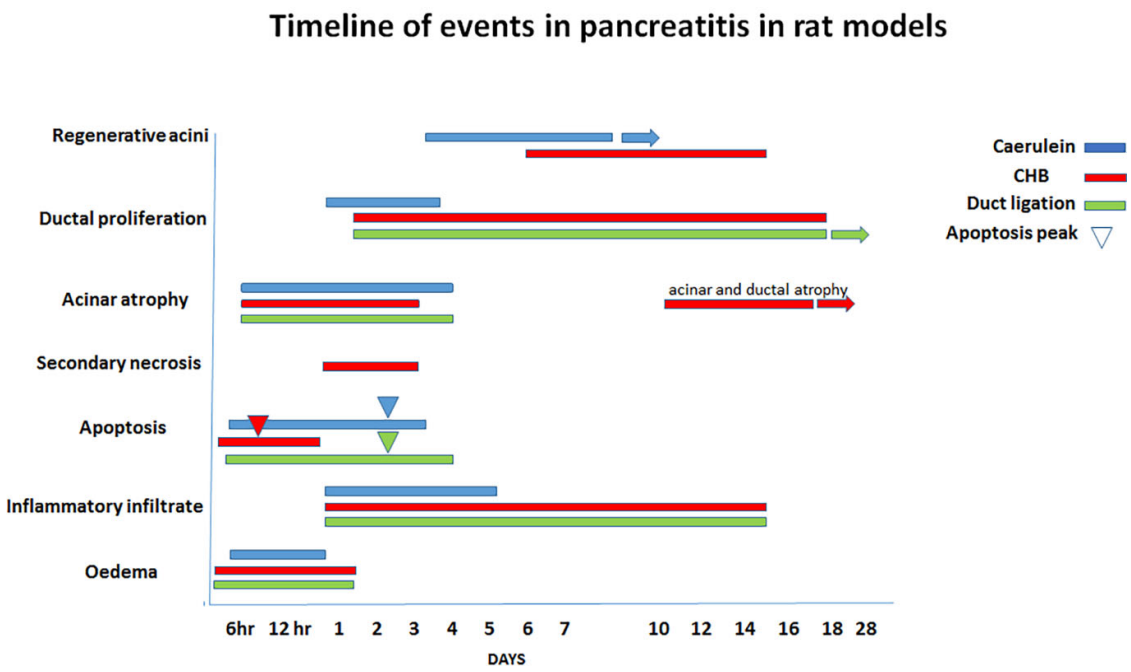

Figure 8.1 Timeline of events in pancreatitis in the rat models

Experimental animal models of pancreatitis vary in their relevance to clinical disease, including the basic features of injury and repair, regeneration, proliferation, atrophy, cell death and inflammation. These models form a basis for studying pancreatic regeneration during pancreatitis, because of their inherent similarities and differences. The caerulein model regenerated quickly and comprehensively, whereas the regeneration was focal and non-progressive in the CHB model and the duct ligation model did not show any regeneration.

8.3 REGENERATION

In humans one of the issues with the pancreas being inaccessible to direct observation applies to regeneration. That the pancreas regenerates when symptoms wane is an assumption but there is no direct evidence that this occurs. Tissue replacement and turnover, the role of pluripotent stem cells and the mechanical aspects of embryonic development are central to understanding regeneration. Stem cells play a role in other organs, for example liver, during regeneration, however a true stem cell has not been identified in pancreas. The tubular complexes, also known as acinar to ductal metaplasia, are the epithelial structures remaining after injury and they upregulate normally duct specific proteins, such as cytokeratins, as seen in this report. In the caerulein model though large numbers of acinar cells are destroyed, viable acinar cells

remain in most lobules. Ultrastucturally and in immunohistochemistry regenerating acinar cells are seen protruding from tubular complexes, in duct to acinar differentiation however one can assume that many acinar cells are replaced by expansion of the surviving cells in this model as has been reported before.[222] Duct to islet differentiation was noted in this caerulein model, as also seen in other pancreatic injury.[105, 258] In a diphtheria toxin transgenic mouse model where acinar cells are obliterated regeneration of acinar cells is due also to duct to acinar differentiation and not self-renewal.[56] In the CHB and duct ligation models no acinar cells remain. In the CHB model no acinar cells were seen in electron microscopy forming from the tubular complexes however they were seen frequently forming next to islet cells and forming in nests in the middle of connective tissue as did new islet tissue. The source of this regeneration was not determined and the acinar cells though normal looking did not persist. Acini, duct cells and tubular complexes died by apoptosis until rats had pancreatic exocrine insufficiency, maldigestion and muscle wasting and were euthanased. The duct ligation model showed no regeneration at all. Persistent injury in the form of ductal ligation ensured that the tubular complexes did not retain the capacity to regenerate acinar cells. How or if the tubular complex cells contribute signals towards ongoing inflammation is a question that requires answers. Acinar cells are normally a source of inflammatory cytokines in pancreatic injury, however once destroyed, other cells, presumably the inflammatory cells provide ongoing signalling towards fibrosis or regeneration.

8.4 FIBROSIS

Excess fibrosis deposition is a system failure. The deposition of ECM in response to injury provides a scaffold so that injured tissue may repair in a supported environment. The repair of tissue such as in wound healing is usually fast and efficient, however restoration of cell populations in pathological repair often fails due to miscommunication of the ECM to coordinate regeneration. This malfunction leads to chronic conditions. Fibrosis, produced by the stellate cells, is a known feature of chronic pancreatitis and pancreatic cancer.[169] The disappearance or persistence of stellate cells correlates with regeneration in the models. In the caerulein model, stellate cells disappear as regeneration occurs. In the duct ligation model, stellate cells persist and regeneration does not occur. In the CHB model stellate cells wane, though fibrosis remains, which suggests that once deposited stellate cells are not required to maintain fibrosis. The persistence of fibrosis may depend on the type of collagen deposited as

the difference between the deposition of collagen I and collagen III in these models was clear. Fibrosis in the caerulein model consisted mainly of collagen III the thinner collagen, however, in the CHB and duct ligation models the collagen laid progressed to more dense collagen I. Collagen I was unable to be degraded by the balance of MMPs and TIMPs in these models. Stellate cells in the duct ligation model may have continued to deposit collagen as they persisted around ducts and tubular complexes.

Mast cells and neutrophils are reported as the first responders in inflammation for host defence,[259] and macrophages and neutrophils in parallel influx in pancreatitis.[95] Dendritic cells, B cells and T cells are reported to infiltrate the injured pancreas early and are able to modulate repair,[53] however, they were not studied here. Early in the rat pancreatitis large numbers of macrophages and stellate cells were observed migrating in the inflammatory infiltrate. Counting of the inflammatory cells was carried out in random fields though concentrated on the areas containing the parenchyma, acinar cells and tubular complexes, rather than areas containing mostly or only connective tissue. For this reason mast cell counts are perhaps lower in totals than the other inflammatory cells as they were often in larger numbers congregated around blood vessels or in connective tissue at the periphery of lobules compared to in the parenchyma and interlobular inflammatory infiltrate. The stellate cells were assessed by area of stained cytoplasm and not as individual cells. As the αSMA immunohistochemistry, a standard method for stellate cells,[79] is a cytoplasmic stain and stellate cells had extremely long processes it was more difficult to separate individual cells, particularly when they were overlapped, encircling tubular complexes. Fibroblasts were not easily distinguished from macrophages in light microscopy. In the literature there are conflicting views on the definition of fibroblasts/myofibroblasts/stellate cells.[148] Their derivation, progenitors, phenotype and function clearly differ in different tissues and they comprise heterogeneous populations. At present, there is no reliable marker to differentiate between quiescent stellate cells versus resident fibroblasts in the pancreas.[148] In this study, ultrastructurally, fibroblasts were identified in the control tissue, just few residing in inter-acinar spaces, containing no lipid droplets. Soon after insult, stellate cells were filled with RER and full and emptied lipid droplets but by day two of the experiments most of the stellate cells had no remaining lipid droplets. Only in the caerulein model after regeneration cells resembling fibroblasts without lipid were seen. Some unidentified inflammatory cells appeared to be apoptotic at later time points in CHB and duct ligation sections, however this was not noted in electron microscopy samples which may have facilitated identification. Stellate cells and macrophages disappeared with regeneration and

fibrosis in the caerulein model, only mast cells remained higher than normal. CHB stellate cell numbers declined much faster and further from 10 days than fibrosis which began to decline from 18 days but still remained higher than control levels. Macrophages paralleled the decline of stellate cells, however mast cell numbers remained high. It appears in the CHB model that stellate cells and macrophages were not required to maintain the level of fibrosis. In duct ligation fibrosis, stellate cells, macrophages and mast cells remained at high levels.

Macrophages are also labelled by phenotype, position and activity. The labelling of macrophages into pro and anti-inflammatory macrophages is perhaps overly simplistic as they are highly plastic cells that change their active state via a spectrum of chemical and physical signals from cellular and environmental cues.[190, 260] Whether resident tissue macrophages were supplemented here by an active recruitment of blood monocytes as has been shown by others[261] was not obvious. Resident macrophages can proliferate in intestinal tissue in response to IL-4 without requirement for blood monocyte recruitment.[262] Mitosis of macrophages was not noted but could have been easily missed as inflammatory cells that were seen in mitosis were not readily identifiable. Macrophages are considered the main inflammatory cell in pancreatitis although peritoneal macrophages are largely responsible for the severity of pancreatitis.[189] Early in the rat pancreatitis the macrophages actively phagocytosed apoptotic acinar cells as previously reported.[216, 222, 263] Macrophages were closely associated with stellate cells in all models and persisted with fibrosis in the CHB and duct ligation models. They may be regulating both inflammation and fibrosis in this pancreatitis. Cross talk between macrophages and stellate cells via the IL-4/IL13 pathway has been demonstrated in chronic pancreatitis *in vivo* and *in vitro*.[264] Pancreatic stellate cells expressed the cytokines that are required to alternatively activate macrophages to a pro fibrotic phenotype and alternatively, macrophages expressed levels of TGFβ and PDGFβ to directly promote stellate cell activation and proliferation. These macrophages also regulated ECM turnover by expressing higher levels of MMPs and TIMPs. Cytokines and growth factors from macrophages regulate the balance of MMPs and TIMPs during nerve repair that potentiates the rate of regeneration.[265] This interaction between macrophages and stellate cells likely determines the balance between fibrosis deposition and resolution and this provides the diversion from the regenerative to the fibrotic state.

Mast cell mediators, chemokines and cytokines are diverse and heterogeneous in both humans and animals.[192] Granule-stored specific proteases and heparin have significant biological

effects relevant to fibrosis including increased collagen synthesis, fibroblast proliferation or differentiation and activating TGFβ. Clinical data from fibrotic pathogenesis in human lung, kidney, cardiac, skin and liver indicates that activated mast cells are implicated in the progression and severity of fibrosis which is supported by pro-fibrotic cell-to cell contact between human mast cells and fibroblasts in co-culture and strong evidence that, in humans, mediators secreted by mast cells exert pro-fibrotic effects directly to fibroblasts.[192] In contrast, mouse and rat models of fibrosis in lung, skin, cardiac, liver, lymph node, adipose tissue using deletion of mast cells has given rise to the incongruity of anti-fibrotic, pro-fibrotic or not involved in fibrosis results.[192] As mast cell numbers were increased, they degranulated and persisted to a certain degree in all models, a role for mast cells in fibrosis in these models is indicated. TGFβ which is upregulated in duct cells in chronic pancreatitis is a stimulator of mast cells and they have been known to induce collagen 1 gene expression in mouse skin fibroblasts.[195] In the fibrotic rat pancreata they were found around tubular complexes, close to stellate cells and macrophages and in the stroma. Mast cells are a source of pro fibrotic stimuli such as TGFβ, PDGF, FGF2 and granulocyte macrophage colony-stimulating factor and they store and release into the interstitial space, matrix components such as hyaluronic acid and chondroitin sulphate all of which can contribute to ECM remodeling.[266]

IHC showed that laminin a component of the basement membrane was disrupted early in the rat pancreatitis, presumably as cells shrank and rounded up with apoptosis. Basement membrane progressed to lay thickly and unevenly around tubular complexes. In the caerulein model laminin levels and basement membrane returned to normal appearance by 10 days, in the CHB and duct ligation models expression was strong and the thick fuzzy appearance looked to be interweaved with stellate cells around some tubular complexes. The abnormal deposition remained in the CHB and duct ligation models at day 18 however were more ordered around regenerating acini in the CHB model. The basement membrane contains laminins and collagens and proteins that crosslink and anchor these fibres. Cellular skeletal architecture and tissue cohesion maintained by laminin and collagen integrity is regulated by integrins. The βintegrin receptor group is largely responsible for cell attachment to the ECM and the lack of integrins interferes with laminin and basement membrane assembly in various other tissues.[267] Pancreatic acini have integrin receptors in their basal lamina[268] but which pancreatic cells express the proteins for cell/basement membrane linkage is unknown. The group of Riopel et al used a loxP-mediated recombination and col1a2-CreERT transgene and tamoxifen administration to remove integrinβ1 from mouse pancreatic cells. This resulted in decreased

ECM protein and integrin loss from acinar cells that further caused disrupted basement membrane and impairment of acinar function. This indicates that integrin-ECM interactions are essential for maintaining exocrine epithelial integrity and that stellate cells regulate pancreas function through maintenance of basement membrane.[269] In the CHB model stellate cell numbers were reduced considerably by 18 days, basement membrane was abnormally laid around tubular complexes and regeneration continued to fail. In the duct ligation model stellate cells remained in high numbers, basement membrane was abnormally laid around tubular complexes and regeneration was non-existent. Basement membrane appeared normal around blood vessels. It follows in the CHB model that absence of stellate cells may have contributed to the failure of basement membrane integrity to influence regeneration however this theory does not hold true in the duct ligation model. Future studies exploring the role of integrins in these models may provide some answers. Macrophage-derived MMPs also facilitate basement membrane disruption to expedite movement of inflammatory cells to injury sites.[190]

Indisputable in the rat models is that stellate cells, macrophages and mast cells increased in number with the onset of pancreatitis. Local and circulating inflammatory cytokines from inflammatory cells acting through inflammatory signalling pathways such as NFκB and JAK-STAT pathways and developmental signals such as Pdx1, Notch, hippo and Wnt pathways regulate pancreatic regeneration. These complex interactions are the subject of debate and findings are conflicting however recent literature alludes to their important roles in promoting or inhibiting pancreatic regeneration.[53] This suggests that interactions between fibrotic and developmental mechanisms regulate pancreatic regeneration.

8.5 SURVIVIN

Survivin expression was increased in the pancreatitis of the rat models in cells that were proliferating, differentiating and pro or anti apoptotic. Its expression early in pancreatitis may reflect that survivin is involved in determining the cell death pathway that proceeds by either inhibiting or promoting caspase activation. Other authors have reported a role for members of the IAP family, including survivin, to regulate the cell-death response in caerulein-induced pancreatitis.[242, 270] The role of survivin in regeneration is more difficult to define. Survivin expression indicated that cells proliferating, acinar, ductal and inflammatory cells correlated with PCNA staining for cycling cells. Tubular complexes were positive for survivin both in the nucleus and cytoplasm. Tubular complexes showed mitosis when forming so will express

survivin as proliferating cells. They do become apoptotic as was seen particularly in the CHB model so the effect cannot be seen as anti-apoptotic. In the duct ligation model where rats were kept up to 52 weeks the duct cells and tubular complexes persist for many months but finally atrophy (personal communication, Prof Neal Walker, Envoi Pathology, Brisbane, Australia). Tubular complexes were also survivin positive in the caerulein model where acinar cells appear to transdifferentiate from them. Survivin expression in tubular complexes may indicate then that these cells are not terminally differentiated. Survivin expression in alpha cells of islets and in ganglion cells may also reflect their differentiation status or propensity to undergo apoptosis. The adult cells of the islets of Langerhans have little regenerative capacity although conversion of δ and α cells into β cells has been reported in ablation approaches in animal examples[271] and neurons are known to be changed in pancreatitis and contribute to fibrosis.[14] Exactly how or if survivin is involved in the process of regeneration in these models is not clear. The availability of antibodies for the individual splice variants of survivin would be advantageous towards teasing out functions of survivin in pancreatitis. What is apparent is that survivin has increased expression in the cell populations that feature in pancreatitis and therefore provides a subject for future investigation.

8.6 MOUSE

The attempt to produce a model of pancreatitis in the mouse with CHB that had apoptosis as the model of cell death was unsuccessful. Apoptosis occurred arbitrarily between lobules, was not in great numbers except in random areas and coexisted with necrosis. Liver damage occurred at higher doses such that the mice died before sufficient acinar cell death of any type could lead to the loss of parenchyma and pancreatitis. Mice dosed with 50μg/kg caerulein appeared to develop both apoptosis and necrosis to the same degree as this experiment[272] or no cell death effect.[273] Other mouse models have shown necrosis to be the primary mode of cell death in mice. Mice treated with arginine or fed a choline-deficient diet supplemented with DL-ethionine developed necrotic pancreatitis.[274] These models in mice do proceed to pancreatitis of various degrees. The difference in cell death responses between rats and mice was demonstrated as a caspase block in mice.[270] Mice appear to be more susceptible to necrosis than apoptosis through blockage of caspases -8 and-9 in acinar cells. Although this was a failure for our purposes CHB in mice would be an appropriate model to investigate the early events in cell death pathways and a model for investigating liver damage.

8.7 DOG

The CHB model in dogs did not produce complete apoptotic cell death in the pancreas. Results in the dogs were inconsistent probably because they were pound dogs of indeterminate history and therefore with possible unknown pre-existing condition. Nonetheless, the result of CHB administration was primarily liver damage before a significant pancreatic effect, useful information if your small dog has a passion for over consumption of cruciferous vegetables or your forage animals escape into the wrong field. The similarity to xylitol poisoning in dogs is particularly interesting as this is a veterinary presentation in the USA and increasingly in Australia as xylitol is used in snack foods. Further research to elucidate the mechanism of CHB liver damage in dogs may be the key to unlock the mechanism of xylitol poisoning with clinical translation. Speculation on the pancreatic cell death response in dogs is not possible with these results. Assuming pound cats would have the same issues with history as the dogs it would be useful to investigate the effect of CHB in a different higher mammal with purpose breeding such as pigs with due regard to the age of the animals. Pancreatitis in dogs remains a clinical issue for veterinarians and is worthy of further investigation.

8.8 FUTURE DIRECTIONS

Currently I am collaborating with a group of researchers at the University of Otago, Dunedin, New Zealand on a project with activins. Activins are members of the TGFβ family likely involved with pancreatic stellate cell activation, and fibrosis. We are investigating immunohistochemistry for activins and their regulators Smads on tissue microarrays made from the paraffin tissue blocks from the rat models along with a commercial tissue array for human pancreatic pathologies. This work is novel and thus far shows promising results.

8.9 CONCLUSION

This research has the potential to add to the emerging field of regeneration biology. We must understand the mechanisms to restore cell populations and their function to damaged tissues. Understanding embryonic development, analysing cell and tissue growth, identifying pluripotent and stem cells and the supportive cells that promote tissue repair is required to develop cell-based therapies for those with chronic disease. It is clear from this report that

inflammatory cells and basement membrane play an important role as a permissive or detrimental local environmental in regeneration from pancreatitis. The roles of the individual cell populations, their mechanisms and mediators are complex but interconnected. Uncovering the obstacles to tissue regeneration remains an important goal for researchers to develop clinical therapies especially in organs with limited regenerative capacity. There are differences between humans and rats in metabolic terms, in genetic background, with laboratory rats subject to clinical inbreeding and strict environmental conditions and diet likely affecting disease mechanisms and phenotypes. Human tissue is collected mainly in the later stages of pancreatitis or is rarely available consequently it is necessary to continue the search for suitable animal models that share general histological and pathological responses with regards to inflammation, cell death and regeneration in pancreatitis.

BIBLIOGRAPHY

1. Kleeff J, Whitcomb DC, Shimosegawa T, et al. Chronic pancreatitis.. Nat Rev Dis Primers. 2017;7 17060.
2. Yadav D, Lowenfels AB. Trends in the epidemiology of the first attack of acute pancreatitis: a systematic review. Pancreas 2006;33:323-330.
3. Schreyer AG, Jung M, Riemann JF, et al. S3 guideline for chronic pancreatitis - diagnosis, classification and therapy for the radiologist. German Society of Digestive and Metabolic Diseases (DGVS 2014;186:1002-1008.
4. Sarner M. Pancreatitis: definitions and classification. In: The Exocrine Pancreas: Biology, Pathobiology and Diseases. New York: ed VLW Go et al, Raven Press, 1986.
5. Longnecker DS. Pathology and pathogenesis of disease of the pancreas. Am J Pathol. 1982;107:103-121.
6. Machicado JD, Yadav D. Epidemiology of Recurrent Acute and Chronic Pancreatitis: Similarities and Differences. Dig Dis Sci. 2017;62:1683-1691.
7. Klöppel G. Toward a new classification of chronic pancreatitis. J Gastroenterol. 2007;42:Suppl 17:55-1757.
8. Milosavljevic T, Kostic Milosavljevic M, Krstic M, et al. Classification of chronic pancreatitis. Dig Dis. 2010;28:330-333.
9. Talukdar R, Vege SS. Acute pancreatitis. Curr Opin Gastroenterol. 2015;31:374-379.
10. Nesvaderani M, Eslick GD, Cox MR. Acute pancreatitis: update on management. . Med J Aust. 2015;202:420-423.
11. Burris H, Storniolo AM. Assessing clinical benefit in the treatment of pancreas cancer: gemcitabine compared to 5-fluorouracil. Eur J Cancer. 1997;33:Suppl 1:S18-22.
12. Mahadevan V. Anatomy of the pancreas and spleen. Surgery 2016;34:261–265.
13. Ibukuro K. Vascular anatomy of the pancreas and clinical applications. Int J Gastrointest Cancer 2001;30:87-104.
14. Li Q, Peng J. Sensory Nerves and Pancreatitis. Gland Surgery 2014;3:284-292.
15. Dolensek J, Rupnik MS, Stozer A. Structural similarities and differences between the human and the mouse pancreas. Islets 2015;7:e1024405.
16. Bilchik AJ, Leach SD, Zucker KA, et al. Experimental Models of Acute Pancreatitis. Journal of Surgical Research. 1990;48:639-647.

17. Tsuchitani M, Sato J, Kokoshima H. A comparison of the anatomical structure of the pancreas in experimental animals. J Toxicol Pathol 2016;29:147-54.
18. Jamieson JD. The exocrine pancreas and salivary glands. In: Histology, Cell and Tissue Biology. London: ed Leon Weiss, MascMillan, 1983.
19. Slack JMW. Developmental biology of the pancreas. Development 1995;121:1569-1580.
20. Boorman GA, Sills RC. Exocrine and endocrine pancreas. In: Pathology of the Mouse: Reference and Atlas. Vienna, IL: Cache River Press, 1999.
21. Githens S. The pancreatic duct cell: Proliferative capabilities, characteristics, metaplasia, isolation and culture. J Paediatr Gastroenterol Nutr. 1988;7:486-506.
22. Leeson TS, Leeson R. Close association of centroacinar/ductular and insular cells in the rat pancreas. Histol Histopath. 1986;1:33-42.
23. Lutcke H, Scheele GA, Kern HF. Time course and cellular site of mitotic activity in the exocrine pancreas of the rat during sustaining hormone simulation. Cell Tissue Res. 1987;247:385-391.
24. Longnecker DS. Anatomy and Histology of the Pancreas. Pancreapedia: Exocrine Pancrease Knowledge Base. 2014;147:1181-1182.
25. Ekholm R, Zelander T, Edlund Y. The ultrasound organization of the rat exocrine pancreas 1. Acinar cells. 2. Centroacinar cells, intercalary and intralobular duts. J Ultrastructural Research 1962;7:62-72.
26. Watanabe O, Baccino FM, Steer ML, et al. Supramaximal caerulein stimulation and ultrastructure of rat pancreatic acinar cell: early morphological changes during development of experimental pancreatitis. Am J Physiol. 1984;246:G457-G467.
27. Ham AW. Histology, eighth edition. . Philadelphia: JB Lippincott Co., 1979.
28. Kern HF. Fine structure of the human exocrine pancreas. In: The Exocrine Pancreas: Biology, Pathobiology and Diseases. New York: ed VLW Go et al, Raven Press, 1986.
29. Bockman DE. Anatomy of the pancreas. In: The Exocrine Pancreas: Biology, Pathobiology and Diseases. New York: ed VLW Go et al, Raven Press, 1986.
30. Case RM, Argent BE. Bicarbonate sercretion by pancreatic duct cells: mechanism and control. In: The Exocrine Pancreas: Biology, Pathobiology and Diseases. New York: ed VLW Go et al. Raven Press, 1986.
31. Pelletier M, Perreault C, Landry D, et al. Ontogeny of human epidermal Langerhans cells. Transplantation. 1984;38:544-546.

32. Walling A, Freelove R. Pancreatitis and prancreatic cancer. Prim Care Clin Office Pract. 2017;44:609-620.
33. Raimondi S, Maisonneuve P, Lowenfels AB. Epidemiology of pancreatic cancer: an overview. Nat Rev Gastroenterol Hepatol. 2009;6:699-708.
34. Manohar M, Verma AK, Venkateshaiah SU, et al. Pathogenic mechanisms of pancreatitis. World J Gastrointest Pharmacol Ther 2017;8:10-25.
35. Kingsnorth A, O'Reilly D. Acute pancreatitis. BMJ. 2006;332:1072-1076.
36. da Silva S, Rocha M, Pinto-de-Sousa J, et al. Acute Pancreatitis Etiology Investigation: A Workup Algorithm Proposal. Gastroenterol. 2017;24:129-136.
37. Ali UA, Issa Y, Hageraars JC, et al. Risk of recurrent pancreatitis and progression to chronic pancreatitis after a first episode of acute pancreatitis. Clinical Gastroenterology and Hepatology. 2016;14:738-746.
38. Raimondi S, Lowenfels AB, Morselli-Labate AM, et al. Pancreatic cancer in chronic pancreatitis; aetiology, incidence, and early detection. Best Pract Res Clin Gastroenterol 2010;24:349-58.
39. Walling A, Freelove R. Pancreatitis and Pancreatic Cancer. Prim Care 2017;44:609-620.
40. Shah AP, Mourad MM, Bramhall SR. Acute pancreatitis: current perspectives on diagnosis and management. J Inflamm Res 2018;11:77-85.
41. Dellinger EP, Forsmark CE, Layer P, et al. Determinant-based classification of acute pancreatitis severity: an international multidisciplinary consultation. Ann Surg 2012;256:875-80.
42. Banks PA, Bollen TL, Dervenis C, et al. Classification of acute pancreatitis--2012: revision of the Atlanta classification and definitions by international consensus. Gut 2013;62:102-11.
43. Schneider A, Löhr JM, Singer MV. The M-ANNHEIM classification of chronic pancreatitis: introduction of a unifying classification system based on a review of previous classifications of the disease. J Gastroenterol. 2007;42:101-119.
44. Majno G, Joris I. Apoptosis, oncosis, and necrosis. An overview of cell death. Am J Pathol 1995;146:3-15.
45. Kroemer G, Galluzzi L, Brenner C. Mitochondrial membrane permeabilization in cell death. Physiol Rev 2007;87:99-163.
46. Kerr JF, Wyllie AH, Currie AR. Apoptosis: a basic biological phenomenon with wide-ranging implications in tissue kinetics. . Br J Cancer. 1972;26:239-257.

47. Nikoletopoulou V, Markaki M, Palikaras K, et al. Crosstalk between apoptosis, necrosis and autophagy. Biochim Biophys Acta 2013;1833:3448-3459.
48. Wu J, Huang Z, Ren J, et al. Mlkl knockout mice demonstrate the indispensable role of Mlkl in necroptosis. Cell Res 2013;23:994-1006.
49. Tait SW, Ichim G, Green DR. Die another way--non-apoptotic mechanisms of cell death. J Cell Sci 2014;127:2135-44.
50. Morisset J, Guan D, Jurkowska G, et al. Endogenous cholecystokinin, the major factor responsible for dietary protein-induced pancreatic growth. Pancreas 1992;7:522-529.
51. Tsiotos GG, Barry MK, Johnson CD, et al. Pancreas regeneration after resection: Does it occur in humans? . Pancreas 1999;19:310-313.
52. Demcollari I, Cujba AM, Sancho R. Phenotypic plasticity in the pancreas: new triggers, new players. Current Opinion in Cell Biology 2017;49:38-46.
53. Murtaugh LC, Keefe MD. Regeneration and repair of the exocrine pancreas. Ann Rev Physiol. 2015;77:229-249.
54. Desai BM, Oliver-Krasinski J, De Leon DD, et al. Preexisting pancreatic acinar cells contribute to acinar cell, but not islet βcell, regeneration. J. Clin. Investig. 2007;117:971-977.
55. Strobel O, Dor Y, Alsina J, et al. In vivo lineage tracing defines the role of acinar-to-ductal transdifferentiation in inflammatory ductal metaplasia. . Gastroenterology 2007;133:1999-2009.
56. Criscimanna A, Speicher JA, Houshmand G, et al. Duct cells contribute to regeneration of endocrine and acinar cells following pancreatic damage in adult mice. Gastroenterology 2011;141:1451-1462.
57. Krah NM, De La O JP, Swift GH, et al. The acinar differentiation determinant PTF1A inhibits initiation of pancreatic ductal adenocarcinoma. Elife 2015;7:4.
58. Kopp JL, von Figura G, Mayes E, et al. Identification of Sox9-dependent acinar-toductal reprogramming as the principal mechanism for initiation of pancreatic ductal adenocarcinoma. . Cancer Cell 2012;22:737-750.
59. Miyatsuka T, Kaneto H, Shiraiwa T, et al. Persistent expression of PDX-1 in the pancreas causes acinar-to-ductal metaplasia through Stat3 activation. . Genes & Development 2006;20:1435-1440.
60. Ricard-Blum S. The collagen family. Cold Spring Harb Perspect Biol 2011;3:a004978.

61. Volk SW, Iqbal SA, Bayat A. Interactions of the Extracellular Matrix and Progenitor Cells in Cutaneous Wound Healing. Adv Wound Care (New Rochelle) 2013;2:261-272.
62. Jarvelainen H, Sainio A, Koulu M, et al. Extracellular matrix molecules: potential targets in pharmacotherapy. Pharmacol Rev 2009;61:198-223.
63. Paulsson M. Basement membrane proteins: structure, assembly, and cellular interactions. Crit Rev Biochem Mol Biol 1992;27:93-127.
64. Yurchenco PD. Basement membranes: cell scaffoldings and signaling platforms. Cold Spring Harb Perspect Biol 2011;3.
65. Pozzi A, Yurchenco PD, Iozzo RV. The nature and biology of basement membranes. Matrix Biol 2017;57-58:1-11.
66. Ramos-Lewis W, Page-McCaw A. Basement membrane mechanics shape development: Lesson from the fly. Matrix Biol 2018.
67. Kadono G, Ishihara T, Yamaguchi T, et al. Immunohistochemical localization of type IV collagen alpha chains in the basement membrane of the pancreatic duct in human normal pancreas and pancreatic diseases. Pancreas 2004;29:61-6.
68. Otte JM, Schwenger M, Brunke G, et al. Expression of hepatocyte growth factor, keratinocyte growth factor and their receptors in experimental chronic pancreatitis. Eur J Clin Invest 2001;31:865-75.
69. Karsdal MA, Nielsen SH, Leeming DJ, et al. The good and the bad collagens of fibrosis - Their role in signaling and organ function. Adv Drug Deliv Rev 2017;121:43-56.
70. Zhang G, Young BB, Ezura Y, et al. Development of tendon structure and function: regulation of collagen fibrillogenesis. J Musculoskelet Neuronal Interact 2005;5:5-21.
71. Pawelec KM, Best SM, Cameron RE. Collagen: a network for regenerative medicine. J Mater Chem B 2016;4:6484-6496.
72. Sweeney SM, Orgel JP, Fertala A, et al. Candidate cell and matrix interaction domains on the collagen fibril, the predominant protein of vertebrates. J Biol Chem 2008;283:21187-97.
73. Scheele S, Nystrom A, Durbeej M, et al. Laminin isoforms in development and disease. J Mol Med (Berl) 2007;85:825-36.
74. Aumailley M. The laminin family. Cell Adh Migr 2013;7:48-55.
75. Colognato H, Yurchenco PD. Form and function: the laminin family of heterotrimers. Dev Dyn 2000;218:213-34.

76. Miner JH. Basement Membranes. In: P MR, ed. The extracellular marix: an overview. Heidelberg Dordrecht London New York: Springer 1984:117-145
77. Tunggal P, Smyth N, Paulsson M, et al. Laminins: structure and genetic regulation. Microsc Res Tech 2000;51:214-27.
78. Grose R, Werner S. Wound-healing studies in transgenic and knockout mice. Mol Biotechnol 2004;28:147-66.
79. Pakshir P, Hinz B. The big five in fibrosis: Macrophages, myofibroblasts, matrix, mechanics, and miscommunication. Matrix Biol 2018.
80. Olsen AL, Bloomer SA, Chan EP, et al. Hepatic stellate cells require a stiff environment for myofibroblastic differentiation. Am J Physiol Gastrointest Liver Physiol 2011;301:G110-8.
81. Schuppan D, Surabattula R, Wang XY. Determinants of fibrosis progression and regression in NASH. J Hepatol 2018;68:238-250.
82. Trautwein C, Friedman SL, Schuppan D, et al. Hepatic fibrosis: Concept to treatment. J Hepatol 2015;62:S15-24.
83. Georges PC, Hui JJ, Gombos Z, et al. Increased stiffness of the rat liver precedes matrix deposition: implications for fibrosis. Am J Physiol Gastrointest Liver Physiol 2007;293:G1147-54.
84. Liu X, Xu J, Brenner DA, et al. Reversibility of Liver Fibrosis and Inactivation of Fibrogenic Myofibroblasts. Curr Pathobiol Rep 2013;1:209-214.
85. Popov Y, Sverdlov DY, Sharma AK, et al. Tissue transglutaminase does not affect fibrotic matrix stability or regression of liver fibrosis in mice. Gastroenterology 2011;140:1642-52.
86. Andoh A, Takaya H, Saotome T, et al. Cytokine regulation of chemokine (IL-8, MCP-1, and RANTES) gene expression in human pancreatic periacinar myofibroblasts. Gastroenterology 2000;119:211-9.
87. Ebert M, Kasper HU, Hernberg S, et al. Overexpression of platelet-derived growth factor (PDGF) B chain and type beta PDGF receptor in human chronic pancreatitis. Dig Dis Sci 1998;43:567-74.
88. Luttenberger T, Schmid-Kotsas A, Menke A, et al. Platelet-derived growth factors stimulate proliferation and extracellular matrix synthesis of pancreatic stellate cells: implications in pathogenesis of pancreas fibrosis. Lab Invest 2000;80:47-55.
89. Kloppel G, Detlefsen S, Feyerabend B. Fibrosis of the pancreas: the initial tissue damage and the resulting pattern. Virchows Arch 2004;445:1-8.

90. Qian LW, Mizumoto K, Maehara N, et al. Co-cultivation of pancreatic cancer cells with orthotopic tumor-derived fibroblasts: fibroblasts stimulate tumor cell invasion via HGF secretion whereas cancer cells exert a minor regulative effect on fibroblasts HGF production. Cancer Lett 2003;190:105-12.
91. Armstrong T, Packham G, Murphy LB, et al. Type I collagen promotes the malignant phenotype of pancreatic ductal adenocarcinoma. Clin Cancer Res 2004;10:7427-37.
92. Wu Y, Looi C, Subramaniam K, et al. Soluble factors from stellate cells induce pancreatic cancer cell proliferation via Nrf2-activated metabolic reprogramming and ROS detoxification. Oncotarget 2016;7:36719-36732.
93. Lohr M, Schmidt C, Ringel J, et al. Transforming growth factor-beta1 induces desmoplasia in an experimental model of human pancreatic carcinoma. Cancer Res 2001;61:550-5.
94. Fujita H, Ohuchida K, Mizumoto K, et al. Tumor-stromal interactions with direct cell contacts enhance proliferation of human pancreatic carcinoma cells. Cancer Sci 2009;100:2309-17.
95. Vonlaufen A, Apte MV, Imhof BA, et al. The role of inflammatory and parenchymal cells in acute pancreatitis. J Pathol 2007;213:239-48.
96. Aoki H, Ohnishi H, Hama K, et al. Autocrine loop between TGF-beta1 and IL-1beta through Smad3- and ERK-dependent pathways in rat pancreatic stellate cells. Am J Physiol Cell Physiol 2006;290:C1100-8.
97. Ohnishi H, Miyata T, Yasuda H, et al. Distinct roles of Smad2-, Smad3-, and ERK-dependent pathways in transforming growth factor-beta1 regulation of pancreatic stellate cellular functions. J Biol Chem 2004;279:8873-8.
98. Tahara H, Sato K, Yamazaki Y, et al. Transforming growth factor-alpha activates pancreatic stellate cells and may be involved in matrix metalloproteinase-1 upregulation. Lab Invest 2013;93:720-32.
99. Jaster R, Sparmann G, Emmrich J, et al. Extracellular signal regulated kinases are key mediators of mitogenic signals in rat pancreatic stellate cells. Gut 2002;51:579-84.
100. Masamune A, Kikuta K, Satoh M, et al. Alcohol activates activator protein-1 and mitogen-activated protein kinases in rat pancreatic stellate cells. J Pharmacol Exp Ther 2002;302:36-42.
101. Masamune A, Kikuta K, Satoh M, et al. Protease-activated receptor-2-mediated proliferation and collagen production of rat pancreatic stellate cells. J Pharmacol Exp Ther 2005;312:651-8.

102. McCarroll JA, Phillips PA, Park S, et al. Pancreatic Stellate Cell Activation by Ethanol and Acetaldehyde: Is it Mediated by the Mitogen-Activated Protein Kinase Signaling Pathway? Pancreas 2003;27:150-160.
103. Kimmelman AC, Hezel AF, Aguirre AJ, et al. Genomic alterations link Rho family of GTPases to the highly invasive phenotype of pancreas cancer. Proc Natl Acad Sci U S A 2008;105:19372-7.
104. Tsukamoto H, Towner SJ, Yu GS, et al. Potentiation of ethanol-induced pancreatic injury by dietary fat. Induction of chronic pancreatitis by alcohol in rats. Am J Pathol. 1988;131:246-257.
105. Walker NI, Winterford CM, Kerr JF. Ultrastructure of the rat pancreas after experimental duct ligation. II. Duct and stromal cell proliferation, differentiation, and deletion. Pancreas 1992;7:420-34.
106. Puig-Divi V, Molero X, Salas A, et al. Induction of chronic pancreatic disease by trintrobenzene sulfonic acid infusion into rat pancreatic ducts. . Pancreas 1996;13:417-424.
107. Sparmann G, Merkord J, Jaschke A, et al. Pancreatic fibrosis in experimental pancreatitis induced by dibutyltin dichloride. Gastroenterology 1997;112:1664-72.
108. Menke A, Adler G. TGFbeta-induced fibrogenesis of the pancreas. Int J Gastrointest Cancer 2002;31:41-6.
109. Vogelmann R, Ruf D, Wagner M, et al. Effects of fibrogenic mediators on the development of pancreatic fibrosis in a TGF-beta1 transgenic mouse model. Am J Physiol Gastrointest Liver Physiol 2001;280:G164-72.
110. Sugiyama M, Kobori O, Atomi Y, et al. Effect of oral administration of protease inhibitor on pancreatic exocrine function in WBN/Kob rats with chronic pancreatitis. Pancreas 1996;13:71-9.
111. Deng X, Wang L, Elm MS, et al. Chronic alcohol consumption accerlerates fibrosis in response to cerulein-induced pancreatitis in rats. Am J Pathol. 2005;166:93-106.
112. Perides G, Tao X, West N, et al. A mouse model of ethanol dependent pancreatic fibrosis. Gut 2005;54:1461-1467.
113. Pereda J, Sabater L, Cassinello N, et al. Effect of simultaneous inhibition of TNF-alpha production and xanthine oxidase in experimental acute pancreatitis: the role of mitogen activated protein kinases. Ann Surg 2004;240:108-16.
114. Tasci I, Deveci S, Turna T, et al. Allopurinol in rat chronic pancreatitis. Pancreas 2007;35:366-371.

115. Vaquero E, Molero X, Tian X, et al. Myofibroblast proliferation, fibrosis, and defective pancreatic repair induced by cyclosporin in rats. Gut 1999;45:269-277.
116. Gómez JA, Molero X, Vaquero E, et al. Vitamin E attenuates biochemical and morphological features associated with development of chronic pancreatitis. Am J Physiol Gastrointest Liver Physiol. 2004;287:G162-169. .
117. Menke A, Yamaguchi H, Gress TM, et al. Extracellular matrix is reduced by inhibitiion of transforming growth factor β1 in pacreatitis in the rat. Gastroenterology 1997;113:295-303.
118. Zion O, Genin O, Kawada N, et al. Inhibition of transforming growth factor beta signaling by halofuginone as a modality for pancreas fibrosis prevention. Pancreas 2009;38:427-425.
119. Zion O, Genin O, Kawada N, et al. Inhibition of Transforming Growth Factor β Signaling by Halofuginone as a Modality for Pancreas Fibrosis Prevention. Pancreas 2009;38:427-435.
120. Kaku T, Oono T, Zhao H, et al. IS-741 attenuates local migration of monocytes and subsequent pancreatic fibrosis in experimental chronic pancreatitis induced by dibutyltin dichloride in rats. Pancreas. 2007;34:299-309.
121. Shimizu K, Shiratori K, Kobayashi M, et al. Troglitazone inhibits the progression of chronic pancreatitis and the profibrogenic activity of pancreatic stellate cells via a PPARgamma-independent mechanism. Pancreas. 2004;29:67-74.
122. Yamada T, Kuno A, Ogawa K, et al. Combination therapy with an angiotensin-converting enzyme inhibitor and an angiotensin II receptor blocker synergistically suppresses chronic pancreatitis in rats. J Pharmacol Exp Ther. 2005;313:36-45.
123. Wernig G, Chen SY, Cui L, et al. Unifying mechanism for different fibrotic diseases. Proc Natl Acad Sci U S A 2017;114:4757-4762.
124. Afratis NA, Selman M, Pardo A, et al. Emerging insights into the role of matrix metalloproteases as therapeutic targets in fibrosis. Matrix Biol 2018.
125. Cui N, Hu M, Khalil RA. Biochemical and Biological Attributes of Matrix Metalloproteinases. Prog Mol Biol Transl Sci 2017;147:1-73.
126. Klein T, Bischoff R. Physiology and pathophysiology of matrix metalloproteases. Amino Acids 2011;41:271-90.
127. Schuppan D, Ashfaq-Khan M, Yang AT, et al. Liver fibrosis: Direct antifibrotic agents and targeted therapies. Matrix Biol 2018.

128. Apte MV, Haber PS, Darby SJ, et al. Pancreatic stellate cells are activated by proinflammatory cytokines: implications for pancreatic fibrogenesis. Gut 1999;44:534-41.
129. Bachem MG, Schneider E, Gross H, et al. Identification, culture, and characterization of pancreatic stellate cells in rats and humans. Gastroenterology 1998;115:421-32.
130. Schneider E, Schmid-Kotsas A, Zhao J, et al. Identification of mediators stimulating proliferation and matrix synthesis of rat pancreatic stellate cells. Am J Physiol Cell Physiol 2001;281:C532-43.
131. Elsasser HP, Adler G, Kern HF. Time course and cellular source of pancreatic regeneration following acute pancreatitis in the rat. Pancreas 1986;1:421-9.
132. Elsasser HP, Adler G, Kern HF. Fibroblast structure and function during regeneration from hormone-induced acute pancreatitis in the rat. Pancreas 1989;4:169-78.
133. Saotome T, Inoue H, Fujimiya M, et al. Morphological and immunocytochemical identification of periacinar fibroblast-like cells derived from human pancreatic acini. Pancreas 1997;14:373-82.
134. Kato Y, Inoue H, Fujiyama Y, et al. Morphological identification of and collagen synthesis by periacinar fibroblastoid cells cultured from isolated rat pancreatic acini. J Gastroenterol 1996;31:565-71.
135. Gress TM, Muller-Pillasch F, Lerch MM, et al. Balance of expression of genes coding for extracellular matrix proteins and extracellular matrix degrading proteases in chronic pancreatitis. Z Gastroenterol 1994;32:221-5.
136. Sato T, Niikawa J, Usui I, et al. Pancreatic regeneration after ethionine-induced acute pancreatitis in rats lacking pancreatic CCK-A receptor gene expression. J Gastroenterol 2003;38:672-80.
137. Lee MS, Gu D, Feng L, et al. Accumulation of extracellular matrix and developmental dysregulation in the pancreas by transgenic production of transforming growth factor-beta 1. Am J Pathol 1995;147:42-52.
138. Sanvito F, Nichols A, Herrera PL, et al. TGF-beta 1 overexpression in murine pancreas induces chronic pancreatitis and, together with TNF-alpha, triggers insulin-dependent diabetes. Biochem Biophys Res Commun 1995;217:1279-86.
139. Saotome T, Inoue H, Fujimiya M, et al. Morphological and immunocytochemical identification of periacinar fibroblast-like cells derived from human pancreatic acini. Pancreas 1997;14:373-382.

140. Apte MV, Haber PS, Applegate TL, et al. Periacinar stellate shaped cells in rat pancreas: identification, isolation, and culture. Gut 1998;43:128-33.
141. Wake K. Perisinusoidal stellate cells (fat-storing cells, interstitial cells, lipocytes), their related structure in and around the liver sinusoids, and vitamin A-storing cells in extrahepatic organs. Int Rev Cytol 1980;66:303-53.
142. Watari N, Hotta Y, Mabuchi Y. Morphological studies on a vitamin A-storing cell and its complex with macrophage observed in mouse pancreatic tissues following excess vitamin A administration. Okajimas Folia Anat Jpn 1982;58:837-58.
143. Kordes C, Sawitza I, Gotze S, et al. Stellate cells from rat pancreas are stem cells and can contribute to liver regeneration. PLoS One 2012;7:e51878.
144. Haber PS, Keogh GW, Apte MV, et al. Activation of pancreatic stellate cells in human and experimental pancreatic fibrosis. Am J Pathol 1999;155:1087-95.
145. Erkan M, Adler G, Apte MV, et al. StellaTUM: current consensus and discussion on pancreatic stellate cell research. Gut 2012;61:172-8.
146. Lardon J, Rooman I, Bouwens L. Nestin expression in pancreatic stellate cells and angiogenic endothelial cells. Histochem Cell Biol 2002;117:535-40.
147. Lua I, Li Y, Zagory JA, et al. Characterization of hepatic stellate cells, portal fibroblasts, and mesothelial cells in normal and fibrotic livers. J Hepatol 2016;64:1137-1146.
148. Nielsen MFB, Mortensen MB, Detlefsen S. Identification of markers for quiescent pancreatic stellate cells in the normal human pancreas. Histochem Cell Biol 2017;148:359-380.
149. Phillips PA, Wu MJ, Kumar RK, et al. Cell migration: a novel aspect of pancreatic stellate cell biology. Gut 2003;52:677-82.
150. Shimizu K, Kobayashi M, Tahara J, et al. Cytokines and peroxisome proliferator-activated receptor gamma ligand regulate phagocytosis by pancreatic stellate cells. Gastroenterology 2005;128:2105-18.
151. Marrache F, Pendyala S, Bhagat G, et al. Role of bone marrow-derived cells in experimental chronic pancreatitis. Gut 2008;57:1113-20.
152. Sparmann G, Kruse ML, Hofmeister-Mielke N, et al. Bone marrow-derived pancreatic stellate cells in rats. Cell Res 2010;20:288-98.
153. Phillips PA, Wu MJ, Kumar RK, et al. Cell migration: a novel aspect of pancreatic stellate cell biology. Gut 2003;52:677-682.

154. McCarroll JA, Phillips PA, Kumar RK, et al. Pancreatic stellate cell migration: role of the phosphatidylinositol 3-kinase(PI3-kinase) pathway. Biochem Pharmacol 2004;67:1215-25.
155. Phillips PA, McCarroll JA, Park S, et al. Rat pancreatic stellate cells secrete matrix metalloproteinases: implications for extracellular matrix turnover. Gut 2003;52:275-82.
156. Paulo JA, Urrutia R, Banks PA, et al. Proteomic analysis of an immortalized mouse pancreatic stellate cell line identifies differentially-expressed proteins in activated vs nonproliferating cell states. J Proteome Res 2011;10:4835-44.
157. Wehr AY, Furth EE, Sangar V, et al. Analysis of the human pancreatic stellate cell secreted proteome. Pancreas 2011;40:557-66.
158. Apte MV, Phillips PA, Fahmy RG, et al. Does alcohol directly stimulate pancreatic fibrogenesis? Studies with rat pancreatic stellate cells. Gastroenterology 2000;118:780-94.
159. Apte MV, Wilson JS. Stellate cell activation in alcoholic pancreatitis. Pancreas 2003;27:316-20.
160. McCarroll JA, Phillips PA, Santucci N, et al. Vitamin A inhibits pancreatic stellate cell activation: implications for treatment of pancreatic fibrosis. Gut 2006;55:79-89.
161. Jaster R, Hilgendorf I, Fitzner B, et al. Regulation of pancreatic stellate cell function in vitro: biological and molecular effects of all-trans retinoic acid. Biochem Pharmacol 2003;66:633-41.
162. Zhao YQ, Liu XH, Ito T, et al. Protective effects of rhubarb on experimental severe acute pancreatitis. World Journal of Gastroenterology 2004;10:1005-1009.
163. Rane SG, Lee JH, Lin HM. Transforming growth factor-beta pathway: role in pancreas development and pancreatic disease. Cytokine Growth Factor Rev. 2006;17:107-119.
164. Ahmed S, Bradshaw AD, Gera S, et al. The TGF-β/Smad4 Signaling Pathway in Pancreatic Carcinogenesis and Its Clinical Significance. J Clin Med. 2017;5:1.
165. Crisera CA. The ontogeny of TGF-beta1, -beta2, -beta3, and TGF-beta receptor-II expression in the pancreas: implications for regulation of growth and differentiation. . J Pediatr Surg 1999;34:689-693.
166. Böttinger EP, Jakubczak JL, Roberts IS, et al. Expression of a dominant-negative mutant TGFbeta type II receptor in transgenic mice reveals essential roles for TGF-

beta in regulation of growth and differentiation in the exocrine pancreas. EMBO J 1997;16:2621-2633.

167. Shek FW, Benyon RC, Walker FM, et al. Expression of transforming growth factor-beta 1 by pancreatic stellate cells and its implications for matrix secretion and turnover in chronic pancreatitis. Am J Pathol 2002;160:1787-98.
168. Apte MV, Pirola RC, Wilson JS. Pancreatic stellate cells: a starring role in normal and diseased pancreas. Front Physiol 2012;3:344.
169. Omary MB, Lugea A, Lowe AW, et al. The pancreatic stellate cell: a star on the rise in pancreatic diseases. J Clin Invest 2007;117:50-9.
170. Fitzner B, Muller S, Walther M, et al. Senescence determines the fate of activated rat pancreatic stellate cells. J Cell Mol Med 2012;16:2620-30.
171. Klonowski-Stumpe H, Fischer R, Reinehr R, et al. Apoptosis in activated rat pancreatic stellate cells. Am J Physiol Gastrointest Liver Physiol 2002;283:G819-26.
172. Vonlaufen A, Phillips PA, Xu Z, et al. Withdrawal of alcohol promotes regression while continued alcohol intake promotes persistence of LPS-induced pancreatic injury in alcohol-fed rats. Gut. 2011;60:238-246.
173. Kim N, Yoo W, Lee J, et al. Formation of vitamin A lipid droplets in pancreatic stellate cells requires albumin. Gut 2009;58:1382-90.
174. Glass A, Kundt G, Brock P, et al. Delayed response toward activation stimuli in pancreatic stellate cells. Pancreas 2006;33:293-300.
175. Bynigeri RR, Jakkampudi A, Jangala R, et al. Pancreatic stellate cell: Pandora's box for pancreatic disease biology. World J Gastroenterol 2017;23:382-405.
176. Masamune A, Shimosegawa T. Signal transduction in pancreatic stellate cells. J Gastroenterol 2009;44:249-60.
177. Gress T, Muller-Pillasch F, Elsasser HP, et al. Enhancement of transforming growth factor beta 1 expression in the rat pancreas during regeneration from caerulein-induced pancreatitis. Eur J Clin Invest 1994;24:679-85.
178. Ohnishi N, Miyata T, Ohnishi H, et al. Activin A is an autocrine activator of rat pancreatic stellate cells: potential therapeutic role of follistatin for pancreatic fibrosis. Gut 2003;52:1487-93.
179. Charrier A, Brigstock DR. Regulation of pancreatic function by connective tissue growth factor (CTGF, CCN2). Cytokine Growth Factor Rev 2013;24:59-68.

180. Gao R, Brigstock DR. Connective tissue growth factor (CCN2) in rat pancreatic stellate cell function: integrin alpha5beta1 as a novel CCN2 receptor. Gastroenterology 2005;129:1019-30.
181. Mews P, Phillips P, Fahmy R, et al. Pancreatic stellate cells respond to inflammatory cytokines: potential role in chronic pancreatitis. Gut 2002;50:535-41.
182. Klonowski-Stumpe H, Reinehr R, Fischer R, et al. Production and effects of endothelin-1 in rat pancreatic stellate cells. Pancreas 2003;27:67-74.
183. Liu Y, Du L. Role of pancreatic stellate cells and periostin in pancreatic cancer progression. Tumour Biol 2015;36:3171-7.
184. Jalleh RP, Aslam M, Williamson RC. Pancreatic tissue and ductal pressures in chronic pancreatitis. Br J Surg 1991;78:1235-7.
185. Watanabe S, Nagashio Y, Asaumi H, et al. Pressure activates rat pancreatic stellate cells. Am J Physiol Gastrointest Liver Physiol 2004;287:G1175-81.
186. Duffield JS, Forbes SJ, Constandinou CM, et al. Selective depletion of macrophages reveals distinct, opposing roles during liver injury and repair. J. Clin. Investig. 2005;115:56-65.
187. Stout RD, Jiang C, Matta B, et al. Macrophages sequentially change their functional phenotype in response to changes in microenvironmental influences. J. Immunol. 2005;175:342-349.
188. Mosser DM, Edwards JP. Exploring the full spectrum of macrophage interaction. . Nat. Rev. Immunol. 2008;8:958-969.
189. Shrivastava P, Bhatia M, World J gastroenterol -. Essential role of monocytes and macrophages in the progression of acute pancreatitis. . World J gastroenterol, 2010;16:3995-4002.
190. Vanella. K, Wynn T. Mechanism of organ injury and repair by macrophages Ann Rev Physiol 2017;79.
191. Fadok V, Bratton DL, Konowal A, et al. Macrophages That Have Ingested Apoptotic Cells In Vitro Inhibit Proinflammatory Cytokine Production Through Autocrine/Paracrine Mechanisms Involving TGFb, PGE2, and PAF. J. Clin. Investig. 1998;101:890–898.
192. Bradding P, Pejler G. The controversial role of mast cells in fibrosis. Immunological Reviews. 2018;282:198-231.

193. Galli SJ, Tsai M, Gordon JR, et al. Analyzing mast cell development and function using mice carrying mutations at W/c-kit or Sl/MGF (SCF) loci. Ann N Y Acad Sci 1992;664:69-88.
194. Braganza JM. Mast cell: pivotal player in lethal acute pancreatitis. Qjm 2000;93:469-76.
195. Esposito I, Friess H, Kappeler A, et al. Mast cell distribution and activation in chronic pancreatitis. Hum Pathol 2001;32:1174–1183.
196. Mukai K, Tsai M, H. S, et al. Mast cells as sources of cytokines, chemokines, and growth factors. Immunological Reviews. 2018;282:121-150.
197. Gordon JR, Galli SJ. Promotion of mouse fibroblast collagen gene expression by mast cells stimulated via the Fc epsilon RI. Role for mast cell-derived transforming growth factor beta and tumor necrosis factor alpha. Journal of Experimental Medicine. 1994;180:2027-2037.
198. Altieri DC. Survivin - The inconvenient IAP. Semin Cell Dev Biol. 2015;39:91-96.
199. Li F, Ling X. Survivin study: an update of "what is the next wave"? J Cell Physiol 2006;208:476-86.
200. Li F. Role of survivin and its splice variants in tumorigenesis. Br J Cancer. 2005;92:212-216.
201. Lens SM, Vader G, Medema RH. The case for Survivin as mitotic regulator. Curr Opin Cell Biol. 2006;18:616-622.
202. Satoh K, Kaneko K, Hirota M, et al. Expression of survivin is correlated with cancer cell apoptosis and is involved in the development of human pancreatic duct cell tumors. Cancer 2001;92:271-8.
203. Hasel C, Bhanot UK, Heydrich R, et al. Parenchymal regression in chronic pancreatitis spares islets reprogrammed for the expression of NFkappaB and IAPs. Lab Invest 2005;85:1263-75.
204. Tashiro M, Nakamura H, Taguchi M, et al. Expression of survivin after acute necrohemorrhagic pancreatitis in rats. Pancreas 2003;26:160-5.
205. Case RM. Is the rat pancreas an appropriate model of the human pancreas? Pancreatology 2006;6:180-90.
206. Su KH, Cuthbertson C, Christophi C. Review of experimental animal models of acute pancreatitis. HPB 2006;8:264-286.

207. Jurkowska G, Grondin G, Morisset J. Involvement of endogenous cholecystokinin in pancreatic regeneration after cerulein-induced acute pancreatitis. Pancreas 1992;7:295-304.
208. Argdassi AA, Mayerle J, Christochowitz S, et al. Animal models for investigating chronic pancreatitis. Fibrogenesis and Tissue Repair 2011;1:26.
209. Saluja AK, Dudeja V. Relevance of animal models of pancreatic cancer and pancreatitis to human disease. . Gastroenterology 2013;144:1194-1198.
210. Schneider A, Whitcomb DC, Singer MV. Animal models in Alcoholic pancreatitis-what can we learn? . Pancreatology 2002;2:189-203.
211. Mizunuma T, Kawamura S, Kishino Y. Effects of injecting excess arginine on rat pancreas. . J. Nurt. 1984;114:467-471.
212. Dawra R, Sharif R, Phillips P, et al. Development of a new mouse model of acute pancreatitis induced by administration of l-arginine. Am J Physiol Gastrointest Liver Physiol 2007;292:G1009-1018.
213. Hegyl P, Rakonczay ZJ, Sari R, et al. Arginine induced experimental pancreatitis. . World J Gastroentero 2004;10:2003-2009.
214. Weaver C, Bishop AE, Polak JM. Pancreatic changes elicited by chronic administration of excess l-arginine. . Exp Mol Pathol 1994;60:71-87.
215. Wallig MA, Gould DH, van Steenhouse J, et al. The relationship of vehicle to target organ toxicity induced by the naturally occurring nitrile 1-cyano-2-hydroxy-3-butene. . Fundam Appl Toxicol 1988;12:377-385.
216. Kelly L, Reid L, Walker N. Massive acinar cell apoptosis with secondary necrosis, origin of ducts in atrophic lobules and failure to regenerate in cyanohydroxybutene pancreatopathy in rats. 1999;80:217-226.
217. Nishie K, Daxenbichler ME. Toxicology of glucosinolates, related compounds (nitriles, R-goitrin, isothiocyanates) and vitamin U found in cruciferae. . Fd Cosmet Toxicol. 1980;18:159-172.
218. Pound AW, Walker NI. Involution of the pancreas after ligation of the pancreatic ducts. I: a histological study. Br J Exp Pathol 1981;62:547-58.
219. Schmidt RM, Whitcomb DC. Genetically defined models of chronic pancreatitis. Gastroenterology 2006;131:2012-2015.
220. Karnovsky MJ. A formaldehyde-glutaraldehyde fixative of high osmolality for use in elctron microscopy. J Cell Biol 1965;27:137A-138A.

221. Kerr JF, Gobé GC, Winterford CM, et al. Anatomical methods in cell death. Methods Cell Biol. 1995;46:1-27.
222. Reid LE, Walker NI. Acinar cell apoptosis and the origin of tubular complexes in caerulein-induced pancreatitis. Int J Exp Pathol 1999;80:205-15.
223. Luttenberger T, Schmid-Kotsas A, Menke A, et al. Platelet-derived growth factors stimulate proliferation and extracellular matrix synthesis of pancreatic stellate cells: implications in pathogenesis of pancreas fibrosis. Lab Invest.;80:47-55.
224. Tomonobu T, Leaki U, Hironori M, et al. Studies on caerulein (FI6934). Absorption, distribution, metabolism and excretion of caerulein. . Japan. J. Pharmacol. 1975;25:747-762.
225. Etemad B, Whitcomb DC. Chronic pancreatitis: diagnosis, classification, and new genetic developments. Gastroenterology 2001;120:682-707.
226. Yokota T, Denham W, Murayama K, et al. Pancreatic stellate cell activation and MMP production in experimental pancreatic fibrosis. J Surg Res. 2002;104:106-111.
227. Muller-Pillasch F, Gress TM, Yamaguchi H, et al. The influence of transforming growth factor beta 1 on the expression of genes coding for matrix metalloproteinases and tissue inhibitors of metalloproteinases during regeneration from cerulein-induced pancreatitis. . Pancreas 1997;15:168-175.
228. Winwood PJ, Schuppan D, Iredale JP, et al. Kuppffer cell-derived 95-kDa type IV collagenase/gelatinase B: characterisation and expression in cultured cells. . Hepatology 1995;22:304-315.
229. Nakae H, Endo S, Inoue Y, et al. Matrix metalloproteinase-1 and cytokines in patients with acute pancreatitis. Pancreas 2003;26:134-138.
230. Dal-Secco D, Wang J, Zeng Z, et al. A dynamic spectrum of monocytes arising from the in situ reprogramming of CCR2+ monocytes at a site of sterile injury. J Exp Med. 2015;212:447-456.
231. Yonetci N, Oruc N, Ozutemiz O, et al. Effects of Mast-Cell Stabilization in Cerulein-Induced Acute Pancreatitis in Rats. Int J Gastrointest Cancer 2001;29:163-172.
232. Shukla SA, Veerappan R, Whittimore JS, et al. Mast cell ultrastructure and staining in tissue. Methods Mol Biol. 2006;315:63-76.
233. Jaskiewicz K, Nalecz A, Rzepko R, et al. Immunocytes and activated stellate cells in pancreatic fibrogenesis. Pancreas 2003;26:239-242.

234. Youssef N, Petitjean B, Bonte H, et al. Non-alcoholic duct destructive chronic pancreatitis: a histological, immunohistochemical and in-situ apoptosis study of 18 cases. Histopathology 2004;44:453-61.
235. Xu X, Rivkind A, Pikarsky A, et al. Mast cells and eosinophils have a potential profibrogenic role in Crohn disease. Scand J Gastroenterol 2004;39:440-7.
236. Crook NE, Clem RJ, Miller LK. An apoptosis-inhibiting baculovirus gene with a zinc finger-like motif. J Virol. 1993;67:168-174.
237. Altieri DC. Survivin in apoptosis control and cell cycle regulation in cancer. Prog Cell Cycle Res 2003;5:447-52.
238. Wu X, Zhang Q, Wang X, et al. Survivin is required for beta-cell mass expansion in the pancreatic duct-ligated mouse model. PLoS One 2012;7:e41976.
239. Ouhtit A, Matrougui K, Bengrine A, et al. Survivin is not only a death encounter but also a survival protein for invading tumour cells. Frontiers in Science 2007;12:1260-1270.
240. Zangermeise-Wittke U, Simon HU. An IAP in action. The multiple roles of survivin in differentiation, immunity and malignancy Cell Cycle. 2004;3:1121-1123.
241. Mareninova OA, Sung KF, Hong P, et al. Cell death in pancreatitis: caspases protect from necrotizing pancreatitis. J Biol Chem 2006;281:3370-81.
242. Yuan J, Liu Y, Tan T, et al. Protein kinase d regulates cell death pathways in experimental pancreatitis. Front Physiol 2012;3:60.
243. M. J. Escaping cell death: survival proteins in cancer. . Exp Cell Res 1999;248:30-43.
244. Liggins C, Orlicky DJ, Bloomquist LA, et al. Developmentally regulated expression of Survivin in human pancreatic islets.. . Pediatr Dev Pathol. 2003;6:392-397.
245. Wang H, Gambosova K, Cooper ZA, et al. EGF regulates survivin stability through the Raf-1/ERK pathway in insulin-secreting pancreatic beta-cells. BMC Mol Biol 2010;11:66.
246. Vera-Portocarreroa L, Westlund KN. Role of Neurogenic Inflammation in Pancreatitis and Pancreatic Pain. . 14 2005;4.
247. Schafer C, Tietz AB, Goke B. Pathophysiology of acute experimental pancreatitis: lessons from genetically engineered animal models and new molecular approaches. Digestion 2005;71:162-72.
248. Wallig MA, Kore AM, Crawshaw J, et al. Separation of the toxic and glutathione-enhancing effects of the naturally occurring nitrile cyanohydroxybutene. . Fundam. Appl. Toxicol. 1992;19:598-606.

249. Barres BA, Hart IK, Coles HS, et al. Cell death and control of cell survival in the oligodendrocyte lineage Cell 1992;70.
250. Coles HS, Burne JF, Raff MC. Large-scale normal cell death in the developing rat kidney and its reduction by epidermal growth factor. . Development 1993;118:777-784.
251. Howie SE, Harrison DJ, Wyllie AH. Lymphocyte apoptosis – mechanisms and implications in disease. Immunol Rev. 1994;142:141-156.
252. Wallig MA, Jeffrey EH. Enhancement of pancreatic and hepatic glutathione levels in rats during cyanohydroxybutene intoxication. Fundam Appl Toxicol, 1990;14:144-159.
253. Clutton S. The importance of oxidative stress in apoptosis Br Med Bull. 1997;53:662-668.
254. Edinger AL, Thompson CB. Death by design: apoptosis, necrosis or autophagy. Current Opinion in Cell Biology 2004;16:663-669.
255. Fujimoto K, Hosotani R, Doi R, et al. Role of neutrophils in cerulean-induced pancreatitis in rats: possible involvement of apoptosis. Digestion 1997;58:421-430.
256. Jäättelä M. Multiple cell death pathways as regulators of tumour initiation and progression. . Oncogene 2004;23:2746-2756.
257. Ulmasov B, Oshima K, Rodriguez MG, et al. Differences in the degree of cerulein-induced chronic pancreatitis in C57BL/6 mouse substrains lead to new insights in identification of potential risk factors in the development of chronic pancreatitis. . A. Am J Pathol 2013;183:692-708.
258. Rosenberg l, Rafaeloff R, Clas D, et al. Induction of islet cell differentiation and new islet formation in the hamster. further support for a ductular origin. Pancreas 1996;13:38-46.
259. Forbes SJ, Rosenthal N. Preparing the ground for tissue regeneration: from mechanism to therapy. Nature Medicine 2014;20:857-869.
260. Van Gassen N, Staels W, Van Overmeire E, et al. Consise Review: macrophages: versatile gatekeepers during pancreatic βcell development, injury, and regeneration. . Stem cells translational medicine 2015;4:555-563.
261. Mikami Y, Takeda K, Shibuya K, et al. Do Peritoneal Macrophages Play an Essential Role in the Progression of Acute Pancreatitis in Rats? Pancreas 2003;27:253-260.

262. Jenkins SJ, Ruckerl D, Thomas GD, et al. IL-4 directly signals tissue-resident macrophages to proliferate beyond homeostatic levels controlled by CSF-1. J. Exp. Med. 2013;210.
263. Walker NI. Ultrastructure of the rat pancreas after experimental duct ligation. I. The role of apoptosis and intraepithelial macrophages in acinar cell deletion. . Am. J. Pathol. 1987;126:439-451.
264. Xue J, Sharma V, Hsieh MH, et al. Alternatively activated macrophages promote pancreatic fibrosis in chronic pancreatitis. Nat Commun. 2015;18:7158.
265. La Fleur M, Underwood JL, Rappolee DA, et al. Basement membrane and repair of injury to peripheral nerve: defining a potential role for macrophages, matrix metalloproteinases, and tissue inhibitor of metalloproteinases-1. . J Exp Med. 1996;184:2311-2326.
266. Hügle T. Beyond allergy: the role of mast cells in fibrosis Swiss Med Wkly. 2014;3:144.
267. Riopel MM, Li J, Liu S, et al. beta1 integrin-extracellular matrix interactions are essential for maintaining exocrine pancreas architecture and function. Lab Invest 2013;93:31-40.
268. Motta PM, Macchiarelli G, Nottola SA, et al. Histology of the exocrine pancreas. Microsc Res Tech. 1997;37:384-398.
269. Means AL, Leach SD. Lineage commitment and cellular differentiation in exocrine pancreas. Pancreatology 2001;1:587-96.
270. Mareninova OA, Sung KF, Hong P, et al. Cell death in pancreatitis: caspases protect from necrotizing pancreatitis. . J Biol Chem. 2006;281:3370-3381.
271. Zhou Q, Melton DA. Pancreas regeneration. Nature. 2018;557:351-358.
272. Zhang J, Rouse RL. Histopathology and pathogenesis of caerulein-, duct ligation-, and arginine-induced acute pancreatitis in Sprague-Dawley rats and C57BL6 mice. Histol Histopathol. 2014;29:1135-1152.
273. Walgren J, Mitchell MD, Whiteley LO, et al. Evaluation of two novel peptide safety markers for exocrine pancreatic toxicity. Toxicol Sci. 2007;96:184-193.
274. Chan YC, Leung PS. Acute pancreatitis: animal models and recent advances in basic research. Pancreas 2007;34:1-14.
275. Lampel M, Kern HF. Acute interstitial pancreatitis in the rat induced by excessive doses of pancreatic secretagogue. Virchows Arch A Pathol Anat Histol. 1977;373:97-117.

276. Bhatia M, Wallig MA, Hofbauer B, Lee HS, Frossard JL, Steer ML, Saluja AK. Induction of apoptosis in pancreatic acinar cells reduces the severity of acute pancreatitis. Biochem Biophys Res Commun 1998;246:476-483.

277. Gruber BL. Mast cells: accessory cells which potentiate fibrosis. Int Rev Immunol 1995;12:259-279

278. Accessory organs of the digestive system. Physiology Plus 2017. http://physiologyplus.com/accessory-organs-of-the-digestive-system-and-their-functions. Accessed 14th January, 2019.

APPENDIX 1

Puchtler's (Picro-) Sirius Red for fibrosis

Picro-sirius red solution	
Sirius red F3B	0.5g
Saturated aqueous picric acid	500ml
Acetic Acid water	5ml
Distilled water	110ml

Bring sections to water. Optionally stain nuclei with an acid resistant nuclear stain. Wash well with water. Stain in Picro-Sirius red solution for 1 hour. Wash with 2 changes of acetic acid water. Dehydrate with ethanol, clear in xylol, mount with depex.

Nuclei=blue, cytoplasm=yellow, collagen=red
Histological and Histochemical Methods, J.A. Kiernan (1999), Butterworth Heinemann Oxford, England, and Woburn, MA., USA; Sirius Red F3B,BDH laboratory supplies, Poole, England.

Alcian Blue/Nuclear-fast Red for mast cells

1% Alcian Blue in 0.7N HCl	
0.7N HCl rinse	
Nuclear Fast Red	0.1g
5% aluminium sulphate aqueous	100ml
Filter before use	

Bring sections to distilled water. Stain in Alcian blue solution for 1.5 hours. Rinse quickly in distilled water. Wash in 0.7N HCl for 1 minute. Stain in Nuclear Fast Red solution 10 minutes. Rinse quickly in water. Dehydrate in ethanol, clear in xylol, mount with depex.

Alcian Blue 8GX, BDH Laboratory Supplies, Poole England.
Nuclear Fast Red, Chroma 1A 402, Chroma-Gesellschaf, Stuttgart.

Toluidine Blue stain for semi thin epoxy sections

Epoxy sections cut 0.5-1.0 µm thick

Distilled water	100 mls
Toluidine blue	1 gram
Sodium tetraborate	1 gram

Add chemicals to boiling water and agitate for 30 minutes. Allow to cool before use. Heat slides on the hot plate for 5 minutes; apply 3 drops of stain; leave for 30-60 seconds. Do not let slide dry. Rinse under running water to remove excess stain. Differentiate in three changes 1-2 mins each of absolute ethanol. Wipe back of slide and dry on hotplate. Blow gently on slide to avoid 'tide' lines. Coverslip with depex.

Mayer's Acid Haemalum

Haematoxylin	1.0g
Sodium iodate	0.2g
Potassium aluminium sulphate	50g
Distilled water	1000 mls
Dissolve overnight then add	
Chloral hydrate	50g
Citric acid	1.0g

The stain has a working life of one month and may be stored for six months. The original formula of Mayer (Mitth. Zool. Stat, Neapel., X, 1, 1891; Toxic) differed in detail from that given, however the latter is accepted as Mayer's formulation.

Eosin

Eosin	1 gm
70% Ethanol	1 litre

[HCl precipitated Eosin Y, C.I. 45380]

10% neutral buffered formalin

37% formaldehyde is the approximate saturation point for formaldehyde gas in water. 10% formalin is a histologist's term and refers to a 1:10 dilution of 37% formaldehyde in buffer, effectively 4% formaldehyde.

$NaH_2PO_4.2H_2O$	4.5 grams
Na_2HPO4	5.85 grams
Formaldehyde 37%	100 mls
Distilled water	900 mls

4% neutral buffered paraformaldehyde

Made by mixing 4 grams of paraformaldehyde powder in 0.1M phosphate buffer pH 7.4. Paraformaldehyde will readily dissolve in neutral to alkaline-buffered solutions. It will not dissolve in distilled water or acidic solutions without the addition of large quantities of sodium hydroxide.

Paraformaldehyde	4 grams
0.1M phosphate buffer	100 mls

Heat the buffer to 50^{o}C and add the paraformaldehyde, stir till dissolved. It is important that the temperature of the buffer is not significantly higher than 50^{o}C as 1 or more small NaOH pellets may need to be added to help dissolve the paraformaldehyde. Cool and check pH Fix for 12 to 24 hours depending on size, use/store at room temperature.

Fixed tissues are transferred to 70% ethanol, or 0.1M phosphate buffer if the samples are for electron microscopy. Paraformaldehyde solutions should be prepared fresh or used within a month.

0.1M Phosphate buffer

Add 36 mls of dibasic sodium phosphate with 14 mls of mono sodium phosphate and 50 mls of distilled water, pH to 7.4

Karnovsky's fixative

Fixative/perfusate for electron microscopy. Addition of calcium chloride to the solution will improve the preservation of cell membranes.

4% paraformaldehyde, 4% glutaraldehyde, 0.1% calcium chloride in 0.1M sodium cacodylate pH 7.3 buffer.

Sodium cacodylate	2.14	grams
Paraformaldehyde	4.0	grams
Calcium chloride	0.1	gram
Water	84	mls
Glutaraldehyde 25%	16	mls

Heat water to 50^{o}C and add the paraformaldehyde, stir till dissolved. 1 small NaOH pellet may need to be added to help dissolve the paraformaldehyde. Cool to room temperature and add the sodium cacodylate and calcium chloride. Stir till dissolved and pH to 7.3. Immediately before use add the glutaraldehyde and mix thoroughly.

Either perfuse animals with Karnovsky's for 10 - 20 minutes, remove the target tissues, dice into blocks 1mm^3 and fix for a further 2 hours by immersion or remove target tissues dice in to 1mm^3 blocks and fix by immersion for a minimum of 4 hours

Warning sodium cacodylate contains arsenic, a known carcinogen. Paraformaldehyde is a suspected carcinogen. Glutaraldehyde in highly toxic by contact and its vapours can cause sensitisation and respiratory distress.

Antigen Retrieval

0.01M Citrate pH6.0, 5 minutes at 125°C
0.001M EDTA/0.01M Tris pH 8.8, 15 minutes at 105°C
0.1% porcine trypsin 30 minutes at room temperature 15 mins at 37°C
20ug/ml proteinase K in 0.05M Tris-Hcl, 0.01M $CaCl_2$ pH8.0 10 minutes at room temperature
HCl 0.2N 15 mins at 37°C
Chymotrypsin 0.5% 10 mins at 37°C
Heat retrieval was performed in a Biocare Medical Decloaking Chamber

Proteinase K Digestion

To make 20µg/ml Proteinase K add:
100 microlitres of 2.0 mg/ml Proteinase K to
10 ml of 0.05M Tris.Cl /0.01M calcium chloride pH 8.0
Proteinase K Promega cat# V302B 155567

Chymotrypsin Digestion

Chymotrypsin 0.05g, Sigma Aldrich C4129-1G
$CaCl_2$ 0.05g, Sigma Aldrich C2661-500g
dH_20, 10 ml
Incubate for 10 min at 37°C, adjust pH to 7.8 using NaOH.

0.01M (10mM) sodium citrate buffer pH 6.0 for antigen heat retrieval

Sodium Citrate Buffer (10mM) - Tween 20 (0.05%) pH 6.0
Dissolve 2.94 g Tri-sodium citrate in 1000 ml distilled water
Adjust to pH 6.0
Add 0.5 ml of Tween 20 and mix well

0.001M ethylenediamine tetra acetic acid (EDTA) pH 8.8-9.0 for antigen heat retrieval

Tris/EDTA (10/1 mM) pH 9
Add 1.21 g of Tris and 0.37 g of EDTA to 1000 ml of distilled water
Adjust to pH 9 if necessary

0.01M Phosphate buffered Saline

100ml saline + 0.026g KH_2PO_4 + 0.115g Na_2HPO_4

Tris buffer/Tween

Tris Buffer (10mM) - Tween 20 (0.05%) pH 10
Dissolve 1.21 g Tris Base in 1000 ml distilled water
Adjust to pH 10 using 1M NaOH
Add 0.5 ml Tween 20 and mix well

Secondary antibody/detection reagent:

DAKO Envision™ + Dual Link System-HRP (DAB+), Dako Code K4065
MACH1 Universal HRP-Polymer detection, Biocare Medical
Jackson donkey goat ant- rabbit 1:300 20 minutes at RT

Glass slides, Menzel Superfrost Plus™

Selected antibody and supplier details

Amylase rabbit anti-human, lot 86H8840, Sigma
Caspase rabbit anti-cleaved caspase3, ASP175, Cell Signaling cat no 9661S
Caerulein sulfated C9026, lot 121H02111, CAS No. 17650-98-5 Sigma peptides and amino acids
CD68, monoclonal mouse anti-human clone PG-M1 code M0876, Lot 016, DAKO
CD117/c-kit rabbit polyclonal cat CP151a, Biocare Medical

Cytokeratin AE1/AE3 mouse anti-human, lot 0019B, DAKO

Glucagon porcine anti-human NCL-GLUCp, Novacastra

PCNA (Proliferating cell nuclear antigen) (AB-1) Monoclonal mouse NA03, Oncogene research products, Calbiochem

αSMA smooth muscle actin, monoclonal mouse IgG2a isotype, clone 1A4, Sigma A2547

Survivin rabbit anti-human clone 71G4B7, Cell Signaling cat #2808

Survivin rabbit polyclonal, NB500-201, lot P1, Novus Biologicals

Biocare Medical, 60 Berry Drive, Pacheco, CA 94553, USA

Calbiochem 10394 Pacific Centr Court, San Diego, CA 92121

Dako Australia Pty Ltd Berry Street, North Sydney, NSW.

Jackson Immunoresearch Inc, 872 West Baltimore Pike, West Grove, PA, USA 19390

Novacastra, Leica Biosystems, Wetzlar, Germany

Novus Biologicals, **In Vitro Technologies** 7-9 Summit Road Noble Park North, VIC 3174

Sigma-Alrich Merck, 12 Anella Ave, Castle Hill NSW 2154